Frontiers in Head and Neck Trauma:

Clinical and Biomechanical

FINAL REPORT

Grant #N00014-96-1-1234

MEDICAL
COLLEGE
OF WISCONSIN

Narayan Yoganandan, Ph.D.
Professor

Department of Neurosurgery

June 26, 1998

Defense Technical Information Center
8725 John J. Kingman Road – Suite 0944
Ft. Belvoir, VA 22060-6218

Re: Grant Number N00014-96-1-1234

To Whom it May Concern:

Enclosed is a copy of the proceedings entitled "Frontiers in Head and Neck Trauma: Clinical and Biomechanical" resulting from the above partial funding. As stipulated in the ONR letter dated September 4, 1996, we have enclosed a copy of form SF-298 along with the proceedings, and in addition, a copy of the SF-298 along with four copies of the proceedings are also being mailed to the ONR in Arlington, Virginia.

We sincerely thank the ONR for providing partial funding for this most important research endeavor that we strongly believe to be of significant benefit to the Navy and other scientific professionals.

Sincerely,

Narayan Yoganandan, Ph.D.
Professor and Chairman, Biomedical Engineering

Frank A. Pintar, Ph.D.
Director, Neuroscience Laboratories

Rodney W. Kison 7/1/98
Director, Grants & Contracts

tw
Enclosures

Froedtert West
9200 West Wisconsin Avenue
Milwaukee, Wisconsin 53226
(414) 384-3453

REPORT DOCUMENTATION PAGE

Form Approved
OMB No. 0704-0188

1. AGENCY USE ONLY *(Leave blank)*	2. REPORT DATE	3. REPORT TYPE AND DATES COVERED
	6/19/98	Final 9/1/96 - 6/19/98

4. TITLE AND SUBTITLE
FRONTIERS IN HEAD AND NECK TRAUMA:
Clinical and Biomechanical

5. FUNDING NUMBERS

6. AUTHOR(S)
Narayan Yoganandan, Ph.D., Frank A. Pintar, Ph.D.
Sanford J. Larson, M.D., Ph.D.

7. PERFORMING ORGANIZATION NAMES(S) AND ADDRESS(ES)
Medical College of Wisconsin
8701 Watertown Plank Road
Milwaukee, WI 53226

8. PERFORMING ORGANIZATION REPORT NUMBER
MCW-NS-980615

9. SPONSORING / MONITORING AGENCY NAMES(S) AND ADDRESS(ES)
Office of Naval Research
Ballston Centre Tower One, 800 N. Quincy Street
Arlington, VA 22217-5660

10. SPONSORING / MONITORING AGENCY REPORT NUMBER
N00014-96-1-1234

11. SUPPLEMENTARY NOTES

a. DISTRIBUTION / AVAILABILITY STATEMENT
Approved for public release

12. DISTRIBUTION CODE

13. ABSTRACT *(Maximum 200 words)*

Clinical and biomedical aspects of head and neck injuries are covered in this presentation. Recent research stemming from laboratory-driven experimental and mathematical models, and clinical and epidemiological investigations are discussed. Topics covered include the basic anatomy of the head and neck of the pediatric and adult human population; the effects of the presence of uncovertebral joints in the adult human neck; and radiographic, computed tomography and magnetic resonance imaging of craniocerebral and cervical trauma. An evaluation is made of the Hybrid III anthropomorphic test device with the human neck structure. Inertial loading of the human neck and its implications in the production of whiplash injuries are given. Mathematical modeling describes continuum mechanics-type buckling models, and numerical finite element techniques to evaluate the effect of clinical procedures such as surgery and stabilization. Instrumentation techniques are discussed for the upper and lower cervical spine. Head and neck injury issues in Naval Aviation are also presented.

14. SUBJECT TERMS
Head and Neck

15. NUMBER OF PAGES

16. PRICE CODE

17. SECURITY CLASSIFICATION OF REPORT	18. SECURITY CLASSIFICATION OF THIS PAGE	19. SECURITY CLASSIFICATION OF ABSTRACT	20. LIMITATION OF ABSTRACT

ADULT AND CHILD

HEAD ANATOMY

Joseph S. Cheng, Kenneth W. Reichert

Abstract

A brief overview of the normal anatomy of the adult and child head is presented. The information was culled from a variety of sources, including major textbooks and papers. Although not a complete work, the intent of this chapter is to orient the reader with some of the major anatomical structures.

1. Adult Anatomy of the Skull

The skeletal structures of the head are divided into three main parts: neurocranium (housing the brain), face and base. The term skull generally refers to the entire bony structures located in the head. Cranium (Latin for helmet) refers to the fused regions only, that is without the mandible. The adult neurocranium is a series of irregularly shaped flat bones fused together (Figure 1). Eight bones make up the neurocranium: frontal, two parietal, two temporal, occipital, sphenoid and ethmoid. The sphenoid and ethmoidal bones are smaller and provide the junction with the face and anterior base of the skull. The calvaria consists of the frontal, parietal and occipital bones that form the bulk of the convexity on top. The lateral aspect of the sphenoid bone meets the temporal bone

to form the lateral region of the head. Below is an overview on the main bones of the neurocranium.

1.1 Frontal Bone

The frontal bone is generally considered a single entity, although its development occurred as two separate pieces divided by the metopic suture along the midline (Figure 2). Shaped similarly to an arrow head with a slight triangular shape, the superior lateral edges are bordered by the parietal bones forming the coronal suture. The bregma is located at the superior apex and defines the intersection of the coronal suture (running side to side) with the sagittal suture (running from front to back and dividing the parietal bones along the midline). The anterior-inferior aspect of the frontal bone forms the orbital roofs, with the medial portion forming the roof of the nose by abutting the ethmoid bone. The glabella indicates the flattened region between the two supraciliary ridges. The anterior portion of the temporalis muscle attaches at the posterior-lateral portion of the frontal bone (Figure 3).

1.2 Parietal Bone

The parietal (paries, Latin for wall) are rectangular and irregularly shaped bones located laterally on either side of the skull (Figure 4). The anterior edge of the bone articulates with the frontal bone forming the coronal suture. Posteriorly, it meets the occipital bone with the division between forming the lambdoid suture. The superior aspect meets the opposite parietal bone and forms the sagittal suture between them. Inferiorly, a small region of the anterior parietal bone is bound by the sphenoid bone, but mainly by the temporal bone. The temporalis muscle attaches to the middle of the bone in a semilunar fashion, forming the temporal ridges along its course. The middle meningeal artery courses along the underside of the parietal bones, forming a groove in the bone. It generally begins at the anterior-inferior angle and quickly divides into multiple branches as it travels in a superior-posterior direction. Fractures through this site may injure this artery producing an epidural hematoma that is considered a neurosurgical emergency. Although the force of impact creates a dural separation, the pressure of the pulsatile artery will generate enough force to progressively strip the dura from the inner table of the skull. Failure to emergently decompress and stop the high pressure arterial bleeding will further damage the underlying brain with possible herniation and death.

1.3 Temporal Bone

The pair of temporal bones resides in the inferolateral portion of the skull bordered by the occipital bone posteriorly, parietal bone superiorly and the sphenoid bone inferoranteriorly. The temporal bone is divided into three sections: squamous, mastoid and petrous portions. The squamous portion is named due to its scale-like form, being thin with a smooth convex outer surface. This smooth surface is marred by the indentation of the deep temporal artery that courses up the posterior aspect. The middle meningeal artery follows the medial aspect of the squamous bone, and fractures to the thin region may injure the artery. The temporalis muscle separates the squamous portion superiorly from the mastoid region in the posterior-inferior region. The tip of the muscle insertion ends anteriorly at the zygomatic process, the bony arch that extends outwards from the temporal bone to meet the zygomatic bone, otherwise known as the "cheek bone". The smooth, thin region of the squamous portion is quite distinctive compared to the rough surface of the mastoid portion. Numerous hollowed spaces, the mastoid air cells, reside in the mastoid portion of the bone although these may be absent in some patients. These cells communicate with the mastoid antrum, a larger air space lined with a mucous membrane and from which communication with the cavity of the tympanum or middle ear is achieved. Injuries to the mastoid region may cause bleeding into the air cells, causing "Battle's sign" or a dark bluish discoloration just behind the ear. Skull fractures that violate the air cells as well as the meningeal covering may

produce pneumocephaly or air trapped in the neurocranium, which is readily detected on a computed tomography (CT) scan.

1.4 Occipital Bone

The occipital bone lies at the most posterior portion of the skull and is separated from both parietal bones superiorly by the lambda sutures (Figure 5). Inferiorly, it articulates with the mastoid and petrosal portions of the temporal bone. The base of the occipital bone rests above the atlas or first cervical vertebra, which then rotates about the axis or second cervical vertebra. The articulation of the occipital bone upon C1-C2 vertebrae or the atlantoaxial region, constitutes a specialized formation that provides the majority of the rotational head motion. The base of the occipital bone contains the foramen magnum, a large opening in the bone that allows for the passage of the spinal cord as it evolves from the lower brainstem. This inferior portion of the brainstem, the medulla oblongata, rests in a groove along the anterior aspect of the occipital bone just above the foramen magnum.

1.5 Sphenoid Bone

Situated at the anterior base of the skull, the sphenoid bone resembles a large butterfly in shape. The body lays midline and is cavitated by the sphenoid sinuses, while the ala or wings are spread out laterally and divided into greater and lesser portions. Various foramina or holes in the bone provide passageways to vascular and nervous structures. Belying the Latin terminology meaning "wedge", the sphenoid may be better described as a foundation, as it truly is the base of the cranial bones, juxtaposing against all the other cranial bones as well as some of the facial ones. The body of the sphenoid bone is fenestrated with a large cavity sitting anteriorly forming the sphenoid sinus. The sinus is actually formed by a pair of irregularly shaped hollowed openings separated in the midline by a thin septum of bone. The sinus communicates anteriorly with the ethmoid bone, and basilar skull fractures through this region will show up on CT scans as an air fluid level. Along the superior surface of the bone lies the sella turcica, in which resides the pituitary gland. The optic groove lies anterior to the sella, extending into the optic canal in which the ophthalmic artery and the optic nerve course after the fibers have crossed at the optic chiasm. Anteriorly, the sphenoid articulates with the ethmoid spine that continues to form the cribiform plate. The cribiform plate is where the first cranial nerve, supporting olfaction or the sense of smell, is located and injury to this region may produce cerebral spinal fluid rhinorrhea. Posteriorly on the body, a shallow depression continues down into the occipital bone forming the clivus. The clivus appears as a "slide" on which lays the upper portion of the pons.

The greater wing of the sphenoid lies inferiorly to the lesser wing and protrudes antero-laterally to articulate with the frontal and parietal bones. Developing as a smooth concave surface along the underside of the neurocranium, it forms the region known as the middle fossa. Along the lateral edge of the ala is a groove in which the frontal branches of the middle meningeal artery runs. The lesser wings are thin, triangular structures that are anterior-superior to the greater wings with the inner specula of bone forming the anterior clinoid process, which abuts the optic canal. Just inferior to the clinoid lays the superior orbital fissure in which cranial nerves III, IV, V-1 (first branch), and VI course through as well the superior ophthalmic vein.

1.6 Ethmoid Bone

The ethmoid bone lies between the orbits and consists of thin plates of bone forming a cuboid shape with multiple sinuses extending throughout this region (Figure 6). It is divided into four main parts: lamina cribosa is a horizontal plate forming the roof, lamina perpendicular forming the perpendicular septum dividing the midline, and the two lateral masses of air cells paired along either side of the midline. The lamina cribosa forms the cribiform plate, the superior aspect of which arises a thin triangular process of bone resembling a "roosters comb" pointing into the anterior fossa. This is known as the crista galli and provides an attachment site for the falx cerebri.

The perpendicular plate of the ethmoid bone arises from the inferior aspect of the horizontal plate and provides the bone core of the nasal septum. The lateral masses are multiple pockets of air cells forming the ethmoidal sinuses. The outer surface of each lateral mass is a smooth plate of bone, the os planum, forming the inner wall of the orbit.

1.7 Sutures

The various bones of the neurocranium are juxtaposed at the edges by sutures (sutura, Latin for seam) which initially develop as a linear fibrous joint between the bones. These eventually fuse into an uneven coaptation in the adult with only a minimal amount of fibrous tissue present between the bones. These sutures may often form web-like patterns along their course with the small bony islands imbedded in the main suture line known as wormian bones or ossa triquetra. The three main sutures along the vertex of the neurocranium include the sagittal (interparietal) suture dividing the parietal bones, the coronal (frontoparietal) suture between the frontal and parietal bones, and the lambdoid (occipitoparietal) suture between the occipital and parietal bones. The bregma refers to the junction of the sagittal and coronal suture, while the lambda refers to the junction of the sagittal and the lambdoid suture.

1.8 Facial Bones

The facial bones consist of fourteen bones: two nasal, two superior maxillary, two lachrymal, two malar, two palate, two inferior turbinate, vomer and inferior maxillary bones. These bones form the housing for most of the sensory structures of the human, including sight, smell and taste. The structures for hearing lie laterally within the temporal bone.

2. Adult Anatomy of the Brain

The cranial vault in the skull of modern man is actually smaller than that of the Neanderthal man, with a current capacity of 1,370 cc (cubic centimeters) versus 1,450 cc. So it would seem that intelligence does not necessarily correlate with the size of the brain. With a range of 950 to 2,200 cc, the adult brain weighs an average of 1400 g (grams), comprises less than 2 percent of the total body weight, and yet receives over 20 percent of the blood flow. Along with the spinal cord, the brain is part of the central nervous system and is generally considered in three main parts: cerebrum, cerebellum and brain stem. The entire nervous system of the human is classified into the central nervous system (CNS) and the peripheral nervous system. The CNS is differentiated from the peripheral nervous system not only by its location, but also by cellular characteristics of the neurons. The neurons of the peripheral nervous systems have their axons covered by a myelin sheath as well as a neurilemma formed by specialized Schwann cells. The neurilemma is able to facilitate nerve regeneration in axonal injuries in the peripheral nervous system but not cell body injuries. The CNS neurons only have a myelin sheath around its axons, and lesions here are replaced with scarring from glial cells. Underneath the protective skull (neurocranium), the brain is covered by three membranes: dura mater, arachnoid mater and pia mater. The dura mater (Latin for hard mother) is a thick fibrous membrane attached to the skull. The dura mater is composed of two layers, the periosteal lying toward the skull, and the meningeal that lies towards the brain. Injuries to the middle meningeal artery may cause stripping of the dura away from the skull forming an epidural hematoma that manifests as a displacing convex mass on the CT scan. The arachnoid mater (Latin for web-like mother) is a thin, lattice structure that, along with the pia mater, provides the potential space for the 150 cc of cerebral spinal fluid (CSF) in the average adult. The arachnoid mater is adjacent to the dura mater, but it is not tightly bound to it and a potential space exists between the two layers. This region forms the subdural space, which may be involved in trauma, forming a subdural hematoma. Subdural hematomas are mass lesions that appear as a crescent shape on the CT scan, differentiating it from an epidural hematoma. The pia

mater (Latin for tender mother) is a thin covering that intimately adheres to the surface of the brain and follows all the convexities of the cortex.

The brain is actually mobile, floating in the sea of CSF that provides both nutrition and a buffer to forces around the brain. While weighing 1400 g in the air, the brain weighs only 50 g while suspended in CSF. However, this buffering may contribute to injuries in rapid acceleration and deceleration situations producing coup and counter-coup injuries, (named) depending on the location of brain injury in relation to the direction of the force. An example of rapid deceleration may be seen in the case of a motor vehicle crash. As the patient's skull strikes the windshield and stops suddenly, the inertia of the brain floating in the CSF still continues to carry it forward. The impact against the front of the skull causes contusions to the soft brain tissue in a coup injury. Recoil backwards from the impact may then damage the opposite pole in a counter coup nature. A severe form of this type of injury is seen in shaken baby syndrome, where no signs of external trauma are seen in the child, although the brain has undergone significant injury.

2.1 Cerebrum

The cerebrum is the largest of all the regions of the brain, and is situated at the rostral or uppermost aspect of the central nervous system (Figure 7). Comprised of two duplicate images that are divided in the midline, the cerebrum is involved in the higher functions of the human. These functions include memory, thought, creativity, intelligence, speech, sensation and voluntary motion. The primary cellular unit of the brain is the neuron, which looks like a comet in the sense of a cell body followed by a long axon. These nonregenerating cells are lost daily by the thousands, with the maximum number of neurons present at birth. Humans are estimated to have among 20 to 200 billion neurons at birth, whose numbers decrease with age. The cell bodies form the gray matter of the brain, overlying their axons that form the white matter of the brain. The gray matter is located along the periphery forming a mantle, with the white matter and isolated neuronal nuclei forming the bulk of the interior or core. The surface of the brain develops in a convoluted fashion, forming gyri ("peaks") and sulci ("valleys"). These gyri and sulci are further grouped together into lobes, based on anatomical placement, although they also form regions of different functions. Sulci form the basis of certain anatomical landmarks along the surface of the brain with deep sulci known as fissures. The longitudinal fissure runs along the midline and divides the two hemispheres of the cerebrum. The central sulcus lies in a perpendicular direction to the longitudinal fissure between the frontal and parietal lobes. The central sulcus not only provides an anatomical landmark, it also provides the division of two major functional regions. Anteriorly, the pre-central gyrus controls motor function as the primary motor cortex, while the post-central gyrus lying posterior to the sulcus is involved in sensation as the primary somatic sensory cortex. The lateral sulcus lies laterally and runs in a superior-posterior direction to separate the temporal lobe from the frontal and parietal regions. A smaller sulcus is the parietal-occipital sulcus that separates the parietal and occipital lobes.

There are six main lobes of the human brain: frontal, parietal, occipital, temporal, insular, and limbic. The insular and limbic lobes (also known as the Island of Reil) are located medially along the underside. All lobes are derived from anatomical location except the limbic lobe that is a functional classification formed from the marginal edges of the frontal, parietal, occipital and temporal lobes. Dominance of the hemispheres is dictated by the area for speech as well as the "handedness" of a person, while the nondominant hemisphere is then responsible for the nonverbal higher level functions. Ninety percent of the population is right handed with the speech center of all these individuals located in the left hemisphere. However, in left-handed people there is still a 50 percent left hemispheric dominance.

2.2 Frontal Lobe

As with all the lobes of the brain, the frontal lobes are comprised of two mirror images separated in the midline. It is the largest of the lobes of the brain and is situated anteriorly. It is separated by the central sulcus from the parietal lobes posteriorly, and from the temporal lobes

inferiorly as divided by the lateral sulcus. The convolutions of the surface are generally divided into four regions: superior, middle and inferior frontal gyri, as well as the pre-central gyrus. The inferior frontal gyrus is subdivided further into the pars orbitale, pars triangularis and pars obicularis. The importance of the inferior region is that the pars triangularis and obicularis form Broca's area in the dominant hemisphere. This area is responsible for controlling the major motor component of speech. Injuries to Broca's area will manifest as an expressive aphasia, a frustrating situation where the patient is unable to speak coherent words and sentences although they are able to hear and understand others with minimal difficulty. Most people perceive the frontal lobe to be involved only with higher levels of thought such as planning, personality and judgment, but the functions of this region are much more diverse. Major portions of the frontal lobe are devoted to motor control of the body, and injury to this region produces the classic picture of contralateral hemiparesis. The functional regions of the pre-central gyrus may be represented by a homunculus, or "a little man", in mapping out the primary motor control of the body. This representation of the motor strip indicates which parts of the body will lose voluntary control if that cortical site is injured. Neurons in the primary motor cortex project directly towards the spinal cord, while the secondary and tertiary regions (premotor areas) of control anterior to it, facilitate the transformation of thought into movement.

2.3 Parietal Lobe

The parietal lobe is situated between the other lobes located along the surface of the cerebral convexity. Separated from the frontal lobe by the central sulcus anteriorly and posteriorly by the parietal-occipital sulcus from the occipital lobe, the parietal lobe lies just under the region of the cranium conveniently known as the parietal bone. In the lateral and inferior direction, the parietal lobe is separated from the temporal lobe by the lateral sulcus, also known as the Sylvian fissure. The primary sensory cortex is located along the anterior border of the parietal lobe in the post-central gyrus.

2.4 Temporal Lobe

Stemming from the posterior body of the brain, the temporal lobe can be perceived as a peninsula in morphology. It lays inferior to the lateral sulcus and can be divided into three regions: superior, middle and inferior temporal gyri. Just medial to the posterior edge of the superior gyrus, several gyri lie in an oblique fashion forming the transverse gyri of Heschl. These small gyri constitute the primary auditory cortex in the human and are integral in the ability to perceive sound. Along the inner aspect of the temporal lobe lies the parahippocampal gyrus that dictates the primary olfactory cortex or the sense of smell. Lesions to this area, as well as auras of seizures with a focus here, may be perceived as olfactory hallucinations by the patient.

2.5 Occipital Lobe

Residing along the posterior region of the brain is the occipital lobe. Sitting on top of the tentorium cerebelli, it is separated from the parietal lobe anteriorly by the parietal-occipital sulcus, although this is not as deep or distinctive of an anatomical landmark like the central sulcus. The occipital lobe is divided by the Y-shaped calcarine fissure into the cuneus and lingual gyri. The cortical cells along either side of the calcarine fissure constitute the primary visual cortex, where input from the retina traverse to in a topographical fashion. Lesions to any of the quadrants of the two occipital lobes divided by the calcarine fissure may be mapped directly to visual field deficits by either confrontational testing or more sophisticated visual field tests.

2.6 Insular Lobe

The insula of the brain is not visible from the surface unless the frontal and temporal lobes are retracted. This lobe forms a triangular region with the surface divided into the gyri breves and longus (Latin for short and long).

2.7 Limbic Lobe

The limbic (Latin for border) lobe is not a true anatomical lobe, being differentiated by its function. It is present in all mammals and is considered to be one of the "oldest" portions of the brain in terms of evolutionary qualities. It is formed from the innermost margins of the frontal, parietal and temporal lobes with its pathways around and inferior to the thalamus (Figure 8). It is divided into the subcallosal, cingulate, parahippocampal, hippocampal, and the dentate gyri. It shares with the temporal lobe the function of olfaction, but the limbic lobe also provides the area for emotion and various autonomic functions such as feeding and sexual behavior. Functions for memory are located within the hippocampus. This region is actively involved in the processing, storage and recall of memories with the dominant hemisphere involved in the verbal memories and the nondominant hemisphere involved in the nonverbal ones.

2.8 Cerebellum

Integral in balance and refined movements, the cerebellum lies under the occipital lobe separated by a thick layer of connective tissue known as the tentorium cerebelli. With an estimated 15 to 20 billion neurons, the cerebellum functions as a major site of motor control. Although injuries to the cerebellum do not cause paralysis, injury here will cause ataxia, dysmetria, loss of muscle tone and loss of balance. As with the cerebral hemispheres, the cerebellum is mirrored down the midline along the vermis, forming the two lateral lobes or hemispheres of the cerebellum. The morphology is also similar to the cerebrum with a mantle consisting of the cell bodies (gray matter) overlying their projections of axons (white matter). Multiple small nuclei or collections of cell bodies lie within the white matter forming the fastigial, globoid, emboliform and the dentate nuclei. The surface of the cerebellum resembles that of a walnut with multiple cerebellar folia (Latin for leaf-like) forming parallel rows of gyri and sulci.

2.9 Brainstem

Residing in front of the cerebellum and providing the connecting pathway from the cerebrum to the spinal cord, the brainstem contains the more vital structures of human survival (Figure 9). Coma may be produced from injury to this region. Major structures at the level of the brainstem include the pons, medulla, fourth ventricle, midbrain and diencephalon. The major structures of the diencephalon are further subdivided into the thalamus, hypothalamus and subthalamic regions.

2.10 Cranial Nerves

Twelve sets of nerves originate from the brainstem region and proceed outward to innervate peripheral structures. Due to their origin from the brain, they are dubbed the cranial nerves. They are:

I. Olfactory nerve (sense of smell) - This short nerve arises from just above the optic chiasm to course to the cribiform plate. Named the first cranial nerve due to its most rostral location, this "nerve" (actually a direct CNS extension) provides us with a sense of smell;

II. Optic nerve (vision) - Connecting the retina to the brain. Injury to this cranial nerve will cause blindness. Tumors arising from close proximity to this nerve, such as in the pituitary, will cause loss of vision as one of its initial symptoms;

III. Oculomotor nerve (eye movement) - This nerve provides that majority of the movement of the eyeball including the pupil as well as the eyelids. Two other cranial nerves IV and VI, assist in movement of the eyeball or globe;

IV. Trochlear nerve (eye movement) - The trochlear nerve controls the superior oblique muscle of the globe allowing for a down and in movement;

V. Trigeminal nerve (facial sensation) - This nerve provides the majority of sensation to the face, being divided into three zones by its three major branches (hence, Trigeminal): V-1 (Ophthalmic), V-2 (Maxillary) and V-3 (Mandibular). In a comatose patient, brainstem function may be tested by eliciting the corneal reflex. A cotton swab is touched lightly against the cornea of the eye, with a blink of movement response indicative of an intact sensory arc from the V-1 portion of this cranial nerve. A motor component of this nerve is the control of the muscles of mastication or chewing, as well as the temporal muscle;

VI. Abducens nerve (eye movement) - By controlling the lateral rectus muscle in moving the eyeball laterally, the abducens nerve functions with the oculomotor and trochlear nerves in controlling eye movement. This is one of the longest cranial nerves and one of the most easily injured. Head trauma can often present with an abducens palsy (one eye moving medially but the other unable to move laterally giving double vision);

VII. Facial nerve (facial movement) - This nerve controls the muscles of facial expression except for the muscles of mastication as noted in the trigeminal nerve. Accessory functions also include the control of the lacrimal glands for tearing, and a sensory input for taste from the anterior two-thirds of the tongue;

VIII. Vestibulocochlear nerve (hearing and balance) - The eighth cranial nerve is composed of two components, the cochlear (hearing) and the vestibular (balance). The structures within the inner ear that are responsible for translating air movement (percussion waves) into neuronal impulses also provide a sense of balance by the three perpendicularly oriented semi-circular canals;

IX. Glossopharyngeal nerve (swallowing) - This nerve has a sensory component in the posterior one-third of the tongue as well as a motor component in the upper pharyngeal muscles and the parotid gland (producing saliva);

X. Vagus nerve (visceral control) - Unlike the other cranial nerves that supply the region of the head, the vagus nerve assists in much of the motor control and sensory input of the visceral components or organs. The vagus is a major component in the parasympathetic autonomic system with long fibers extending to the throat, heart, lungs and intestines;

XI. Spinal accessory nerve (neck movement) - This cranial nerve courses downward to innervate the sternocleidomastoid and the upper trapezius muscles. In spinal cord injury, care must be taken to differentiate function of this nerve (trapezius function with shoulder shrug) versus that of the cervical cord (deltoid function with arm abduction); and

XII. Hypoglossal nerve (tongue movement) - The last cranial nerve, named for its origin most inferiorly, controls the movement of the tongue as well as some of the muscles in the neck (strap muscles).

2.11 Ventricles

There are areas within the brain that are essentially hollow regions filled with CSF, these areas form the ventricular system. There are four ventricles present, two lateral, and the third and the fourth. The majority of CSF is formed within the ventricular system by the choroid plexus, a convoluted vascular structure that resembles a cauliflower protruding from the walls of the ventricles in various areas. The majority of the choroid plexus lie within the two lateral ventricles, from where the CSF flows into the third ventricle between them via the foramen of Monroe. From the third ventricle, CSF travels through the Sylvian aqueduct into the fourth ventricle, located in front of the cerebellum at the level of the pons. The fourth ventricle has three holes or foramen (the single foramen of Magendie in the midline and the two foramina of Luschka laterally) from which the CSF exits the brain into the subarachnoid space. Any blockage of the CSF flow, from either a mass lesion or clotting blood from a subarachnoid hemorrhage, will cause noncommunicating

hydrocephalus. This condition occurs as the production of CSF occurs at a relatively constant rate 0.3 to 0.4 cc/min., irrespective of the pressures and volume of CSF within the CNS. Noncommunicating hydrocephalus is evident on the CT scan with dilation of the ventricles and subsequent compression and thinning of the brain from the increased internal pressure. The CSF flow around the brain provides mechanical as well as nutritional support, and is eventually reabsorbed at the vertex through the Pachioni granulations on the sagittal sinus, the large venous structure at the vertex of the brain.

2.12 Vascular Supply

The brain is supplied by two main arterial systems, the internal carotid artery anteriorly and the vertebrobasilar artery posteriorly. The common carotid artery arises from the aorta and bifurcates or divides into the external and internal carotid arteries in the neck. The external carotid artery supplies the majority of the face and scalp while the internal carotid artery proceeds to the region under the optic chiasm where it forms an anastomotic loop with the basilar artery known as the Circle of Willis (Figure 10). The two vertebral arteries course up to the brain posteriorly through the cervical spine and join to form the basilar artery at the level of the pons. The basilar artery then continues upward to form the posterior aspect of the Circle of Willis. Three main pairs of cerebral arteries develop from the Circle of Willis: anterior, middle and posterior cerebral. Although the Circle of Willis provides an anastomotic network to provide a continuous blood supply in the event of obstruction of any of the feeding vessels, the internal carotid supplies the majority of the anterior and middle cerebral arteries, while the basilar artery provides the bulk of the posterior cerebral artery's flow. The anterior cerebral artery supplies the bulk of the medial aspect of the cerebral hemispheres while the middle cerebral artery supplies the majority of the lateral aspect of the hemispheres. The posterior cerebral artery then supplies the occipital portions of the brain and surrounding vicinity not covered by the other two systems. The rich network of blood vessels then run off into large venous lakes known as sinuses. These sinuses are formed partially within the layers of the dura and proceed to drain into the jugular veins to return to the heart via the superior vena cava (Figure 11).

3. Developmental Anatomy of the Brain

Unlike the static anatomy of the adult head, the head anatomy of the child is still in development and various aspects will vary with age. Although general features are present, the basic underlying bony characteristics do not develop until the age of two in most cases, and completion of growth does not occur until the second decade of life. To better understand the head and neck anatomy of the child, it may help to begin with the initial development at the embryonic stages. Initially after conception, the clump of rapidly dividing cells begin to resemble a more organized pattern forming the embryo. The cells of the human embryo are categorized into layers. These are the ectoderm (outer), mesoderm (middle) and endoderm (inner), named by the location of the cell layers. Along the ectoderm, a specialized region of cells form the neural plate from where the structures of the nervous system are formed by cellular division. This process of growth is termed neural induction. As the cells along the outermost edge proliferate more rapidly, it creates an indentation or "groove" along the midline known as the neural groove. This process continues, with the margins growing up and around to form the neural tube, with closure initially at the area of the neck, and proceeding in both the rostral (toward the head) and caudal (towards the tail) directions. From the neural tube, the various components of the central nervous system will develop. Failure of closure of the neural tube will produce a plethora of defects, an example of which is spina bifida, if the caudal portion fails to close properly. The extent of the closure defect will determine the developmental severity, ranging from spina bifida occulta to myelomeningocele. Once closed, the neural tube represents all of the components of the nervous system, with the rostral portion forming the cerebral hemispheres and brainstem, and the caudal portion into the spinal cord. From the mesodermal layer comes the formation of the skeletal structures that surround and protect the nervous system. Cells from this middle layer will develop into

specialized regions and form paired, block-like masses known as somites. These regions are arranged around the neural tube in a symmetric pattern and develop into the vertebral column and segmental musculature. These events then form the basic blueprint of the human skeleton and nervous system, from which growth in utero will proceed until birth.

4. Neonatal and Pediatric Anatomy of the Skull

The properties of the newborn skull are quite unlike the adult skull biomechanically as well as morphologically. The skull is more of a viscoelastic nature than the rigid adult skull to allow for the accommodation of growth. Although skull fractures occur in traumatic head injuries in children, they have a lower incidence than the adult population and many authors have reported the presence of extra-axial hematomas without a skull fracture. These factors may highlight the point of increased elasticity in children's skulls. Although underdeveloped bone plates are present, the pliability of the infant skull arises from the large unfused sutures and fontanelles. Growth of the skull is especially rapid within the first two years of life, and will reach 90 percent of its adult volume by the age of ten years. Morphologically, the neurocranium surrounding the brain is significantly larger than the face with ratios between 3:1 to 4:1. Although adult features of the skull will develop by two years of age, the neurocranium to face ratio will continue to decrease reaching 2:1 to 2.5:1 by the age of six. Teratogenic effects that hinder brain growth will cause a smaller neurocranium to face ratio, while increased intracranial volume such as with hydrocephalus will increase this ratio. At birth, the cranial vault has developed into plates of bones with the main areas of growth located at the fibrous joints between them termed synchondrosis. The linear regions between the plates are termed sutures, while the larger patches of connective tissue are known as fontanelles. The central layer of the sutures forms the bulk of the connective tissue, with parallel regions surrounding the periphery. Growth then occurs mainly at the central region and along the surface of the bony plates. This process of bony development is by intramembranous ossification, where the connective tissue matrix is replaced by bony tissue. Natural variations may occur in the regions surrounding the larger sutures, as smaller convoluted sutures may form bony islands called wormian bones.

4.1 Sutures

The frontal bone is divided down the midline by the metopic suture, and outlined posteriorly by the coronal suture. The parietal bones are two symmetric plates covering the lateral aspect of the skull and are separated by the sagittal suture in the midline. Anteriorly, they are abutted by the coronal suture, posteriorly by the lambdoidal suture, and inferiorly by the squamosal suture. The occipital bone or more specifically, the squamous portion of the occipital bone, is formed by the lambdoidal suture that comes down symmetrically from the lambdoid, and merges into the posterior-lateral fontanelle. The mendosal suture, or "false" suture may extend posteriorly into the occipital bone from the posterior-lateral fontanelle, but will only proceed partially and not connect with any other suture lines. The temporal bones as well as the exoccipital portion of the occipital bone then reside inferiorly to the squamousal suture. The sutures will continue to diminish in size with age, but closure will occur at different intervals. The metopic suture generally closes at three years of age, and the mendosal suture by two years of age. However, these may be present in adults in up to 10 percent of the population. Complete fusion of the bony plates with obliteration of the sutures occurs at around 20 years of age, when the skull has reached its definitive size.

4.2 Fontanelles

The "soft spots" or fontanelles on a newborn's head, are larger patches of fibrous tissue that are located between the bony plates of the skull. There are six major or constant fontanelles, with variable smaller or accessory fontanelles usually located along the sagittal suture. The six

major fontanelles are the anterior, posterior, and the paired anterior-lateral and posterior-lateral. The anterior fontanelle is located along the bregma or the intersection of the coronal, sagittal and metopic sutures. The posterior fontanelle is located along the lambda, which is the intersection of the sagittal and lambdoidal sutures. The anterior-lateral fontanelles are located along the pterion, which is the intersection of the coronal and squamousal suture. The posterior-lateral fontanelles are then along the asterion or the intersection of the lambdoidal and squamosal sutures. Closure of the fontanelles occurs at various times, similar to the sutures. The anterior fontanelle may be reduced to a fingertip size within the second year of life, while the posterior fontanelle may have already closed by the time of birth.

References

[1] Alexander, Proctor. *Advanced Trauma Life Support Course for Physicians.* American College of Surgeons, 1993.

[2] Ford, McLaurin. Mechanisms of Extradural Hematomas. *J Neurosurgery* 1963:20: 760-769.

[3] Galbraith. Age-distribution of extradural hemorrhage without skull fracture. *Lancet* 1973:1: 1217-1218.

[4] Mealy. Acute extradural hematoma without demonstrable skull fractures. *J Neurosurgery* 1960:17: 27-34.

[5] Cambell, Cohen. Epidural hemorrhage and the skull of children. *Surg Gynecol Obstet* 1951:92: 257-280.

[6] Carpenter. *Core Text of Neuroanatomy.* Williams & Wilkins, Baltimore, 1991.

[7] Dorland. *Dorland's Illustrated Medical Dictionary*, 26th Edition. WB Saunders, Philadelphia, 1985.

[8] Martin. *Neuroanatomy: Text and Atlas.* Elsevier, New York, 1988.

[9] Kandel, Schwartz. *Principles of Neural Science.* Elsevier, New York, 1985.

[10] Netter. *Atlas of Human Anatomy.* Ciba-Geigy, New Jersey, 1989.

[11] Cheek. *Pediatric Neurosurgery: Surgery of the Developing Nervous System*, 3rd Edition. WB Saunders, Philadelphia, 1994.

[12] Touloukian. *Pediatric Trauma*, 2nd Edition. Mosby Year Book, Philadelphia, 1990.

[13] Barkin. *Pediatric Emergency Medicine: Concepts and Clinical Practice.* Mosby Year Book, Philadelphia, 1992.

[14] Moroteaux, Faure, Fessard, et al. *Bone Diseases of Children.* JB Lippincott, Philadelphia, 1979.

[15] Silverman, Kuhn, Berdon, et al. *Caffey's Pediatric X-Ray Diagnosis: An Integrated Imaging Approach.* Mosby, Philadelphia, 1993.

[16] Loftus (ed). *Neurosurgical Emergencies*, Volume I. AANS, Chicago, 1994.

Figure Captions

Figure 1: Side, front and bottom views of the adult skull.

Figure 2: Frontal bone.

Figure 3: Temporalis muscle insertion.

Figure 4: Parietal bone.

Figure 5: Occipital bone.

Figure 6: Ethmoid bone.

Figure 7: Cerebral cortex.

Figure 8: Medial aspect of the brain.

Figure 9: Brainstem (front and side views)

Figure 10: Circle of Willis.

Figure 11: Venous sinuses.

Figure 1

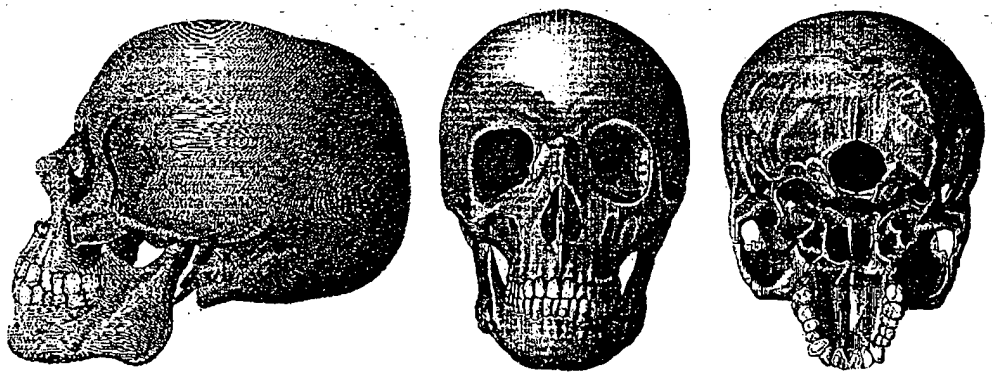

Figure 2

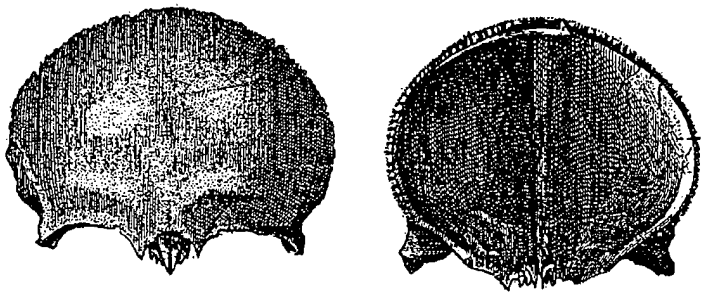

Figure 3

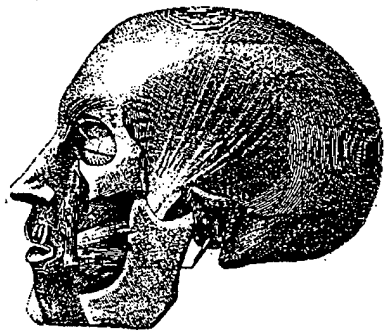

Figure 4

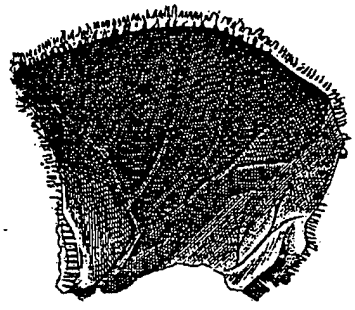

Figure 5

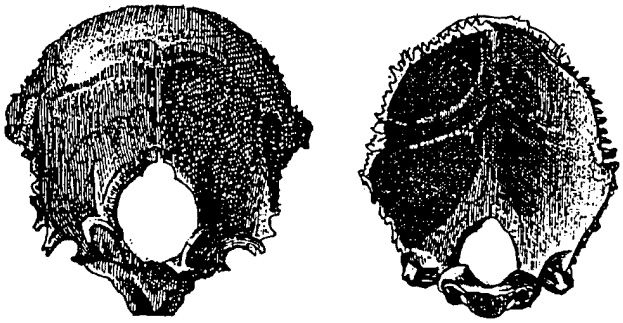

Figure 6

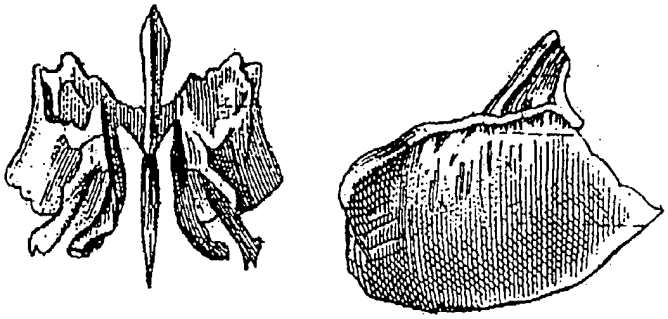

Figure 7

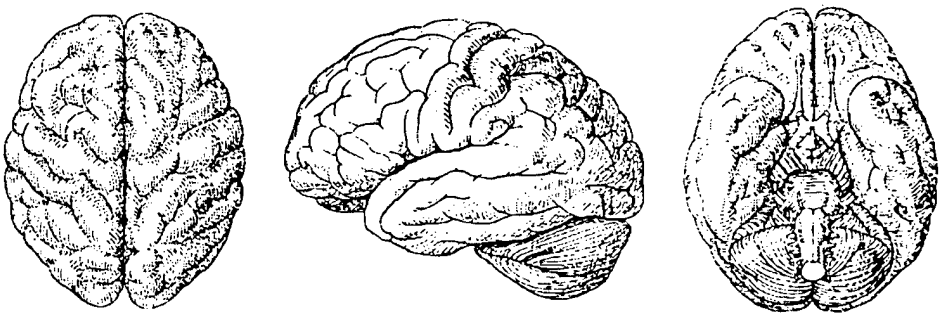

Figure 8

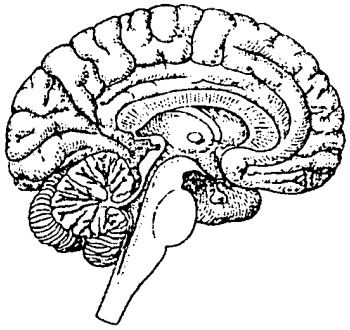

Figure 9

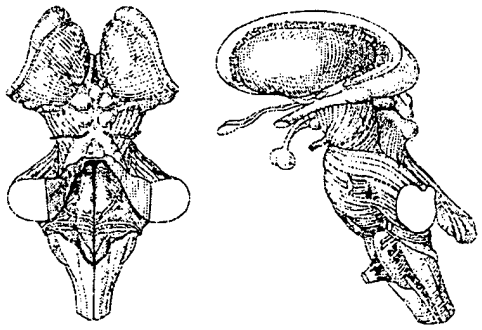

Figure 10

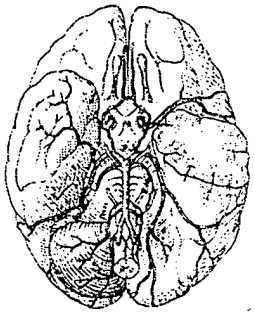

Figure 11

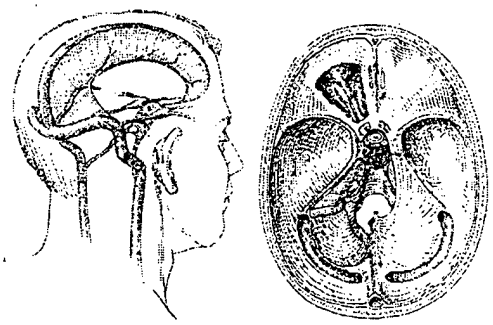

ADULT AND CHILD NECK ANATOMY

Christopher E. Wolfla

Abstract

The purpose of this chapter is two-fold. First, basic anatomy of the human neck is presented. Second, major differences between the adult neck and child neck are discussed. A comprehensive description of human neck anatomy is beyond the scope of this chapter. The reader is therefore, referred to any number of sources for information not found herein. Emphasis is given to the load-bearing structures of the neck.

1. Anatomy of the Adult Neck

The anatomy of the neck may be divided into two major compartments. The anterior compartment which is encircled by the pretracheal fascia contains the trachea, esophagus and related structures. The posterior compartment which is encircled by the prevertebral fascia contains the spinal cord, vertebra, paraspinous muscles and related structures [1] (Figure 1). Both compartments are encircled with a dual layer of investing fascia which separates to encompass the sternocleidomastoid and trapezius muscles.

1.1 Pharynx, Larynx, Trachea, Esophagus

In the most dorsal portion of the oral cavity lies the pharynx (Figure 2). The cranial portion of the pharynx is divided into the oropharynx and nasopharynx by the soft palate. The anterior arch of C1 is palpable just above the soft palate in the nasopharynx in most individuals. Caudally, the laryngeal pharynx lies dorsal to the larynx and continues on as the esophagus. The entrance to the larynx lies ventral to the laryngeal pharynx and is protected by the epiglottis. The caudal continuation of the larynx is the trachea. The hyoid bone lies at the level of C3, the thyroid cartilage lies at the level of the C4-C5 disc, and the cricothyroid membrane lies at the level of C6 [2]. The thyroid gland lies just anterior to the larynx at the level of C6 [1].

1.2 Arteries of the Neck

Carotid Artery: These arteries arise bilaterally in the chest from the aorta and its branches. The right common carotid artery arises from the innominate artery, the first major branch of the aorta. The left common carotid artery generally arises as the second major branch of the aorta. In approximately 10 percent of cases, the left common carotid artery arises from the innominate artery. The carotid arteries ascend through the neck within the carotid sheath, which also contains the vagus nerve and internal jugular vein. At approximately the C4 level, the carotid bifurcates into two major branches, the internal and external carotid arteries (Figure 3). This bifurcation is higher on the left side in 50 percent of cases and higher on the right in 22 percent. The external carotid artery gives off numerous branches, and supplies the majority of the extracranial structures of the head. In addition, the middle meningeal artery supplies the intracranial dura mater. The occipital artery, the fifth branch of the external carotid artery, has important anastamotic connections with the deep cervical artery, a branch of the costo-cervical trunk. The internal carotid artery ascends without branching to the skull base. Initially, the internal carotid artery lies lateral to the external, though at higher levels it moves to a more medial location. It terminates at the circle of Willis where it bifurcates into the anterior and middle cerebral arteries. There are a limited number of potential anastamotic sites between the internal and external carotids [3].

Vertebral Artery: These arteries arise bilaterally from the subclavian arteries in the chest. They then ascend anterior to the longus coli muscles to the anterior surface of the C7 transverse processes. The vertebral arteries, as well as a plexus of veins, typically then enter the C6 transverse foramina and ascend through subsequent adjacent transverse foramina. As the arteries ascend they give off multiple lateral spinal and muscular branches. The lateral spinal branches provide blood supply to portions of the spinal cord and the vertebral bodies. The muscular branches are important potential sources of collateral blood flow in the event of a proximal occlusion of the vertebral artery. At the level of the C2 transverse foramen, the vertebral arteries take an abrupt lateral turn before looping into the transverse foramen of C1. At the level of the C1 transverse foramen, the vertebral arteries make another abrupt posterior and medial turn before traversing the vertebral groove of C1 to pierce the dura matter at the cervicomedullary junction. The vertebral arteries terminate by uniting to form the basilar artery intracranially. As the vertebral arteries ascend, they become progressively closer. The distance between the vertebral arteries decreases from a mean of 35.16 mm at C7 to 26.67 mm at C3. The diameter of the vertebral arteries is 1.5 mm to 2.0 mm smaller than the transverse foramina. Occasionally, a transverse process may have duplicate transverse foramina. In this instance, the vertebral artery is usually transmitted by the more medial foramen [4].

1.3 Veins of the Neck

The major veins draining the head and neck are the internal jugular, vertebral and external jugular veins (Figure 4). Unlike the large veins of the extremities, none are valved. The internal jugular veins are the continuations of the sigmoid sinuses bilaterally. Frequently, the right internal jugular vein and sigmoid sinus preferentially drain the superior sagittal sinus, while the left internal

jugular vein and sigmoid sinus preferentially drain the straight sinus [5]. The scalp is drained by the deep cervical vein, which communicates with the superior sagittal sinus via emissary veins and with the sigmoid sinus via the occipital veins. The external jugular vein, along with the common facial vein, drains the cavernous sinus and pterygoid venous plexi. Rich anastamoses exist between the intracranial and extracranial venous systems. These provide multiple alternative drainage pathways in the event of occlusion or surgical ligation of any of the major neck veins. These anastamoses unfortunately, also provide a nearly unimpeded path for the spread of infection into the intracranial space.

1.4 Spinal Cord

The spinal cord begins at the cervicomedullary junction. Its origin is marked externally by the appearance of the first cervical rootlets. The spinal cord is surrounded by the pia mater, arachnoid and the dura mater. The pia mater is closely applied to the outer surface of the spinal cord. The arachnoid is a finely trabeculated layer between the pia and dura mater. Cerebrospinal fluid is normally present between the arachnoid and pia mater. The dura mater is the outermost covering of the spinal cord. It is thicker than the pia mater or arachnoid and is continuous with the intracranial dura mater. Between the dura mater and the bony walls of the neural canal is the epidural space which contains numerous epidural veins as well as epidural fat.

The mean cross-sectional area of the spinal cord at the C2 level is 56.0 square mm. This value increases to 58.3 square mm at C6, the region of the cervical enlargement. Below C6, the cross-sectional area of the spinal cord falls off rapidly, reaching a value of 42.6 square mm at the T1 level. As one moves caudally, the cervical spinal cord becomes progressively more flattened in the anteroposterior direction. The proportion of spinal grey matter is highest in the region of the cervical enlargement, ranging from 18.3 to 20.5 percent (6).

The ascending and descending white matter tracts of the spinal cord are arranged into bundles, most subserving relatively discreet functions. In general, the dorsal white matter tracts are ascending and convey impulses concerned with light touch and proprioception. The anterior and lateral spinothalamic tracts are also ascending and carry impulses concerned with pain and temperature sensation. The anterior, anterolateral and lateral corticospinal tracts are descending and carry impulses concerned with voluntary, discrete and skilled movements [7].

Arising from the anterior and posterior surfaces of the spinal cord, the anterior and posterior rootlets combine to form the ventral and dorsal roots of the spinal nerves at each level. In addition, from the C1 to the C5 level, a small number of rootlets emerge from the lateral surface of the spinal cord. These rootlets unite posterior to the dentate ligaments and ascend into the skull base to form the spinal portion of the spinal accessory nerve. From the C6 to C8 level, the mean number of anterior rootlets which combine to form a single ventral root ranges from 20.2 to 25.4. The mean number of posterior rootlets which combine to form a single dorsal root ranges from 9.0 to 12.7. The mean distance from the midline of the spinal cord to the anterior rootlet exit zone ranges from 1.53 mm to 1.75 mm, while the mean distance from the midline of the spinal cord to the posterior rootlet zone ranges from 3.2 mm to 4.0 mm. The clinical significance of this relationship is that a more medial disc herniation, not related to the neural foramen, may cause radicular symptoms due to compression of the anterior rootlets near the exit zone. The length of the rootlets from their exit zone to the neural foramen ranges from 4.8 mm to 21.2 mm for anterior rootlets, and from 3.7 mm to 19.8 mm for posterior rootlets [8].

The blood supply of the anterior two-thirds of the spinal cord is via the anterior spinal artery, while that of the posterior one-third of the spinal cord is via the paired posterior spinal arteries (Figure 5). The anterior spinal arteries originate intracranially as the last branches of the vertebral artery and then join to form a single descending branch. The posterior spinal arteries originate from the ipsilateral vertebral arteries. While there are numerous anastamoses between the posterior spinal arteries, there are few, if any, anastamoses between the anterior and posterior spinal arteries [9].

1.5 Spinal Nerves

In the region of the neural foramen the spinal rootlets combine to form the cervical nerve roots. In the lateral portion of the neural foramen, the sensory fibers, mostly derived from the posterior rootlets, synapse at the dorsal root ganglion. From there, the roots continue on to supply more distal structures. The first through fourth cervical roots combine to form the cervical plexus. The phrenic nerve, which supplies the diaphragm, is derived from the third, fourth and fifth cervical roots. The fifth through eighth cervical roots, as well as the first thoracic root, combine to form the brachial plexus. The brachial plexus continues on to supply the shoulder, arm and hand. The long thoracic nerve is formed from small branches, fifth, sixth and seventh cervical roots. This nerve supplies the serratus magus muscle. The long thoracic nerve is especially susceptible to injury, which results in "winging" of the scapula.

1.6 Cranial Nerves

A number of cranial nerves descend from the skull base to supply the neck. The seventh cranial nerve or facial nerve, in addition to supplying the muscles of facial expression, supplies the platysma, stylohyoid and digastric muscles of the neck. The ninth cranial nerve or glossopharyngeal, supplies the stylopharyngeus muscle and provides sensation to a portion of the pharyngeal wall. The glossopharyngeal nerve also supplies the carotid body, a chemosensitive organ located in the carotid bifurcation. The tenth cranial nerve or vagus nerve, travels with the carotid artery and internal jugular vein on its way to the chest and abdomen. As it descends, it gives off sensory branches to the lower pharynx and motor branches to the constrictors of the pharynx. In the chest, the vagus nerve gives off a large branch, termed the recurrent laryngeal nerve, which ascends back into the neck to supply the inferior pharyngeal constrictor and the majority of the muscles to the larynx. The eleventh cranial nerve or spinal accessory nerve, supplies the sternocleidomastoid and trapezius muscles. Finally, the twelfth cranial nerve or hypoglossal nerve, supplies all of the intrinsic and the majority of the extrinsic muscles of the tongue.

2. Vertebra

The neck contains seven cervical vertebrae (Figure 6). The first (atlas), second (axis) and seventh cervical vertebrae are significantly different in structure than the others. The atlas articulates with the skull base via the occipital condyles. The seventh cervical vertebra articulates with the first thoracic vertebra and has some features of both cervical and thoracic vertebrae. Movement of the neck is not evenly distributed amongst the cervical vertebra. Fifty percent of neck flexion and extension occurs between the occiput and C1, with remainder distributed throughout the remainder of the cervical spine. Of this remaining flexion and extension, the C5-C6 level is responsible for slightly more motion than the other levels, which may account for its frequent involvement in cervical degenerative disease. Likewise, nearly 50 percent of axial rotation occurs at the C1-C2 articulation, with the remainder nearly evenly distributed amongst the remaining levels. All other movements of the cervical spine are complex movements associated with some component of flexion/extension and axial rotation [2].

Each cervical vertebra is composed of a number of parts (Figure 7). The most dorsal structure is the spinous process which is readily palpable on the back of the neck. From C2 through C6, the mean spinous process length ranges from 28.5 mm (C5) to 34.2 mm (C6). The mean length of the C7 spinous process is 45.7 mm [10]. It is palpably larger than the upper cervical vertebra and is often referred to as the vertebra prominens.

The spinous process gives way to the lamina, the dorsal wall of the neural canal. The mean width of the neural canal ranges from 22.9 mm (C3) to 25.8 mm (C6), while the depth of the neural canal ranges from 15.2 mm (C7) to 21.0 mm (C2). For this reason, the cross-sectional area of the neural canal is greatest at C2 (374.5 square mm) and least at C7 (223.8 square mm) [10].

The laminae are contiguous with the lateral masses bilaterally (Figure 8). The lateral mass of the cervical spine is analogous to the pars interarticularis of the thoracic and lumbar spine in that it is the structure which joins the superior and inferior articular processes of the facet joints. The mean width of the lateral masses is 11.56 mm, while the mean height of the lateral masses is 14.49 mm. Ventral to the lateral masses course the vertebral artery and cervical nerve roots, in all but the upper outer quadrant [11].

Above and below the lateral masses are the paired facet joints. The facet joints are made up of one projection from each adjacent vertebral level. The superior facet process extends cranially from the lower vertebral level. The inferior facet process extends caudally from the vertebral level above and lies dorsal to the superior facet process. The height of the superior facet processes ranges from 10.2 mm (C6) to 18.0 mm (C2), while that of the inferior facet processes ranges from 10.8 mm (C5) to 13.9 mm (C7). The width of the superior facet processes ranges from 10.8 mm (C3) to 18.0 mm (C2). These dimensions result in subaxial facet surface areas ranging from 79.5 square mm (superior facet process of C6) to 107.0 square mm (superior facet process of C5). The mean distance between the centerline of the superior facet processes at each level ranges from 30.3 mm (C2) to 39.9 mm (C6). The mean distance between the centerline of the inferior facet processes at each level ranges from 33.6 mm (C7) to 40.5 mm (C5). Unlike the thoracic and lumbar facets, the cervical facets are oriented nearly coronally [12].

The dorsal structures are connected to the vertebral body ventrally by the pedicles. The pedicles range in length from 6.7 mm (C6) to 9.4 mm (C2). The width of the cervical pedicles ranges from 4.8 mm (C3) to 8.0 mm (C2). The pedicles are angled medially 39 (C2) to 48 (C4 and C5) degrees. Preliminary investigations indicate that screws placed into the cervical pedicles may have a significantly higher pull-out strength than screws placed into the lateral masses, by virtue of their longer effective length. Placement of these screws is technically demanding [13]. Above each pedicle exits one cervical nerve root through the neural foramen. The cervical neural foramen is bounded superiorly by the pedicle of the next vertebral level above, inferiorly by the pedicle of the adjacent vertebral level, anteriorly by the uncinate process of the adjacent vertebral level, and posteriorly by the superior facet process of the adjacent vertebral level. The mean height of the neural foramen ranges from 7.4 mm (C3-4, C4-C5) to 8.6 mm (C5-C6, C6-C7), while the anterior-posterior width of the neural foramen ranges from 4.5 mm (C3-C4) to 7.0 mm (C6-C7) [14]. The pedicle of C7 is unique in that it is associated with two cervical roots. The C7 root passes above the C7 pedicle, while the C8 root, which has no corresponding vertebra, passes below the C7 pedicle.

Projecting laterally from the vertebral bodies are the transverse processes. Cervical vertebrae have two distal projections, the anterior and posterior tubercles. The distance between the tips of the transverse processes, from C2-C6, ranges from 46.4 mm (C5) to 52.6 mm (C2). The transitional seventh cervical vertebra has slightly longer transverse processes, with a mean distance of 66.6 mm between the tips [10]. The transverse processes have holes, the transverse foramina, through which the vertebral arteries pass bilaterally. The medial wall of these foramina is relatively close to the lateral border of the vertebral body, with this distance ranging from 0.8 mm (C2-C3) to 1.6 mm (C4-C5). The distance between the medial walls of the transverse foramina at each level ranges from 26.02 mm (C4) to 31.52 mm (C7) [15].

The most ventral structures are the vertebral bodies. These bodies are roughly oval shaped masses with a slight flattening dorsally, where they make up the ventral wall of the neural canal. The size of the vertebral bodies increases as one moves lower in the cervical spine. The mean anterior vertebral body height ranges from 13.27 mm (C5) to 14.79 mm (C7), while the mean posterior vertebral body height ranges from 14.06 mm (C6) to 15.14 mm (C7). The anteroposterior diameter ("depth") of the vertebral bodies at the superior endplate increases from 15.9 mm at C3 to 17.63 mm at C7. The anteroposterior diameter of the vertebral bodies at the inferior endplate ranges from 16.67 mm at C3 to 18.07 mm at C6. All of the vertebral bodies therefore, become slightly deeper from the superior to the inferior surface, except for C7 [16].

On either side of the vertebral endplates are the uncovertebral joints or "Luschka joints." Not true synovial joints, they consist of small upturned projections on either side of the superior

endplates of C3 through C7. These projections, termed uncinate processes, articulate with similarly rounded regions on either side of the inferior endplates of C2 through C6. The mean height of the uncinate processes ranges from 5.8 (C4-C5) to 8.1 mm (C5-C6), while the mean width ranges from 5.3 (C4-C5) to 6.7 mm (C6-C7). The distance between the tip of the uncinate process and the vertebral body above ("width") the uncovertebral joint, ranges from 1.0 (C2-C3, C6-C7) to 1.5 mm (C4-C5). This distance increases from 3.3 (C6-C7) to 4.5 mm (C3-C4) with discectomy and intervertebral disc space distraction [15]. On the anterior surface of the vertebral bodies runs the paired, longitudinally oriented longus coli muscles. These muscles originate at C1 and extend to the upper thoracic spine. As these muscles descend, they gradually separate. The mean distance between the medial borders of these muscles increases from 4.5 at C2-C3 to 23.5 mm at C6-C7 [15].

Between the vertebral bodies are the intervertebral discs. The axial shape of the intervertebral discs roughly parallels the shape of the vertebral body endplates above and below. In the sagittal section, the discs frequently appear slightly wedge shaped because the anterior height is greater than the posterior height. The outer region of the disc is made up of the annulus fibrosis. The annulus fibrosis is composed of approximately 12 lamellae, whose fibers are tilted 60 to 70 degrees from the long axis of the spine. Adjacent lamellae have fibers oriented in opposite directions, creating a lattice. The annulus fibrosis is thinner dorsally, adjacent to the neural canal. The inner region of the intervertebral disc is made up of the nucleus pulposis. The nucleus pulposis is composed of a complex mixture of proteoglycans, collagen and water. The composition of the nucleus pulposis changes with aging, primarily due to loss of water. The endplates form the interface between the intervertebral discs and the vertebral bodies above and below. The endplates are composed of hyaline cartilage similar to that found in articular cartilage [17]. The mean width of the disc space ranges from 22.0 mm (C3-C4) to 28.7 mm (C2-C7), while the depth of the disc space ranges from 17.9 mm (C2-C3) to 20.8 mm (C6-C7). The undistracted mean disc space height ranges from 3.3 mm (C4-C5) to 4.5 mm (C5-C6). Distracted, the mean disc space height increases from a minimum of 8.5 mm at C2-C3 and C6-C7 to a maximum of 9.0 mm at C5-C6 [15].

C1: The first cervical vertebra or atlas, articulates with the cranial base above, via the occipital condyles and with the second cervical vertebra or axis below (Figure 9). The atlas is composed of an anterior and a posterior arch, paired lateral masses and transverse processes, and two broad pairs of articular processes. The atlas is unique in that it does not have a true vertebral body and is not associated with an intervertebral disc. Additionally, while the atlas does have a spinous process, it is usually very small and not palpable clinically (Figure 10). The mean exterior anteroposterior diameter of the atlas is 45.8 mm, while the mean height is 15.4 mm. The mean overall width, measured from the tips of the transverse processes, is 78.6 mm. As this width is significantly greater than that of the subaxial cervical vertebra, the transverse processes of the atlas constitute an important and readily palpable landmark for cranial base surgery. The anteroposterior diameter of the inside of the C1 ring is 31.7 mm, while the width of the neural canal is 32.2 mm [18]. The inner surface of the anterior arch has a unique additional articular surface which articulates with the dens or odontoid process of the axis. It is important to remember, when considering the anteroposterior diameter of the neural canal at the level of C1, that the dens occupies approximately one-third of this space. Anomalies of the posterior arch of the atlas are not uncommon [19].

C2: The second cervical vertebra or axis, articulates with the atlas above and the third cervical vertebra below (Figure 11). Many components of the lower half of the axis are similar to those of the subaxial cervical vertebra. A number of the relevant properties of these components have been discussed previously. The dominant feature of the axis is the dens or odontoid process. This structure projects cranially to articulate with the inner surface of the anterior arch of the atlas. The mean diameter of this articular surface is 15.5 mm. The mean height of the dens, measured from base to tip, is 23.3 mm, while the mean height measured from the inferior endplate of C2 to the tip of the dens is 39.9 mm. The upper portion of the dens is slightly larger than the base. The mean anteroposterior diameter of the dens is 11.2 mm in the upper portion and 10.8 mm in the

lower portion. The lateral diameter of the dens is 10.8 mm in the upper portion and 9.9 mm in the lower portion. The dens is angled posteriorly a mean of 9 degrees, though this angle is somewhat variable [20]. Of the remaining features of the axis, several merit additional discussion. The spinous process of the axis is broad, bifid and much larger than that of C3 through C6. It is readily palpable on the dorsal aspect of the neck. The superior articular surface of C2 is much larger than that of the subaxial cervical vertebra. It has a mean surface area of 211.3 square mm on the left, and 205.1 square mm on the right [12]. The inferior endplate of C2 is relatively small, with a mean width of 18.7 mm and a mean depth of 16.2 mm. The inferior endplate slopes forward with a mean inclination of 4.1 degrees [20].

C7: The seventh cervical vertebra is a transitional vertebra between the cervical and thoracic spine. Again, many of its relevant properties have already been discussed. The spinous process of C7, in addition to being much longer than the spinous processes of C3 through C6, is not usually bifid, making it an important surgical landmark. The transverse processes of C7, though longer than that of the other lower cervical vertebra, possess only a single distal tubercle. Additionally, the transverse foramina of C7 tend to be proportionally smaller, as they typically do not transmit the vertebral artery at this level.

3. Ligaments

The vertebrae are bound together and to the head by a number of ligaments. The dens is attached to the skull base in the midline by the apical ligament and laterally by the paired alar ligaments [9]. The alar ligaments limit axial rotation and side bending of the occipito-atlanto-axial complex [21]. The atlas is attached to the axis by the transverse ligament and the accessory atlantoaxial ligaments (Figure 12). The transverse ligament is the primary structure involved in keeping the dens closely applied to the posterior surface of the anterior arch of the atlas.

The vertebral bodies are joined together by the anterior and posterior longitudinal ligaments. The anterior longitudinal ligament extends from the clivus to the sacrum as a continuous band (Figure 13). It is wider in the region of the intervertebral discs, but thicker in the region of the vertebral bodies. The cranial-most portion of the anterior longitudinal ligament is termed the anterior atlanto-occipital membrane. The posterior longitudinal ligament originates on the inner surface of the clivus and also extends to the sacrum as a continuous band (Figure 14). The cranial-most portion of the posterior longitudinal ligament is termed the tectorial membrane. The posterior longitudinal ligament is wide over the disc spaces and quite narrow over the vertebral bodies.

The posterior elements (spinous processes, lamina and facets) are also joined together by a number of ligaments. The supraspinous and nuchal ligaments run longitudinally over the dorsal aspect of the cervical spinous processes as a single band. The intraspinous ligament joins adjacent pairs of spinous processes. The ligamentum flavum runs from the undersurface of the lamina above to the superior margin of the lamina below at each level. There is a small midline cleft in this ligament at each level. The ligamentum flavum functions to stabilize the spine in extension. It is highly susceptible to hypertrophy with degenerative conditions of the cervical spine. Finally, the facet joints possess typical synovial membranes and fibrous joint capsules. Though more lax than the capsules of the thoracic and lumbar spine, the facet joint capsules function to stabilize the spine in extension [9].

4. Differences Between the Child Neck and Adult Neck

4.1 Airway

The airway of the infant and small child differs significantly from that of the adult. The epiglottis is displaced cephalad and anteriorly in comparison with that of the adult. This, combined with the large size of the head relative to the neck, small mandibular size and large tongue, may

make endotracheal intubation extremely difficult. In children less than eight years of age, the trachea is smallest at the level of the cricoid cartilage [22]. This makes the airway of the young child particularly susceptible to subglottic stenosis after prolonged endotracheal intubation.

4.2 Proportional Length

The head and neck of the child are proportionally larger and heavier than those of the adult. The ratio of the length of the upper body segment (vertex to symphysis pubis) to the lower body segment (symphysis pubis to floor) decreases from approximately 1.7 at birth to approximately 1.0 during adulthood [23]. These differences predispose the child to flexion and extension injuries with sudden acceleration or deceleration.

4.3 Ossification

Vertebral bodies form from ossification of cartilaginous models originating from primitive mesenchymal tissue. Ossification does not take place uniformly throughout the vertebral body. Instead, it occurs at discreet sites termed ossific nuclei. In the subaxial cervical spine, there are three ossific nuclei at each vertebral level, one in the vertebral body and one in each neural arch. The atlas develops from only two ossific nuclei (one in each neural arch), as it does not have a true vertebral body. The axis is the most complicated of the cervical vertebra. It develops from five separate ossific nuclei, two in the dens, one in the vertebral body, and one in each neural arch. At birth, the lower cervical vertebra is usually composed of three nonfused, partially ossified components: body (or centrum) and neural arches. The atlas is usually composed of two components, neural arches. Prior to birth, the two ossific nuclei of the dens have usually ossified and fused. Therefore, at birth, the axis is usually composed of four components: dens, body (or centrum) and neural arches. The vertebra continues to ossify throughout childhood, sometimes developing secondary ossific nuclei. Ossification of the atlas is complete from six to nine years of age, the dens at twelve years of age, and the bodies and neural arches of C2 through C7 at 15 to 16 years of age [24].

4.4 Disc and Ligaments

The nucleus pulposus develops from remnants of the notocord that are pushed aside during formation of the vertebral bodies [24]. The proportion of water and proteoglycans in the child's disc is higher than that of the adult [17]. The cartilaginous endplates of the vertebral bodies have an indistinct and stronger interface with the nucleus pulposus than do adult endplates, making them less susceptible to separation [24]. The ligaments of the pediatric spine are more elastic than those of the adult, allowing considerable longitudinal stretching of the spinal column without fracture. In addition, the incomplete development of facet and uncovertebral joints makes the cervical spine more mobile and less able to withstand forces of flexion and rotation. In young children, the distance between the anterior surface of the dens and the posterior arch of the atlas may normally be as high as 3 mm to 5 mm. Twenty percent of children may have overriding of the anterior arch of the atlas on the dens in extension. Finally, as many as 45 percent of children may have nonpathologic subluxation ("pseudosubluxation") at C2-C3 [25].

References

[1] Anderson JE. *Grant's Atlas of Anatomy*. 8th Edition. Williams & Wilkins, Baltimore, 1983.

[2] Hoppenfield S. *Physical Examination of the Spine and Extremities*. Appleton and Lange, Norwalk, 1976: 105-132.

[3] Osborn AG. Introduction to Cerebral Angiography. Harper and Row, Philadelphia, 1980: 33-142.

[4] Heary RF, Albert TJ, Ludwig SC, Vaccaro AR, Wolansky LJ, Leddy TP, Schmidt RR. Surgical anatomy of the vertebral arteries. *Spine* 1996:21: 2074-2080.

[5] Carpenter MB. *Core Text of Neuroanaromy*. 4th Edition. Williams & Wilkins, Baltimore, 1991.
[6] Kameyama T, Hashizume Y, Ando T, Takahashi A. Morphometry of the normal cadaveric cervical spinal cord. *Spine* 1994:19: 2077-2081.
[7] Carpenter MB. *Core Text of Neuroanaromy*. 4th Edition. Williams & Wilkins, Baltimore, 1991: 83-114.
[8] Kubo Y, Waga S, Kojima T, Matsubara T, Kuga Y, Nakagawa Y. Microsurgical anatomy of the lower cervical spine and cord. *Neurosurgery* 1994:34: 895-902.
[9] Parke WW, Sherk HH. Normal adult anatomy. In: *The Cervical Spine*. Sherk HH, Dunn EJ, Eismont FJ, Fielding JW, Long DM, Ono K, Penning L, Raynor R(eds). JB Lippincott Company, Philadelphia, 1989: 11-32.
[10] Panjabi MM, Duranceau J, Goel V, Oxland T, Takata K. Cervical human vertebrae: Quantitative three-dimensional anatomy of the middle and lower regions. *Spine* 1991:6: 861-869.
[11] Pait TG, McAllister PV, Kaufman HK. Quadrant anatomy of the articular pillars (lateral cervical mass) of the cervical spine. *J Neurosurg* 1995:82: 1011-1014.
[12] Panjabi MM, Oxland T, Takata K, Goel V, Duranceau J, Krag M. Articular facets of the human spine: Quantitative three-dimensional anatomy. *Spine* 1993:18: 1298-1310.
[13] Jones EL, Heller JG, Silcox DH, Hutton WC. Cervical pedicle screws versus lateral mass screws: Anatomic feasibility and biomechanical comparison. *Spine* 1997:22: 977-982.
[14] Ebraheim NA, An HS, Xu R, Ahmad M, Yeasting RA. The quantitative anatomy of the cervical nerve root groove and the intervertebral foramen. *Spine* 1996:21: 1619-1623.
[15] Pait TG, Killefer JA, Arnautovic KI. Surgical anatomy of the anterior cervical spine: The disc space, vertebral artery, and associated bony structures. *Neurosurgery* 1996:39: 769-776.
[16] Seong-Hoon O, Perin NI, Cooper PR. Quantitative three-dimensional anatomy of the subaxial cervical spine: Implication for anterior spinal surgery. *Neurosurgery* 1996:38: 1139-1144.
[17] Hulkins DWL. Disc structure and function. In: *The Biology of the Intervertebral Disc*, Volume 1. Ghosh P (ed). CRC Press, Inc., Boca Raton, 1988: 1-38.
[18] Doherty BJ, Heggeness MH. The quantitative anatomy of the atlas. *Spine* 1994:19: 2497-2500.
[19] Anderson JE. *Grant's Atlas of Anatomy*. 8th Edition. Williams & Wilkins, Baltimore, 1983: 5(1)-5(50).
[20] Doherty BJ, Heggeness MH. Quantitative anatomy of the second cervical vertebra. *Spine* 1995:20: 513-517.
[21] Dvorak J, Panjabi MM. Functional anatomy of the alar ligaments. *Spine* 1987:22: 183-189.
[22] Hammer GB, Krane EJ. Perioperative care of the child with acute neurological disease. In: *Pediatric Neurosurgical Intensive Care*. Andrews BT, Hammer GB (eds). AANS, Park Ridge, 1997: 25-35.
[23] Needlman RD. Assessment of growth. In: Nelson Textbook of Pediatrics. Behrman RE, Kliegman RM, Arvin AM (eds). WB Saunders, Philadelphia, 1996: 63-67.
[24] Sherk HH, Parke WW. Developmental anatomy. In: *The Cervical Spine*. Sherk HH, Dunn EJ, Eismont FJ, Fielding JW, Long DM, Ono K, Penning L, Raynor R (eds). JB Lippincott Company, Philadelphia, 1989: 1-10.
[25] Menezes AH, Osenbach RK. Spinal cord injury. In: *Pediatric Neurosurgery*. Cheek WR, Marlin AE, McLone DG, Reigel DH, Walker ML (eds). WB Saunders, Philadelphia, 1994: 320-343.

Figure Captions

Figure 1: Cross-sectional anatomy of the neck below the level of the carotid bifurcation.

Figure 2: Sagittal section of the neck showing divisions of the pharynx.

Figure 3: Major arteries of the neck.

Figure 4: Veins of the head and neck.

Figure 5: Arterial supply of the spinal cord, showing the relationship between the anterior and posterior spinal arteries, anterior and posterior rootlet exit zones, lateral rootlet exit zone for the spinal roots of the spinal accessory nerve, and spinal grey matter.

Figure 6: Cervical vertebra, posterior lateral view.

Figure 7: Mid-cervical vertebra, from above.

Figure 8: Mid-cervical vertebra, from behind. The box marks the approximate location of the lateral mass. Note the upturned uncinate processes.

Figure 9: Atlas, from above.

Figure 10: Atlas, from behind. Note the width of the transverse processes (Compare with Figures 7 and 8).

Figure 11: Axis, from the side. Note the slope of the inferior endplate.

Figure 12: Atlas, axis, and atlantoaxial ligaments, from above. Note the thickness of the transverse ligament.

Figure 13: Anterior longitudinal ligament.

Figure 14: Mid-cervical vertebra, from above, showing the subaxial ligaments.

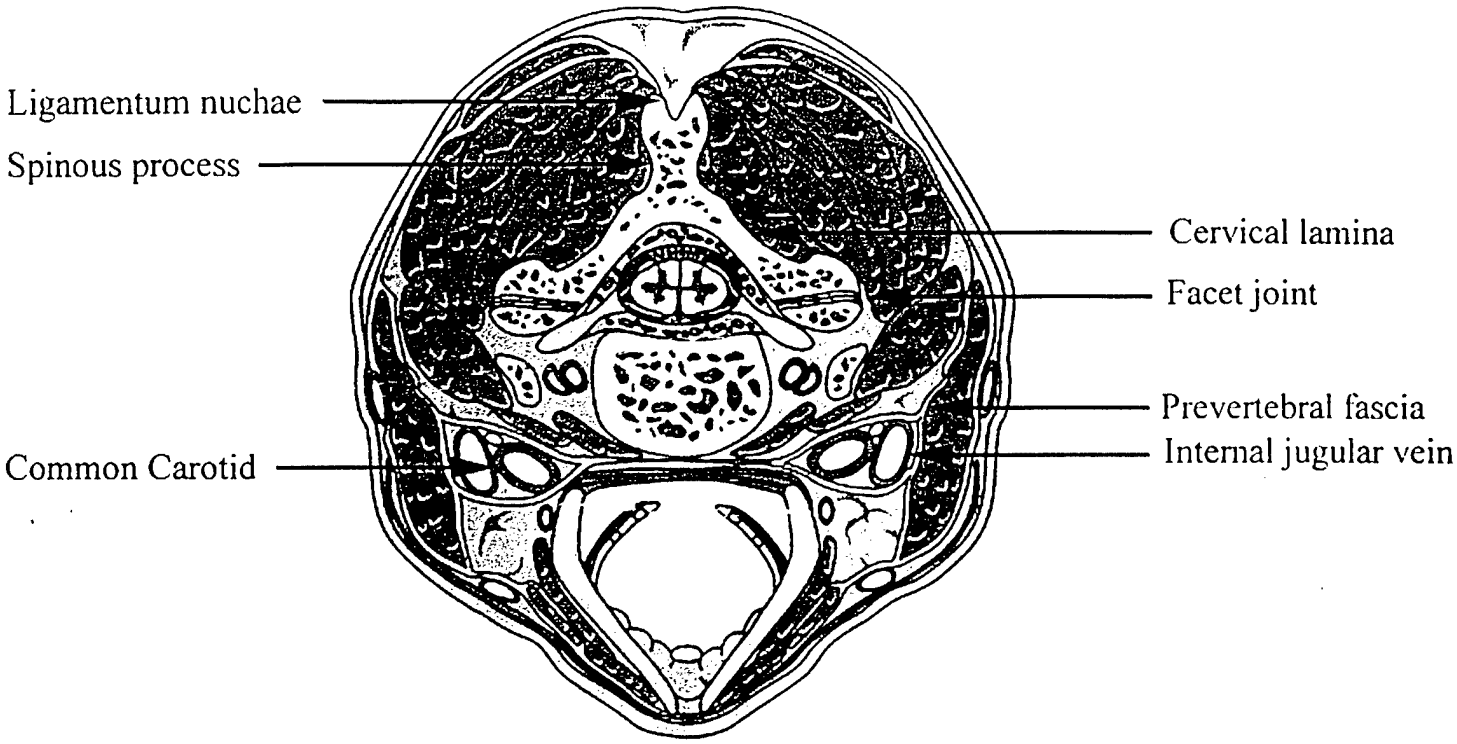
Ligamentum nuchae
Spinous process
Cervical lamina
Facet joint
Prevertebral fascia
Internal jugular vein
Common Carotid

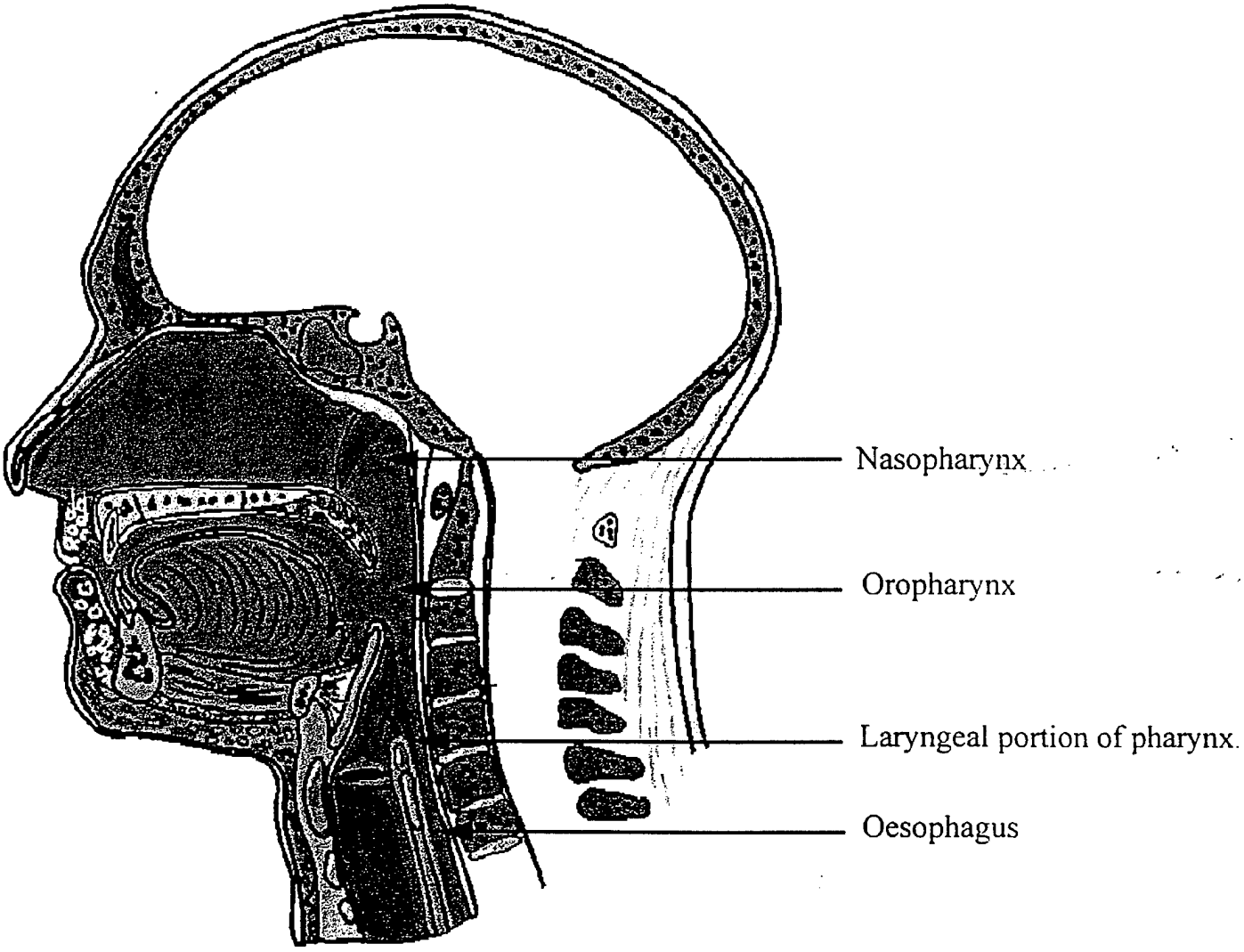
Nasopharynx
Oropharynx
Laryngeal portion of pharynx
Oesophagus

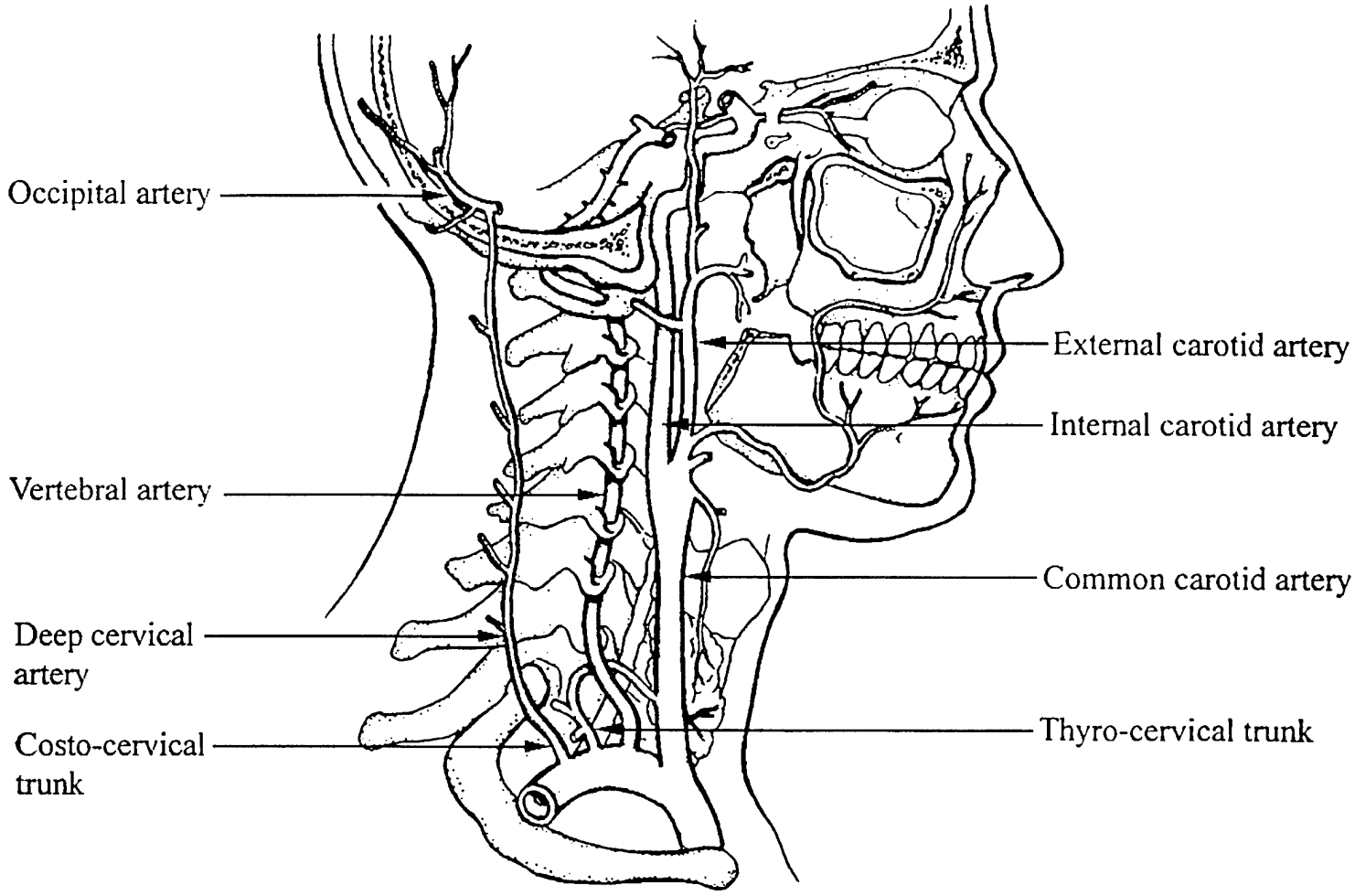
Occipital artery
External carotid artery
Internal carotid artery
Vertebral artery
Common carotid artery
Deep cervical artery
Thyro-cervical trunk
Costo-cervical trunk

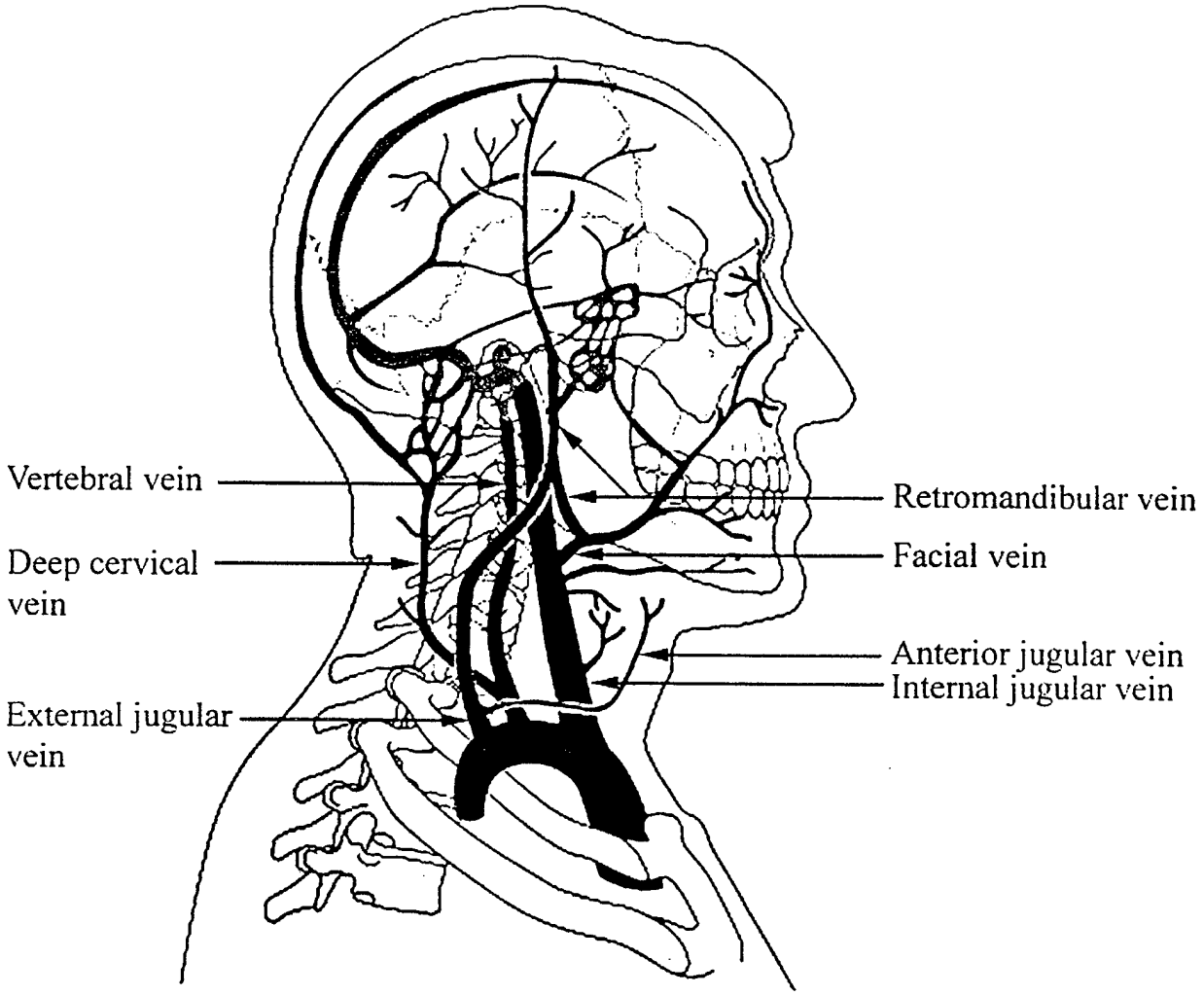
Vertebral vein
Deep cervical vein
External jugular vein
Retromandibular vein
Facial vein
Anterior jugular vein
Internal jugular vein

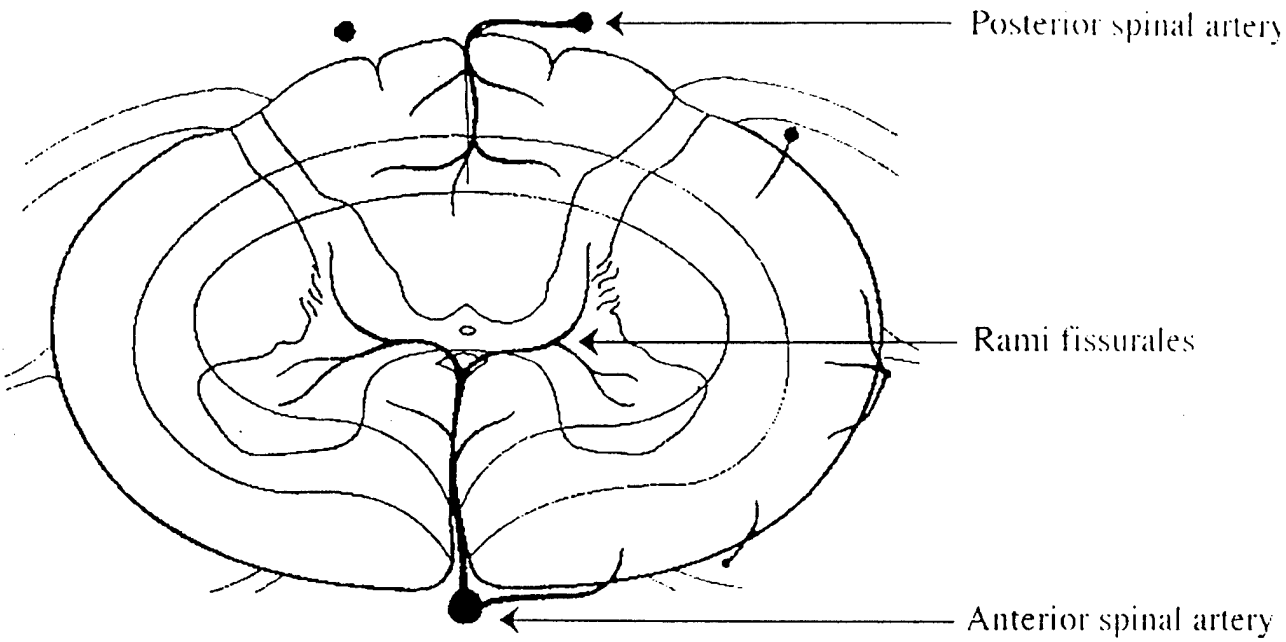
Posterior spinal artery
Rami fissurales
Anterior spinal artery

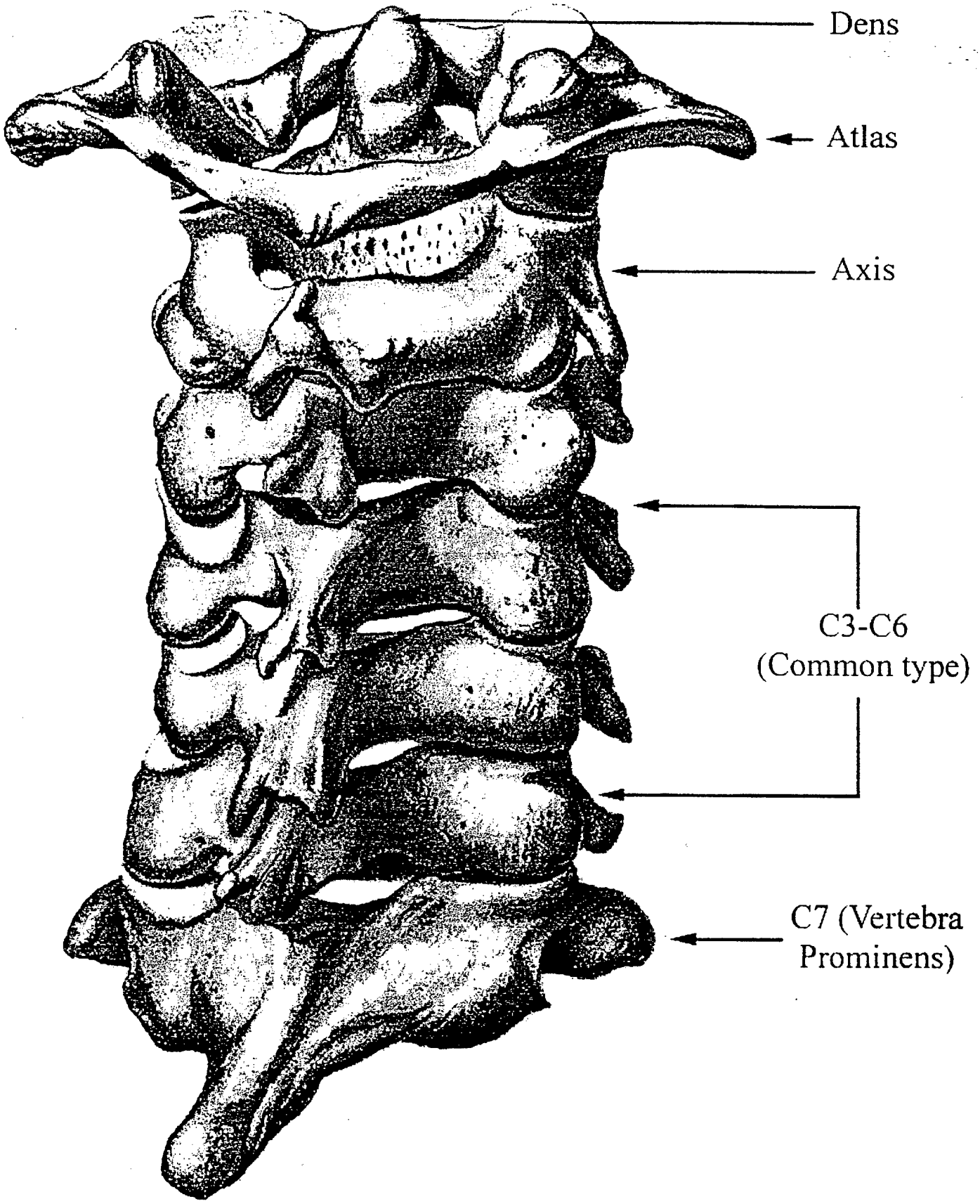
Dens
Atlas
Axis
C3-C6
(Common type)
C7 (Vertebra
Prominens)

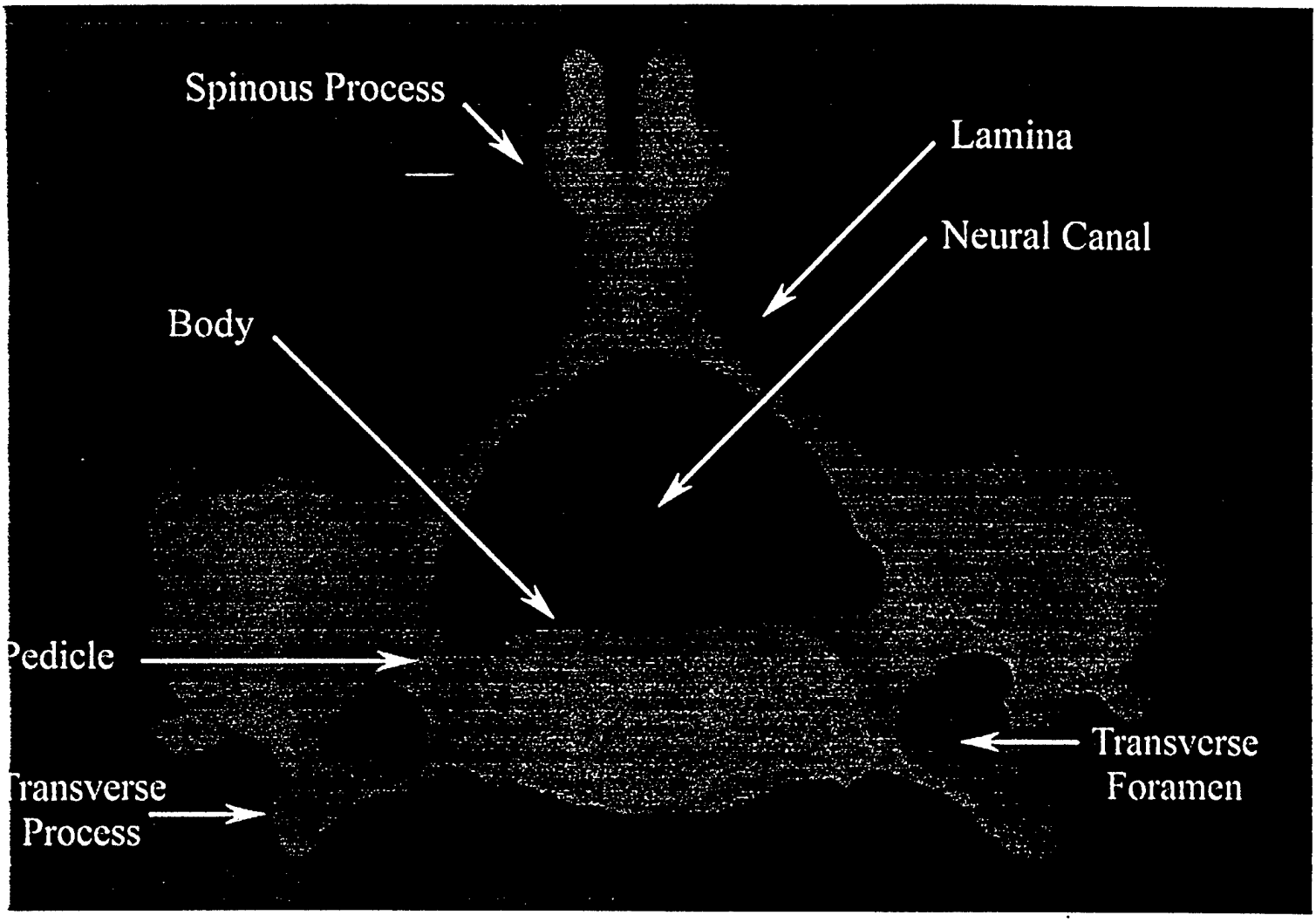
Spinous Process
Lamina
Neural Canal
Body
Pedicle
Transverse
Foramen
Transverse
Process

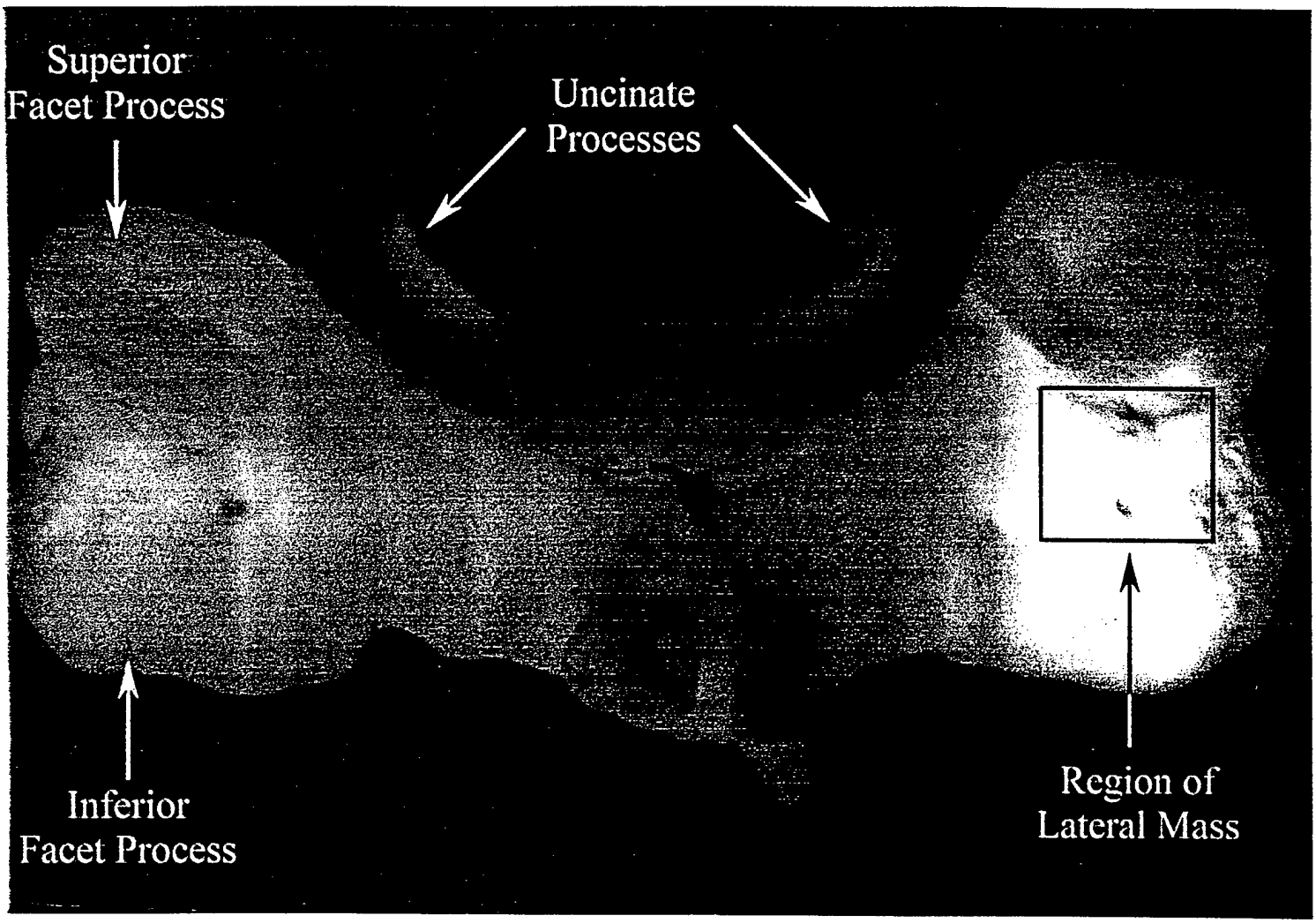
Superior
Facet Process
Uncinate
Processes
Inferior
Facet Process
Region of
Lateral Mass

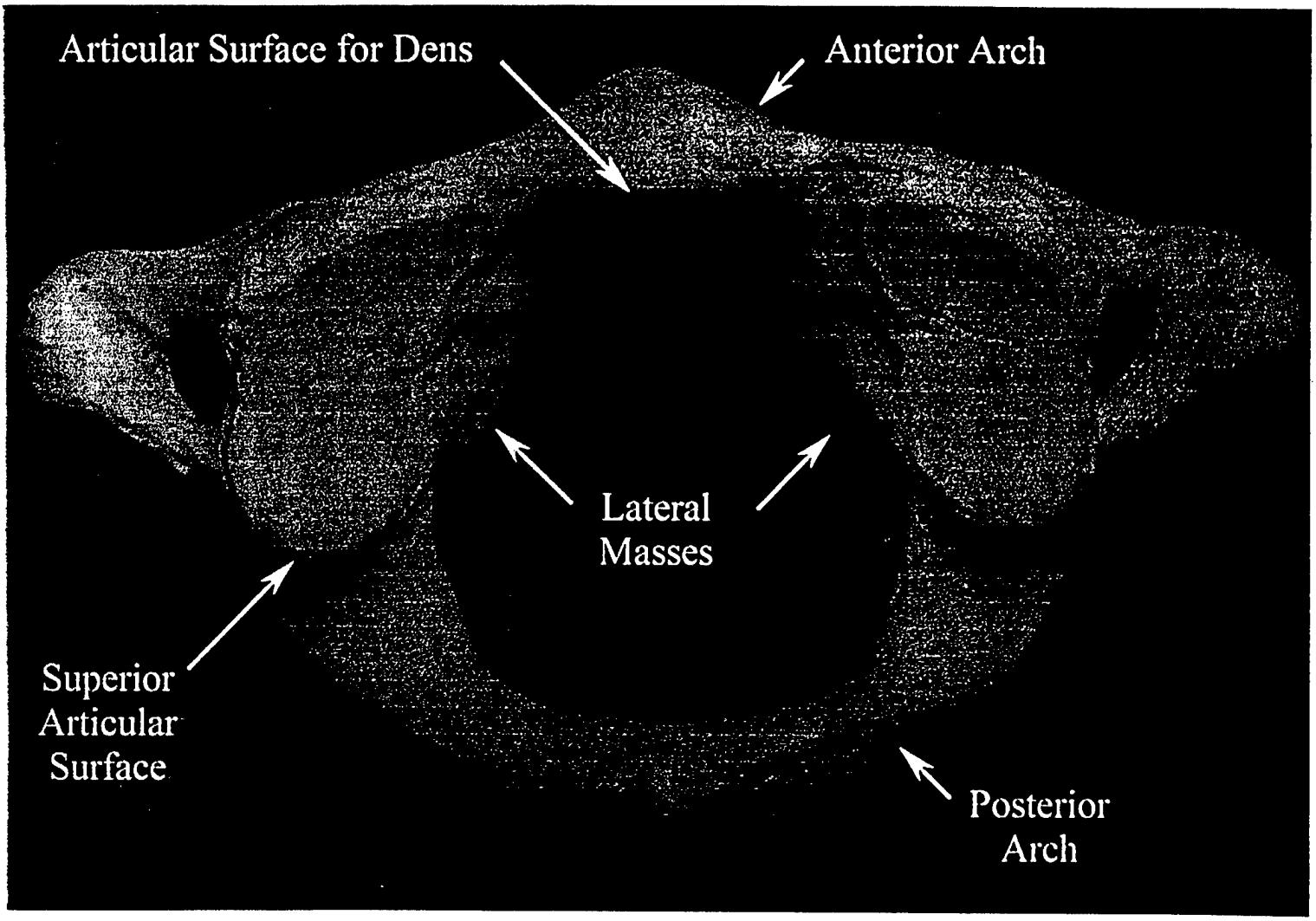
Articular Surface for Dens
Anterior Arch
Lateral Masses
Superior Articular Surface
Posterior Arch

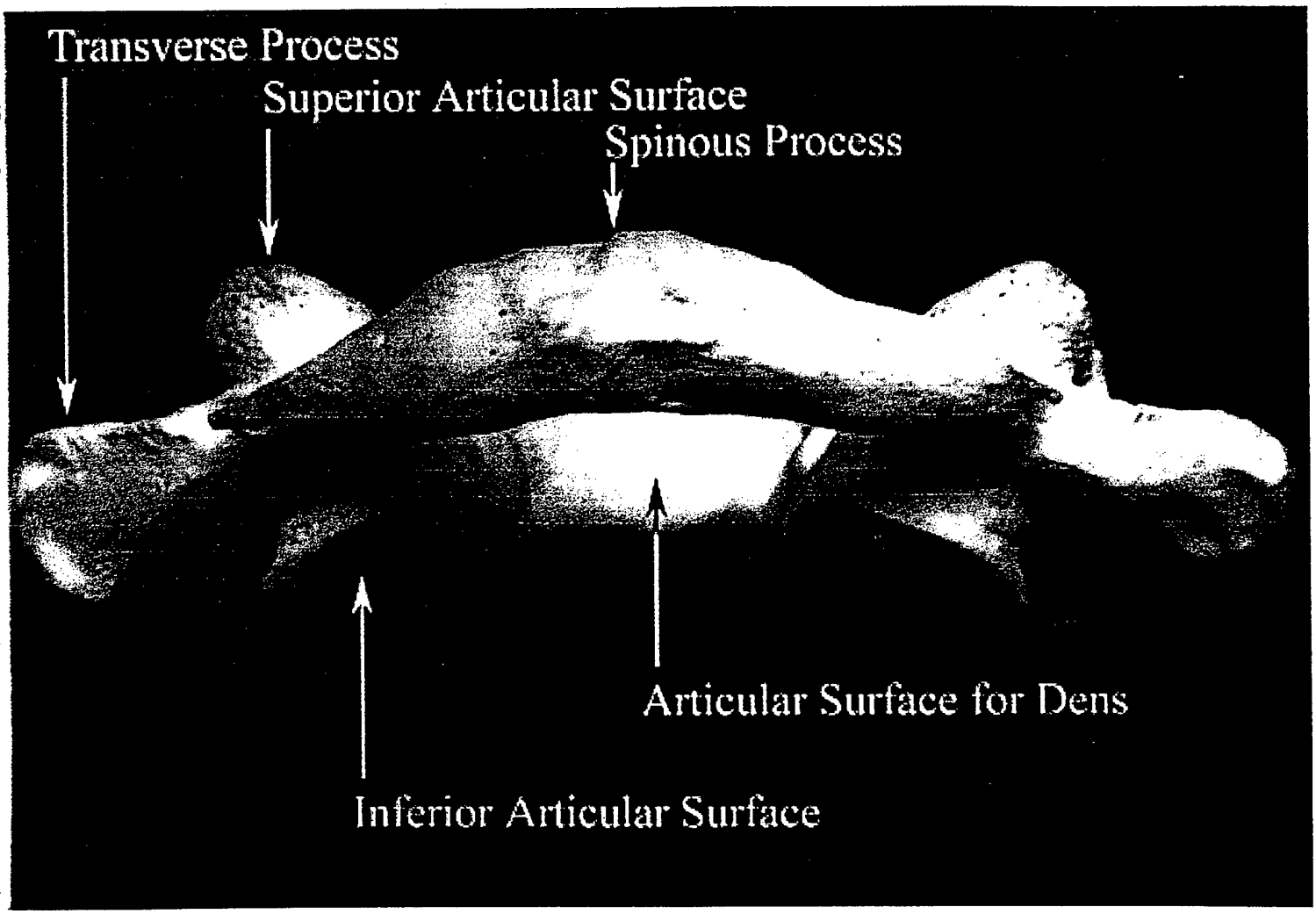
Transverse Process
Superior Articular Surface
Spinous Process
Articular Surface for Dens
Inferior Articular Surface

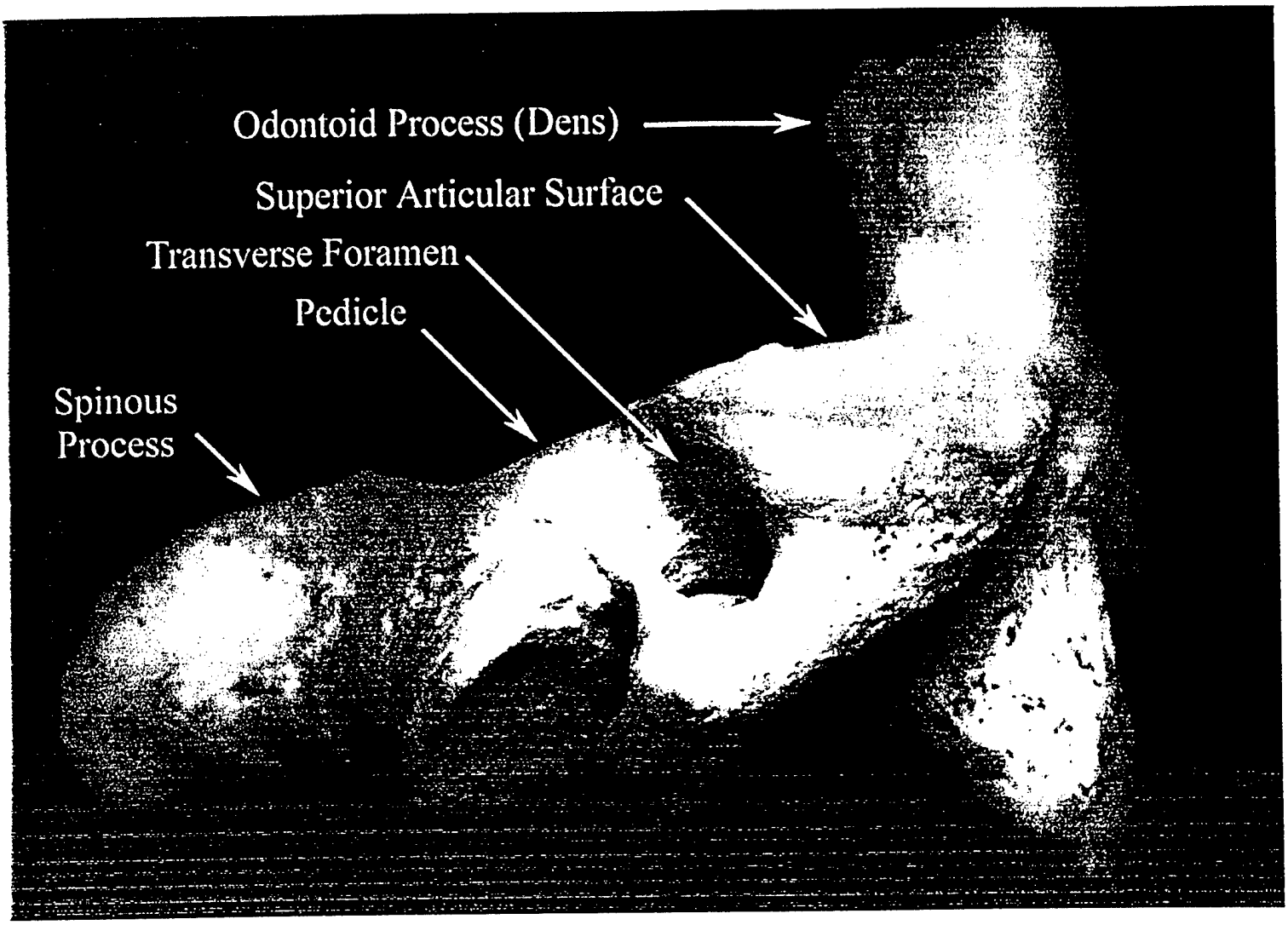
Odontoid Process (Dens)
Superior Articular Surface
Transverse Foramen
Pedicle
Spinous Process

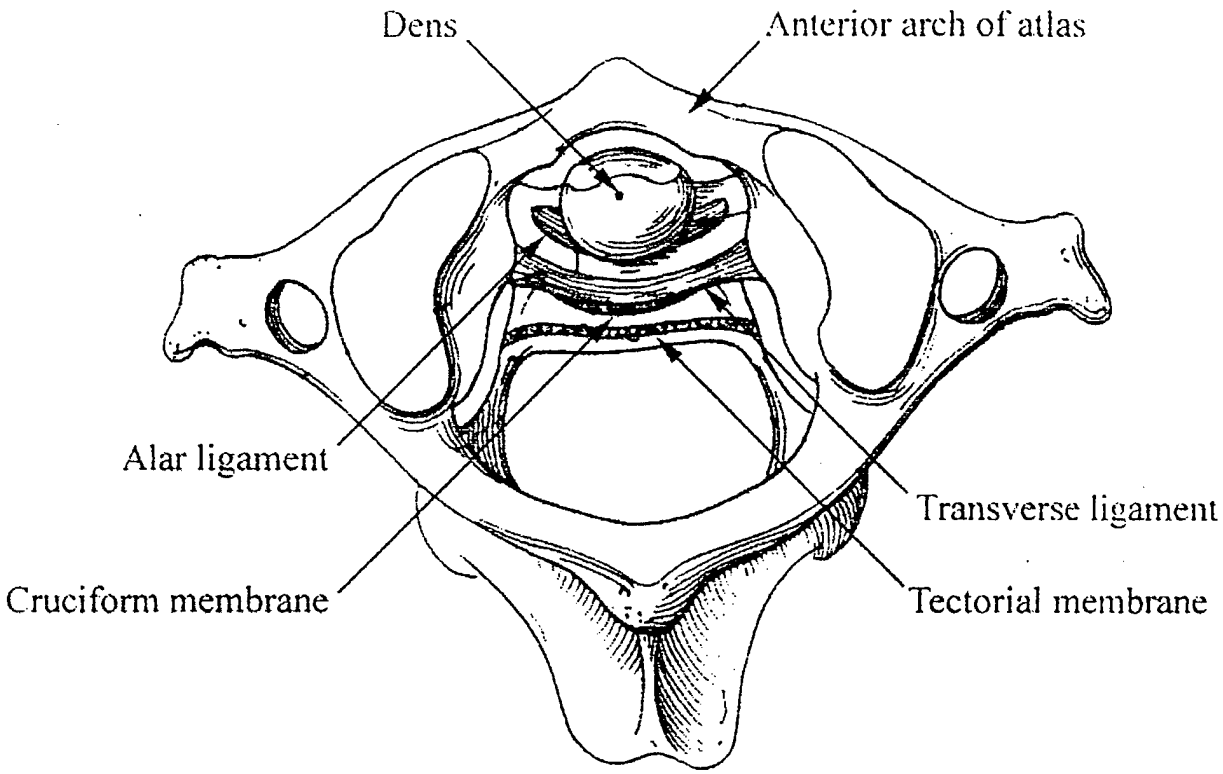
Dens
Anterior arch of atlas
Alar ligament
Transverse ligament
Cruciform membrane
Tectorial membrane

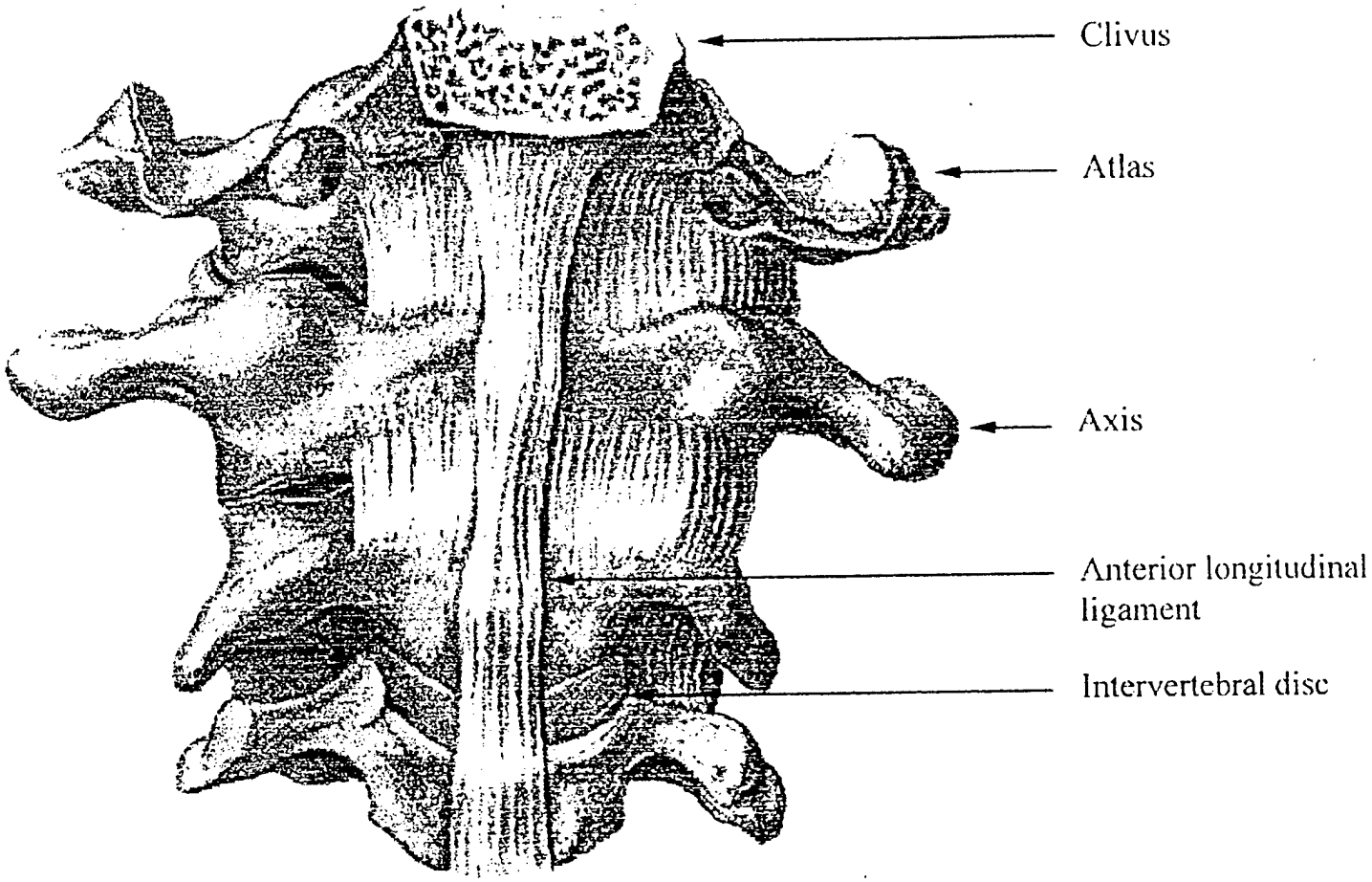
Clivus
Atlas
Axis
Anterior longitudinal ligament
Intervertebral disc

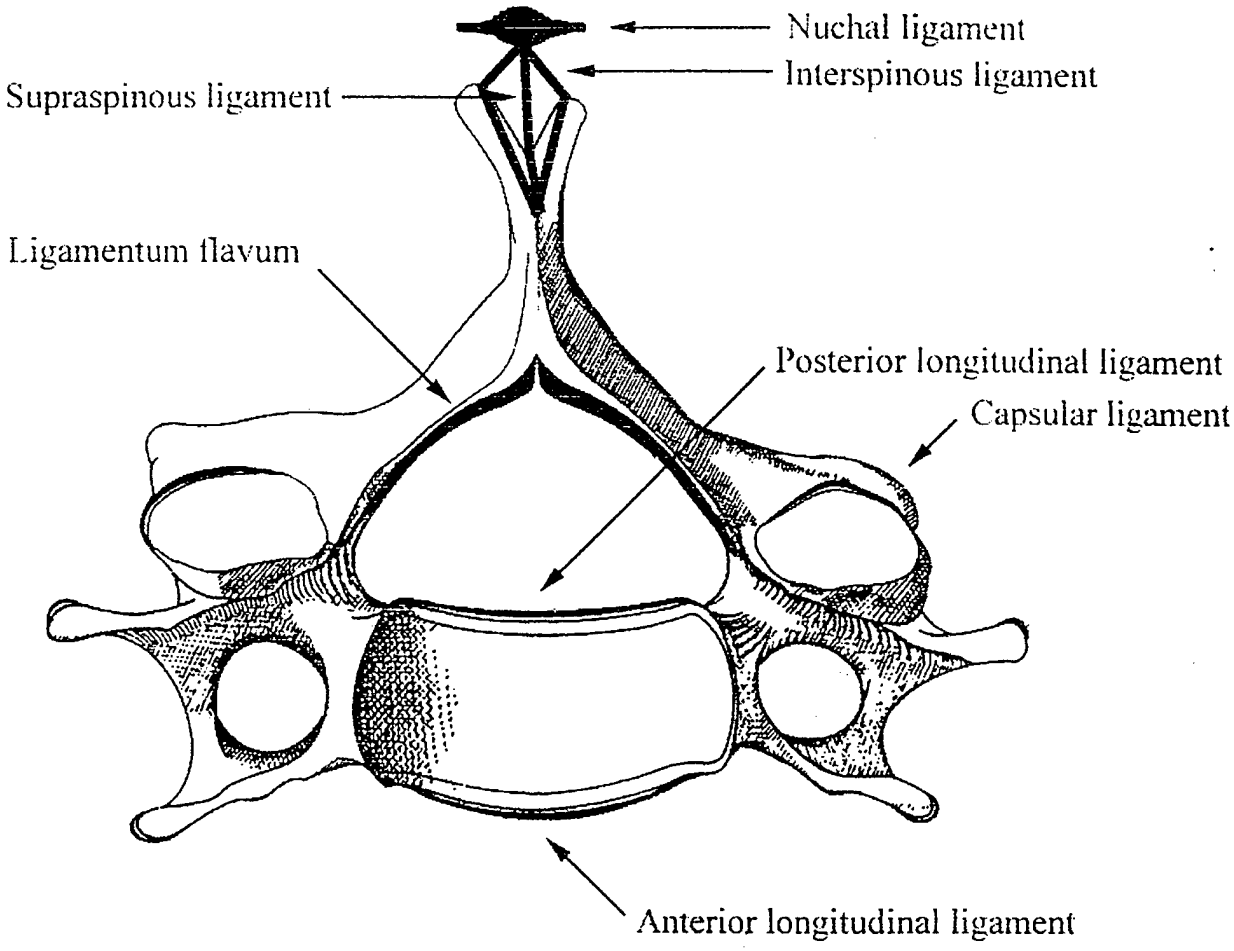
Nuchal ligament
Interspinous ligament
Supraspinous ligament
Ligamentum flavum
Posterior longitudinal ligament
Capsular ligament
Anterior longitudinal ligament

HUMAN CERVICAL SPINE UNCOVERTEBRAL JOINT ANATOMY

Srirangam Kumaresan, Narayan Yoganandan, Frank A. Pintar

Abstract

Although uncovertebral joints have been identified in the human cervical spine, systematic quantitative anatomical studies have not been undertaken. Since the various components of the cervical column contribute to its kinematic and biomechanical responses, it is important to understand the anatomy of these structures. Using cryomicrotomy techniques, sequential anatomic sections from the human cadaver C2 to T1 structures were analyzed to qualitatively describe and quantitatively document the three-dimensional details of the uncovertebral joints. Bilateral dorsal to ventral length, medial to lateral depth, and caudal to cranial height measurements were obtained. The structure appears as a synovial joint and is located laterally in the intervertebral joint. The well-developed larger joints are observed in the mid to lower cervical (C3-C7) regions and the smaller joints appear in the most cranial and caudal (C2-C3, C7-T1) levels ($p<0.05$). The uncovertebral joints in the mid to lower cervical region extend further ventrally compared to the most cranial and caudal levels. The height of the uncovertebral joints is equal to the height of the lateral discs throughout the extent of the joint. These quantitative three-dimensional descriptions assist in describing the uncovertebral joints in finite element models to understand its effects on the cervical spine biomechanical behavior. This study may offer insights into the segmental kinematic differences seen in the adult cervical spine.

1. Introduction

The human spinal column has unique regional anatomical features. In addition to the morphologic variations among the vertebrae and the intervertebral disc components in the lumbar, thoracic and cervical columns, distinct characteristic features of the various joints are also noted in

these structures. While the lumbar column is devoid of the intercostal articulations found in the thoracic spine, the cervical spine contains the most characteristic joints in the vertebral body-disc medium. These joints found lateral to the intervertebral discs are commonly termed as uncovertebral, neurocartilage or Luschka's joints [1].

It is important to define the quantitative anatomy of the cervical spine components such as the facet joint orientation, intervertebral disc height variations from the anterior to the posterior direction, and the three-dimensional morphology of the vertebra to understand the biomechanical behavior [2-7]. While many studies have documented these types of data, there is a paucity of deterministic information on the anatomy of the uncovertebral joints. Like the other joints of the cervical spine, uncovertebral joints contribute to the biomechanical load carrying capacity and the internal structural mechanics of the neck. However, the lack of data on the anatomical details have restricted our understanding of its effects on the intervertebral biomechanics. A significant majority of previous experimental and analytical studies including finite element models have ignored this structure on the cervical spine response [8]. Therefore, an understanding of the detailed quantitative anatomy of uncovertebral joints is needed to delineate its role in cervical spine biomechanics. These data may have clinical significance in the diagnosis of spinal disorders and to develop surgical procedures and instrumentation. In addition, quantitative definition on the size of uncovertebral joints assists in the development of clinically relevant mathematical models. The only available dimension is by roentgenogram observations but this two-dimensional value does not represent the exact location and depth of the uncovertebral joint at each intervertebral level [9]. In this chapter, the three-dimensional quantitative anatomical details of uncovertebral joints from C2 to T1 levels are presented.

2. Methods

The anatomy of uncovertebral joints was obtained using a 33 year old human cadaver OC-T2 structure [10]. Radiographs of the specimen were taken to ensure the absence of spinal abnormalities. It was prepared by deep freezing to prevent drainage of blood and cerebrospinal fluid, the entrance of air into the specimen, and to preserve the structural relationships between the soft and the hard tissues. Before cryosectioning, methyl-cellulose gel was poured around the frozen specimen and allowed to set for approximately 48 hours. A heavy duty cryomicrotome was used for obtaining sequential anatomic sections of the specimen [11]. The OC-T2 structure was sliced at 0.025 mm intervals from ventral to dorsal edge and documented photographically at every 1 mm. After each cryosection, a slab of dry ice was placed on the freshly sectioned specimen to quick-freeze. Ethyl alcohol was applied on the surface to enhance the contrast of the different tissues. A 35 mm camera was used with high-definition color slide film to take photographs of each section. Three views were selected for photographic purposes; an overall view from OC-T2, and close-up views from OC-C4 and C4-T2. Further close-up views were obtained to identify structures more clearly. A millimeter scale was placed on the side of the specimen in each section.

Photographic slides obtained in each cryosection image were used to define the anatomy. Each slide section was projected and the bilateral boundaries of uncovertebral joints were traced. The projection of the slide considerably magnified (20 times) the anatomical details of the relatively small uncovertebral joints. The joint was identified as a distinctly darker color from the disc boundary confined lateral to the anulus of the intervertebral disc at every spinal level. Quantitatively, the joint was defined between the uncinate processes of the caudal vertebral body and the corresponding under-surface of the cranial vertebral body. The slide showing the overall view was used to identify the intervertebral disc level in the close-up view. The tracing of the joint boundaries at each coronal section and sequential stacking of these tracings provided the three-dimensional geometrical details of the joint. The tracings were digitized to obtain the coordinates of the joint boundaries. Independent measurements were done at different times to check to insure repeatability. The measurements of the coordinates were made with respect to a fixed reference point. The adopted anatomical coordinate system was: X-axis corresponds to posterior to anterior (dorsal to ventral), Y-axis from right to left (medial to lateral), and Z-axis from inferior to superior

(caudal to cranial) directions. The shape of the joint was idealized to conform to a rectangular solid. The mean values including the standard deviations of the medial to lateral depth (Y-axis measurement) and the caudal to cranial height (Z-axis measurement) of the joint were obtained. The dorsal to ventral length of the joint was measured along the X-axis. For simplicity, these dimensions are referred to as the depth, height and length, respectively. Analysis of variance (ANOVA) and paired t-test analyses were conducted to determine the statistical differences between the measured joint dimensions.

3. Results

The cryosectioning images from the ventral edge of the intervertebral discs to the end of the dorsal edge indicated the following. The uncovertebral joints were noted bilaterally from C2 to T1 spinal levels. At each level, it appeared as a synovial joint bordered inferiorly by the uncinate processes of the caudal vertebral body and superiorly by the corresponding under-surface of the cranial vertebral body, and medially by the outer layer of the lateral circumference of disc anulus and laterally by the nerve root. The inclined joints were directed superiorly and laterally. They merged with the outer layers of anulus ventrally and dorsally. The joint height was approximately equal to the lateral disc height from anterior to posterior of the joint. The lateral cranial edge of the joint coincided with the boundary between the disc and the superior vertebral body. In general, the joints terminated at the dorsal edge of the discs and were parallel to the respective uncinate processes of the caudal vertebral bodies. The joints in the mid to lower cervical (C3-C7) region extended further ventrally compared to the most cranial (C2-C3) and caudal (C7-T1) levels.

No statistically significant differences ($p>0.05$) were found between the left and right side dimensions in either the depth, length, or height of the joint at each spinal level. This result suggested a symmetrical joint at each level. The depth did not show statistically significant variations on a level-by-level basis (Figure 1). The overall average depth of the joint (independent of spinal level) was 3.8 mm ($\pm$ 1.8). The length and height of the joint demonstrated significant variations among the regions. Consequently, these dimensions were grouped for further analysis. The larger height (3.1 mm $\pm$ 0.6) was noted in the C5-C7 regions and the lower height (2.5 mm $\pm$ 0.8) was noted in the remaining counterparts. These data were statistically significantly different ($p<0.05$). The length had significantly higher ($p<0.05$) mean values (8.3 mm $\pm$ 0.5) in the C3-C6 region followed by the C6-C7 level and was the smallest in the most cranial (C2-C3) and caudal (C7-T1) levels (4.2 mm $\pm$ 0.5). These data revealed that the well-developed larger joints were in the mid and lower cervical (C3-C7) regions and the smaller joints were in the most cranial and caudal regions (C2-C3, C7-T1). The lateral disc heights anterior from the starting and termination of the uncovertebral joint are given in figure 2. These data indicated that the joint heights were approximately equal to the lateral disc height from the starting and termination of the joint, i.e., during the path of the Luschka's structure. The disc heights significantly increased anterior to Luschka's joint. In other words, the disc height decreases substantially from the anterior to the posterior direction as soon as uncovertebral joint begins to appear.

4. Discussion

Anatomical studies of the human cervical spine have routinely used radiography, computed tomography (CT), magnetic resonance imaging (MRI), gross dissection combined with macroscopic visualization, light microscopy and cryomicrotomy [3,9,11-13]. Radiographs are not easily amenable for detailed quantified measurements particularly when the tissue involved is a joint structure. While x-rays and CT scans delineate the bony morphology, soft tissue and joint details are only inferential from these imaging modalities. Magnetic resonance images describe the soft tissue details in the gray scale format. However, radiographs, CT and MRI scans cannot clearly define the contrasting soft tissue details especially at the joints. Cryomicrotome sectioning

of cadaver specimen is an ideal method to describe and quantify the soft and hard tissue anatomy [14-16]. The technique involves a serial trimming of the frozen, undecalcified cadaver specimens to identify the undistorted anatomic characteristics. The *in situ* freezing limits the drainage of the cerebrospinal fluid and the blood from the specimen, and the entrance of the air into the specimen. It also preserves the natural color of the tissues. In addition, freezing helps to maintain the internal structural relationships between the soft tissues and the supporting elements. Therefore, this method provides qualitative and quantitative anatomic descriptions of uncovertebral joints.

The present study obtained the three-dimensional geometrical data of the joint at every level of the cervical spine by sequential coronal cryosectioning from ventral to dorsal edges of the intervertebral discs. The statistical results revealed that the joints are symmetrical. Results also indicated that uncovertebral joints in the middle levels (C3-C7) extend more ventrally compared to the upper (C2-C3) and the lower (C7-T1) intervertebral levels. Further, the joints do not appear in the T1-T2 levels. These qualitative descriptions regarding the regional variations correlate well with literature [17]. In addition, the current observation of the joint merging with the outer layer of intervertebral anulus fibers ventrally and dorsally correlates with the reporting of Luschka [18]. The inclined, superior and lateral orientation of the joint matches with Luschka's findings [1]. The shape of uncovertebral joints was idealized into a regular and mathematically definable geometry as done in previous studies to quantify the cervical and lumbar spine anatomy [19]. This approach helps to better describe these joints in numerical models. Furthermore, the level-by-level data were grouped to delineate its regional characteristics in the human cervical spine. The statistically derived groupings revealed that the well-developed larger joints are present in the mid and in the lower cervical (C3-C7) regions, and the smaller joints are found in the cranial and caudal (C2-C3, C7-T1) levels. The results indicated that the joint heights are equal to the lateral disc height from the starting and termination of the joint. Recent studies have shown the intervertebral kinematics to vary with the spinal level even in intact cervical spinal columns under external static and dynamic loading [20,21]. The presently observed unique regional variations of uncovertebral joints may help explain some of these differences in the local kinematics among various cervical levels.

Hall reported the morphological development of uncovertebral joints in the fetus, newborn, 14 year old and degenerated spine specimens [18]. Loose connective tissues were found lateral to the disc in the fetus and newborn specimens. A densely organized vascular connective tissue with no joint cavity between the tissue and the uncinate processes was found in the 14 year old spine. Based on these observations, Hall concluded a lack of joint cavity in the developing state of this region. However, the joint cavity appeared during growth, and development of uncovertebral anatomy did not depend on the gross degeneration and thinning of intervertebral discs. Similarly, Penning reported that in the first twenty years, the joints appear as a synchondroses (fibrocartilage joint) like the intervertebral discs and after this period, they transform into diarthrosis [17]. This delayed transformation of a fibrocartilaginous joint into a synovial joint (diarthrosis) raises the controversy whether the joint is a true joint or not. Some anatomists consider uncovertebral joints as small synovial articulations between the opposing superior and inferior margins of the adjacent vertebrae and therefore, a true synovial joint [1,9,18,22-25]. In contrast, others have treated the joint as fibrocartilaginous fissures resulting from disc degeneration [26-28]. Because of these foregoing information, a specimen representing a well-developed cervical anatomy was used in the present study. Further, the current observation that found distinctly darker gelatinous substance surrounded by a thin membrane appears to support the consideration that uncovertebral joints may be of the synovial type. In fact, this observation bears further support from histologic studies wherein the synovial joint has been explained as a collection of synovial cells among the connective fibers with no definitive cellular synovial membrane at the surface [29,30].

Despite the complex anatomical characteristics of uncovertebral joints, in the present research, a simplified approach was used to define the geometry as a regular solid with length, depth, and height. As indicated earlier, this is an acceptable methodology to assist the existing finite element models of the human cervical spine to attain a higher level of geometrical complexity by incorporating uncovertebral joints at the respective spinal levels [8,31-34]. In fact, the present results of the dimension and the location of the joint in relation to its adjacent components (e.g., the lateral cranial edge of the joint coincided with the boundary between the disc and the cranial

vertebral body) facilitates an easy incorporation to the already defined vertebral anatomy in these models. We have successfully used this methodology and developed a three-dimensional nonlinear finite element model of the adult human lower cervical spine and experimentally validated under different physiologic loading modes [35]. This model is used to delineate the effect of the uncovertebral joints on the biomechanical response of the cervical spine.

5. Conclusions

The three-dimensional quantitative geometrical details of the uncovertebral joints in the normal human cervical spine are obtained using the cryomicrotome technique. The uncovertebral joints are observed from C2 to T1 intervertebral levels. The joint is bordered laterally by the uncinate processes of the caudal vertebral bodies and by the corresponding under-surface of the cephalad vertebral bodies, and medially by the outer layer of the lateral circumference of the disc anulus and laterally by the nerve roots. The joints are inclined and are directed superiorly and laterally. They merge with the outer layer of disc anulus ventrally and dorsally. Distinct regional variations of the joints are noted. The well-developed larger joints are observed in mid to lower cervical (C3-C7) regions and the smaller joints are noted in the most cranial and caudal (C2-C3, C7-T1) levels. In the mid to lower cervical region they extend further ventrally compared to the most cranial and caudal levels. The present three-dimensional quantitative anatomical data will improve the geometrical descriptions in future mathematical models that may assist in a better understanding of the clinical and biomechanical aspects of the adult human cervical spine.

Acknowledgment: This study was supported in part by PHS CDC Grant R49CCR 507370, DOT NHTSA Grant DTNH22-93-Y-17028, and the Department of Veterans Affairs Medical Center Research.

References

[1] Luschka HV. *Die Halbgelenke des Menschlichen Korpers*, Reimer, Berlin, 1858.

[2] Francis CC. Variations in the articular facets of the cervical vertebrae. *Anatomical Record* 1955:122: 589-602.

[3] Liu YK, Krieger KW, Njus G, Ueno K, Connors M, Wakano K, Thies D. Cervical spine stiffness and geometry of the young human male, 1981, Wright-Patterson AFB, AFAMRL-TR-80-138: Dayton, OH.

[4] Pintar FA, Yoganandan N, Sances A Jr, Reinartz J, Harris G, Larson SJ. Kinematic and anatomical analysis of the human cervical spinal column under axial loading. *SAE Transactions* 1990:98(6): 1766-1789.

[5] Pooni JS, Hukins DW, Harris PF, Hilton RC, Davies KE. Comparison of the structure of human intervertebral discs in the cervical, thoracic and lumbar regions of the spine. *Surg Radiol Anat* 1986:8: 175-182.

[6] Yoganandan N, Pintar FA, Wilson CR, Sances A Jr. In vitro biomechanical study of female geriatric cervical vertebral bodies. *J Biomed Eng* 1990:12(2): 97-101.

[7] Yoganandan N, Pintar FA, Sances A Jr, Maiman DJ. Strength and motion analysis of the human head-neck complex. *J Spinal Disord* 1991:4(1): 73-85.

[8] Yoganandan N, Kumaresan S, Voo L, Pintar F. Finite element applications in human cervical spine modeling. *Spine* 1996:21(15): 1824-1834.

[9] Compere EL, Tachdjian MO, Kernahan WT. The Luschka Joints: Their anatomy, physiology and pathology. *Orthopaedics* 1959:1: 159-168.

[10] Kumaresan S, Yoganandan N, Pintar FA. Methodology to quantify the uncovertebral joint in the human cervical spine. *J Musculoskeletal Research* 1997 (In Press).

[11] Rauschning W. Surface cryoplaning - A technique for clinical anatomical correlations. *Ups J Med Sci* 1986:91: 251-255.

[12] Hadley LA. The covertebral articulations and cervical foramen encroachment. *J Bone Joint Surg* 1957:39A: 910-920.

[13] Krag MH, Weaver DL, Beynnon BD. Morphometry of the thoracic and lumbar spine related to transpedicular screw placement for surgical spinal fixation. *Spine* 1988:13(1): 27-32.
[14] Rauschning W. Computed tomography and cryomicrotomy of lumbar spine specimens - a new technique for multiplanar anatomic correlation. *Spine* 1983:8(2): 170-180.
[15] Pech P, Bergstrom K, Rauschning W, Haughton WM. Attenuation values, volume changes and artifacts in tissue due to freezing. *Acta Radiol* 1987:28: 779-782.
[16] Pintar FA, Yoganandan N, Myers T, Elhagediab A, Sances A Jr. Biomechanical properties of human lumbar spine ligaments. *J Biomech* 1992:25(11): 1351-1356.
[17] Penning L. *Functional Pathology of the Cervical Spine*, Williams & Wilkins Co., Baltimore, MD, 1968.
[18] Hall MC. *Luschka's Joint*, C C Thomas, Springfield, IL, 1965: 141.
[19] Nissan M, Gilad I. The cervical and lumbar vertebrae: An anthropometric model. *Eng Med* 1984:13(3): 111-114.
[20] Yoganandan N, Pintar FA, Arnold P, Reinartz J, Cusick JF, Maiman DJ, Sances A Jr. Continuous motion analysis of the head-neck complex under impact. *J Spinal Disord* 1994:7(3): 420-428.
[21] Cusick JF, Pintar FA, Yoganandan N, Reinartz JM. Biomechanical alterations induced by multilevel cervical laminectomy. *Spine* 1995:20(22): 2393-2399.
[22] Boreadis AG, Gershon-Cohen J. Luschka joints of the cervical spine. *Radiology* 1956:66: 181-187.
[23] Lyon E. Uncovertebral osteophytes and osteochondroses of the cervical spine. *J Bone Joint Surg* 1945:27: 248-253.
[24] Spurling RG, Segerberg LH. Lateral intervertebral disc lesions in the lower cervical region. *JAMA* 1953:151(5): 354-359.
[25] Brain WR, Knight GC, Bull JW. Discussion on rupture of the intervertebral disc in cervical region. *Proc Roy Soc Med* 1948:41: 509-516.
[26] Bovill EG, Drazek JA. An anatomic study of the cervical spine based on clinical-roentgenologic concept of the etiology of brachialgia. *University of Michigan Medical Bulletin* 1950:16: 387-398.
[27] Frykholm R. Lower cervical vertebrae and intervertebral discs. *Acta Chir Scand* 1951:101: 345-359.
[28] Payne EE , Spillane JD. The cervical spine. An anatomic-pathological study of 70 specimens (using a special technique) with particular reference to the problem of cervical spondylosis. *Brain* 1957:80: 571-596.
[29] Wheater PR, Burkitt HG, Daniels VG. *Functional Histology*. 2nd Edition, Churchill Livingston, New York, 1987: 348.
[30] Bloom W, Fawcett DW. *A Textbook of Histology*. 8th Edition, WB Saunders Company, Philadelphia, PA, 1962: 720.
[31] Kleinberger M. Application of finite element techniques to the study of cervical spine mechanics. In: *Proceedings 37th Stapp Car Crash Conference*, San Antonio, TX, 1993, pp 261-272.
[32] Kumaresan S, Yoganandan N, Pintar F, Voo L, Cusick J, Larson S. Finite element modeling of cervical laminectomy with graded facetectomy. *J Spinal Disord* 1997:10(1): 40-47.
[33] Saito T, Yamamuro T, Shikata J, Oka M, Tsutsumi S. Analysis and prevention of spinal column deformity following cervical laminectomy I. Pathogenetic analysis of postlaminectomy deformities. *Spine* 1991:16: 494-502.
[34] Yoganandan N, Kumaresan S, Voo L, Pintar F. Finite element model of the human lower cervical spine. *J Biomech Eng* 1997:119(1): 87-92.
[35] Kumaresan S, Yoganandan N, Pintar F. Age-specific pediatric cervical spine biomechanical responses: Three-dimensional nonlinear finite element models. In: *Proceedings 41st Stapp Car Crash Conference*, Orlando, FL, 1997.

Figure Captions

Figure 1 Average values of the dorsal to ventral length, medial to lateral depth and caudal to cranial height of the uncovertebral joint.

Figure 2 Comparison of the lateral disc height with the uncovertebral joint height.

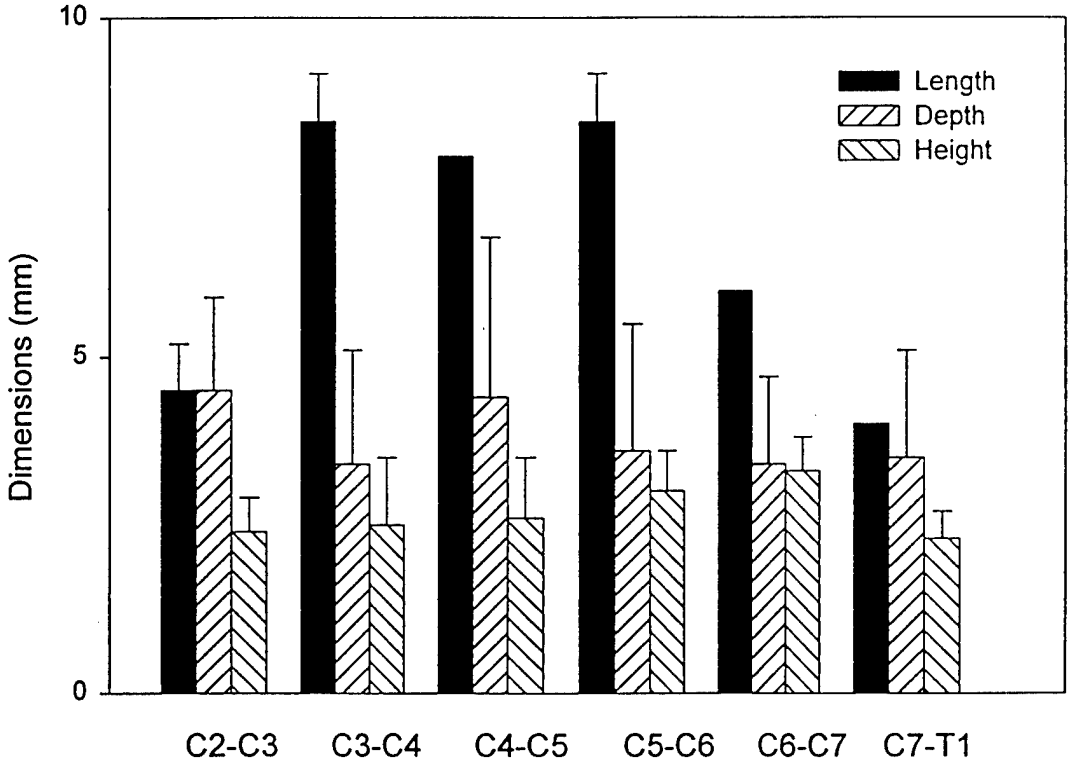

Figure 1 Average values of the dorsal to ventral length, medial to lateral depth and caudal to cranial height of the uncovertebral joint.

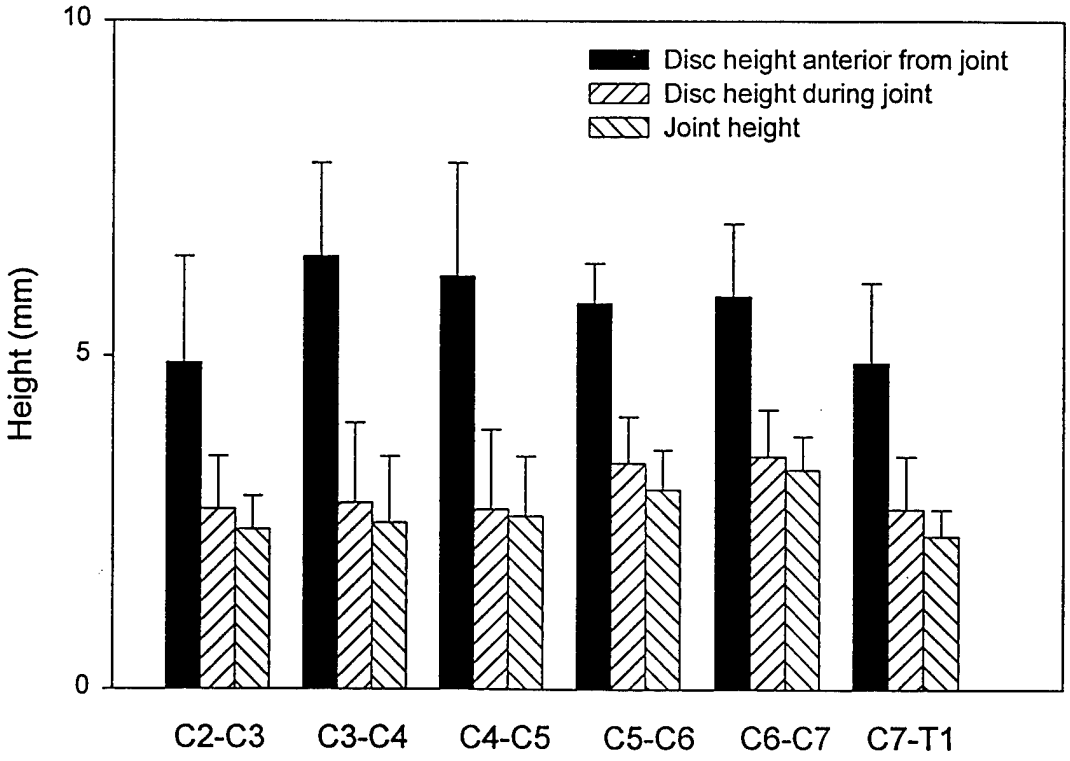

Figure 2 Comparison of the lateral disc height with the uncovertebral joint height.

CT AND MRI OF CRANIO-CEREBRAL AND CERVICAL TRAUMA

William Keenan, David Daniels

Abstract

Computed tomography (CT) and magnetic resonance (MR) imaging are used to evaluate cranial and cervical post-traumatic abnormalities. Computed tomography is initially used to evaluate acute cerebral trauma because it readily identifies acute hematoma and depressed skull fractures, can be used to study an uncooperative patient that would be difficult to study with MR, and can be used to evaluate other areas of the body such as the abdomen and chest. Computed tomography also can effectively demonstrate cervical spine fractures after plain radiographs, show fracture deformity, evidence of soft tissue injury or completely evaluate parts of the spine. Magnetic resonance usually is used after CT if it is necessary to better define areas of cerebral contusion or when an intracerebral hematoma may have an underlying neoplasm or vascular malformation. Magnetic resonance also is used in cases of cervical trauma to demonstrate a herniated disc, epidural hematoma, spinal cord edema and contusion, and ligamentous injury.

1. Introduction

1.1 Cranio-Cerebral Trauma

Computed tomography (CT) and magnetic resonance imaging (MRI) of abnormalities after cranial trauma including extra-axial and intra-axial hematomas, diffuse axonal injury, contusion, brain herniation, edema and ischemia will be described in this chapter.

1.2 Findings in Acute Trauma

1.2.1 Skull and Scalp Injuries

Computed tomography is superior to MR in evaluating skull fractures because of CT's ability to better delineate osseous anatomy. Evaluation of osseous anatomy with CT requires a wide window (i.e., "bone" window technique) such that the scalp and intracranial structures appear dark in contrast to the high density osseous structures appearing white. Depressed skull fractures are easily detected as areas of inward displacement of skull fragments (Figure 1). A linear fracture parallel to the plane of section may not be appreciated with CT and may be better visualized on the lateral scoutview that is used to localize the area of scanning. In addition to using a "bone" window technique to evaluate osseous anatomy, it is crucial to use a narrow window (i.e., "soft tissue" technique) to detect intra-axial injuries and extra-axial hematomas that can be associated with linear and depressed skull fractures. Scalp injuries are also well evaluated with CT scanning. These injuries include scalp lacerations, hematomas and soft tissue swelling. Viewing the scalp at a "bone window" technique permits visualization of subtle areas of scalp soft tissue swelling. However, differentiation of scalp hematoma from soft tissue swelling would require using the "soft tissue" window technique. At every window setting, the air associated with scalp lacerations typically appears black due to its extremely low density in CT scans.

1.2.2 Extra-Axial Hemorrhage

Subdural hematomas (SDH) are more common than epidural hematomas (EDH). The SDH typically result from tearing of cortical veins [1-2]. The SDH are located between dura and arachnoid and typically have a semilunar or crescentic shape (Figure 2). The SDH may extend across suture lines but cannot cross dural attachments. Most SDH are unilateral and positioned peripheral to the frontal and parietal lobes. SDH can also occur between the cerebral hemispheres and are sometimes bilateral. In CT the acute SDH typically is homogeneously and markedly hyperdense with respect to cerebral tissue but may contain some low density areas reflecting hematoma of different ages or cerebrospinal fluid mixed with the hematoma [3]. A small SDH or EDH may be identified using an intermediate window between "soft tissue" and "bone" techniques to appear less dense than that of the skull. The acute SDH may be isodense with the adjacent cerebral tissue in cases of severe anemia or coagulopathies [4-5]. The subacute SDH decreases in density to become nearly isodense to the adjacent cerebral grey matter. However, it can usually be identified with high resolution CT scans due to displacement of the grey-white matter junction. Intravenous contrast agent is usually not required to identify enhancing cortical veins displaced from the inner table by the SDH or to demonstrate an enhancing membrane of a SDH. Chronic SDH are lower in density than adjacent cerebral tissue, and are more commonly crescentic than lens-shaped and may calcify. Repeated hemorrhages in a chronic subdural hematoma can result in the SDH having regions of low and high density [6].

The MR appearance of SDH varies with its age and also with the field strength of the MR scanner. In MR images obtained with a high field strength machine, the hyperacute SDH is usually isointense on T1-weighted images and hyperintense (appearing white) or isointense on T2-weighted images [1]. In this chapter MR images are obtained with a spin echo technique unless stated otherwise. The acute SDH is typically hypointense (appearing dark) on T1- and T2-weighted images [1]. The subacute SDH is hyperintense on T1- and T2-weighted images [1]. The chronic SDH has variable signal intensity on T1-weighted images and typically increased signal intensity on T2-weighted images [1,7-8]. (See section on cerebral hematomas). The EDH typically arises from tearing of the middle meningeal artery or a dural venous sinus, the latter typically in the posterior fossa. The EDH is lens-shaped, can extend across dural attachments but not across sutures, and may enlarge with time (Figure 3) [9]. In CT, the EDH usually appears as a lens-shaped high density extra-axial fluid collection. In some cases however, the EDH has heterogeneous density from blood of different ages [1]. In MR, the acute EDH is isointense on T1-weighted images and hyperintense on T2-weighted images. Subacute and chronic EDH's are usually hyperintense on T1- and T2-weighted images [1]. Acute subarachnoid hemorrhage appears as high density fluid in the basal cisterns on CT (Figure 4). Interhemispheric subarachnoid hemorrhage extends into the adjacent cerebral sulci while subdural hematoma does not. Sometimes a small amount of subarachnoid hemorrhage can be identified in sulci at the

convexities. A small amount of high density subarachnoid hemorrhage may sometimes only be seen in the interpeduncular cistern.

1.2.3 Intra-Axial Injuries

Intracranial hematomas: In CT, acute intracranial hematomas are typically hyperdense. The hematoma is rarely isodense with respect to the adjacent brain if the patient is extremely anemic with a low protein concentration or has a coagulation disorder preventing clot formation [4,10]. If the patient is actively bleeding, the hematoma can have low and high density areas [11]. The density of intracerebral hematomas decreases with time, resorbs from peripheral to central, and becomes isodense with the adjacent cerebral tissue within several days to several weeks. Chronic cerebral hematomas are low in density, may show some rim enhancement for several months, and occasionally may calcify. In MR, the appearance of intracranial hematomas is complex and not completely understood. The MR appearance will vary depending on the pulse sequences used and the field strength of the MR system. The main MR features of an intracranial hematoma using a high field strength MR system are summarized below [12].

Hyperacute hematoma: The hyperacute hematoma is 4-6 hours old. It contains oxyhemoglobin that is diamagnetic and does not affect the appearance of the hematoma in T1- and T2-weighted images. The hematoma has a similar signal to that of grey matter on T1-weighted images, is hyperintense on T2-weighted images due to its high protein/water content, and is markedly hypointense on gradient-echo images.

Acute hematoma: The acute hematoma is 7-72 hours old. Intracellular oxyhemoglobin oxidizes to deoxyhemoglobin that is paramagnetic. The acute hematoma appears isointense with cerebral tissue on T1-weighted images and markedly hypointense on T2-weighted and especially gradient echo images. Adjacent edema has high signal intensity on T2-weighted images in this and subsequent stages.

Subacute hematoma: The subacute hematoma is 4-7 days old. Intracellular hemoglobin continues to oxidize to methemoglobin which is strongly paramagnetic. The early subacute hematoma demonstrates increased signal intensity peripherally and an isointense center on T1-weighted images and is markedly hypointense on T2-weighted and gradient echo images.

Late subacute hematoma: The late subacute hematoma is 1-4 weeks old. Red blood cells in the hematoma lie such that extracellular methemoglobin is present. The late subacute hematoma has high signal intensity on T1- and T2-weighted images, and very low signal intensity on gradient echo images.

Early chronic hematoma: The early chronic hematoma is several months old and gradually becomes smaller. It has high signal intensity on T1- and T2-weighted images due to extracellular methemoglobin. The rim of the hematoma has very low intensity on T2-weighted images due to macrophages at the margin that contain ferritin and hemosiderin that have prominent magnetic susceptibility effects. The hematoma continues to have very low signal intensity on gradient echo images.

Late chronic hematoma: The late chronic hematoma is several months to years old. The hematoma shrinks further, becomes fibrotic and contains macrophages with ferritin and methemoglobin that have strong magnetic susceptibility properties. The hematoma is markedly hypointense on T1- and T2-weighted images, and also on gradient echo images. The strong magnetic susceptibility effects the blood produces such as ferritin and hemosiderin, cause "blooming" or enlargement of the very low signal intensity of hematomas. This is most prominent in chronic hematoma stages with gradient echo imaging, and less prominent in standard T2-weighted spin echo and in turn fast spin echo T2-weighted images. Magnetic susceptibility effects and signal changes from hematomas are more prominent in images obtained with a high field strength system than a low field strength system.

Cortical contusions: Cortical contusions are small areas of hemorrhage. They occur from impaction of the brain against osseous (less often dural ridges), but most frequently at the anterior and inferior aspects of the temporal and frontal lobes [13]. These typically result from acceleration/deceleration injuries. With CT, cortical contusions may be difficult to identify until

one to two days following trauma and then appear as small high density areas that often have a small amount of adajcent edema (Figure 5) [14]. Cortical contusions are usually better identified with MR than CT [15]. Acute cortical contusions have low signal intensity on T2-weighted images with adjacent high signal intensity edema; the contusions are better visualized in T2-weighted gradient echo images than in standard T2-weighted spin echo images and in turn fast spin echo T2-weighted images [1,12]. Late subacute cortical contusions demonstrate high signal intensity on both T1- and T2-weighted images. Old cortical contusions typically have low signal intensity on T1- and T2-weighted images due to hemosiderin formation [12]. (See Intracerebral Hematomas).

Diffuse axonal injury: Diffuse axonal or shearing injury (DAI) is an important cause of morbidity in patients with cranial cerebral trauma [16]. Diffuse axonal injury can occur as a result of acceleration/deceleration or rotation of the brain [1]. The trauma typically occurs at the grey-white junction and less often in the corpus callosum, internal capsule and tectum of the mesencephalon [16]. With CT, DAI may be better shown on delayed scanning as focal areas of hemorrhage having high density [15,17]. With MR, DAI is often better visualized. If nonhemorrhagic, DAI appears as foci of high signal intensity on T2-weighted images [1]. Hemorrhagic DAI can appear as foci of high signal intensity on T1- and T2-weighted images if subacute, and appear as foci of low signal intensity in T2-weighted images (especially gradient echo images) due to hemosiderin formation if chronic (Figure 6) [1].

Other shearing injuries: Brainstem and basal ganglia injuries can be identified as small areas of hemorrhage in the brainstem or basal ganglia that are better shown with MR than with CT [1]. More than the other portions of the brainstem, the mesencephalon may be damaged from contacting the tentorial notch during trauma [16].

Intraventricular hemorrhage: Intraventricular hemorrhage may occur as a result of trauma possibly due to tearing of subependymal veins [18].

1.2.4 Herniations

Cerebral herniations occur when the brain is displaced and major arteries may be compressed resulting in infarction [1]. Subfalcine herniations occur when a cerebral hemisphere is displaced across the midline inferior to the falx cerebri. Resultant compression of the Foramen of Monroe, enlargement of the contralateral lateral ventricle, and infarction from compression of the anterior cerebral artery against the falx cerebri may occur. Progressive supratentorial mass effect may result in downward transtentorial herniation beginning with medial displacement of the medial part of the temporal lobe (uncus and parahippocampal gyrus) through the tentorial notch. A midbrain (Duret) hemorrhage can result from downward displacement of the midbrain [1]. The contralateral cerebral peduncle may be compressed against the opposite edge of the tentorium cerebelli resulting in a deformity of the cerebral peduncle that is designated Kernohan's notch [1]. With further transtentorial herniation, obliteration of all the basal cisterns can occur (Figure 7). Compression of the posterior cerebral artery and other arterial branches of the Circle of Willis can result in infarctions of the occipital lobe, basal ganglia and mesencephalon. Tonsillar herniation occurs when a large posterior fossa mass effect causes the cerebellar tonsils to be displaced beneath the foramen magnum. Downward transtentorial herniation is much more common than upward transtentorial herniation, which may be caused by a posterior fossa mass effect [1]. In cases of subfalcine and transtentorial herniation, CT can demonstrate the shift of midline structures and obliteration of basal cisterns. Sagittal and coronal MR imaging are especially effective for demonstrating the extent of downward transtentorial herniation and the deformity of the brainstem.

Cerebral ischemia and infarction: Cerebral ischemia can result from altered blood flow due to trauma [1]. Cerebral infarction can result from displacement and compression of arteries that occur after different types of herniation [1].

Cerebral edema: Cerebral edema (Figure 8) can involve one or both cerebral hemispheres after cerebral compression, herniation or infarction. Computed tomography can show diffuse cerebral edema causing compression of the lateral and third ventricles, effacement of cerebral sulci, obliteration of the basal cisterns and decreased density of cerebral tissue such that grey and white matter cannot be differentiated. In severe cases of cerebral edema, the Circle of Willis and

cerebellum may appear relatively high in density due to the low density of the cerebral hemispheres.

Abnormal cerebral blood flow: Abnormal cerebral blood flow resulting in cerebral infarction can be due to arterial vasospasm, compression of arterial branches due to herniation or direct injury of blood vessels that can result in vessel occlusion, pseudoaneurysm formation, arterial dissection or arteriovenous fistula formation [1].

Pneumocephalus: Pneumocephalus can be associated with a skull base fracture involving a paranasal sinus or with a skull fracture and an associated dural tear [1]. Intracranial air appears black (very low density) in all cranial CT images despite different filming techniques. Air also appears black (very low signal intensity) in T1- and T2-weighted images.

Findings in Old Trauma: Encephalomacia appears on CT as a low density region that can be associated with some ventricular dilatation and sulcal prominence. In MRI, areas of encephalomalacia usually have low and high signal intensity in T1- and T2-weighted images, respectively. Generalized cerebral atrophy may occur in patients with severe cerebral trauma and appears as dilatation of the ventricles and sulci to a degree greater than expected for the patient's age. The leptomeningeal cyst or "growing fracture" is a post-traumatic cyst that extends through a dural tear and widens margins of an adjacent skull fracture.

2. Cervical Spine Trauma

Plain radiographs (lateral, AP, odontoid views), CT scanning (thin high resolution images filmed at "soft tissue", "bone" window and reformatted imaging techniques) and MR imaging (T1-weighted spin echo, T2-weighted fast spin echo, and T2-weighted gradient echo images) are used to evaluate patients with cervical trauma (Figures 9a-9c). Plain films serve as the initial screening radiographic test for patients with cervical trauma (Figures 10a-10c). The lateral x-ray film demonstrates the relationship between the occiput, atlas and axis, the alignment of the cervical vertebra and the relationship of C7 to T1. The lateral film should include the lower cervical spine and the upper part of T1 to exclude fractures and dislocations of the lower cervical area. If the upper part of T1 is not visualized, a "swimmer's view" or CT scanning can be used to visualize C7-T1. An "open mouth view" should be obtained to evaluate the upper cervical area. The lateral margins of the lateral masses of C1 should align with the lateral margins of the occipital condyles and the articular pillars of C2. If the upper cervical area is not optimally evaluated with plain radiographs, then CT from the occiput (including the margins of the foramen magnum) to upper C3 with sagittal and coronal reformatted images should be obtained to exclude dislocations and fractures. Plain radiographs and subsequent CT scanning can be used to evaluate an area where prevertebral soft tissue swelling is unexplained or associated with a fracture.

Computed tomography scanning better defines osseous detail than MR and also can show subtle fractures that are not detected with plain radiographs. Axial contiguous CT scans can be obtained with 1-3 mm slice thicknesses. Sagittal reformatted images have less anatomic resolution than direct axial images and show better detail if thinner direct axial scans are used. However, 1 mm thick scans are not typically used to obtain reformatted images due to the potential for patient motion. The more common technique is to use 3 mm thick axial CT scans with 2 mm overlap to obtain satisfactory reformatted images. Computed tomography scanning through the shoulders of a patient usually results in loss of anatomic detail particularly if the patient is large. Complex fractures with perched or locked facets may be difficult to conceptualize in the direct axial CT scans but generally can be conceptualized when seen in the sagittal reformatted images. If there is a rotational abnormality after trauma, oblique sagittal or coronal reformatted images could be obtained. Intrathecal contrast agent is required to optimally evaluate the spinal cord contour with CT and also to optimally visualize the root sheaths. When MR imaging is used with CT in trauma cases, intrathecal contrast agent with CT is usually not required. Magnetic resonance can optimally demonstrate the spinal cord. Computed tomography with intrathecal contrast agent may be required to visualize a dural tear which may be difficult to demonstrate with MR.

Magnetic resonance imaging is widely used to evaluate patients with cervical trauma. Motion artifact should be minimized with MR because it can degrade multiple images obtained in the same series. Magnetic resonance compatible traction devices also are required. Magnetic resonance imaging in spinal trauma provides some advantages over CT. With MR, direct multiplanar images can be obtained. Sagittal images are especially useful in evaluating post-traumatic osseous deformity of the spine that includes facet malalignment and bone impaction. Sagittal images also effectively evaluate the contour of the spinal cord. Direct coronal images are also useful in evaluating the skull base and upper cervical area for fracture deformities involving C1 and the dens. Magnetic resonance is superior to CT in showing intrinsic spinal cord damage from hemorrhage, edema and spinal cord transsection. It can also be used to diagnose soft tissue injuries involving the ligaments, prevertebral soft tissue structures and other paraspinal tissues. MR also is excellent for demonstrating extramedullary spinal canal hematomas and herniated discs.

In our institution, MR imaging of the cervical spine consists of a combination of sagittal T1-weighted and fast spin echo T2-weighted images, and also sagittal and axial T2-weighted gradient echo images. The sagittal T2-weighted fast spin echo images show high signal intensity cerebrospinal fluid appearing white creating a "myelogram effect" in which the contour of the cervical spinal cord is well shown, the spinal cord having lower signal intensity than cerebrospinal fluid. Spinal cord edema has high signal intensity on T2-weighted images. The gradient echo images are especially useful to detect areas of acute hematoma within or adjacent to the cervical spinal cord due to their increased sensitivity for magnetic susceptibility effects. Acute hematomas would have very low signal intensity in the gradient echo images and subtler low signal in fast spin echo T2-weighted images. T2-weighted gradient echo images and fat-suppressed T2-weighted fast spin echo images are also useful to determine areas of soft tissue injury that have increased signal intensity. In all types of MR images, cortical bone and ligaments have negligible signal intensity. Ligamentous damage can be identified by evaluating sagittal T2-weighted images and detecting an interruption of the dark signal that represents a combination of ligament and cortical bone. This decreased signal normally is found along the anterior and posterior aspects of the vertebral bodies and intervertebral discs and along the posterior margin of the spinal canal appearing as dark bands. In fast spin echo T2-weighted imaging, a normal intervertebral disc has a similar signal intensity to that of ligaments but a torn intervertebral disc can be detected due to its high signal intensity. A torn disc would be more difficult to demonstrate in sagittal T2-weighted gradient echo images because a normal disc has higher signal intensity than the ligaments. With MR, intra- and extra-medullary and paraspinal hematomas typically do not have high signal intensity on T1- and T2-weighted images immediately after trauma and gradually become hyperintense over a few days. Magnetic resonance can still demonstrate spinal cord compression from an extramedullary hematoma due to its mass effect. The diagnosis of hematoma can be verified due to its very low signal intensity on T2-weighted gradient echo images. Magnetic resonance is excellent for demonstrating the sequelae of acute cord trauma that includes contusion, hemorrhage, transsection and epidural hematoma. Sequelae of old spinal cord injury such as syringohydromyelia, myelomalacia and atrophy are also well visualized. Syringohydromyelia appears as a sharply defined intramedullary cyst having homogeneous low and high signal intensity on T1- and T2-weighted images, respectively, and that may contain transversely oriented septations, and may be associated with an expanded or normal sized spinal cord or possibly a small and misshapen spinal cord following portal collapse of a syrinx. Myelomalacia appears as poorly defined increased signal intensity on T2-weighted images and may be associated with spinal cord atrophy.

References

[1] Osborn AG. Craniocerebral Trauma. In: *Diagnostic Neuroradiology*, Mosby, St. Louis, 1994: 199-247.

[2] Adams JH. Pathology of nonmissile head injury. *Neuroimaging Clin N Amer* 1991:1: 397-410.

[3] Reed D, Robertson WD, Graeb DA, LaPointe JS, Nugent RA, Woodhurst WB. Acute subdural hematomas: Atypical CT findings. *AJNR* 1986:7: 417-421.

[4] Boyko OB, Cooper DF, Grosseman CB. Contrast-enhanced CT of acute isodense subdural hematoma. *AJNR* 1991:12: 341-343.

[5] Stein SC, Young GS, Talucci RC, Greenbaum BH, Ross SE. Delayed brain injury after head trauma: Significance of coagulopathy. *Neurosurgery* 1992:30: 160-165.

[6] Hashimoto N, Sakakibara T, Yamamoto K, et al. Two fluid-blood density levels in chronic subdural hematoma. *J Neurosurg* 1992:77: 310-311.

[7] Fobben ES, Grossman RI, Atlas SW, Hackney DB, Goldberg HI, Zimmerman RA, Bilaniuk LT. MR characteristics of subdural hematoma and hygromas at 1.5T. *AJNR* 1989:10: 687-693.

[8] Hosoda K, Tamaki N, Masumura M, Matsumoto S, Maeda F. Magnetic resonance images of chronic subdural hematomas. J Neurosurg 1987:67(5): 677-683.

[9] Hamilton M, Wallace C. Nonoperative management of acute epidural hematoma diagnosed by CT: The neuroradiologist's role. *AJNR* 1992:13: 853-859.

[10] Kirkpatrick JB, Hayman LA. Pathophysiology of intracranial hemorrhage. *Neuroimaging Clin N Amer* 1992:2: 11-23.

[11] Cohen WA, Wayman LA. Computed tomography of intracranial hemorrhage. *Neuroimaging Clinics N Amer* 1992:2: 75-87.

[12] Osborn AG. Intracranial Hemorrhage. In: Diagnostic Neuroradiology, Mosby, St. Louis, 1994: 154-198.

[13] Gentry LR, Gordersky JC, Thompson B. MR imaging of head trauma: review of the distribution and radiopathologic features of traumatic lesions. *AJNR* 1988:9: 101-110.

[14] Hesselink JR, Dowd CF, Healy ME, Hajek P, Baker LL, Luerssen TG. MR imaging of brain contusions: A comparative study with CT. *AJNR* 1988:9: 269-278.

[15] Gentry LR, Gordersky JC, Thompson B, Dunn VD. Prospective comparative study of intermediate-field MR and CT in the evaluation of closed head trauma. *AJNR* 1988:9: 91-100.

[16] Gentry LR. Head trauma. SW Atlas (ed). In: *Magnetic Resonance Imaging of the Brain and Spine.* Raven Press, New York, 1991: 439-466.

[17] Kelly AB, Zimmerman RD, Snow RB, Gandy SE, Heier LA, Deck MD. Head trauma: Comparison of MR and CT — experience in 100 patients. *AJNR* 1988:9: 699-708.

[18] Lee JP, Lui TN, Change CN. Acute post-traumatic intraventricular hemorrhage analysis of 25 patients with emphasis on final outcome. *Acta Neurol/Scand* 1991:84: 89-90.

Figure Captions

Figure 1: Depressed skull fracture (straight arrow) and soft tissue swelling (curved arrow). Axial CT filmed with a "bone" window technique.

Figure 2: Acute high density subdural hematoma appearing crescentic (long arrows), causing subfalcine herniation (curved arrows), and displacing the contralateral lateral ventricle (short arrow). Axial CT.

Figure 3: Acute epidural hematoma appearing lens-shaped (arrows), and having heterogeneous density due to blood of different ages. Axial CT.

Figure 4: Acute subarachnoid hemorrhage (arrows) appearing as high density fluid in the basal cisterns. Axial CT.

Figure 5: High density hemorrhagic cortical contusion (arrow) at the medial temporal lobe. Axial CT.

Figure 6: Shearing injury in the corpus callosum having adjacent high signal intensity edema (short arrows) as shown in A, a T2-weighted fast spin echo MR image and a hemorrhagic component (long arrow) best shown as a low signal intensity area in B, a T2-weighted gradient echo MR image.

Figure 7: Transtentorial herniation (long arrows) resulting in obliteration of the basal cisterns and causing an area of brainstem hemorrhage (short arrow). Axial CT.

Figure 8: Diffuse cerebral edema resulting in effacement of some cerebral sulci and poor grey and white matter differentiation.

Figure 9: Comminuted fracture of the C5 vertebral body (arrow) in a lateral plain radiograph (A). Sagittal T2-weighted fast spin echo MR image (B). Sagittal reformatted CT scan (C). In B, spinal cord expansion and edema having high signal intensity (asterisk) are shown.

Figure 10: Fracture deformity with malalignment at C4-C5 (open arrow) in a lateral plain radiograph (A). Sagittal T2-weighted MR image (B). Sagittal reformatted CT scan (C). Also evident in B is spinal cord expansion and edema (asterisk), a damaged disc having high signal intensity (arrowheads), some prevertebral hematoma (curved arrow), and a torn posterior longitudinal ligament appearing as an interruption (solid arrow) of the low signal intensity band along the posterior margin of the spinal canal.

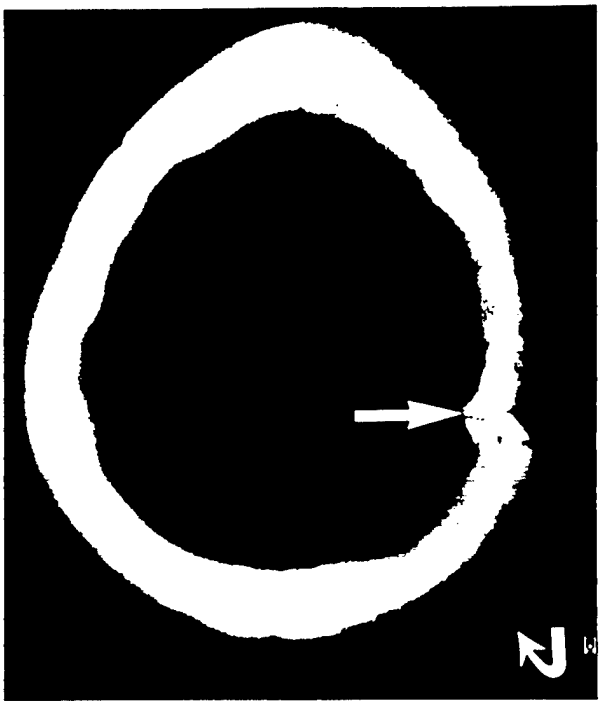

Figure 1: Depressed skull fracture (straight arrow) and soft tissue swelling (curved arrow). Axial CT filmed with a "bone" window technique.

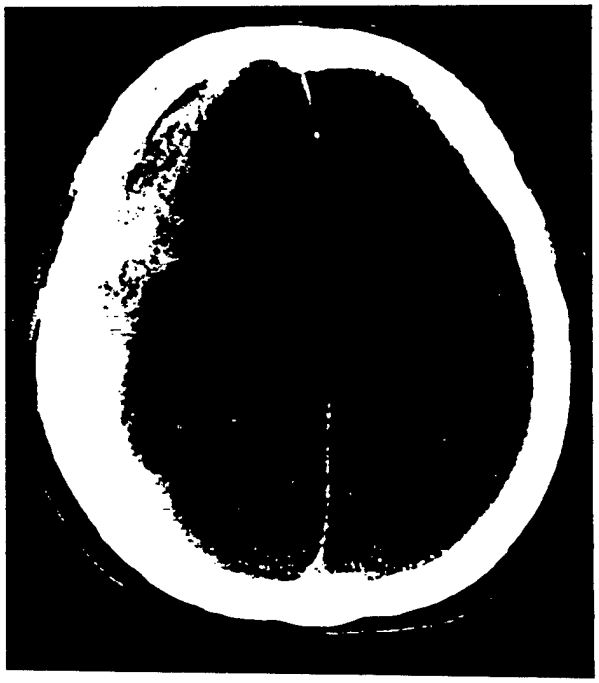

Figure 2: Acute high density subdural hematoma appearing crescentic (long arrows), causing subfalcine herniation (curved arrows), and displacing the contralateral lateral ventricle (short arrow). Axial CT.

Figure 3: Acute epidural hematoma appearing lens-shaped (arrows), and having heterogeneous density due to blood of different ages. Axial CT.

Figure 4: Acute subarachnoid hemorrhage (arrows) appearing as high density fluid in the basal cisterns. Axial CT.

Figure 5: High density hemorrhagic cortical contusion (arrow) at the medial temporal lobe. Axial CT.

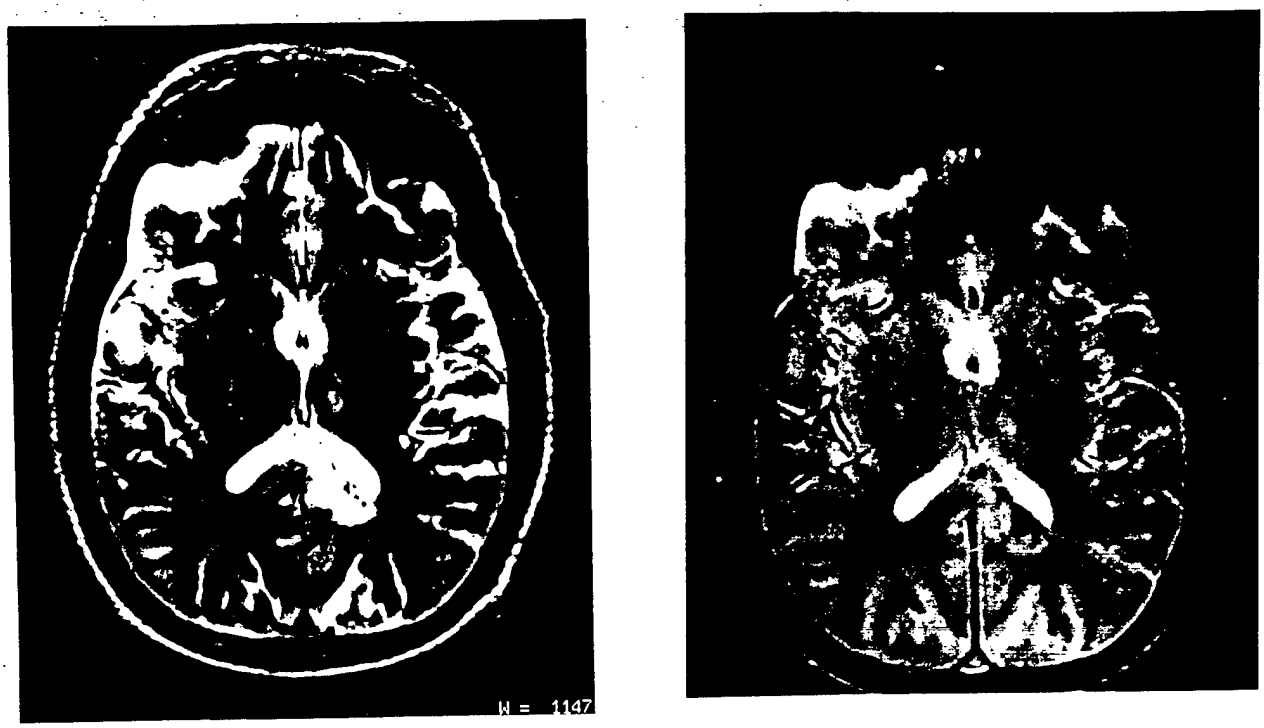

Figure 6: Shearing injury in the corpus callosum having adjacent high signal intensity edema (short arrows) as shown in A, a T2-weighted fast spin echo MR image and a hemorrhagic component (long arrow) best shown as a low signal intensity area in B, a T2-weighted gradient echo MR image.

Figure 7: Transtentorial herniation (long arrows) resulting in obliteration of the basal cisterns and causing an area of brainstem hemorrhage (short arrow). Axial CT.

Figure 8: Diffuse cerebral edema resulting in effacement of some cerebral sulci and poor grey and white matter differentiation.

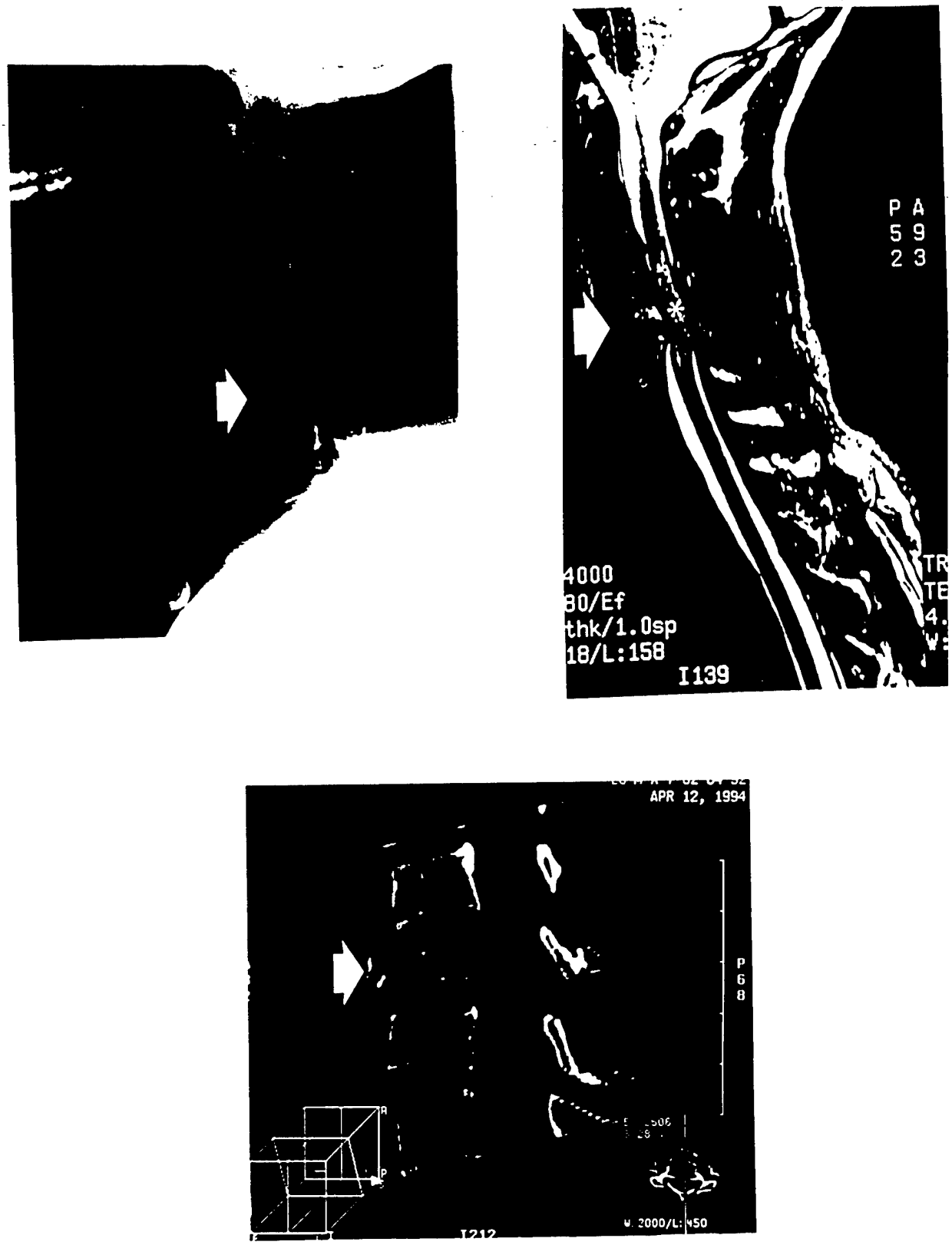

Figure 9: Comminuted fracture of the C5 vertebral body (arrow) in a lateral plain radiograph (A). Sagittal T2-weighted fast spin echo MR image (B). Sagittal reformatted CT scan (C). In B, spinal cord expansion and edema having high signal intensity (asterisk) are shown.

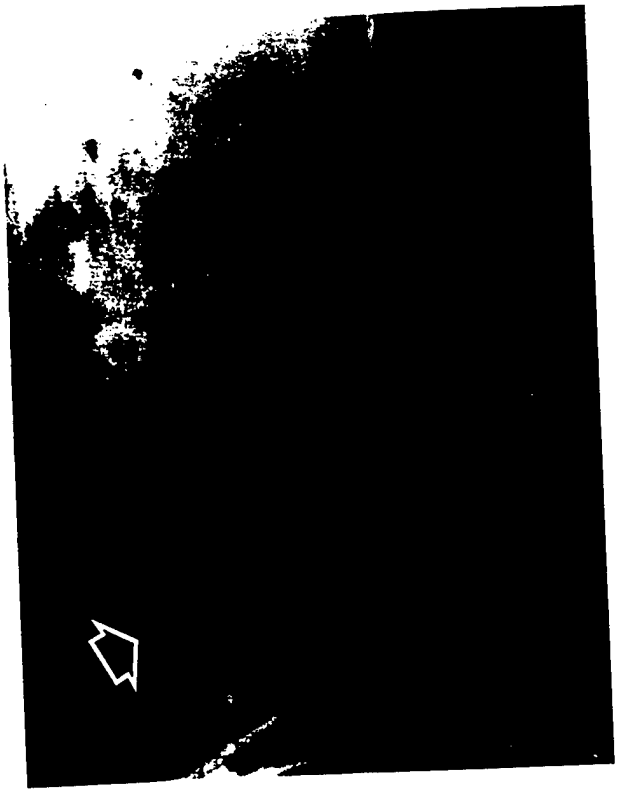

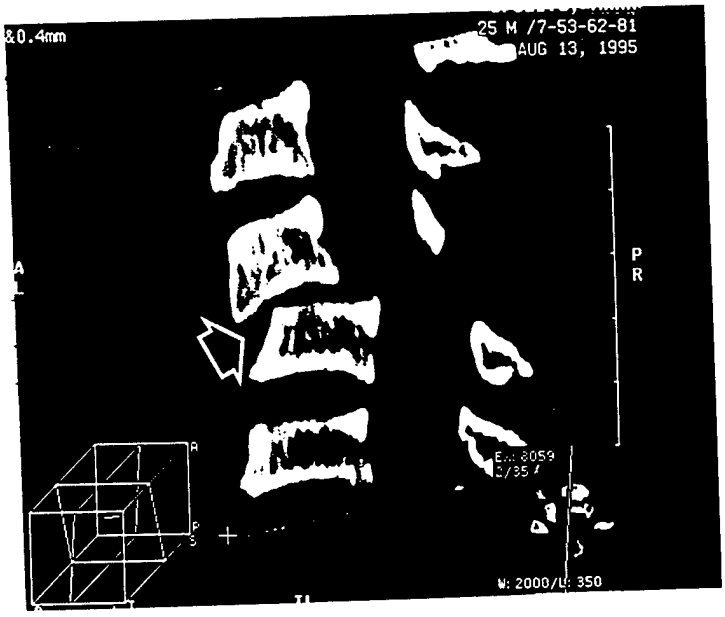

Figure 10: Fracture deformity with malalignment at C4-C5 (open arrow) in a lateral plain radiograph (A). Sagittal T2-weighted MR image (B). Sagittal reformatted CT scan (C). Also evident in B is spinal cord expansion and edema (asterisk), a damaged disc having high signal intensity (arrowheads), some prevertebral hematoma (curved arrow), and a torn posterior longitudinal ligament appearing as an interruption (solid arrow) of the low signal intensity band along the posterior margin of the spinal canal.

CIVILIAN FIREARM

SPINAL CORD INJURY

Denise M. Lemke, James P. Hollowell, Dennis J. Maiman

Abstract

Firearms are among the leading cause of spinal cord injuries in the United States. In many cities, firearm injuries are the most common etiology; nationally, they are the third leading cause. Pathogenesis of the neurological injury is related to direct crush injury or from shock waves. Twenty percent of firearm-related SCI's occur in the cervical spine, 50 percent in the thoracic and 30 percent in the thoracolumbar. Recovery of function is seen less commonly than in patients with fractures. Early management is focused at stabilizing the patient from the typical multiple trauma. Entrance and exit wounds are debrided. SCI patients typically are not given methylprednisolone . Radiography, including myelography and plain films, is typically necessary to precisely find the lesion. Surgery is rarely indicated as neurological improvement cannot be expected to occur. Rather, orthoses are often used to enhance healing of the fracture. At the Medical College of Wisconsin hospitals between 1989 and 1993, 268 patients were admitted with central nervous system trauma due to firearms. Of these, 24 percent were isolated to the spine. Violent crime was the most common cause. C2 was observed to be an increasingly common level of complete spinal cord injury. Lengths of stay were significantly higher than for fracture-related spinal cord injury. Treatment costs ranged from $22,000 to $519,000, with an average reimbursement rate to the hospital of 23 percent. Over 88 percent had public funding only. Wounds to the spinal cord will continue to be a common and extremely expensive cause of spinal cord injury, representing an ongoing epidemic in our cities.

1. Violence in the United States

The right to bear arms is a constitutional right of every American. Since our country's inception, Americans have maintained a strong attachment to firearms. They were used by the early settlers as a means of survival in obtaining food, protection and safety. As the country grew and settlers moved West, firearms continued to be vital tools in their survival. Before the

establishment of the legal system, the firearm was the first choice for settling any type of dispute. The issue of firearm control began with the early establishment of the legal system, yet there was little debate over one's right to bear arms. There has been less and less need for the firearm in our daily life as our culture has evolved, yet the ownership of firearms by civilians is on the rise. Currently, approximately 120-200 million firearms are in the possession of individuals. Approximately 30 percent of the firearms owned by civilians are handguns and account for 90 percent of homicides. Assault weapons account for 10.5%, and the remainder are rifles and shotguns [1-12]. Forty-three to fifty percent of homes have at least one loaded firearm with 25 to 30 percent containing two or more [1,3,5,6,8]. Firearms provide a sense of "safety" to the home owner, yet the risk is 43 times higher that an occupant of the home will be injured by the firearm than the criminal, and suicide risk is five times greater in a home that has a firearm [6,8-9,12,13]. Firearms are now the third leading cause of trauma-related death of our youth, exceeded only by motor vehicle crashes (MVC) and drowning. Thirty percent of homes where a child lives have firearms; this raises the risk for the child to suffer an unintentional injury [1,5-7,9,12,14-16]. There are approximately 732 shootings a day in the US and for every fatal injury there are 5 to 13 nonfatal injuries [2,5,8-9,12,14-19]. Cities now have classified "war zones" when gang and crime-related activity limits the traffic patterns [10,20]. Firearms have become a symbol of power and control in these inner city war zones, and provide a means to secure and defend gang territory. Gang-related violence and inner city crime takes on new meaning with 96 percent of related homicides committed with a firearm in Los Angles County alone. Approximately 26 percent of victims of gang-related homicides have no history of gang affiliation [20]. There is also speculation that gang-related shootings have shifted from the intent to kill to the intent to maim, with an increase in firearm-related spinal cord injuries, especially respirator-dependent tetraplegia. Black males are at the highest risk and are seven times more likely to be killed by a firearm than white males. Just as alcohol is a major contributing factor in MVC, 80 to 85 percent of individuals involved in firearm-related injuries have reportable alcohol or drug levels [7,9-11,15,17,19,21-22]. The injuries, while severe, generally do not cause death in the field requiring the need for emergency medical care [19,20,23-24]. Song et al., detracted the costs for acute emergency care in gang-related shootings for a population of 272 in a 27 month period as $4,828,828 or $5,550 per day for survivors and an average charge of $8,902 for individuals who died after sustaining a firearm injury. Nationally, 85 percent of cases are funded with public aid programs that computes to a reimbursement rate of 23.6 percent [4,7,20].

2. SCI and Firearms

In Wisconsin, firearm injuries rank second to MVC as the leading cause of fatalities [5]. Nationally, firearm-related spinal cord injury (SCI) is the third leading cause and accounts for 13 percent of the population [4,8,25-26]. In comparison, SCI secondary to firearms occurred at a nine percent rate during a 32 month period in the Croatian War, with no reported SCI secondary to firearms during Operation Desert Storm [2,15]. The extent of injury to the spinal cord is related to the velocity of impact, size and type, fragmentation of the missile, and the missile path within the body, spinal column and spinal cord. The kinetic energy defines the extent of damage created by a missile, taking into consideration the mass and velocity. Increasing the velocity or mass will directly increase the missile's wound forming capability [1,17,21-22,25-27]. Tissues can be injured from direct crushing injury or a combination of shock waves and cavitation. Direct tissue injury or crush occurs at the point of entrance and potentially at the exit. A series of waves form as the missile enters a mass, the first is a sonic wave that precedes the missile and creates no displacement or permanent injury to the structure. The secondary wave formation creates a cavitation, displacing tissues and creating increased wounding capabilities. The extent of the injury is directly related to the amount of tissue displaced and the type of tissue cavitated, inelastic (liver) versus flexible tissue (muscle, bowel, lung). Inelastic tissue is more prone to structural disruption because of its lack of flexibility. Secondary cavitation occurs along the path of least resistance, destroying tissue planes by separating tissues that are fixed. The permanent cavity is the result of

tissue, vascular and muscular injury created by the temporary cavitation. In addition, missile impact at the spinal column creates contusive injuries to the cord. The missile itself need not enter the spinal cord to cause traumatic injury [8,22,25-27]. Commonly, the fracture occurs from actual impact of the missile with approximately 33 percent of missiles lodging in the canal. Twenty percent in the cervical, 50 percent in the thoracic, and 30 percent are in the thoracolumbar spines. Seventy-five percent of the patients are paraplegic; 50 percent of the injuries are complete. Recovery of function is seen in 25 percent in complete lesions and 33 percent in incomplete lesions [4,6,8,22,25-27]. The greatest area of documented improvement is injuries sustained in the cervical region.

3. Cost

Average lifetime medical costs are $570,000 for tetraplegia. With approximately 177,000 persons with SCI in the US in 1990, the annual cost of SCI nationally was over 100 billion dollars [4,8,25]. There is limited data nationally on the overall costs associated with traumatic SCI that incorporate the initial trauma care through discharge from rehabilitation. Harvey et al., calculated the initial two years estimated cost for traumatic SCI by surveying various national institutions over an eight year period (1980-1988). The study estimated average hospital costs at $95,203 in isolated SCI and estimated costs of $8,208 for home modification. Other costs include $7,866 a year for services, supplies and adaptive equipment, and $6,269 for assisted care versus institutionalized care.

4. Medical Management

The early focus in the emergency room (ER) aims at stabilizing the patient hemodynamically while maintaining spine precautions. Field assessment will assist in the triage of the patient within the ER to speed appropriate consults. General assessment in the ER is performed to identify additional injuries, assessment of entrance and exit wounds, and should include a complete neurological assessment using the American Spinal Injury Association (ASIA) [8,25-26,28]. The ASIA criterion allows for uniform delineation of functional level 1. Drugs used in the ER may include vasopressors and prophylactic antibiotics. The utilization of methylprednisolone aimed to prevent secondary injury in the general traumatic SCI population, is felt to have limited positive effects on SCI related to firearm injuries and therefore, is not recommended if the spinal cord is involved. However, for bony injuries without canal involvement, steroids are commonly used. Recent drug studies have also excluded firearm injuries from their data collection. Radiographs are performed to determine the extent of injury including the evaluation of the spinal cord, presence of bone fragments, dural injury and spinal instability. Once stability of the spine is proved, the focus of treatment is aimed at the rehabilitation of the patient. Early mobilization and early rehabilitation limit complications associated with bedrest and may improve functional recovery. Orthoses are needed in cases that require surgical stabilization secondary to instability, although the orthosis may be used on an as needed basis for pain management.

5. Surgical Intervention

Surgical intervention in those with firearm-related SCI remains a hotly debated issue. Theoretically, surgical removal of the missile is directed at prevention of complications associated with cerebrospinal fluid leaks, infection, meningitis, pain, migration of missile and neurological decline. However, wound infection and meningitis are rare even with missile retention, and there is no evidence that removal of the missile will lead to neurological improvement. Advocates of nonoperative treatment limit surgical intervention to persistent CSF leaks and the rare patient with

incomplete injuries where the missile acts as a compromising mass [8,22,25-26]. Waters et al., found limited evidence that removal of the missile improves functional motor outcome or post-injury pain syndromes and that surgery may increase dysesthetic pain syndromes. Conversely, Yosida et al., refers to the collaborative 1984 study by the National Spinal Cord Injury Model Systems that demonstrated significant improvement in missiles removed from the thoracolumbar spine. Spinal instability is rare after firearm injuries, and if present, is usually related to transverse fractures of bilateral facets or pedicles. Thus, surgery for spinal stabilization is rarely indicated and requires definitive radiographic evidence of spinal instability.

6. Wisconsin Experience

Two hundred sixty-eight patients were admitted to the Neurosurgery service from July 1989 through June 1993 with firearm induced injuries to the central nervous system. Injuries were classified as head or spine, the latter with or without neurological compromise. Chart was reviewed for demographics, presence of illicit drugs and alcohol, circumstances of injury, geographic location of shooting, location of injury, associated injuries, surgical intervention, complications and length of stay. Sixty-six percent of the injuries were isolated to the head and 24 percent involved the spine. Death rate was 52 percent for isolated head injuries while no deaths occurred from spinal injuries, with or without SCI. The most common identified circumstance of the shooting was violent crime that included domestic and gang-related disputes, homicide attempts with known and unknown assailants and victims of crime-related activity as in robbery. The specifics of injury were often obscured by the reluctance of the victim to discuss events. The mean patient age was 26 years (range: 13 to 59 years). Eighty-six percent of the patients were males and accounted for 93 percent of violent crimes. Fifty percent of the injured were under the influence of drugs and/or alcohol. The overall breakdown of the circumstance of shooting included suicide attempt (4.3%), accidental (4.3%), attempted homicide and/or violent crime (89%), and law enforcement sequelae (2.2%). Racial analysis revealed 22.4 percent of the victims were white, 65.5 percent African-American, 8.6 percent Hispanic, and 3.5 percent other. Specific characteristics of the injuries revealed that 54 percent of victims were shot from the front, 28 percent from behind and 18 percent from the side, without significant right or left side predominance. Only six percent of the individuals demonstrated an exit wound. Seventy-one percent incurred a single wound while 29 percent of individuals suffered multiple wounds. Analysis of the location of spinal injuries revealed 14 percent occurred at the cervical level, 70 percent at the thoracic level, and 16 percent at the lumbar level. Forty-six percent of individuals suffered incomplete SCI; 54 percent were complete SCI; 75 percent were paraplegic, 25 percent were tetraplegic. T12 was the most common level of injury for complete and incomplete paraplegia with seven individuals in each category. Eighty-five percent of tetraplegics suffered a complete injury. C2 was the most common level of complete SCI in the tetraplegia group with three individuals, followed by C5 with two individuals. All C2 tetraplegics were close-range assaults; all had posterior entrance wounds and represented deliberate efforts to produce C2 tetraplegia. Hospitalization, for the purpose of this study, is defined as admission to the trauma room until discharge after acute rehabilitation. Length of stay (LOS) was 8 to 173 days with a mean of 60 days. Acute care LOS averaged 23 days and rehabilitation LOS averaged 36 days. Length of stay varied relative to level of injury and health care needs. Total hospitalization in the ventilator tetraplegic ranged from 97 to 173 days with the average for 1993 at 117 days. Nonventilator tetraplegics LOS ranged from 55 to 90 days.

7. Economic Factors

Treatment costs ranged from $22,789 to $519,314. The mean total for the study group was calculated at $111,131 per individual. The $519,314 figure reflects the cost for an individual who suffered a missile injury to the neck rendering the individual a C2 ventilator dependent

tetraplegic in the year 1991. The addition of a ventilator adds $400.00 per day to the treatment costs bringing the average charge for a ventilator dependent tetraplegic to $330,118, or three-fold the mean cost in this study. Total treatment costs were $6,334,085 with actual reimbursement of $2,550,260, a collection rate of less than 40 percent. Public funding was the sole support for 88.8 percent of these patients. Medicaid accounted for 71.4 percent of this amount. The remaining 13.4 percent was a Wisconsin based public funding program entitled Victim of Crime. Commercial insurance payers represented only 2.2 percent of the entire group, with a reimbursement rate of 51.5 percent. Public funding received reimbursement at a rate of 23.6 percent. Actual recovered costs averaged $19,000 per patient for a total reimbursement of $2,550,260 for the 57 individuals.

8. Prevention

If one addresses the pattern of firearm injuries in the US and utilization of health care resources, preventing firearm injuries should be an economic and health care focus. Treatment of victims of trauma is essential to our society; prevention is viewed as key in decreasing the number of traumatic injuries and optimizing the health care cost [1,3,7,12,14,16,24]. Prevention can take the form of paternalistic intervention as in the enforcement of the seatbelt law, enforcement in the drunk driving laws or as advocacy groups (MADD, Think First) which promote programs in education and awareness. The methods used in firearm awareness are debatable, though with the continued decline in fatalities related to motor vehicle crashes, one has to consider the positive effects of these preventive programs. In the past, firearm safety programs have not resulted in any correlation with decreased unintentional injury. Indeed, studies of firearm owners following such programs show that owners are more likely to store their firearms loaded and unlocked [23]. The Brady Act attempted to provide a means to control the continued influx of weapons on the street by requiring a five day waiting period to allow for a police check on firearm purchases. This only addresses the legitimate individual purchasing a firearm and falls short of the desired intent of eliminating firearms on the street. The majority of firearms on the streets are bought illegally. Present laws require an individual to be 21 to purchase a firearm; studies in Illinois and Wisconsin, report that 33 percent of male high school juveniles own a handgun [21,24]. Many cities have offered "gun buy back" programs, and in Wisconsin over 100 firearms were returned from juveniles alone in a one year period. Financial costs to society for medical costs as well as public assistance are an increasing burden [1,3,12,16-17]. Because public funding provides reimbursement at only 24 percent, the treating hospitals are subjected to significant unreimbursed costs. This impacts directly on the economic stability of our society and stresses the need for ongoing intervention aimed at preventing injuries. Prevention appears to be essential and further development of programs aimed at firearm awareness are needed to alter the present course of violence within our society.

Defining the "War Zone" may avert some firearm injuries, though the use of firearms in the inner cities is increasingly commonplace to the point of being a primary source of death in our minority populations. Education is self-limiting as preventive programs are geared to the middle class population and do not address the crux of the problem: poverty, illegal drug trafficking, gang-related activities, limited parental or extended family support, family violence and an increasing lack of respect of life [3]. Thus, educational programs promoting firearm control are self-limiting and other solutions will have to be brought forth.

References

[1] Blendon RJ, Young JT, Hemenway D. The American public and the gun control debate. *JAMA* 1996:275: 1719-1722.

[2] Carey MC. Analysis of wounds incurred by US army seventh corps personnel treatment in corps hospitals during operation desert storm, February 20 to March 10, 1991. *J Trauma, Injury, Infection & Critical Care* 1996:40: S165-S169.

[3] Conway T. The internist's role in addressing violence. *Arch Intern Med* 1996:156: 951-956.

[4] Harvey C, Wilson SE, Greene CG, Berkowitz M, Stripling TE. New estimate on the direct cost of traumatic spinal cord injuries: Results of a nationwide survey. *Paraplegia* 1992:30: 834-850.

[5] Katcher ML. Firearm injuries among children and adolescents: I. The facts. *Wisconsin Medical Journal* 1994:93(10): 511-515.

[6] Kellermann AL, Reay DT. Protection or Peril? An analysis of firearm-related deaths in the home. *New Eng J Med* 1986:314: 1557-1560.

[7] Koop CE, Lundberg GD. Violence in America: A public health emergency. Time to bite the missile back. *JAMA* 1992:267: 3075-3076.

[8] Landy HJ, Arias J, Green B. Penetrating Injuries In Contemporary Management of Spinal Cord Injury. ED Benzel, (ed). *Amer Assoc Neurosurgical Surgeons*, Park Ridge, IL., 1995: 177-185.

[9] Ordog GJ, Wasserberger J, Ackroyd G. Hospital costs of firearm injuries. *J Trauma Injury, Infection & Critical Care* 1995:38(2): 291-298.

[10] Sayre JW. Gunshot violence in the united states: A growing threat to all. A Physician's personal view. *Bulletin New York Academy of Medicine* 1995:72: 31-45.

[11] Velmahos GC, Degiannis E, Hart K, Souter I, Saadia R. Changing profiles in spinal cord injuries and risk influencing recovery after penetrating injuries. *J Trauma Injury, Infection and Critical Care* 1995:38: 334-337.

[12] US Department of Health and Human Services, Healthy People 2000: National Health Promotion and Disease Prevention Objectives. 1990: 226-282.

[13] Wintemute G, Hancock M, Loftin C. Policy options on firearm violence. In: *Improving the Health of the Poor: Strategies for Prevention.* SE Samuels, MD Smith (eds). 1992: 80-96.

[14] Injury Prevention: Meeting the Challenge. National Committee for Injury Prevention and Control. *Amer J Preven Med* 1989:5(3): 261-267.

[15] Rukovansjki M. Spinal cord injuries caused by missile weapons in the Croatian war. *J Trauma, Injury, Infection & Critical Care* 40(3): S189-S192.

[16] US Department of Health and Human Services, The Third National Injury Control Conference: Prevention of Violence (Position Paper) 1991: 188-198.

[17] Fackler ML. Gunshot wound review. *Ann Emerg Med* 1996:28: 194-203.

[18] National Committee for Injury Prevention and Control. Injury Prevention: Meeting the Challenge; Firearm injuries. *Amer J Prev Med* 1995:5: 261-261.

[19] Vasser MJ, Kizer K. Hospitalization for firearm-related injuries: A population-based study of 9562 patients. *JAMA* 1996:275: 1734-1739.

[20] Song DH, Naude GP, Gilmore DA, Bongard F. Gang warfare: The medical repercussions. *J Trauma, Injury, Infection & Critical Care* 1996:40: 810-815.

[21] Kellermann AL, Lee RK, Mercy JA, Banton J. The epidemiological basis for the prevention of firearm injuries. *Ann Rev Public Health* 1991:2: 17-40.

[22] Yosida GM, Garland D, Waters RL. Gunshot wounds to the spine. *Orthopedic Clinics of North America* 1995:26: 109-116.

[23] Sinauer N, Annest JL, Mercy, JA. Unintentional, nonfatal firearm-related injuries: A preventative public heath burden. *JAMA* 1996:275: 1740-1743.

[24] Webster DW, Chaulk CP, Teret SP, Wintemute G. Reducing firearm injuries. *Issues in Science and Technology* 1991: 73-79.

[25] Waters R. Gunshot wounds to the spine: The effects of the missile fragments in the spinal canal. *J Amer Paraplegia Society* 1984:989: 30-33.

[26] Waters RL, Hu SS. Penetrating Injuries of the Spinal Cord. In: *The Adult Spine: Principles and Practice.* JW Frymoyer (ed). Raven Press, Ltd, New York, 1991: 815-826.

[27] Valsamis MP. Pathology of trauma. *Neurosurgery Clinic of North American* 1994:5: 175-183.

[28] American Spinal Injury Association (ASIA) International Medical Society of Paraplegia (IMSOP). International Standards for Neurological & Functional Classification of Spinal Cord Injury. Chicago, IL: ASIA/IMSOP, 1992.

DYNAMIC COMPARISON OF THE HYBRID III AND HUMAN NECK

Anthony Sances, Jr.

Abstract

The dynamic axial compressive responses of the Hybrid head-neck were compared with the intact human cadaver head-neck complex. The Hybrid III head-neck was tested under dynamic loading at rates up to 7.2 m/s. Inertially compensated forces, axial deformations and distal generalized six-axis load cell histories were gathered at dynamic sampling rates. The localized axial compressions of the neck were obtained using retroreflective target information and high-speed photography. The Hybrid III dummy responded with nonlinear and rate stiffening characteristics with minimal initial softening. This was in contrast to the human cadaver tissues wherein initial softening characteristics were present in the force-deformation curves. The Hybrid III neck was found to be at least two times stiffer compared to the human under similar dynamic axial compressive loading. Furthermore, the shape of the Hybrid III force-deformation response was different from the human cadaver tissues. These differences must be included to properly extrapolate the results from the Hybrid III to predict injury in real-world vehicular crash environments.

1. Introduction

Anthropomorphic test devices, often called manikins, are used to predict injury in crash environments such as motor vehicle rollovers. Injuries are predicted using mechanical indices such as forces and moments. The indices are obtained from studies including human cadaver tissue experimentation under different modes of external loading. To realistically estimate trauma, the dummy should be biofidelic, i.e., the response should mimic the human. The widely used Hybrid

III dummy is based on the biomechanical data from the 1970s [1]. It was developed to predict injury in frontal impact. The vehicular environment at that time was predominantly unrestrained. Since then, numerous biomechanical studies have been conducted to determine the response of the human and human cadaver tissues under different modes from quasi-static to dynamic rates of loading [1-10]. This study describes the response of the dummy neck at higher real-world rates of axial loading for comparison with the dynamic human cadaver corridors [5].

2. Materials and Methods

Axial compressive loading tests were conducted using the Hybrid III dummy head-neck system using a custom-designed electrohydraulic testing device. The Hybrid III head-neck preparation was placed on the platform of the testing apparatus via a six-axis load cell at the base. Retroreflective targets were attached to the aluminum rings at every level of the neck. Targets were also attached to the head and piston of the testing device. Accelerometers were fixed to the head and the piston. Tests were conducted at loading rates up to 7.2 m/s. The load was applied to the top of the unconstrained head. Initially, the piston was allowed to travel in the air and after attaining the desired velocity, the piston impacted the head. The test was documented with a high-speed video camera (4500 full frames/sec). The piston force, acceleration and displacement as a function of time, were recorded with the uni-axial force gage, the accelerometer and the linear variable differential transformer attached in-series with the actuator of the testing apparatus, respectively. The generalized force and moment histories from the upper neck and distal six-axis load cell were gathered as a function of time. All data were collected digitally according to the SAE J211b specifications. Retroreflective target data provided the local deformations of the neck. Data processing included the derivation of the force-deformation responses. These force-deformation curves at different dynamic rates of loading were compared with similar data obtained from human cadaver tests.

3. Results

The input force-deflection responses were nonlinear at all loading rates. With increasing loading rates, the inertially compensated loads from the piston force gage were higher than the forces recorded by the six-axis load cell at the distal end (Figure 1) and the upper neck load cell that was similar. A review of the high-speed video photography and target analysis indicated the following: the head-neck system responded with an initial deformation of the head followed by the compressions from the neck segments. Relatively uniform compressions of the different neck segments (evidenced by the shortening of the rubber between the aluminum rings) occurred throughout the loading process. The Hybrid III head-neck system demonstrated stiffening with increasing rates of loading. The Hybrid III neck was at least two times stiffer than the human cadaver tissues under similar dynamic axial compressive loading.

4. Discussion

An earlier study demonstrated the differences between the axial compressive response of the Hybrid III head-neck system and the human tissue under compressive loading at low rates of force application [9]. The Hybrid III was shown to be three to four times stiffer compared to the human cadaver tissue, suggesting an over-estimation of the forces at a specific deflection level. Further, with loading rates from 2.54 to 254 mm/s, this earlier study indicated that the Hybrid III dummy neck increases in stiffness. McElhaney et al., reported that the Hybrid III dummy neck is significantly stiffer than the human cadaver cervical spine with slowly applied quasi-static type combined bending and axial loads. This study included compression-flexion, tension-flexion, compression-lateral bending, tension-lateral bending, compression-extension and tension-

extension [3]. Myers et al., reported that the Hybrid III dummy neck is 10 to 50 times stiffer than the human cadaver depending on the end condition [4]. In frontal impact simulations under dynamic loading, studies have shown that the Hybrid III neck "is much too stiff" [11-12]. Similar observations were noted in this series of dummy tests at higher rates of axial loading. The compressions of the Hybrid III dummy neck are relatively uniform under dynamic loading compared to nonuniform local deformations of the intact human cadaver head-neck complex under similar axial compressive loads [5]. These differences are caused by the variations in the local/segmental stiffnesses of the human cervical spine that are not included in the construction of the Hybrid III neck. The human cadaver corridors consistently indicated an initial softening phase that was not present in the Hybrid III [6]. These differences in the stiffness, initial softening, deformations along the length of the dummy neck and the shape of the force-deformation curves must be included to extrapolate the results the human. White et al., developed an advanced dummy neck that includes the well-known human head-lag (not present in Hybrid III dummy) and presents an improvement in the flexion and the extension responses [11,13-14]. However, the differences were higher in the axial compressive stiffness characteristics at the higher loading rates. The Hybrid III does not reliably predict injury for rear-end collisions. For this purpose, the rear impact dummy (RID) was developed. However, it is limited to low-speed impacts [14]. For better injury prediction, an improved dummy head-neck system should be developed to account for the differences in the dynamic axial compressive characteristics.

Acknowledgment: This study was supported in part by the Department of Veterans Affairs Medical Research Service.

References

[1] Foster JK, Kortge JO, Wolanin MJ. A biomechanical based crash test dummy. In: *Proceedings 21st Stapp Car Crash Conference*, New Orleans, LA, October 19-21, 1977, pp 973-1014.

[2] Ewing CL, Thomas DJ, Sances A Jr, Larson SJ (eds). *Impact Injury of the Head and Spine*. CC Thomas, Springfield, IL, 1983: 785 pp.

[3] McElhaney JH, Doherty BJ, Paver JG, Myers BS, Gray L. Combined bending and axial loading responses of the human cervical spine. In: *Proceedings 32nd Stapp Car Crash Conference,* Atlanta, GA, October 17-19, 1988, pp 21-28.

[4] Myers BS, McElhaney JH, Richardson WJ, Nightingale RW, Doherty BJ. The influence of end condition on human cervical spine injury mechanism. In: *Proceedings 35th Stapp Car Crash Conference*, San Diego, CA, November 18-20, 1991, pp 391-399.

[5] Pintar FA, Sances A Jr, Yoganandan N, Reinartz JM, Maiman DJ, Suh JK, Unger G, Cusick JF, Larson SJ. Biodynamics of the total human cadaver cervical spine. In: *Proceedings 34th Stapp Car Crash Conference*, Orlando, FL, November 4-7, 1990, pp 55-72.

[6] Pintar FA, Yoganandan N, Voo LM, Cusick JF, Maiman DJ, Sances A Jr. Dynamic characteristics of the human cervical spine. *SAE Transactions* 1995:104(6): 3087-3094.

[7] Sances A Jr, Myklebust JB, Maiman DJ, Larson SJ, Cusick JF, Jodat R. The biomechanics of spinal injuries. *CRC Crit Rev Bioeng* 1984:11: 1-76.

[8] Sances A Jr, Thomas DJ, Ewing CL, Larson SJ, Unterharnscheidt F (eds). *Mechanisms of Head and Spine Trauma*. Aloray, Goshen, NY, 1986: 746.

[9] Yoganandan N, Sances A Jr, Pintar FA. Biomechanical evaluation of the axial compressive responses of the human cadaveric and manikin necks. *J Biomech Eng* 1989:111(3): 250-255.

[10] Sances A Jr, Myklebust JB, Larson SJ, Cusick JF, Weber RC, Walsh PR. Bioengineering analysis of head and spine injuries. *CRC Crit Rev Bioeng* 1981:2(15): 1-79.

[11] Seemann MR, Muzzy WH, Lustick LS. Comparison of human and Hybrid III head and neck dynamic response. In: *Proceedings 30th Stapp Car Crash Conference*, San Diego, CA, October 27-29, 1986, pp 291-311.

[12] Svensson MY, Lovsund P. A dummy for rear-end collisions - Development and validation of a new dummy neck. In: *International Conference on the Biomechanics of Impacts*, Verona, Italy, 1992: 299-310.

[13] Thunnissen J, Wismans J, Ewing C, Thomas DJ. Human volunteer head-neck response in frontal flexion: A new analysis. In: *Proceedings 39th Stapp Car Crash Conference*, Coronado, CA, November 8-10, 1995, pp 439-460.

[14] White RP, Zhao Q, Rangarajan N. Development of an instrumented biofidelic neck for the NHTSA advanced frontal test dummy. In: *15th International Conference on Experimental Safety of Vehicles*, Melbourne, Australia, 1996, pp 1-13.

Figure Caption

Figure 1: Light bar corresponds to average dynamic stiffness (N/mm) for 20 human cadaveric head-neck complexes tested at 3 to 8 m/s [6]. Dark bars correspond to dynamic stiffness (N/mm) of the Hybrid III head-neck system at 0.9 m/s, 5.7 m/s and 7.2 m/s. All are for vertical compression loading tests .

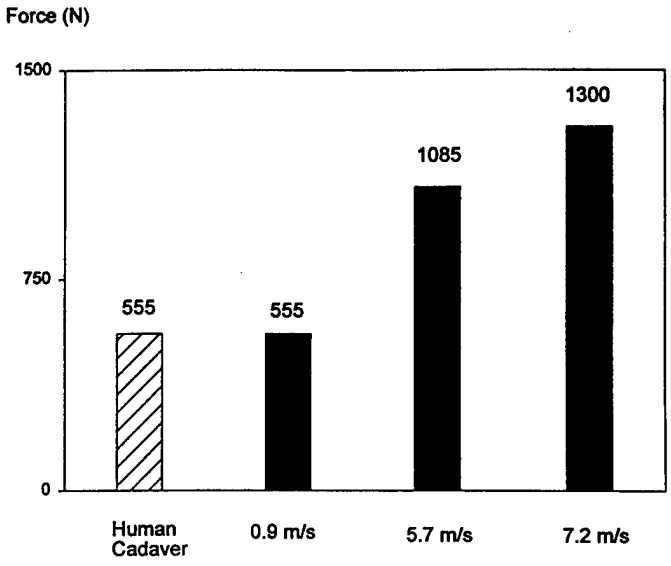

Figure 1: Light bar corresponds to average dynamic stiffness (N/mm) for 20 human cadaveric head-neck complexes tested at 3 to 8 m/s [6]. Dark bars correspond to dynamic stiffness (N/mm) of the Hybrid III head-neck system at 0.9 m/s, 5.7 m/s and 7.2 m/s. All are for vertical compression loading tests .

EXPERIMENTAL SYSTEM TO INVESTIGATE WHIPLASH INJURY BIOMECHANICS

Anthony Sances, Jr.

Abstract

Substantial experimental cervical spine biomechanics studies have been conducted using slowly applied forces/moments or dynamically applied forces with contact. In contrast, few studies have been conducted to delineate the biomechanics of the structure under inertial "noncontact" type whiplash forces. An experimental methodology to induce inertial loads is reported in this chapter. A mini-sled pendulum system was designed to test specimens (e.g., intact human cadaver head-neck complex) at sub-failure or failure levels under loading modalities such as flexion, extension and lateral bending. The system allows acceleration input with varying wave-forms. The system can dynamically record the input and output strength information such as forces, accelerations, moments and angular velocities. It can also obtain the temporal overall and local kinematic data of the cervical spine segments. This system permits a total biomechanical structural analysis of the cervical spine under whiplash or other modes. In this chapter, the feasibility of the methodology is demonstrated by subjecting the human cadaver head-neck complex with musculature and skin to inertial flexion and extension. This method can be used to compare the human data and advanced dummy designs.

1. Introduction

Biomechanical evaluations of the human cervical spine are routinely conducted in a laboratory environment using mathematical and/or human cadaver experimental models [1-5]. These include an isolated component (e.g., ligament), intervertebral joint (e.g., functional spinal unit), intact ligamentous column (e.g., C2-T1 spine), and intact head-neck complexes with and without the accompanying passive musculature. Depending on the type of

evaluation and the level of complexity, these models delineate the "passive" biomechanical response. Routinely, quasi-static load vectors (e.g., pure moment) have been used to induce the external loading (insult) at sub-failure levels to define parameters such as sagittal rotations and instability [3]. Recent studies have described the mechanisms of injury under traumatic forces induced by high-speed dynamic loading [6-7]. These studies have replicated severe neck injuries such as wedge and burst compression fractures encountered in a clinical environment. These types of insults belong to the "contact type" force application. It is well known that the human neck can be traumatized under dynamic forces applied to the structure in an inertial mode, i.e., impact forces are not directly applied via contact [8-12]. To better understand the structural mechanics of the human head-neck complex, it is important to apply these noncontact type forces in a controlled environment. A methodology is reported in this chapter to induce inertial loading to an *in vitro* experimental model. In addition, it was designed to allow for multi-axis (flexion, extension, lateral bending) and multiple acceleration/deceleration testing at sub-failure and failure levels with varying wave forms (G-time histories). The methodology permits analysis of the temporal structural kinetics and the related pathoanatomical alterations.

2. Materials and Methods

A mini-sled pendulum system was designed to house the specimen (e.g., human cadaver head-neck complex) and the loading assembly. The mini-sled consists of two 2.5 m long precision ground rails rigidly attached to a 1.5 m high steel frame. Four precision rolled ball bearings form the interface between the cart assembly and the rails. The cart assembly was designed to accept a six-axis load cell and allow for a vertical axis of rotation of the specimen to permit different loading modes. A flat surface was attached to the cart assembly to accept the impact from the pendulum. The hollow cylindrical pendulum impactor assembly was designed to accept varying masses. A load cell was attached at the leading face of the impactor. Varying energy absorbing material surfaces can be fixed to its face [13].

An accelerometer was rigidly attached to the rear face of the pendulum. A uniaxial load cell was attached to the leading face of the impactor to record the input longitudinal forces. A six-axis load cell was attached to the inferior fixation of the test specimen to record the generalized force-time (and moment) histories. In addition, an accelerometer was placed at this level. At the superior end (head) a triaxial accelerometer and a triaxial angular velocity sensor were attached to measure the linear and angular components of the acceleration and velocity, respectively. All information were gathered using a digital data acquisition system according to the SAE J211b specifications. A high-speed video camera was used.

The intact human cadaver head-neck complex was rigidly fixed at the inferior end. The preparation was mounted with the posterior soft tissue including the ligamentum nuchae and the skin. The anterior region was devoid of spinal musculature and the skin to facilitate target placement for obtaining the localized kinematics. However, ligaments were not violated. Retroreflective targets were placed on the mastoid process of the skull, anterior regions of the exposed vertebral bodies and lateral masses at each cervical level [7].

The specimen was inserted into the fixation on the mini-sled. The initial orientation was under the flexion (anterior region facing the impactor) or extension (posterior region facing the impactor) mode. By rotating the specimen in the fixture housed in the mini-sled 180 degrees, the orientation was changed from flexion to extension or vice-versa. The specimen was subjected to noncontact inertial loading by impacting at the inferior end with the pendulum at 4.6 m/s.

3. Results

The generalized force histories demonstrated bending moment and shear forces to be predominant during the loading phase with minimal off-axis forces (lateral shear or axial load) or moments suggesting that the head-neck complex is primarily subjected to a planar-type dynamic input. The acceleration-time histories were unimodal. The kinematic analysis quantified the response of the cervical spine (Figure 1). The high-speed video photographic analysis demonstrated differing kinematics and head-cervical spinal column signatures under flexion and extension at the same initial impact velocity in a temporal sequence. Under whiplash loading, the translation of the inferior end from the posterior to anterior direction occurred after pendulum contact. The motion was found to be similar to the human torso going forward secondary to a rear impact in real-world whiplash loading [14]. The lower cervical spine

went into an extension mode because of this translation. The inertia of the head with a concomitant inferior end translation caused the head to lag producing an S-curve in the cervical column. This S-curve was produced by flexion in the upper cervical complex (head-C2) and extension in the mid and lower cervical column (Figure 1). The early local upper cervical flexion concomitant with the lower cervical extension was later followed by a uniform extension loading signature in the entire head-neck complex. For loading from the anterior to the posterior direction simulating a frontal impact, the upper cervical spine went into extension first while the lower cervical spine went into local flexion, and later, the upper cervical spine also went into flexion resulting in a unimodal flexion modality.

4. Discussion

This study developed a reproducible experimental method to induce inertial noncontact-type forces to an *in vitro* cadaver human head-neck complex model. Traditional biomechanical models using single-level or multi-level motion segments were not used because of a lack of the connecting structures and its relevance to *in vivo* situations. The mini-sled pendulum experimental set-up permitted a measurement of the biodynamic strength (e.g., forces, accelerations, moments) as well as the overall and local motion information (retroreflective target movements) using the principles of high-speed data acquisition and photography, thus quantifying the kinetic responses of the structure. The mini-sled pendulum set-up has the ability to shape the acceleration pulse. The mass of the pendulum and velocity of the impact can be individually varied. The acceleration level and the wave form shape can be tuned by a suitable combination of spring and dashpot (e.g., foam) materials placed at the front edge of the impacting striker or on the leading face of the cart assembly. Instrumentation devices such as accelerometers at the rear face of the pendulum striker and the leading edge of the specimen together with the load cells on the pendulum and the specimen have the ability to provide a complete time history quantification of the biomechanical strength variables. High-speed photographic equipment records the test event as well as the motion of the retroreflective targets. Because the optics and the strength information from all the channels are synchronized, a full analysis of the response is possible. These data can be used for the development and validation of a detailed mathematical model (e.g., finite element model) of the human head-neck complex. The testing equipment and the associated high-speed instrumentation devices are an integral part of the methodology. In addition, this experimental test set-up has the potential to use instrumentation devices such as a nine-axis accelerometer array on the head or accelerometers on individual cervical vertebrae. The optical tracking system is also an integral part of the experimental design. This system consisting of the high-speed camera together with the retroreflective targets placed at every level of the head-neck complex will facilitate the analysis of localized temporal deformations of the spinal segments. For example, micro level motions representing facet joint capsule stretch and the associated anterior vertebral body and intervertebral disc compressions can be obtained. These data may have clinical relevance since the concept of facet motion has been implicated to cause pain in the human neck secondary to inertial noncontact loads [15].

Another feature of the experimental test set-up includes testing of physical models such as anthropomorphic test devices (e.g., Hybrid III manikin head-neck structure) to investigate the dynamic mechanical response of the model in relation to the human. The system also allows data to be obtained from the upper six-axis load cell of the Hybrid III manikin structure by merely adding this instrumentation to the data collection apparatus. With the additional upper neck data, it will be possible to evaluate the load transmission from the occiput (upper neck) to the lower cervical region or vice-versa. Alternate designs of the physical model to closely match the human biomechanical response can be accomplished with the present methodology [16-17]. The posterior skin and musculature included in the experimental model can be used to assess the contribution to the biodynamic response by conducting repeat experiments without these tissues. Likewise, the response of the human head-neck complex without the posterior musculature, i.e., the intact ligamentous cervical column, can be used to validate a detailed finite element model of the cervical spine [18-19]. Our methodology also allows testing of cervical columns with degenerative conditions such as stenotic canal, osteophytes and spondylosis, and iatrogenically altered spines such as facetectomy and laminectomy to delineate their biomechanical characteristics under inertial impact.

5. Summary

A methodology was developed to apply inertial noncontact flexion, extension, lateral bending and oblique loading to an intact head-neck complex. Because of the nature of the mini-sled pendulum equipment design, it is

possible to conduct dynamic studies simulating rear (whiplash loading), frontal (forward flexion) and oblique impact tests. The methodology included a dynamic recording of biomechanical data at high-sampling rates [20]. The temporal local and overall kinematics of the head-neck complex can be delineated. An analysis of the segmental rotations is presented [21]. The hypothesis that differing local extension/flexion motions occur in the upper cervical region concomitant with local flexion/extension motions in the lower cervical spine under frontal/rear (whiplash) impact during the early stages of external loading, may elucidate the biomechanics of injury in real-world situations.

Acknowledgment: This study was supported in part by DOT NHTSA Grant DTNH22-93-Y-17028, and the Department of Veterans Affairs Medical Research Service.

References

[1] Sances A Jr, Myklebust JB, Maiman DJ, Larson SJ, Cusick JF, Jodat R. The biomechanics of spinal injuries. *CRC Crit Rev Bioeng* 1984:11: 1-76.

[2] Yoganandan N, Sances A Jr, Pintar FA. Biomechanical evaluation of the axial compressive responses of the human cadaveric and manikin necks. *J Biomech Eng* 1989:111(3): 250-255.

[3] Sherk HH, Dunn EJ, Eismont FJ, Fielding JW, Long DM, Ono K, Penning L, Raynor R. *The Cervical Spine.* Second Edition, JB Lippincott Co., Philadelphia, PA, 1989: 881.

[4] Sances A Jr, Thomas DJ, Ewing CL, Larson SJ, Unterharnscheidt F (eds). *Mechanisms of Head and Spine Trauma.* Aloray, Goshen, NY, 1986: 746 pp.

[5] McElhaney JH, Paver JG, McCrackin HJ, Maxwell GM. Cervical spine compression responses. In: *Proceedings 27th Stapp Car Crash Conference,* San Diego, CA, October 17-19, 1983, pp 163-177.

[6] Pintar FA, Yoganandan N, Voo LM, Cusick JF, Maiman DJ, Sances A Jr. Dynamic characteristics of the human cervical spine. *SAE Transactions* 1995:104(6): 3087-3094.

[7] Pintar FA, Sances A Jr, Yoganandan N, Reinartz JM, Maiman DJ, Suh JK, Unger G, Cusick JF, Larson SJ. Biodynamics of the total human cadaver cervical spine. In: *Proceedings 34th Stapp Car Crash Conference*, Orlando, FL, November 4-7, 1990, pp 55-72.

[8] Barnsley L, Lord S, Bogduk N. Clinical Review - Whiplash Injury. *Pain* 1994:58: 283-307.

[9] Barnsley L, Lord SM, Wallis BJ, Bogduk N. The prevalence of chronic cervical zygapophyseal joint pain after whiplash. *Spine* 1995:20(1): 20-26.

[10] Aprill C, Dwyer A, Bogduk N. Cervical zygapophyseal joint pain patterns II: A clinical evaluation. *Spine* 1990:15(6): 458-461.

[11] Dwyer A, Aprill C, Bogduk N. Cervical zygapophyseal joint pain patterns I: A study in normal volunteers. *Spine* 1990:15: 453-457.

[12] Ewing CL, Thomas DJ, Lustick L, Muzzy WH, Williams G, Majewski PL. The effect of duration, rate of onset and peak sled acceleration on the dynamic response of the human head and neck. In: *Proceedings 20th Stapp Car Crash Conference*, Dearborn, MI, October 18-20, 1976.

[13] Yoganandan N, Pintar FA. Inertial loading of the human cervical spine. *J Biomech Eng* 1997 (In Press).

[14] Geigl BC, Steffan H, Dippel C, Muser MH, Walz F, Svensson MY. Comparison of head-neck kinematics during rear-end impact between standard Hybrid III, RID neck, volunteers and PMTO's. In: *IRCOBI*, Brunnen, Switzerland, 1995: 261-270.

[15] Bogduk N, Aprill C. The prevalence of cervical zygapophyseal joint pain, a first approximation. *Spine* 1993:17: 744-747.

[16] White RP, Zhao Q, Rangarajan N, Haffner M, Eppinger M, Kleinberger M. Development of an instrumented biofidelic neck for the NHTSA advanced frontal test dummy. In: *15th International Conference Experimental Safety of Vehicles*, Melbourne, Australia, 1996, pp 1-13.

[17] Ono K, Kanno M. Influences of the physical parameters on the risk to neck injuries in low impact speed rear-end collisions. *Accid Anal and Prev* 1996:28(4): 493-499.

[18] Yoganandan N, Kumaresan S, Voo L, Pintar F. Finite element applications in human cervical spine modeling. *Spine* 1996:21(15): 1824-1834.

[19] Kleinberger M. Application of finite element techniques to the study of cervical spine mechanics. In: *Proceedings 37th Stapp Car Crash Conference,* San Antonio, TX, November 7-8, 1993, pp 261-272.

[20] Yoganandan N, Pintar FA, Sances A Jr, Voo LM, Cusick JF. Inertial flexion-extension loading of the human neck. *Adv Bioeng* 1995:31: 45-46.

[21] Yoganandan N, Pintar FA, Cusick JF. Cervical spine kinematics under inertial flexion-extension. In: *11th North American Spine Society Proceeding*, Vancouver, BC, 1996, pp 265-266.

Figure Caption

Figure 1: Kinematics of the head-neck complex due to whiplash loading.

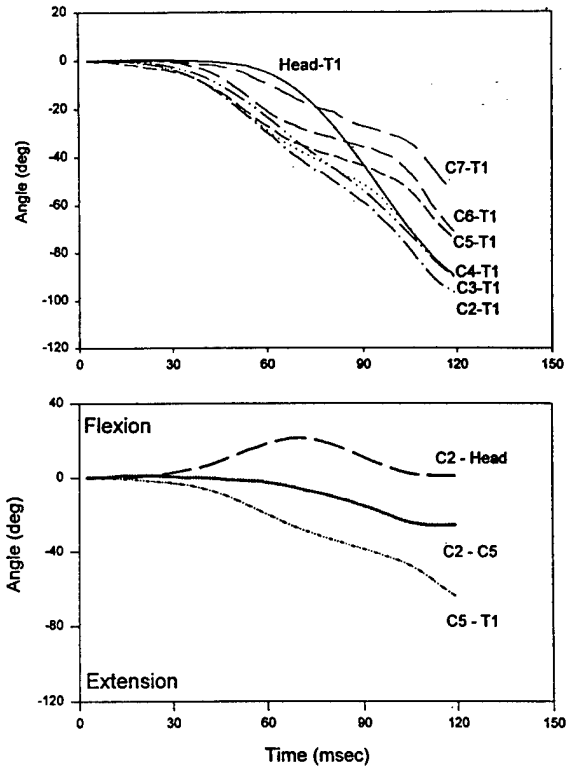

Figure 1: Kinematics of the head-neck complex due to whiplash loading.

BIOMECHANICAL ASSESSMENT OF WHIPLASH

Narayan Yoganandan, Frank A. Pintar

Abstract

Whiplash injury is a problem with significant impact. The annual estimated cost in the United States alone is approximately four and one-half billion dollars. In the United Kingdom the cost is estimated at two and one-half billion pounds. Health care providers, biomedical engineers and others have contributed to the recognition and understanding of the injury and patient management. There is a lack of consensus with regard to the injury production despite these advancements. Numerous mechanisms of injury have been proposed. However, no single study has completely evaluated the efficaciousness of any particular mechanism of injury. A critical review is presented in this chapter on the existing human cadaver and human volunteer studies dealing with the identification and derivation of the mechanisms of injury. The requirements of a human cadaver model to quantify the clinical and biomechanical aspects of whiplash are delineated. Our recent laboratory studies on this topic are also described. Results indicate the following. During the initial phases of the extension whiplash loading, the upper cervical spine-head undergoes local flexion concomitant with a lag of the head while the mid-lower cervical column is in local extension thus establishing a reverse curvature. This reverse curvature may result in a stretching of the upper head-neck complex which may lead to sub-occipital headaches. With continuing application of the dynamic loading, the inertia of the head catches up with the cervical spine and approximately at the end of the loading phase, the entire head-neck complex is fully under extension. In contrast, the lower cervical spine facet joints demonstrate both local compression and sliding along the joint throughout the loading phase. While both the anterior- and posterior-most regions of the facet joint slide, the posterior-most regions of the joint compress more than the anterior-most regions thus exhibiting, on a temporal basis, a "pinching" mechanism. These differing local micro motions of the facet joint may provide a biomechanical explanation for neck pain reported by whiplash patients.

1. Introduction

Extensive research has been conducted on the dynamic response of the human body secondary to high velocity impact (e.g., frontal collisions). For over 40 years the Stapp Car Crash, the American Association of Automotive Medicine, the International Research Committee on the Biokinetics of Impact, and the Experimental

Safety Vehicle (now called the Enhanced Safety of Vehicle) Conferences, have provided a forum for presentation of such research. In addition, medical conferences hosted by various disciplines (e.g., medicine, radiology, orthopedic surgery) over the last five decades have enriched the clinical awareness and knowledge of the management of a severely injured patient, and these presentations together with archival systems have improved the quality of life in our society. The advent of systems such as airbags, seatbelts and vehicle component design improvements have been possible through these investigations. However, relatively few studies are available to clearly delineate the dynamic biomechanics of the human head-cervical spine complex in low-speed, rear-end, postero-anterior type impact. A commonly reported outcome secondary to impact is whiplash.

To analyze complaints following railway incidents, "Railway Spine" was the phraseology used in 1886 by Erichsen. The complaints included headache and neck pain. To describe the spinal motion in eight cases of neck injury secondary to motor vehicle crashes, Crowe used the term "whip lash" in 1928. These are cited in Griffiths et al [1]. The term whiplash has proliferated in published medical literature since 1945. Many different terminologies have also been used. They include, cantilever injury, hyperextension injuries, cervical sprain/strain and acceleration-deceleration syndrome [1-4]. It is estimated that 86 percent of all neck injuries seen clinically result from motor vehicle crashes and that 85 percent of these injuries are secondary to rear-end crashes [2,5]. Because of these findings, and since the inception of the term whiplash, it has been primarily dedicated to refer to the sequelae of events stemming from vehicular rear-end crashes wherein the sitting human body is initially accelerated from the posterior to anterior direction through dynamic impact. The whiplash event to the neck occurs because the torso is accelerated forward prior to the head inducing a lag. This "head lag" defines the movement of the neck to result in an initial S-curve followed by an extension motion in the human cervical spine [6]. A critical review is presented in this chapter on the existing human cadaver and human volunteer experimental studies dealing with the identification and derivation of the mechanisms of whiplash injury. Our recent laboratory studies on this topic are also described in this chapter.

2. Epidemiology

The Quebec Task Force monograph provides a summary of the clinical epidemiology of whiplash injury [7]. A recent symposium held in November 1996 in Belgium, further emphasizes the significance of impact of this problem [8]. Although both frontal and rear impacts contribute to whiplash injuries, rear-end crashes are responsible for about 85 percent of all whiplash trauma [9-10]. Precise estimates for the actual incidence and the associated economics of the injury are not easily available. This is primarily due to the multitude of variables involved in the production and assessment of trauma. Vehicular factors, occupant demographics and positioning at the time of the crash, and collision variables together with the human tolerance constitute a significant body of parameters responsible for the injury sequelae; symptoms may be acute or chronic. Another confounding factor is associated with the litigious environment [11-12]. A generally reported incidence rate of whiplash injury is about 1 in 1000 in Western countries, and approximately 25 percent of the patients become chronic with 10 percent suffering serious pain [13]. Based on the human life span, Barnsley estimated that 0.5 percent of the population have chronic pain and 0.2 percent have severe pain [13]. Studies from the European countries have expressed growing concern with this injury. For example, Swedish data indicate that more than 50 percent of all "traffic injuries" with long-term consequences involve the human neck [14]. This study further indicates that whiplash injury, classified to belong to the AIS = 1 (Abbreviated Injury Scale) category, leads to long-term problems in 10 percent of cases compared to 0.1 percent for all other injuries, a 100 fold change [15]. In the United Kingdom, seatbelt usage increased the incidence of whiplash injury [16].

A 1995 report by the Insurance Institute of Highway Safety indicated the incidence of minor neck injuries to be 270 per 1000 in rear crashes compared to 62, 65, and 82 in frontal, side and rollover collisions, respectively [17]. This suggests a propensity of approximately three to four times in rear crashes compared to the other modes of injury causation. In Japan, minor neck injuries (AIS = 1) accounted for approximately 50 percent of car-to-car crashes, with a gradual increase from 43.9 percent in 1985 to 50.8 percent in 1991 [18]. About 95 percent of all neck injuries occurred in rear-end crashes with 15 to 20 percent of occupants suffering from prolonged symptoms; seatbelt laws were promulgated in 1986 in Japan. This finding of the increase in neck injury despite the restraint legislation, parallels the above cited study from the United Kingdom.

Neither the physical damage to the vehicle nor the speed or the velocity change secondary to the rear-end crash bears relationship to these types of low level (AIS = 1) cervical spine injuries [19-22]. From a vehicle

component perspective, seat (stiff vs. flexible), restraint system, and headrest (type and location with respect to the human anthropometry) have been studied for their (in)ability to minimize whiplash trauma [23-24]. Other studies have investigated the increased incidence of soft tissue neck injury in four-door versus two-door cars [25]. The influence of the position of the occupant within the vehicle on the incidence of whiplash injury indicated a higher susceptibility for the front compared to the rear seat occupant [26]. Factors such as age and sex were included in this earlier study. Studies have also reported a higher susceptibility for females compared to males [17].

An incidence of 391,717 AIS = 1 neck injuries with associated medical costs of $501 per nonhospitalized patient and $15,002 per hospitalized patient have been reported [27]. These injuries lead to an annual overall cost of approximately $356 million at an average per patient medical cost of $1,000. It must however, be appreciated that routine epidemiological measures for this minor AIS = 1 injury often elude the system as the symptomatology can be latent initially and the tertiary care procedures are not a common inclusion course for data acquisition [28]. The liability claims in the United States due to rear-end crashes are estimated to be more than ten billion dollars per year [29]. The annual cost of whiplash associated injury in the United Kingdom is estimated at 2.5 billion pounds and this figure represents approximately 0.4 percent of the gross national product [30].

The National Accident Sampling System, a computerized database, allows for the estimation of the incidence of various events including occupant injuries. For example, we have reported studies describing the epidemiology and injury biomechanics of the human cervical spine in vehicular crashes by examining this database from 1979 to 1986 [31]. However, this system that has been collecting data all across our country since 1979 cannot be used to obtain precise estimates on the subject of this study as chronicity is not an input variable, i.e., follow-up data collection is not a part of this database. Another factor is that this database only codes the top six injuries sustained in a tow-away crash which often tends to leave out the minor, latent or prolonged soft tissue trauma to the neck. Furthermore, not all cases with whiplash trauma result from tow-away crashes. For example, the 1993 study by Maag et al., that investigated a large sample of neck injury claims indicated that approximately 25 percent of claims occurred in crashes with property damage only, indicating a delayed symptomatology [32]. The patient after the crash may not be immediately seen by a physician in the emergency room. These characteristic features have partially obliterated the community from arriving at an exact estimate of the prevalence and incidence of injury. However, the aforementioned research studies from various sources clearly emphasize the magnitude of the problem. In the next section, we have provided an overview of the biomechanical aspects of whiplash injury research.

3. Biomechanical Studies

Several approaches have been used to understand the behavior of the human head-neck complex under inertial whiplash type loading. They include mathematical and physical models, experiments using animals, and human volunteer and human cadaver evaluations [4,6,20,33-37,40-50]. This cited literature is not all inclusive.

Mathematical studies have provided a basic understanding of the biomechanics of the structure. Appendix A provides a brief description of some of the mathematical work in this area. Because of a lack of precise definition of the hard and soft tissue properties and the associated three-dimensional geometrical definition of the human head-neck complex, existing mathematical approaches including lumped parameter, finite element and occupant simulation models have limited application particularly in the investigations of the clinical biomechanics of whiplash injury mechanisms. Therefore, other modeling approaches are necessary to determine the dynamic mechanisms of injury under whiplash loading.

Physical models (briefly presented in Appendix A) of the human head-neck complex have not attained the level of detail to provide accurate descriptions of segmental spinal mechanics. For example, the neck of the widely used Hybrid III manikin consists of three aluminum cylinders interconnected by rubber with no differentiation or direct parallelism among the spinal levels. This representation is inadequate to delineate the differences in the motion along the human cervical spinal column. Furthermore, this physical model lacks biofidelity as its head does not lag the neck motion during inertial flexion or extension loading; this lag has been demonstrated in human volunteers and human cadaver tests [51-52]. Consequently, other modeling approaches are necessary to delineate the dynamic mechanisms of injury.

Experimental animal studies have the unique feature of documenting the physiologic responses to trauma. Results from quadruped models, which do not bear a complete one-to-one correspondence with the human structure, have to be scaled appropriately to describe the mechanics of the human head-neck complex. Since precise scaling

laws do not presently exist, findings from these studies are only a first step in the understanding of the biomechanics of whiplash. Difficulties associated with obtaining detailed temporal definitions of the localized kinematics of the structure using optical and/or imaging techniques during the impact event, further renders the delineation of the dynamic mechanisms of injury a formidable task. It must be noted that it is almost impossible to conduct these experiments with high-speed radiography and at injury producing levels because of ethical and technical considerations. Consequently, other types of experimental models are necessary to achieve these objectives.

Human volunteer tests have the unique feature of eliminating the scaling problems associated with animal experiments. Because of experimental difficulties and other constraints, it is only possible to determine the overall kinematics of the head-neck complex at sub-injury levels. Furthermore, instrumentation that can be used in these studies is limited; for example, it is not possible to introduce optical targets at every level of the cervical column and determine the temporal kinematics under high-speed photography as tissue dissection cannot be done. High-speed x-rays are limited in their capabilities because of technological constraints, their ability to obtain clear segmental dynamic information (e.g., facet joint motions at every msec), and above all, the radiation exposure to the human volunteer often poses difficulties in not only obtaining the approval from the IRB/human studies committees but also in obtaining subjects for the study. Despite these limitations, the sub-injury level experiments can provide important information on several factors including the overall macroscopic motions as viewed by a high-speed camera, the physiologic response characteristics, and the associated input impact variables such as the accelerations at the cervico-thoracic level. Human volunteer studies are described in a later section in this chapter. Cervico-thoracic acceleration data at this level can serve as input to conduct controlled experimentation with added instrumentation using intact human cadaver head-neck complexes so that realistic estimates of the temporal and localized spinal motion can be obtained. These data will delineate the dynamic mechanisms of injury under whiplash forces. This hybrid protocol, as explained later, is followed in our studies.

4. Human Cadaver Studies: Literature Review

During the years 1967-1971, Mertz and Patrick reported data from two embalmed human cadavers and a human volunteer [45-46]. The human cadavers were 66 (#1035) and 69 (#1089) years of age, 60.8 and 59 kg in weight, 162 and 170 cm in height. The head weights were 2.85 and 4.13 kg. Cadaver 1035 was used earlier in windshield, shoulder harness and steering wheel evaluation programs, and cadaver 1089 was tested to determine the force-deflection characteristics of the chest [53]. Radiography from these earlier tests revealed fractures to the head/face with no radiological evidence of damage to the neck. Consequently, the specimens were determined to be suitable to conduct additional experiments to investigate whiplash injury biomechanics. For both the cadavers and the human volunteer (47 years old, 72.6 kg, 173 cm tall, head weight 4.9 kg), tests were run at 16 kph (10 mph) and 36.8 kph (23 mph) rear impact speeds. A horizontal accelerator was used in all tests. The equivalent sled speeds were 14.4 kph (9 mph) and 24 kph (15 mph), respectively.

The simulation sequences in the cadavers consisted of two series, one with the head support followed by one without the head support. For the head support series, the first run was with a rigid seatback at 14.4 kph (9 mph) sled speed, and the remaining runs were conducted at 24 kph (15 mph) sled speed. The degree of seatback rigidity was incrementally increased and for the final run the seatback was fully rigid. The simulation sequence for the case of no head support was identical. The authors stated that "subsequent sets of x-rays were taken after any simulation in which damage to the cervical spine was suspected to have occurred".

The simulation sequence for the single human volunteer test series consisted of head supported and head unsupported series with rigid seatback configuration. For the head supported series, the first run was at 14.4 kph (9 mph) sled speed and in the subsequent runs, the severity was increased. The final run was 23.5 kph (14.7 mph) sled speed. Two runs were conducted with no head support, the first run at 13.4 kph (8.4 mph) and the second run at 14.2 kph (8.9 mph) sled speeds.

Using the head acceleration data, neck reactions including neck torque, acceleration at the center of gravity of the head, and head angular accelerations were computed. In all tests with no headrest for the human volunteer and human cadavers, the subjects were lap belted and the seatback was not allowed to rotate. For the 16 kph (10 mph) simulation, the pulse times for the volunteer traces were longer than for cadavers. The maximum neck torques for these 16 kph simulations were 20.2 Nm (14.9 foot pounds) and 37.4 Nm (27.6 foot pounds) for the two cadavers (1035 and 1089). In contrast, the human volunteer neck torque was 16.7 Nm (12.3 foot pounds). The maximum head-neck extension was 64 and 61 degrees for the two cadavers. The human volunteer responded with an extension

of 27 degrees. For cadavers 1035 and 1089, the computed shear forces were 245 and 400 N, and the axial neck forces were 187 and 312 N, respectively. In contrast, for the human volunteer tests, the shear and axial forces were 218 N and 125 N. The tensing action of the human volunteer prior to rear-end collision was considered to be responsible for the differences in these biomechanical parameters. The maximum shear and axial forces under static loading for the human volunteer were reported by the authors to be 846 N and 1135 N, respectively.

The computed shear forces for cadavers 1035 and 1089 in the high severity 36.8 kph (23 mph) simulations were 271 N and 441 N; the axial neck forces were 418 and 503 N; the maximum torques were 34.4 Nm (25.4 foot pounds) and 44.8 Nm (33.0 foot pounds). No human volunteer tests were conducted at this speed. Radiographic data indicated minor damage between the C3 and C4 vertebrae for cadaver 1035. No damage was observed for cadaver 1089. The authors' analysis indicated a tolerance level of 27.7 Nm (20.4 foot pounds) for a 2.86 kg head weight (cadaver 1039) and 40 Nm (29.5 foot pounds) for a head weight of 4.13 kg (cadaver 1089). These levels are based on a scaling of the actual torques with the relative head weight differences between the cadaver and the human volunteer. The reader is referred to the original article for further details [45-46].

In the 1971 report, Mertz and Patrick plotted the torque at the occipital condyles with respect to the head position relative to the torso for the two cadavers along with human volunteer data [45]. The cadaver response curves indicated a "progressive loosening" of the components of the neck with increased number of runs. A response envelope was proposed for hyperextension using the three subjects on a qualitative basis. Based on earlier studies, a torque level of 23.7 Nm (17.5 foot pounds) was considered noninjurious under static conditions. Mertz and Patrick chose a dynamic torque level of 47.5 Nm (35 foot pounds) to be noninjurious and deduced the injury tolerance to be 61 Nm (45 foot pounds) for ligamentous damage under hyperextension. This was done as follows. Since cadaver 1035, which sustained minor C3-C4 ligamentous damage with a maximum neck torque of 34.4 Nm (25.4 foot pounds), had a small head weight of 2.85 kg compared to the 72.6 kg human volunteer whose head weight was 4.9 kg, a rationale was made to scale this torque based on the mass of the head. The injury threshold for the torque developed at the occipital condyles of 61 Nm (45 foot pounds) was recommended for ligamentous damage under hyperextension (applicable to the 50 percentile adult male). The Society of Automotive Engineers publication indicates a torque of 57 Nm (42 foot pounds) to represent the AIS = 3 level injury; in contrast, a torque of 47 Nm (35 foot pounds) is considered noninjurious [15,54].

In 1972, Clemens and Burow investigated the mechanisms of injury secondary to whiplash forces with sled tests using 21 unembalmed human cadaver torsos [47]. The specimens were isolated at the T10 level and mounted on a flat rigid plate. In all but one, the head was transected at the base of the skull and a spherical wooden measuring head was inserted. The preparations were divided into no headrest (49 to 88 years old) and simulated headrest (70 to 93 years old) groups. The simulated headrest was constructed from a 4 cm foam rubber covered 5 x 25 cm "planed board". Tests in the no headrest group were conducted at velocities ranging from 19.1 to 24.6 kph. The speed in the simulated headrest group was 25.3 kph. The weight of the 16 preparations in the no headrest group ranged from 4.7 to 8.7 kg. Five tests in the no headrest group had four preparations weighing from 3.7 to 8.7 kg, and the remaining one, a T10-head specimen, had a weight of 14.3 kg. In all tests, a steel backrest with foam upholstery was used to support the torso such that the torso was in contact with the upholstery and the backrest was level with the shoulder. In the no headrest group of tests, the kinematics indicated the following: acceleration of the torso lasting for 30 to 40 msec lead to the rotation of the head while the neck was in extension. Maximum head rotations were coincident with the peak of the input deceleration pulse. Injuries occurred to the disc (90%) followed by ruptures of the anterior longitudinal ligament (80%), ruptures of the joint capsules (40%), posterior vertebral body and spinous process fractures (30%), ligamentum flavum ruptures (10%) and posterior longitudinal ligament ruptures (10%). In contrast, in tests with the headrest, there was an increased translation of the thorax initiating a relative motion between the head and the thorax which resulted in a "slight" forward flexion of the neck. No injuries occurred in this group. Tension and shear forces were considered by Clemens and Burow to be the determinants for whiplash injury instead of head acceleration.

In 1974, Marar reported data from seven human cadaver specimens that were manually loaded by a hyperextension force (termed in the original article as backward rotation force) with the head lying free at the edge of the table [55]. This rearward rotation produced vertebral fractures in five specimens. In all specimens however, the anterior longitudinal ligament was torn at the fracture site and the posterior longitudinal ligament was intact. In three cadavers with the fracture of the vertebral body just below the pedicle produced by the backward rotation force, a "strong" posterior displacement force was manually applied simultaneously with backward rotation. This resulted in a posterior subluxation of the "upper spine" on the lower cervical column. The displaced upper segment returned to its initial position with the removal of the external manual force. Spinal cord constriction occurred only in these

three cadavers that had been subjected to a strong backward displacement force in addition to backward rotation. In contrast, the cord was normal in specimens sustaining only the backward rotation force. The maximum inward bulging of the ligamentum flavum occurred when the cervical spine was 30 degrees short of complete hyperextension. These experiments indicated that rotation plays a lesser role in hyperextension injuries of the cervical spine, a finding contradictory to Roaf who emphasized the importance of rotation in spinal trauma [56]. Therefore, the mechanism of injury was found to be a combination of hyperextension and backward shearing with little contribution from lateral rotation.

In 1992, Shea et al., reported data from nine female human cadaver occiput to T1 specimens (age 56 to 95 years; mean 74, standard deviation 15) that were quasistatically loaded under tension to failure at a loading rate of 5 mm/s [57]. The specimens were pre-extended at an angle of 30 degrees. Failure loads, extension bending moments and axial tensile displacements were 400 N (standard deviation: 148), 4.0 Nm (standard deviation: 3.1), and 18.8 mm (standard deviation: 7.7), respectively. Failure generally occurred at C5-C6 and C6-C7 levels. Tears of the anterior longitudinal ligament and the intervertebral disc occurred at least at one level. These spinal levels also had the most severe degree of degeneration compared to the other segments. These data indicate the effects of degeneration on the combined tension-extension loading on the ligamentous cervical spine. Since these studies were quasistatic, additional investigations are needed to evaluate the response of the cervical spine with dynamic loading rates using male and younger specimens.

In a parallel study, Yoo et al., investigated the alterations in the neuroforaminal diameter secondary to static postural variations using five human cadaver C3-C7 columns fixed at C2 and T1 levels [58]. With an axial pre-compressive load of 4.4 kg, the specimens were subjected to neutral and flexion-extension alone (10, 20, 30 degrees in each mode) and a combination of neutral and flexion-extension (20 degrees in each mode) with an axial rotation of 20 degrees. The neuroforaminal diameters compared to the neutral position were significantly reduced ($p < 0.01$) secondary to 20 and 30 degrees of extension (10 and 13%, respectively). In contrast, the diameters increased by 8 and 10 percent, respectively, at 20 and 30 degrees of flexion ($p < 0.01$). Axial rotation combined with extension did not show significant changes compared to the unimodal values. However, ipsilateral rotation induced an additive effect in the narrowing of the neuroforaminal space. While the principal emphasis of the investigation was directed towards conservative patient management evaluating the efficacy of immobilization in a flexion versus an extension position, these results emphasize the need to perform additional biomechanical studies to determine the effects of dynamic whiplash loading on the local spinal component kinematics. These studies are important particularly when one considers the fact that the encroachment of the space may lead to root compression resulting in injury.

Geigl et al., in 1994, reported 49 sled tests using six human "post-mortal test objects" at impact velocities of 6 to 15 kph [59]. The two female and four male cadavers ranged in age from 50 to 79 years of age. Mean sled decelerations ranged from 1.3 to 8.7 G. The specimens were oriented with initial head angles ranging from -45 to +45 degrees. The distance between the head and headrest ranged from none to 16 cm. High-speed photography at 1000 frames/sec was used to determine the kinematics. Rearward head rotation initiated 60 to 100 msec after impact. After 100 to 160 msec, the head began to rotate forward while the shoulders had already translated forward, i.e., the head lagged the shoulder motion. Rearward head rotation was the least (10 to 15 degrees) with an initial contact of the head with the head restraint, and was the maximum with a 16 cm clear distance between the head and the head restraint. Head to mid-cervical spine motion initiated after 50 to 80 msec following impact. The motion resulted in upper cervical spine flexion. Peak relative rotation of up to 45 degrees occurred between 100 and 130 msec. These observations were also found to be true for the human volunteer tests (described below). Geigl et al., concluded that it is important to avoid extreme relative movement between the head, neck and torso to minimize human neck injury.

5. Human Volunteer Studies: Literature Review

In 1955, Severy et al., conducted one of the early studies on human volunteers [20]. They reported two rear impact tests with lap-belted human volunteers in the struck and bullet cars. The struck car was a 1947 model Plymouth and the bullet car was a 1941 model Plymouth. The human volunteers were instrumented on the head with accelerometers. At bullet car speeds of 13.1 kph (8.2 mph) and 15 kph (9.4 mph), the sitting volunteer in the target car responded with peak head accelerations of 5.0 and 2.9 G, respectively. Injuries to the head and neck were not reported. The accelerations of the body of the vehicle were 2.0 and 2.5 G, respectively. The body posture and

the state of preparedness at the time of impact were considered to influence the potential for whiplash injury. Severy et al., concluded that flexion was not the exclusive mechanism of neck injury but extension may also play a role.

Mertz and Patrick analyzed data from a human volunteer and two human cadavers. These are discussed earlier. In 1993, McConnell et al., conducted 10 car-to-car rear impact tests using four three-point belt restrained healthy male human volunteers (age 45 to 56 years) at velocities ranging from 3.3 to 9.24 kph [43]. The kinematics were obtained from high-speed cameras operating at 500 frames/sec. Each subject was exposed from three to seven collisions over an 11 day period. Two subjects reported mild neck discomfort lasting approximately five hours. One subject had mild neck discomfort the following day, which lasted three days. The kinematics were divided into the following phases: phase I consisted of the first 100 msec after bumper contact. In the first 50 msec, the human body did not respond with motion. At about 60 msec, the hips and the low back moved forward and upward. In phase II (100 to 200 msec), at about 100 msec, the upper trunk began moving forward and upward. After 120 msec, the neck appeared to be axially compressed and straightened as the top of the neck began moving upward and rearward. By 160 msec, the forward and upward movement of the upper torso pulled the base of the neck into tension and started the forward motion of the head even as the occiput continued to tip downward towards the headrest. In phase III (200 to 300 msec), at 200 msec, the upward motion of the torso stopped after raising about 9 cm and a head rotation of 45 degrees. At this juncture, the head started to reverse its motion into a forward one. By 250 msec, the trunk, neck and head were descending along the seatback with the restraint system taking the load. In phase IV (300 to 400 msec), after 300 msec, this descent action was complete. At 400 msec, the head showed the most forward excursion and began to rebound. Phase V (400 to 600 msec) was the restitution phase. The kinematics of these subjects were similar at 4 and 8 kph change in velocities although the higher velocity resulted in increased magnitudes in the kinematics. The early upward neck movement and the initial forward head motions were attributed to the upward "lofting" action by the inclined seatback, acceleration related straightening of the spinal curvatures against the seatback, and the normal postural muscle tone of the upper neck. In the 6 to 8 kph runs, the initial axial compression at the top of the neck accelerated the head upward about 1 to 1.5 G, as the base of the neck was pulled forward and downward by a brief axial tension through the rearward extended cervical spine of about 2 to 4.5 G. Compression-tension was suggested as the injury mechanism for whiplash by McConnell et al.

In 1993, in a parallel study, Wess et al., exposed five male volunteers (age ranging from 25 to 43 years) to rear crashes at barrier equivalent speeds of 4 to 13 kph [60]. Each volunteer was exposed to up to 12 runs. Minor neck pain lasting approximately two days was reported. Kinematic data were not reported. Based on these tests, the authors stated that neck extension and head accelerations are below human tolerance for soft tissue injury in healthy adult males.

In 1994, Geigl et al., reported 37 sled tests using 25 human volunteers at impact velocities of 6 to 12 kph [59]. The two female and 23 male volunteers ranged in age from 20 to 60 years. Mean sled decelerations ranged from 1.2 to 4.1 G. The subjects were oriented with an initial head angle ranging from -15 to +15 degrees. The distance between the head and the headrest ranged from zero to 8 cm. High-speed photography at 1000 frames/sec was used to determine the kinematics. No injuries were reported. The kinematic data were similar between their human cadaver tests (described earlier) and the human volunteers.

In 1994, Matsushita et al., discussed results of radiographic studies of the human neck subjected to rear impact using a sled equipment. Nineteen volunteers with age ranging from 21 to 61 years (16 male, 3 female) were tested at velocities from 2.5 to 4.8 kph [61]. Forward leaning, neutral, rotated and lateral bending postures were considered. Three subjects were tensed and the remaining 16 were in a relaxed state before the test. High-speed photography and radiography records were obtained at 200 and 90 frames/sec, respectively. Head accelerations ranged from 1.4 to 6.3 G. Hyperextension did not occur in any test. Five subjects complained of mild discomfort with localized neck pain the following morning that lasted two to four days. In the forward leaning or the stooped-shoulder posture, the upper torso was not in contact with the seatback and the extension of the thoracic spine resulted in a compressive loading to the cervical column. Cervical flexion occurred prior to extension during the straightening of the thoracic and cervical spines. In contrast, for the upright and reclined postures, the torso was immediately pushed away (forward) from the seatback, the chest and shoulders descended with the rearward deflection for the seatback and the compressive loading of the neck did not occur. Matsushita et al., concluded that the initial curvatures of the cervical and thoracic columns were the significant factors for whiplash injury causation.

In 1994, Szabo et al., examined the effects of varying spinal morphology on whiplash injury causation by subjecting five instrumented three-point belted human volunteers (2 female, 3 male) to a change in velocity of approximately 8 kph [41]. The bullet vehicle was a 1981 model Ford Escort and the target vehicle was a 1982 model Ford Escort. The spine morphology was documented by magnetic resonance imaging. The morphology was

reported for four out of five subjects. Two of these four subjects were normal and the other two had a minor degree of spinal degeneration. From a disc bulge perspective, two were normal, one had minor and the other had a moderate protrusion. All tests were conducted over a two day period. High-speed photographic analysis (camera operating at 500 frames/sec) indicated that the translational and rotational motions occur "exclusively" in the sagittal plane. Resultant head accelerations ranged from 10.1 to 13.7 G with pulse durations of 15 to 40 msec. Accelerations of the lower cervical spine (approximately at the first thoracic vertebral level) ranged from 4.5 to 7.4 G. Head accelerations lagged the lower cervical spine accelerations. Four out of five volunteers complained of headache after impact which resolved "immediately". One female volunteer reported minor transient neck stiffness in the morning following the test. No objective spinal changes were detected in the post-test magnetic resonance images. Szabo et al., indicated that the 8 kph rear impact change in velocity is within the human neck injury tolerance for normal and some pre-existing spinal abnormalities, and females, thus extending their previous studies from the normal male population. This study did not determine any muscle responses. The kinematics were similar for all the subjects during the phase wherein the occupant moved rearward with respect to the vehicle. They were different in the rebound phase presumably due to the variations in the muscle activities. Hyperextension/flexion did not occur. Since no jaw motion relative to the cranium was observed, Szabo et al., further concluded that their tests fail to support the prevalence of the temporo-mandibular joint injury during whiplash loading.

In 1995, McConnell et al., extended their earlier study to include higher velocity (5.8 to 10.9 kph) tests [44]. A total of 14 crashes were conducted with seven male human volunteers (32 to 59 years of age, 76 to 118 kg in weight, and 173 to 188 cm in height). Both driver and right front seat passenger positions were considered in the study. Four subjects sustained three exposures each, one subject underwent four exposures and the other two subjects had one exposure each. All exposures occurred in three consecutive days. All subjects reported some test-related discomfort symptoms that included fleeting headache and muscle soreness. High-speed data were gathered at 250 frames/sec. The kinematics, divided into five phases as reported in their earlier study, demonstrated similar patterns in this series of higher severity impact. The earlier proposed tension-extension mechanism of injury was found to apply for this series. Hyperextension was not attributed to be the causal mechanism for whiplash symptoms sustained by the subjects in this series of tests. This was based on the following: the uncoiling or straightening of the thoracic spinal curvature occurring between 60 to 80 msec after bumper contact together with the rearward deformations of the seatback were responsible for ramping. During this period, the head was stationary despite the forward translation of the base of the neck. By about 100 msec, the top of the head began to move while the base of the neck continued to translate. The head rotated 10 to 15 degrees between 110 to 170 msec and then started to translate forward with the neck continuing in its forward path. The head reached its peak rearward rotation around 180 to 200 msec and the maximum neck extension was 18 to 51 degrees. McConnell et al., concluded that tension-extension (not hyperextension) was the mechanism of whiplash injury.

In a study reported in 1996, Ono and Kanno conducted sled tests simulating car-to-car impact using three male belt-restrained human volunteers (22 to 43 years of age) at speeds of 2, 3 and 4 kph [18]. The head rotated forward at about 50 msec at which time the sled acceleration attained its peak value, which was considered by the authors to coincide with the onset of whiplash. The head started rotating rearward at approximately 100 msec, the time when the sled ceased its acceleration. The bending moment and the shear force in the neck reached their maxima at approximately 110 msec. These neck parameters approached zero magnitudes around 200 msec. The study did not find differences between the sitting and reclined postures in the neck shear or moment. The axial forces were higher for the reclined posture than the sitting posture. In contrast, the head rotation was higher which resulted in hyperextension of the neck. In the case of a normal height headrest, while the moment and the axial forces were the lowest, the authors' suggested that shear forces may actually increase. Although electomyographic activities were recorded, no data were reported in the article. Ono and Kanno concluded that neck bending moment, axial and shear forces, and the head rotations must be determined for a proper understanding of the whiplash neck injury mechanism.

The above cited studies by Matsushita et al., Mertz and Patrick, Ono and Kanno, Severy et al., Szabo et al., and West et al., did not quantify the muscle activity of the human volunteer prior to rear impact [18,20,41-42,45-46,60-61]. Consequently, accurate inferences cannot be drawn in these human volunteer studies with regard to the preparedness of the subject before impact. Muscle activities may affect the spinal kinematics which result in alterations in the local spinal component load sharing.

In 1996, Szabo and Welcher conducted ten car-to-car tests with five instrumented (4 male, 1 female) human volunteers and monitored muscle activities [62]. Electromyographic data were obtained using surface mounted electrodes in the anterior paracervical, posterior paracervical, trapezius and paralumbar muscles. The seatbelted volunteers were 22 to 54 years of age. The velocity change used in the study was 10 kph for the struck vehicle. The

head restraint conditions included two types. One was a standard seat integrated restraint and the other type included a modification of this head restraint with 50 mm padding to reduce the horizontal gap with the human volunteer. Each subject was exposed twice to impact (one in each head restraint type) over a two day period. The struck vehicle was a 1976 model Volvo. Kinematic data were obtained from a high-speed camera operating at 500 frames/sec. Injuries were not reported by the human volunteers. Pre-impact muscle activities were commensurate with the relaxed seated posture. The initial muscle activity occurred 100 to 125 msec following the bumper contact from the bullet vehicle. Since full muscle tension does not develop until 60 to 70 msec after the onset of muscle activity, it can be concluded that it takes approximately 160 to 190 msec for activation. At this juncture, sagittal plane kinematics indicated that the cervical spine was in extension. Full muscle tension "likely" did not develop until the spine went into an extension mode. Similar onset times were recorded in the cervical extensor and flexor muscles. The muscle response times were not significantly different between the two types of head restraint. However, decreases occurred in the head acceleration and displacement, and cervical extension for the 50 mm padded restraint case. Szabo and Welcher concluded that pre-tensing of supporting muscles may be a factor in whiplash.

6. Critique

Soft tissue injury to the cervical spine may occur individually or in combination in the ligaments, nerves, muscles, discs, blood vessels and fractures/dislocations. Common whiplash symptoms include: focal trauma, headache, posterior cervical pain, referred pain, radiculitis and afferent sympathetic function. Clinically and radiographically it is difficult to precisely identify the painful motion segment in patients with prolonged symptoms [63]. Because of the multiplicity of the structures and the levels involved, inconclusive epidemiology, variable clinical findings, and a paucity of biomechanical studies including human volunteer and cadaver tests, mathematical models and *in vivo* animal evaluations, no accepted general consensus exists regarding the sequelae and the mechanism of whiplash injury.

Neck pain and headache are the two most common symptoms/outcomes of whiplash injury; other common complaints include pain in the upper back and extremities [9,64-67]. The cervical spine is replete with pain sensitive structures including the facet joints, anulus of the discs, ligaments, muscles, nerve roots, synovial joints and arteries of the vertebrae [68]. Dynamic kinematic changes to these components may result in trauma: stretching of the spinal ligaments, muscles, stretching or compression of the nerve roots, disturbance of the integrity of the facet joints, and compressive disc herniation inducing stimulation of the anulus fibrosus may all be the potential mechanisms. Evidence has been presented to relate whiplash injury to the cervical components [13,69]. If the injury is sub-occipital, pain may be experienced in the head, if it is between the sub-occipital region and the fifth intervertebral disc space, it may occur in the neck itself (posterior region) and/or shoulders, and if the injury is inferior to this level, pain may ensue in the neck, shoulders, back and extremities. Muscle injury secondary to stretching during the dynamic phase may affect the associated nerve complex stimulating pain or headache. For example, pain may be referred to the occipital region via the C2-C3 sensory roots, which may be activated due to excessive segmental stretching of the head-C2-C3 complex due to a local flexion of the upper cervical spine in the dynamic hyperextension phase (see our studies below), and potentially to the area of the orbitofrontal vertex by the C1 sensory root. This may trigger a headache in a whiplash injured patient.

Using human volunteers, Bogduk and his associates delineated the pain pattern secondary to the blockage of the zygapophyseal (facet) joints [70]. The characteristic areas of pain referred from these joints were mapped [71]. These investigations were conducted on 10 symptomatic human volunteers. Studies were also conducted to document lesion to this complex in the form of occult fractures of the joints or the facet pillar [72-73]. Tears of the joint capsule were reported in whiplash patients on radiograms [74]. Using autopsy material, soft tissue lesions and facet bony damages have been identified in subjects with a diagnosis of hyperextension injury [75-77]. These clinical studies emphasize the role of the cervical facet joints in whiplash patients. Controlled dynamic biomechanical studies delineating the kinematic sequelae of these components in relation to the input impact variables are however, not yet available.

Another spinal component that may contribute to whiplash to a lesser degree is nerve root injury secondary to the constriction of the neuroforamina. The nerve root may become contused producing possible axonal injury. Local crush injuries have been reported in whiplash arising from a "pincer-like" action in the neuroforamina [2]. The absence of an epineurium in the spinal nerve roots accentuates its susceptibility for trauma. Applying a simplified uniaxial quasistatic load of 4.4 kg on human cadaver C3-C7 columns, it has been demonstrated that the

neuroforamina decreases its size with increasing degrees of hyperextension ($p < 0.01$), and ipsilateral rotation induces additive effects on this decrease [78]. Since human spinal tissues are rate sensitive, dynamic load applications similar to those encountered in rear-end collisions may have different biomechanical effects on the human head-neck complex [79]. Studies are not available to determine the changes under these dynamic loads. These changes are likely to be different when the intact head is included in the experimental model as it is well known that the inertial effects contribute to added changes in the intervertebral motions [80-81]. It may be necessary to temporally measure the changes in the neuroforaminal diameter during whiplash loading to quantify the kinematics of this component. This requires sophisticated instrumentation. It is important to note that quantifications of the overall and local mechanisms of injury during the whiplash loading phase with particular reference to the facet joint kinetics (and kinematics) and upper cervical-head motions will address the most common locations of whiplash associated problems.

Previous hypotheses regarding the mechanism of injury have involved overall movements of the head-neck complex. For example, earlier postulates indicated "acute flexion followed by extension" [67]. This was later disproved by the seminal work of Severy using controlled laboratory investigations suggesting extension followed by flexion during a rear-end impact to be the overall mechanism [20]. More recently, hypertranslation of the head has been postulated as a mechanism [82]. The concept of our research (described later) regarding the overall mechanism is a hybrid of these proposals. Further rationale for our studies is delineated below.

The above discussed experimental modeling studies using human cadavers and human volunteers form a primary database for the understanding of whiplash injury biomechanics. Human volunteer exposures in real-world vehicles have the unique feature of monitoring the physiological response during and after whiplash loading. The use of car-to-car rear-end impact crash scenarios can assess the efficacy of vehicular interiors such as head restraints, and seat and seatback strength. However, practical and ethical limitations constrain the extension of these experiments into the injury producing range and to higher velocities. Although the overall kinematics of the head-neck complex in relation to the human torso and the associated vehicle seating system can be determined using high-speed photography, accurate determination of the temporal motions of the dynamic cervical spine structures on a level-by-level (segmental) or on a component basis is difficult. A moving vehicle together with the difficulty in instrumenting the test subject and placing the high-speed cameras to track the above described motions pose considerable challenges. In addition, the strength-related variables such as the forces and moments on the cervical spine cannot be measured in these tests. To determine the strength and motion-related biomechanical parameters, i.e., to describe the kinetics due to whiplash loading, human cadaver experiments are necessary. The following factors have to be considered to achieve these objectives: experimental model, instrumentation, loading, and data acquisition and analysis.

6.1 Experimental Model

Real-world whiplash injury is primarily due to vehicular rear-end impact. Because the human body is accelerated due to impact from the rear, it is important to include the appropriate masses of the head and neck structures in any experimental model focused to delineate the biomechanics of whiplash. The initial masses of the various structural components impart inertial effects during dynamic loading. Mass and time factors play a role. The traditional one- or two-level motion segment (vertebra-disc-vertebra) experimental models are inadequate not only because of the unique upper cervical anatomy, but also they cannot adequately address the segmental changes associated with whiplash loading. Furthermore, it is difficult to include the surrounding neck musculature and the skin in these models. Levels that can be tested will only include below the axis because of the lack of intervertebral disc between the atlas and axis. Therefore, motion segment models have to be extended to include the entire cervical spine column. Although the entire cervical column model can be prepared with the surrounding soft tissue structures to include the human neck anatomy, fixation at the proximal end will introduce artifactual boundary conditions rendering the model less than accurate. Furthermore, it is not possible to determine the upper cervical spine kinetics as occipital attachments are consciously excluded. Any artificial surrogate used to replace the actual head of the human cadaver will be approximate in terms of its placement, as the center of gravity of the intact head in relation to the cervical spine cannot be precisely determined, and the dynamic characteristics of the artificial surrogate head cannot mimic the actual dynamics of the intact head attached to the cervical spinal column. These considerations obviously lead to the use of the entire intact head-neck complex; the preparation includes the ligamentous column, musculature, skin, and the intact cranium and its contents. Needless to say, because of the inclusion of the intact head, not only the actual attachments to the upper cervical spine and the surrounding musculature are included, but

also the actual mass of the head along with its eccentric placement on the cervical spine is automatically incorporated into the model. It must be noted that because of the cadaver nature of the experimental model, these structures account for the passive response. Because most dynamic injury to the human tissues and more specifically to the neck occur very early in the trauma event (first 100 msec), and because it has been determined that active muscle contraction does not begin before 100 msec during whiplash loading, the human cadaver is an appropriate model for these studies [62,83-87].

6.2 Instrumentation

It is imperative to use appropriate instrumentation that can record the strength and the kinematics-related parameters to determine the kinetics of the structure. To measure the forces and bending moments in the three anatomical planes, a six-axis load cell can be attached to the inferior preparation of the intact head-neck complex. This will provide the generalized force histories. Accelerometers (e.g., nine-axis array) and velocity sensor arrays (e.g., triaxial or uniaxial sensors) can be attached to the intact head. These sensors can be used to determine the linear and angular accelerations and velocities, and also to compute the moments at the occipital condyles during whiplash loading. In addition, miniature accelerometers can be fixed to the cervical vertebrae to obtain the local acceleration responses. All the above described sensors are capable of recording the data in a dynamic mode. To obtain the kinematics of the structure, biomechanical studies have traditionally used transducers such as strain gauges. However, these types of instruments are difficult to use in the intact head-neck preparation. For example, attaching strain gauges to the bony regions of the cervical vertebrae is a challenging task as the model includes soft tissue structures, it is time consuming, and above all, increases the demand on the channel capabilities of the data acquisition system. Furthermore, difficulties in the calibration procedures together with the sensor break-down during loading introduce limitations on the deformation response characterization. The use of optical techniques is an effective way to obtain the dynamic deformation responses. These techniques minimize the above hindrances as no electronic cabling systems are necessary and the data can be recorded using high-speed photography/imaging. Retroreflective targets can be easily placed close to the various cervical spine joints and at various locations in the bones. These procedures serve as a means to determine the local component (e.g., facet joint), and the overall and segmental motions of the head-neck complex.

6.3 Loading

As indicated earlier, whiplash loading is a dynamic event which renders the traditional procedures of static loading inapplicable. In addition, since whiplash is inertially induced, i.e., not caused by a direct blow to the neck or the head, pure moment type or impact loading methods are also inapplicable. The impact from the rear in the real-world accelerates the human torso forward inducing an acceleration-time history at the cervico-thoracic level. This acceleration-time history imparts inertial loading to the superior neck and head structures. Therefore, it is appropriate to apply these types of acceleration-time histories as input to the experimental model at the distal end of the preparation. These factors generally preclude the use of devices such as drop towers and electrohydraulic testing systems to apply whiplash loading to the head-neck complex. Repeatability and reproducibility are among the principal requirements of the loading device used to apply the acceleration-time pulse to simulate whiplash loading. The loading device must also be calibrated with physical models such as the Hybrid III anthropomorphic manikin so that future parallel experimentation can be conducted to assess the biofidelity of any physical model. A mini-sled pendulum device is an appropriate choice to meet these requirements. The pendulum serves as a loading device to apply inertial loading to the head-neck complex. By suitably orienting the head-neck structure it is possible to apply inertial loads in extension, flexion and oblique modes simulating the differing human postures in real-world rear crashes. Pendulum raise height will induce various velocities of loading. Furthermore, the pendulum can be designed with various masses and dashpot materials to shape the whiplash input pulse. Accelerometer and load cell sensors attached to the pendulum will determine the forces, velocities and accelerations. The mini-sled will house the properly oriented preparation and following impact loading from the pendulum at the base of the preparation, the run out will induce the intended acceleration.

6.4 Data Acquisition and Analysis

Again, because of the dynamic nature of the applied insult, it is important to record the biomechanical data at high sampling rates of more than 10,000 Hz. Routinely, during impact biomechanics evaluations, the Society of Automotive Engineers 211b specifications are used with regard to the anti-aliasing and filtering of signals. An additional feature in these tests is to synchronize the data acquisition from the sensors (e.g., accelerometers), the optical markers which use high-speed photography, and the loading apparatus. These systems are an integral part of the experimental design. Digital procedures are available to completely synchronize the entire system so that a one-to-one correlation between the kinetic and the kinematic data can be obtained during analysis. Initial data analysis includes the determination of the peak responses in the associated temporal domain coupled with the kinematics. It is important to determine the temporal motions of the cervical spine structures from a segmental and from a component (e.g., facet joint) perspective as these biomechanical parameters may explain the mechanism of whiplash injury. For example, excessive stretching of the upper cervical spine-head complex may explain the mechanism of sub-occipital headaches observed clinically following whiplash injury. In addition, excessive and/or differing facet joint motions in the mid-lower cervical spine may explain neck pain following a real-world rear-end impact. These "microscopic type" mechanistic motions can be investigated using the above described procedures.

As a part of the initial study, using the above rationale, in our laboratory, human cadaver head-neck complexes were tested to determine the dynamic mechanisms of injury. Whiplash type, i.e., inertial dynamic forces, were applied to the distal end of the human cadaver head-neck complex. These advancements are described below.

7. Whiplash Biomechanics Studies at the Medical College of Wisconsin

7.1 Methods and Experimental Design

These studies were initially sponsored by the Office of Naval Research in 1994 in an attempt to develop to a finite element model of the cervical spine, and a preliminary analysis from our testing protocol was presented in 1995 [49]. Studies are still on-going to completely understand the biomechanics of whiplash. A mini-sled pendulum equipment was designed to house the human cadaver head-neck complex and the loading assembly. Recent articles by Yoganandan, Pintar and co-workers provide the rationale needed for designing a mini-sled pendulum setup [6,49,88]. The mini-sled consists of two 2.5 m long precision ground rails (19 mm diameter) rigidly attached to a steel frame 1.5 m high. Four precision rolled ball bearings form the interface between the cart assembly and the rails. To permit different loading modalities, the cart assembly accepts a six-axis load cell and allows for a vertical (z) axis rotation of the specimen under test. A flat surface attached to the cart assembly receives the impact from the pendulum. The hollow pendulum impactor assembly is cylindrical in shape (40 cm long, 15 cm diameter). It is designed such that varying weight (up to 100 kg) can be added in its center thereby adjusting initial momentum input. A load cell is attached at the leading face of the impactor with capabilities to attach energy absorbing materials such as padded surfaces. By properly adjusting the pendulum mass and the energy absorbing material, it is possible to duplicate the acceleration wave forms typically seen in rear-end crashes (e.g., human volunteer pulses recorded at the cervico-thoracic level). Instrumentation devices such as accelerometers at the rear face of the pendulum striker and leading edge of the specimen together with load cells on the pendulum and specimen provide a complete time history quantification of the biomechanical strength variables.

Initial tests were conducted with the anthropomorphic Hybrid III head-neck system to replicate the pulse characteristics and calibrate the mini-sled pendulum equipment. In addition to the above mentioned mini-sled pendulum instrumentation, other instrumentation included accelerometers in the manikin head, angular velocity sensors, accelerometer in the slider of the mini-sled pendulum device, and a triaxial accelerometer at the base of the neck. Because the Hybrid III head-neck is a repeatable and reproducible device, it is possible to arrive at the most appropriate combinations of the mini-sled pendulum mass and the associated energy absorbing materials to match the required acceleration wave form (G-time history) which can then be used to conduct the human cadaver head-neck complex tests. It should also be noted that these instrumentation devices serve as a means to develop standards for whiplash injury assessment as these sensors are already being used in the manikin for compliant testing according to the Federal Motor Vehicle Safety Standards for frontal impact [89]. This methodology of testing the human cadaver head-neck complexes will not only delineate the dynamic mechanisms of injury (described below) but will also accommodate acquisition of other data which can be used to correlate the dynamic kinematics, and assist in the development of biofidelic devices which can predict injury and design safer vehicular interiors. These are the additional long-term goals of our multifaceted research study.

Intact human cadaver head-neck complexes were rigidly fixed at the T2-3 (inferior) end using polymethyl-methacrylate. The superior end (head) was unconstrained. This allowed for the natural end conditions for the cervical spine at the cephalad end. Further, this preparation incorporates the actual inertial contribution from the head as it is neither isolated nor compensated artificially by attaching a physical surrogate. It must be emphasized that due to the mass of the head, the dynamic kinematics of the cervical spine will be significantly affected if proper end conditions are not maintained in the model. The intact head preserves all of the relevant anatomical attachments to the cervical spine and maintains the appropriate mass properties. A standard coordinate axis was used: posterior to anterior direction represented the positive x-axis, right-to-left direction represented the positive y-axis, and inferior to superior direction represented the positive z-axis [81,83,90]. The preparation was mounted with posterior soft tissues including the ligamentum nuchae and the skin. In the anterior region, the skin and muscle were left intact; the esophagus and trachea were removed. To facilitate target placement for obtaining the localized kinematics, the skin and muscle (bilateral) tissue were dissected away. However, ligaments were not violated. Retroreflective targets were placed on the mastoid process of the skull, on the anterior regions of the exposed vertebral bodies, and on the lateral masses at every cervical spinal level according to accepted techniques [84]. Additional smaller flat-head pin targets were fixed into the bony portions of the facet joint such that at least two targets each were seen locally on the superior and inferior facet articulations. The test set-up is shown in Figure 1.

A uniaxial accelerometer (Entran, Inc., Fairfield, NJ) was attached to the rear face of the pendulum for measuring the input accelerations. A uniaxial load cell (Interface, Inc., Scottsdale, AZ) was attached to the leading face of the impactor to record the input dynamic forces. A six-axis load cell (Denton Inc., Rochester Hills, MI) was attached to the inferior fixation of the test specimen to record the generalized force- (and moment) time histories. In addition, an accelerometer placed at this level recorded acceleration at the inferior end. At the superior end (head), a triaxial accelerometer and a triaxial angular velocity sensor were attached to measure the linear and angular components of the acceleration and velocity, respectively. All information was gathered using a digital data acquisition system (ODAS, DSP Technology, San Francisco, CA) according to the SAE J211b specifications at a sampling rate of 12,500 Hz with appropriate anti-aliasing filters and signal conditioning equipment [78,91-94]. A high-speed video camera (Kodak, Model 4540, Rochester, NY) operating at 2,250 to 4,500 full frames/sec was used to capture the impact event and determine the overall temporal kinematics of the retroreflective targets in the sagittal plane which were determined using the principles of continuous motion analysis [86-87,95]. The system also has the flexibility to incorporate custom-designed force transducers made from Kynar piezo-electric film. The transducers are 220 microns in thickness and have a 6 mm square loading area to measure the force transmission through the facet joints during loading. An array of these transducers has successfully been employed in an instrumented artificial spinal cord to study cord forces during a burst fracture event using an intact human cadaver head-neck model [96]. Because the frequency response of this transducer is in the Giga-hertz range, higher frequency events such as failure of tissue components can be sensed. These transducers were inserted into the facet joint capsule by transecting only the lateral portions of the capsular ligaments on one side of the preparation. Another high-speed, high-resolution digital video system was used to capture and determine the localized temporal kinematics of the facet joints using the principles of continuous motion analysis.

Initial tests were conducted with the specimen turned upside down (n = 9) to check the feasibility of the methodology. The initial orientation was under the flexion (anterior region facing the impactor) or the extension (posterior region facing the impactor) mode. By rotating the specimen in the fixture housed in the mini-sled 180 degrees, the orientation was changed from flexion to extension or vice-versa. The specimen was subjected to noncontact type inertial loading by impacting at the inferior end (T2 level) with the pendulum impactor. Velocities of 1.1, 2.3 and 3.5 m/s were chosen in the preliminary study. All the biomechanical information was gathered under each velocity. Following these initial flexion and extension tests with the specimen in an upside down position, a total of seven tests were conducted in the right side up, i.e., normal head-neck orientation. The head-neck complex was oriented such that the head was at the top with the Frankfurt plane horizontal. The mastoid process was aligned over the center of the T1 vertebral body. This orientation of the head-neck complex approximates the normal seated driving position used in human volunteer studies [18,43]. In addition, it is anatomically reproducible in each specimen. The specimens were oriented symmetrically without any accompanying initial head rotation. Loading was applied such that the pendulum impactor contacted the base of the preparation at the inferior end so that the specimen went into an extension mode due to the posterior impact. Some salient results from the right side up extension loading experiments include the following.

7.2 Results

The generalized force-time histories recorded by the six-axis load cell demonstrated bending moment (flexion/extension) and shear (anterior/posterior) forces to be predominant during the loading phase, without any significant off-axis forces (lateral shear or axial load) or moments (torsion or lateral-flexion). This suggests that the head-neck complex of the specimen is primarily subjected to a planar type of dynamic force input. Overall kinematic target analysis revealed the response of the cervical spine to the whiplash loading event (Figure 2). The overall-view camera images were analyzed on a temporal basis to reveal head lag with respect to the base. This resulting translation of the T1 base with respect to the head, produced an S-curve in the spine. The plots in Figure 2 demonstrate this S-curve wherein the upper spine (head-C2) is forced into flexion and the lower spine (C6-T1) is forced into extension. This demonstrates the local temporal segmental kinematic differences in the head-neck complex under inertial extension, i.e., whiplash loading.

The local temporal motions, i.e., head with respect to T1, C2 with respect to T1, and so on, and head-C2, C2-C3, C3-C4, etc., quantified the head lag from cervical motion. The local head-C2 flexion occurs during the initial translation phase (head lag) between torso (T1) and head and continues somewhat as the head "catches up" with the torso and begins extension motion (Figure 2). During this phase, the S-curve forms in the cervical spine. It is only after this phase that overall head-neck extension occurs, the commonly accepted "whiplash motion". This initial reverse curvature between the head and upper cervical spine, compared to the mid-lower cervical spine region is primarily driven by the inertial mass of the head. Posterior stretching of the structures may occur during the local flexion phase of the head-C2 complex, creating soft tissue injuries to structures such as ligaments and/or muscles. It must be noted that this local upper cervical flexion occurs very early in the inertial loading phase, i.e., during the translation of the torso with respect to the head. It is during this period that certain muscles are already actively maintaining the initial orientation of the head-neck complex, but other inactive muscles have not yet reacted to the loading event. Therefore, any stretching of the fibers during this period may induce trauma to the associated structures. This phenomenon may explain the sub-occipital headaches noted clinically in whiplash patients.

The localized component kinematics were also analyzed on a temporal basis. The high-speed, high-resolution camera documented the facet joint movements during the event (Figure 3). Small (1-2 mm diameter) targets on the facet joints documented the sliding and compression/tension movements that occurred in the joint (Figure 4). The C5-C6 facet joint motions were analyzed for the first 100 msec of the event. The upper two graphs in Figure 4 demonstrate that the anteroposterior translation motions of the joint are approximately equal between anterior and posterior target pairs. The superior-inferior motion (compression) however, follows a different pattern. The posterior target pair undergoes compression from 50 to 100 msec, whereas the anterior target pair shows little change. This posterior compression in the facet joint during the initial loading may be a mechanism of injury in the lower facet joints, leading to excitation of local pain fibers. This kind of compression may not be noted as gross injury but may be enough to cause micro-fractures of the cartilage plates and squeezing of the synovial space in these joints. The lower graph in Figure 4 demonstrates transducer output from the 6 mm square force transducer placed in the C7-T1 joint space during the event. Note that this facet joint experiences increasing compressive forces throughout this initial phase. These transducers placed on the contralateral side as the targets further quantify the magnitude of force experienced by the lower facet joints. These fundamental concepts and preliminary data have been reported by Yoganandan, Pintar and co-workers [50,97-98].

The cumulative influence of dynamics in association with the biomechanics of the hard and soft tissues of the human head-neck complex bears relation to the kinetics (kinematics and strength) and presumably to the ensuing symptomatology. The mechanics of the structure, the focus of the our efforts, will act as a catalyst to pursue further research activities to better understand the symptomatology. These investigations could lead to better treatment procedures for the whiplash injured patient. In addition, understanding the dynamic mechanisms of injury will assist in the development of test devices (e.g., Hybrid III dummy) which can be used to predict trauma in rear crashes, and thereby facilitate safer and user-friendly vehicular designs. It must be emphasized that the widely used Hybrid III dummy does not possess proven biofidelity to be used in rear crashes as it was developed in the 1970s for frontal impact assessment [99]. Other recent developments in manikin design also need fundamental biomechanical data for achieving the required biofidelity in order to be used to predict injury in rear crashes [52,100]. When the mechanisms of injury are clearly delineated, it will then be possible to design suitable vehicular interiors such as seats, headrests and restraint systems. Our present intact head-neck complex experimental model together with dynamic inertial whiplash type force application has the potential to further study the mechanics of the structure.

The human cadaver model is the best surrogate to study mechanisms of injury in the human condition. Under dynamic loading conditions the mass and mass moment of inertia properties are essentially the same as those

for the *in vivo* human. The human cadaver model also allows for direct invasive measurements that are impossible to obtain in the human volunteer studies. The lack of muscle tone is a disadvantage of the present cadaver model. However, under dynamic loading conditions it has been generally acknowledged that muscle contraction does not occur until 150 msec or more after the initiation of the event. In a recent study examining the electromyographic signals from the neck musculature during human volunteer rear impact auto collisions, it was found that initial muscle activation did not occur until 100 msec after event start. These authors also noted that full muscle contraction did not occur until 150-170 msec after event onset when the head-neck was already in extension [62]. Similar findings have been confirmed by Kaneoka and Ono [101]. Recent work by Pope and co-workers with human volunteer tests under whiplash loading conditions also demonstrate muscle activation at greater than or equal to 100 msec [102]. Since our laboratory data indicate that injury occurs before this time, active muscle contraction does not appear to be a major factor. Many studies in dynamic biomechanics confirm the notion that trauma occurs early in the dynamic event when acceleration/deceleration is most severe [81,83-85,103-104]. Compression-related injuries of the cervical spine for example, occur before the head motion can influence the outcome [85]. The protective action of muscle activation serves to reduce the magnitude and duration of dynamic loading (acceleration/deceleration) to the head and neck structures during whiplash loading [102]. It is logical therefore, that without this protective component (first 100 msec), the spine could be more susceptible to injury. In the living human, the head is held upright by activation of certain anterior and posterior muscle groups. These muscle groups essentially pre-align the head with respect to the cervical spine prior to loading. It can also be noted that these muscles are generally situated deeper and closer to the vertebrae. Since there are sudden angular changes between the vertebrae during the initial phase, these contracting muscles may be highly susceptible to damage.

Our multi-faceted experimental design includes the use of a mini-sled apparatus which allows for inputting the acceleration-time histories recorded at cervico-thoracic levels in human volunteer rear crash tests, the use of various transducers to obtain parameters such as head velocities and accelerations, the use of targets placed at the various spinal components to determine the local kinematics of the head-neck complex, and the use of miniature transducers in the facet capsule at various cervical levels to obtain the relative temporal forces in these components. This design duplicates a rear impact crash scenario to the inferior end of the head-neck complex so that an evaluation can be made of the overall and localized kinematics, and the associated kinetics (e.g., facet loads) to understand the dynamic mechanisms of whiplash injury.

7.3 Summary

We have made attempts to describe the dynamic kinetics (and kinematics) of the human head and neck during whiplash loading [6,49-50]. The experimental model included the intact head to delineate the head to upper cervical spine motions. In addition, the entire neck structure including the ligamentous cervical spinal column up to the first thoracic level, the neck musculature, the ligamentum nuchae and the skin were maintained. Using a specially designed and calibrated mini-sled pendulum, the acceleration-time pulse was applied to the human cadaver specimen. A six-axis load cell at the inferior thoracic end documented the dynamic force and moment histories in the three anatomic planes to quantify the strength characteristic biomechanics of the human cervical spine. Retroreflective targets were placed at every vertebral level of the head-neck complex including the head and also at the cervical facet joints (Figure 1). Using high-resolution and high-speed digital video cameras, the overall (head to T1), segmental (e.g., occiput to C2), and local (e.g., C4-C5 anterior regions of the facet joint) motions were described on a temporal basis.

The head-neck complex primarily sustains the inertially applied flexion/extension loading in a sagittal mode, i.e., off-axis forces and moments are relatively insignificant. During the initial phases of the extension loading in whiplash, the upper cervical spine-head undergoes local flexion concomitant with a lag of the head while the mid-lower cervical column is in local extension, thus establishing a reverse curvature. This reverse curvature may result in stretching of the upper head-neck complex which may lead to sub-occipital headaches. With continuing application of the dynamic loading, the inertia of the head catches up with the cervical spine and approximately at the end of the loading phase, the entire head-neck complex is under the extension mode.

In contrast, the lower cervical spine facet joints demonstrate local compression and sliding along the joint throughout the loading phase. While both the anterior- and posterior-most regions of the facet joint slide, the posterior-most region of the joint compresses more than the anterior-most region thus exhibiting, on a temporal basis, a "pinching" mechanism. These differing local micro motions of the facet joint may provide a biomechanical basis of cervical pain attributable to the zygapophyseal joints [13]. Although, these initial results are available,

factors such as the initial orientation of the head and neck with respect to the torso and the underlying support structures, thresholds of injury as a function of age, gender and spinal degeneration, and impact severity, are yet to be considered for a full delineation of the mechanisms of whiplash injury.

8. Conclusions

Whiplash injury is a problem with significant impact. The annual estimated cost of this problem in the US alone is approximately four and one-half billion dollars. Health care providers, biomedical engineers and others have contributed to our present recognition and understanding of the injury and the management of whiplash patients. There is a lack of consensus with regard to the injury production despite these advancements. Numerous mechanisms of injury have been proposed. Tension, extension, shear, compression and hyperextension mechanisms are proposed from a modality point-of-view. From an initial alignment viewpoint, variations in the spinal curvatures are reported to be responsible for the injury. The bending moment, shear and axial forces, and head rotation from injury indices' perspective, and spinal segmental changes and muscle activities resulting in local curvature alterations and component motions during the application of the inertial load vector from the posterior to the anterior directions from a dynamic kinematics aspect, have been implicated in one way or another in this context. The effect of the restraint system, the presence or absence or even the location and type of headrest, seat design and other interior components from a vehicular perspective are also attributed to be the causal factors in whiplash injury. Despite these identifications, no single study has completely evaluated the efficaciousness of any particular mechanism of injury.

Although the epidemiology and the developments in this area have basically evolved from the Western countries, because of the increasing use of motor vehicles both in the developed and other countries, whiplash injury is not just confined to the Western population. Concerted efforts are needed to derive the underlying mechanism of injury through an evaluation of the kinetics from overall, local, segmental and component perspectives; arrive at appropriate injury criteria that can be used in the design and development of anthropomorphic dummies; and, design safer motor vehicles. Injury prevention and control can be accomplished using this approach.

Appendix A

A brief overview of the physical and mathematical modeling studies on the topic is given.

A.1 Physical Model Tests

Severy et al., conducted three tests with the Sierra type dummies at bullet vehicle speeds of 11.2 kph (7 mph), 15.8 kph (9.9 mph), and 31.7 kph (19.8 mph) [20]. Differences were noted between the responses of the dummy and the human volunteer. Scott et al., compared a male human volunteer's (50 years of age, 78 kg weight, and 180 cm tall, placed in the driver position) data with the 50th percentile Hybrid III dummy (right front passenger) responses [42]. The details of the development of the Hybrid III neck are reported [105]. The volunteer used in three tests underwent seven impacts. The Hybrid III kinematics were different from the human volunteer in all the different phases during the entire rear-crash impact event. Although tests were conducted with Ito Seki 3DGM-JM50 dummy by Matsushita et al., no results were reported [61]. The Hybrid II dummy tests conducted by Szabo et al., indicated that the manikin is less than biofidelic [41]. The differences in the responses between the human volunteer and the dummy were attributed to the improper back anthropometry, and stiff cervical and lumbar spine constructions. This study underscored the need for the development of a more biofidelic dummy for whiplash injury prediction. Svenson designed a new dummy neck and termed the device "Rear Impact Dummy", RID, for rear impact [106]. The need to validate the dummy with more data was emphasized in this study. Analyses of the different physical models to predict injury in whiplash environments reported herein are not exhaustive. Because of a paucity of data and a consensus on an accurate estimation of the mechanism of injury, the existing physical models are not completely biofidelic and further laboratory research is urgently needed to develop whiplash injury criteria and mechanisms.

A.2 Mathematical Modeling Studies

Yoganandan et al., reviewed the mathematical and finite element models of spinal injuries [107]. With specific reference to the current topic, Martinez and Garcia in 1968, developed a model for analyzing whiplash biomechanics [33]. The closed-form type analysis was developed to determine the head angular and linear accelerations due to a 5 G peak 200 msec pulse. The Orne and Liu's pilot ejection model was extended by McKenzie and Williams in 1971 to study the behavior of the human head-neck and seatback system secondary to whiplash [34,108-109]. Modifications were made to include the atlas and axis which were considered rigid and resembling the other vertebral bodies despite their characteristic differences in the anatomy. A deformable link was used between the head and atlas. The link incorporated the same properties of the intervertebral disc. The model considered the torso and the seatback as rigid. The head and cervical spine geometrical data were obtained from a 188 cm (six feet two inches), 72.6 kg (160 lb) male. The study investigated the effects of seatback stiffness on the head-neck kinetics by subjecting the discrete parameter model of the head, neck and torso to a 5 G, 200 msec pulse. The head lagged the motion of T1. The study indicated that low stiffness could lead to high tensile loading with bending in the lower cervical spine. This was attributed by the authors to contribute to anterior ligament tears and associated structural damage. However, the analysis for the increasing seatback stiffness indicated the possibility of compression in the lower cervical spine. This compressive force with the added bending moment was considered to result in facet fractures. Because of the assumptions, the model is not applicable for extending the analysis beyond the first 171 msec. The authors underscored the need to obtain structural properties of the spinal tissues for a better understanding of whiplash injury biomechanics.

In 1975, Prasad et al., extended their earlier pilot ejection model, which was also based on the Orne and Liu model, to investigate the dynamic response of the spine secondary to forward acceleration [35,108-109]. The model relaxed the rigidity assumption present in the earlier models for the seatback and the torso, and a seatback cushion was added. The vertebrae and head were considered rigid. In contrast, the intervertebral discs were assumed to be deformable. The model accounted for the human spinal curvature. Head restraints were simulated by increasing the height of the seatback. The input pulse simulated a 48 kph rear impact with a velocity change of 24 kph. Belt restraints were not included because it was considered ineffective at this change in velocity. For an elastic seatback with a maximum rotation of 10 degrees, the model indicated the following: for the first 100 msec, the head lagged T1 and the spine translated rearward into the seatback with a simultaneous ramping (movement of the spine upwards

in the seatback). During this time, the relative rotation of the head with respect to T1 was small. At 100 msec the seatback rebounded resulting in a hyperextension of the neck at approximately 150 msec. Angular acceleration of the head did not change appreciably with different types of seatback. In contrast, the head to T1 angular rotation varied from 105 degrees for an elastic seatback with no head restraint, to 45 degrees for a rigid seatback with head restraint. Based on these findings, Prasad et al., concluded that the angular rotation of the head may not be the sole predictor of whiplash injury. The maximum axial neck forces were tensile with no head restraint and compressive with the presence of a head restraint. While the shear force decreased at C3 and C7 with the presence of a head restraint, shear forces at the head-neck junction increased. Greater offset between the spine and the seatback increased the head to T1 angular rotation, torque, axial and shear forces at the head, C3 and C7, and ramping. The reader is referred to the original citation for numeric details [35]. Prasad et al., further compared these data with a human cadaver test (77 kg weight, 73.7 cm sitting height) conducted at 40/45 kph impact velocity. The study demonstrated that a flexible seatback reduces the forces and the bending moments in the spine. Since, in many simulations the model predicted forces at the C3-C4 level were higher compared to the forces at the head-neck junction, whiplash injury was predicted to occur at the C3-C4 levels. Prasad et al., indicated that a proper selection of the seatback stiffness and the head restraint is necessary to control hyperextension-induced whiplash injury.

Goldsmith and co-workers developed a series of physical and mathematical models for head-neck simulations [110-111]. The earlier models of Deng and Goldsmith were exercised in frontal flexion and lateral loading [110]. The model based on the lumped parameter approach included the effects of spinal musculature. Representation of the Hybrid III manikin head-neck system was included in these simulations. However, simulations were not done to analyze the response secondary to whiplash forces. Recently de Jager et al., reported the development of a more detailed head-neck model [112]. The head and the vertebrae were assumed to be rigid. They were connected by linear viscoelastic intervertebral discs, nonlinear viscoelastic ligaments, friction-free facet joints and contractile muscles. Although the model was exercised under frontal and lateral impact modalities, analysis under the whiplash mode was not done. However, this model appears to have the potential to investigate the biomechanical response under rear impact. Further details of this model are given in another chapter in this book.

Acknowledgment: This research was supported in part by DOT NHTSA Grant DTNH22-93-Y-17028, PHS CDC R49CCR507370, and the Department of Veterans Affairs Medical Center Research Service.

References

[1] Griffiths HJ, Olson PN, Everson LI, Winemiller M. Hyperextension strain or "whiplash" injuries to the cervical spine. *Skeletal Radiology* 1995:24: 263-266.

[2] Foreman SM, Croft AC. *Whiplash Injuries. The cervical acceleration/deceleration syndrome.* Second Edition, Williams & Wilkins, Baltimore, MD, 1995: 500.

[3] Teasell RW , Shaprio AP. *Spine. State of the Art Reviews. Cervical flexion-extension/whiplash injuries.* Hanley & Belfus, Philadelphia, PA, 1993: 578.

[4] Sances A Jr, Myklebust JB, Maiman DJ, Larson SJ, Cusick JF, Jodat RW. The biomechanics of spinal injuries. *CRC Critical Reviews in Biomedical Engineering* 1984:11(1): 1-76.

[5] States JD, Korn MW, Masengill JB. The enigma of whiplash injuries. *NY State Med J* 1970:70(1): 83-108.

[6] Yoganandan N, Pintar FA, Cusick JF. Cervical spine kinematics under inertial flexion-extension. In: *11th North American Spine Society*, Vancouver, BC, 1996, pp 265-266.

[7] Spitzer WO, Skovron ML, Salmi LR, Cassidy JD, Duranceau J, Suissa S, Zeiss E. Scientific monograph of the Quebec task force on whiplash-associated disorders: Redefining "Whiplash" and its management. *Spine* 1995:20(8S): 73S pp.

[8] Gunzburg R. In: *Whiplash 1996 International Symposium.* Brussels, Belgium, 1996.

[9] Hohl M. Soft tissue injuries of the neck in automobile accidents: Factors influencing prognosis. *J Bone Jt Surg* 1974:56A: 1675-1682.

[10] Deans GT, McGalliard JN, Rutherford WH. Incidence and duration of neck pain among patients injured in car accidents. *Br Med J* 1986:292: 94-95.

[11] Schrader H, Obelieniene D, Bovim G, Surkiene D, Mickeviciene D, Miseviciene I, Sand T. Natural evolution of late whiplash syndrome outside the medicolegal context. *Lancet* 1996:347: 1207-1211.

[12] Grady D. In one country, chronic whiplash is uncompensated (and unknown). In: *The New York Times*, New York, NY, 1996.

[13] Barnsley L, Lord S, Bogduk N. Clinical Review - Whiplash Injury. *Pain* 1994:58: 283-307.

[14] Koch M, Kullgren A, Lie A, Nygren A, Tingvall C. Soft tissue injury of the cervical spine in rear-end and frontal car collisions. In: *International Research Conference Biokinetics of Impact.* Brunnen, Switzerland, 1995: 273-283.

[15] *AIS. The Abbreviated Injury Scale.* American Association for Automotive Medicine, Arlington Heights, IL, 1990.

[16] Deans GT, McGilliard JN, Kerr M, Rutherford WH. Neck sprain - a major cause of disability following car accidents. *Injury* 1987:18: 10-12.

[17] Kaufmann M, Lancaster K, Rasmussen SJ. *Whiplash Injuries.* Institute Insurance for Highway Safety: Arlington, VA, 1995.

[18] Ono K , Kanno M. Influences of the physical parameters on the risk to neck injuries in low impact speed rear-end collisions. *Accid Anal and Prev* 1996:28(4): 493-499.

[19] MacNab J. Acceleration extension injuries of the cervical spine. In: *The Spine.* RH Rothman, FA Simeone (eds). WB Saunders, Philadelphia, PA., 1982: 647-660.

[20] Severy DM, Mathewson JH, Bechtol CO. Controlled automobile rear-end collisions, an investigation of related engineering and medical phenomena. *Can Serv Med J* 1955:11: 727-759.

[21] Larder DR, Twiss MK, Mackay GM. Neck injury to car occupants using seat belts. In: *29th Annual American Association for Automobile Medicine Conference*, Des Plaines, IL, 1985, pp 153-165.

[22] Hirsch SA, Hirsch PJ, Hiramoto H, Weiss A. Whiplash syndrome. Fact or fiction? *Orthopedic Clinics of North America* 1988:19(4): 791-795.

[23] Nygren A, Gustafsson H, Tingvall C. Effects of different types of headrests in rear-end collisions. In: *10th International Conference on Experimental Safety Vehicles*, 1985, pp 85-90.

[24] O'Neill B, Haddon W, Kelley AB, Sorenson WW. Automobile head restraints: Frequency of neck injury insurance claims in relation to the presence of head restraints. *Am J Publ Health* 1972:62(3): 399-406.

[25] Koch M, Nygren A, Tingvall C. Impairment pattern in passenger car crashes, a follow-up of injuries resulting in long-term consequences. In: *Experimental Safety Vehicles Conference 94-S5-0-02*, Munchen, 1994, pp 776-781.

[26] Lovsund P, Nygren A, Salen B, Tingvall C. Neck injuries in rear end collisions among front and rear seat occupants. In: *Proceedings International Research Conference On Biokinetics of Impact*, Bergisch-Gladbach, F.R.G., 1988, pp 319-325.

[27] Miller T, Pindus N, Douglass J. Medically related motor vehicle injury costs by body region and severity. *J Trauma* 1993:34(2): 270-275.

[28] Viano DC, Gargan MF. Headrest position during normal driving: Implication to neck injury risk in rear crashes. *Accident Analysis & Prevention* 1996:28(6): 665-674.

[29] Blumenstein R. Baseball catcher's mitt helps to inspire a safer, whiplash-resistant auto seat. In: *Wall Street Journal*, New York, NY, December 26, 1995.

[30] Galasko CSB. Whiplash Associated disorders: Cost to society. In: *Whiplash '96*, Brussels, Belgium, 1996, p 55.

[31] Yoganandan N, Haffner M, Maiman DJ, Nichols H, Pintar FA, Jentzen J, Weinshel S, Larson SJ, Sances A Jr. Epidemiology and injury biomechanics of motor vehicle related trauma to the human spine. *SAE Transactions* 1990:98(6): 1790-1807.

[32] Maag U, Laberge-Nadeau C, Xiang TT. Neck strains in car crashes: Incidence, associations, length of compensation and cost to insurer. In: *Proceedings 37th Association Advancement of Automotive Medicine*, San Antonio, TX, 1993, pp 15-26.

[33] Martinez JL, Garcia DJ. A model for whiplash. *J Biomechanics* 1968:1(1): 23-32.

[34] McKenzie JA, Williams JF. The dynamic behavior of the head and cervical spine during "whiplash". *J Biomech* 1971:4(6): 477-490.

[35] Prasad P, Mital N, King AI, Patrick LM. Dynamic response of the spine during +Gx acceleration. In: *Proceedings 19th Stapp Car Crash Conference,* San Diego, CA, 1975, pp 869-897.

[36] Pontius UR, Liu YK. Neuromuscular effects in a dynamic model of the cervical spine. In: *Proceedings NSF Workshop on Voluntary Human Effort*, Gainsville, FL, 1975, pp 147-175.

[37] Ommaya AK , Hirsch AE. Tolerances for cerebral concussion from head impact and whiplash in primates. *J Biomech* 1971:4(1): 13-21.

[38] Ommaya AK, Faas F, Yarnell P. Whiplash injury and brain damage - an experimental study. *JAMA* 1968: 204: 285-289.

[39] Wickstrom JK, Martinez JL, Rodriguez R, Haines DM. Hyperextension and hyperflexion injuries to the head and neck of primates. In: *Neckache and Backache*. ES Gurdjian, LM Thomas (eds). CC Thomas, Springfield, IL., 1970: 108-119.

[40] Domer FR, Liu YK, Chandran KB, Krieger KW. Effect of hyperextension-hyperflexion (whiplash) on the function of the blood-brain barrier of rhesus monkeys. *Exp Neurol* 1979:63: 304-310.

[41] Szabo TJ, Welcher JB, Anderson RD, Rice MM, Ward JA, Paulo LR, Carpenter NJ. Human occupant kinematic response to low speed rear-end impacts. In: *Proceedings SAE Conference*, 1994: 630-642.

[42] Scott MW, McConnell WE, Guzman HM, Howard RP, Bomar JB, Smith HL, Benedict JV, Raddin JH, Hatsell CP. Comparison of human and ATD head kinematics during low-speed rearend impacts. In: *International Congress and Exposition*, Detroit, MI, 1993, pp 1-8.

[43] McConnell WE, Howard RP, Guzman HM, Bomar JB, Raddin JH, Benedict JV, Smith HL, Hatsell CP. Analysis of human test subject kinematic responses to low velocity rear end impacts. In: *International Congress and Exposition*, Detroit, MI, 1993, pp 21-30.

[44] McConnell WE, Howard RP, Van Poppel J, Krause R, Guzman HM, Bomar JB, Raddin JH, Benedict JV, Hatsell CP. Human head and neck kinematics after low velocity rear-end impacts - understanding "whiplash". In: *Proceedings 39th Stapp Car Crash Conference*, San Francisco, CA, 1995, pp 215-238.

[45] Mertz HJ, Patrick LM. Strength and response of the human neck. In: *Proceedings 15th Stapp Car Crash Conference*, Coronado, CA, 1971, pp 207-255.

[46] Mertz HJ, Patrick LM. Investigation of the kinematics and kinetics of whiplash. In: *Proceedings 11th Stapp Car Crash Conference,* Anaheim, CA, 1967, pp 267-317.

[47] Clemens HJ, Burow K. Experimental investigation on injury mechanism of cervical spine at frontal and rear-frontal vehicle impacts. In: *Proceedings 16th Stapp Car Crash Conference,* Detroit, MI, 1972, pp 76-104.

[48] Panjabi MM, Cholewicki J, Babat L, Nibu K, Dvorak J. A new approach to whiplash biomechanics. In: *42nd Orthopaedic Research Society Proceedings*, Atlanta, GA, 1996, p 163.

[49] Yoganandan N, Pintar FA, Sances A Jr, Voo LM, Cusick JF. Inertial flexion-extension loading of the human neck. *Adv Bioeng* 1995:31: 45-46.

[50] Yoganandan N, Pintar FA, Kumaresan S, Cusick JF, Sances A Jr. Cervical spine biomechanics under whiplash loading. *ASME Adv Bioeng* 1997:32: 443-444.

[51] Thunnissen J, Wismans J, Ewing CL, Thomas DJ. Human volunteer head-neck response in frontal flexion: A new analysis. In: *Proceedings 39th Stapp Car Crash Conference,* San Francisco, CA, 1995, pp 439-460.

[52] White RP, Zhao Q, Rangarajan N, Haffner M, Eppinger M, Kleinberger M. Development of an instrumented biofidelic neck for the NHTSA advanced frontal test dummy. In: *15th International Conference on Experimental Safety of Vehicles*, Melbourne, Australia, 1996, pp 1-13.

[53] Mertz HJ. The kinematics and kinetics of whiplash. In: *Engineering Mechanics*. Wayne State University, Detroit, MI., 1967: 370.

[54] SAE Vehicle Occupant Restraint Systems and Components Standards Manual. 1993: SAE HS-13: 254 pp.

[55] Marar BC. Hyperextension injuries of the cervical spine. *J Bone Jt Surg* 1974:56-A(8): 1655-1662.

[56] Roaf R. A study of the mechanics of spinal injuries. *J Bone Joint Surg* 1960:42B: 810.

[57] Shea M, Wittenberg RH, Edwards WT, White AAI, Hayes WC. In vitro hyperextension injuries in the human cadaveric cervical spine. *J Ortho Res* 1992:10: 911-916.

[58] Yoo JU, Zou D, Edwards T, Bayley J, Yuan HA. Effect of cervical spine motion on the neuroforaminal dimensions of human cervical spine. *Spine* 1992:17(10): 1131-1136.

[59] Geigl BC, Steffan H, Leinzinger P, Muhlbauer M, Bauer G. The movement of head and cervical spine during rearend impact. In: *1994 International Conference on the Biomechanics of Impacts*, Lyon, France, 1994.

[60] West DH, Gough JP, Harper GT. Low speed rear-end collision testing using human subjects. *Accident Reconstruction Journal* 1993:5(1): 22-26.

[61] Matsushita T, Sato TB, Hirabayashi K, Fujimura S, Asazuma T, Takatori T. X-ray study of the human neck motion due to head inertia loading. In: *Proceedings 38th Stapp Car Crash Conference,* Ft. Lauderdale, FL, 1994, pp 55-64.

[62] Szabo TJ, Welcher JB. Human subject kinematics and electromyographic activity during low speed rear impacts. In: *Proceedings 40th Stapp Car Crash Conference,* Albuquerque, NM, 1996, pp 295-315.

[63] Algers G, Pettersson K, Hildingsson C, Toolanen G. Surgery for chronic symptoms after whiplash injury. Follow-up of 20 cases. *Acta Orthop Scand* 1993:64(6): 654-656.

[64] Lord S, Bogduk N, Barnsley L. Prevalence of third occipital headache following whiplash. *Orthop Trans* 1992.

[65] Pearce JM. Whiplash injury: A reappraisal. *J Neurol Neurosurg Psychiatry* 1989:52: 1329-1331.

[66] Maimaris C, Barnes MR, Allen MJ. "Whiplash injuries" of the neck: A retrospective study. *Injury* 1988: 19: 393-396.

[67] Gay JR, Abbott KH. Common whiplash injuries of the neck. *JAMA* 1953:152: 1698-1704.

[68] Sherk HH, Dunn EJ, Eismont FJ, Fielding JW, Long DM, Ono K, Penning L, Raynor R. *The Cervical Spine.* Second Edition. JB Lippincott Co., Philadelphia, PA, 1989: 881.

[69] Edmeads J. The cervical spine and headache. *Neurology* 1988:38: 1874-1878.

[70] Dwyer A, Aprill C, Bogduk N. Cervical zygapophysial joint pain patterns I: A study in normal volunteers. *Spine* 1990:15: 453-457.

[71] Aprill C, Dwyer A, Bogduk N. Cervical zygapophyseal joint pain patterns II: A clinical evaluation. *Spine* 1990:15(6): 458-461.

[72] Clark CR, Igram CM, Khoury GY, Ehara S. Radiographic evaluation of cervical spine injuries. *Spine* 1988:13: 742-747.

[73] Abel MS. The radiology of chronic neck pain: Sequelae of occult traumatic lesions. *CRC Crit Rev Diagn Imag* 1982:20: 27-78.

[74] Buonocore E, Hartman JT, Nelson CL. Cineradiograms of cervical spine in diagnosis of soft-tissue injuries. *JAMA* 1966:198: 143-147.

[75] Bucholz RW, Burkhead WZ, Graham W, Petty C. Occult cervical spine injuries in fatal traffic accidents. *J Trauma* 1979:19(10): 768-771.

[76] Jonsson H, Cesarini K, Sahlstedt B, Rauschning W. Findings and outcome in whiplash type neck distortions. *Spine* 1994:19(24): 2733-2743.

[77] Abel MS. Occult traumatic lesions of the cervical vertebrae. *CRC Crit Rev Clin Radiol Nucl Med* 1975:6: 469-553.

[78] Yoganandan N, Pintar FA, Skrade D, Chmiel W, Reinartz JM, Sances A Jr. Thoracic biomechanics with air bag restraint. *SAE Transactions* 1994:102(6): 2597-2607.

[79] Yoganandan N, Pintar FA, Butler J, Reinartz J, Sances A Jr, Larson SJ. Dynamic response of human cervical spine ligaments. *Spine* 1989:14(10): 1102-1110.

[80] Ewing CL, Thomas DJ, Sances A Jr, Larson SJ (eds). *Impact Injury of the Head and Spine.* CC Thomas, Springfield, IL, 1983: 785 pp.

[81] Sances A Jr, Thomas DJ, Ewing CL, Larson SJ, Unterharnscheidt F (eds). *Mechanisms of Head and Spine Trauma.* Aloray, Goshen, NY, 1986: 746 pp.

[82] Penning L. Hypertranslation des Kopfes nach hinten: Teil des Schleuderverletz-ungsmechanismus der HWS? *Orthopade* 1994:23: 268-274.

[83] Pintar FA, Yoganandan N, Voo LM, Cusick JF, Maiman DJ, Sances A Jr. Dynamic characteristics of the human cervical spine. *SAE Transactions* 1995:104(6): 3087-3094.

[84] Pintar FA, Sances A Jr, Yoganandan N, Reinartz JM, Maiman DJ, Suh JK, Unger G, Cusick JF, Larson SJ. Biodynamics of the total human cadaver cervical spine. In: *Proceedings 34th Stapp Car Crash Conference*, Orlando, FL, 1990, pp 55-72.

[85] Nightingale RW, McElhaney JH, Richardson WJ, Myers B. Dynamic responses of the head and cervical spine to axial impact loading. *J Biomech* 1996:29(3): 307-318.

[86] Yoganandan N, Pintar FA, Arnold P, Reinartz J, Cusick JF, Maiman DJ, Sances A Jr. Continuous motion analysis of the head-neck complex under impact. *J Spinal Disord* 1994:7(3): 420-428.

[87] Yoganandan N, Pintar FA, Sances A Jr, Reinartz J, Larson SJ. Strength and kinematic response of dynamic cervical spine injuries. *Spine* 1991:16(10): 511-517.

[88] Yoganandan N, Pintar FA. Inertial loading of the human cervical spine. *J Biomech Eng* 1997:119(3): 237-240.

[89] *Code of Federal Regulations.* National Highway Traffic Safety Administration, Washington, DC, 1995: 407-539 pp.

[90] Pintar FA, Yoganandan N, Sances A Jr, Reinartz J, Harris G, Larson SJ. Kinematic and anatomical analysis of the human cervical spinal column under axial loading. *SAE Transactions* 1990:98(6): 1766-1789.

[91] Yoganandan N, Skrade D, Pintar F, Reinartz J, Sances A Jr. Thoracic deformation contours in a frontal impact. In: *Proceedings 35th Stapp Car Crash Conference*, San Diego, CA, 1991, pp 47-63.

[92] Yoganandan N, Morgan RM, Eppinger RH, Pintar FA, Skrade DA, Sances A Jr. Thoracic deformation and velocity analysis in frontal impact. *J Biomech Engr* 1995:117: 48-52.

[93] Yoganandan N, Morgan RM, Eppinger RH, Pintar FA, Sances A Jr, Williams A. Mechanism of thoracic injury in a frontal impact. *J Biomech Engr* 1996:118: 595-597.

[94] Pintar FA, Yoganandan N, Sances A Jr, Eppinger RH. Instrumentation of human surrogates for side impact. In: *Proceedings 40th Stapp Car Crash Conference,* Albuquerque, NM, 1996, pp 29-42.

[95] Yoganandan N, Pintar FA, Sances A Jr, Maiman DJ. Strength and motion analysis of the human head-neck complex. *J Spinal Disord* 1991:4(1): 73-85.

[96] Pintar FA, Schlick MB, Yoganandan N, Maiman DJ. Instrumented artificial spinal cord for human cervical pressure measurement. *Bio-Med Mat & Eng* 1996:6(2): 219-229.

[97] Yoganandan N, Pintar FA. Facet joint local component kinetics in whiplash trauma. *ASME Adv Bioeng* 1997 (In press).

[98] Yoganandan N, Pintar F, Kleinberger M. Cervical vertebral and facet joint kinematics under whiplash. *J Biomech Eng* (In press).

[99] Backaitis SH, Mertz HJ (eds). *Hybrid III: The First Human-Like Crash Test Dummy.* Society of Automotive Engineers, Warrendale, PA, 1994: 830 pp.

[100] Svensson MY, Lovsund P, Haland Y, Larsson S. The influence of seat-back and head-restraint properties on the head-neck motion during rear-impact. In: *IRCOBI International Conference Biomechanics of Impacts.* Eindhoven, Netherlands, 1993, pp 395-406.

[101] Kaneoka K, Ono K. Personal Communication.

[102] Pope MH, Aleksiev A, Wilder D, Magnusson M, Fusaro V, Spratt K, Goel VK. The role of muscles in whiplash injuries/EMG wavelet analysis. In: *Whiplash '96*, Brussels, Belgium, 1996, pp 20-21.

[103] Levine RS (ed). *Head and neck injury.* Society of Automotive Engineers, Warrendale, PA, 1994: 255 pp.

[104] Nahum AM, Melvin JW (eds). *Accidental Injury: Biomechanics and prevention.* Springler Verlag, 1993: 577 pp.

[105] Foster JK, Kortge JO, Wolanin MJ. A biomechanical based crash test dummy. In: *Proceedings 21st Stapp Car Crash Conference*, New Orleans, LA, 1977, pp 973-1014.

[106] Svensson MY, Lovsund P. A dummy for rear-end collisions - development and validation of a new dummy-neck. In: *IRCOBI International Conference Biomechanics of Impacts*, Verona, Italy, 1992, pp 299-310.

[107] Yoganandan N, Myklebust JB, Ray G, Sances A Jr. Mathematical and finite element analysis of spinal injuries. *CRC Review Biomed Eng* 1987:15(1): 29-93.

[108] Orne D, Liu YK. A mathematical of spinal response to impact. In: *Department of Engineering Mechanics*, University of Michigan, Ann Arbor, MI., 1969, p. 113.

[109] Orne D, Liu YK. A mathematical model of spinal response to impact. *J Biomech* 1971:4(1): 49-71.

[110] Deng YC, Goldsmith W. Response of a human head/neck/upper torso replica to dynamic loading. *J Biomech* 1987:20: 471-498.

[111] Landkof B, Goldsmith W. Impact on a head-neck structure. *J Biomech* 1976:9: 141-151.

[112] de Jager MK. *Mathematical Head-Neck Models for Acceleration Impacts.* Eindhoven University of Technology: Eindhoven, The Netherlands, 1996.

Figure Captions

Figure 1: Head-neck preparation set-up for whiplash loading experiments. The C4-C7 aspect of the spine was filmed at high-speed to obtain the localized movements of the facet joints during loading. Smaller facet joint targets were used to obtain the relative sliding and/or compression kinematics in the joint.

Figure 2: The upper two pictures are taken from images of the digital video camera system at 4500 f/s. The images demonstrate the S-curve that occurs during the first 100 msec of whiplash loading. The upper cervical segments are in flexion and the lower cervical segments are in extension. The upper graph quantifies this motion for these segments for the first 100 msec. The lower plot represents the angular motions at each level with respect to the base.

Figure 3: Images from the high-speed, high-resolution digital video camera system. The above four images were taken at 0, 40, 60, and 78 msec to demonstrate the localized movements in the spinal segments during loading. The first frame includes segment identification. The C5-C6 segment of the image is enlarged in the lower picture to demonstrate the smaller targets used in the facet joint sliding and compression analysis given in Figure 4.

Figure 4: C5-C6 facet joint motions are depicted in the top two plots. The top plot demonstrates the change in the anteroposterior distance (sliding) of the anterior and posterior pairs of targets illustrated in figure 3. Note that both pairs of targets demonstrate similar translations. The middle plot demonstrates the change in the superior-inferior distance from the same target pairs. The posterior targets exhibit more compression than the anterior targets. The sudden compression in the posterior aspect of the facet joint in the initial stages of whiplash loading may be a potential mechanism of injury. The bottom graph is the facet force transducer output recorded during the same event at the C7-T1 level. Note that the C7-T1 joint undergoes compression during this period.

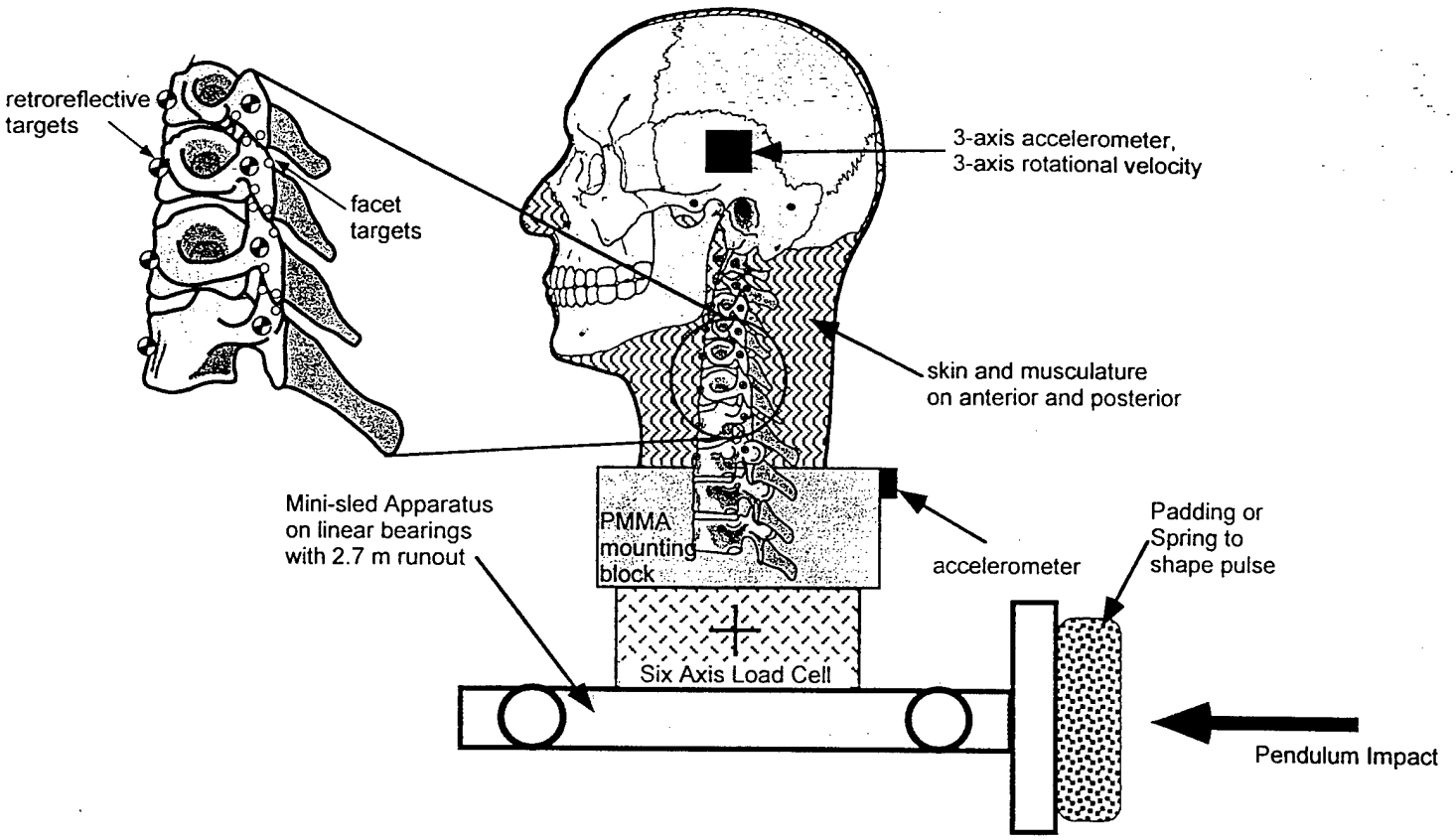
retroreflective targets
facet targets
3-axis accelerometer, 3-axis rotational velocity
skin and musculature on anterior and posterior
Mini-sled Apparatus on linear bearings with 2.7 m runout
PMMA mounting block
accelerometer
Padding or Spring to shape pulse
Six Axis Load Cell
Pendulum Impact

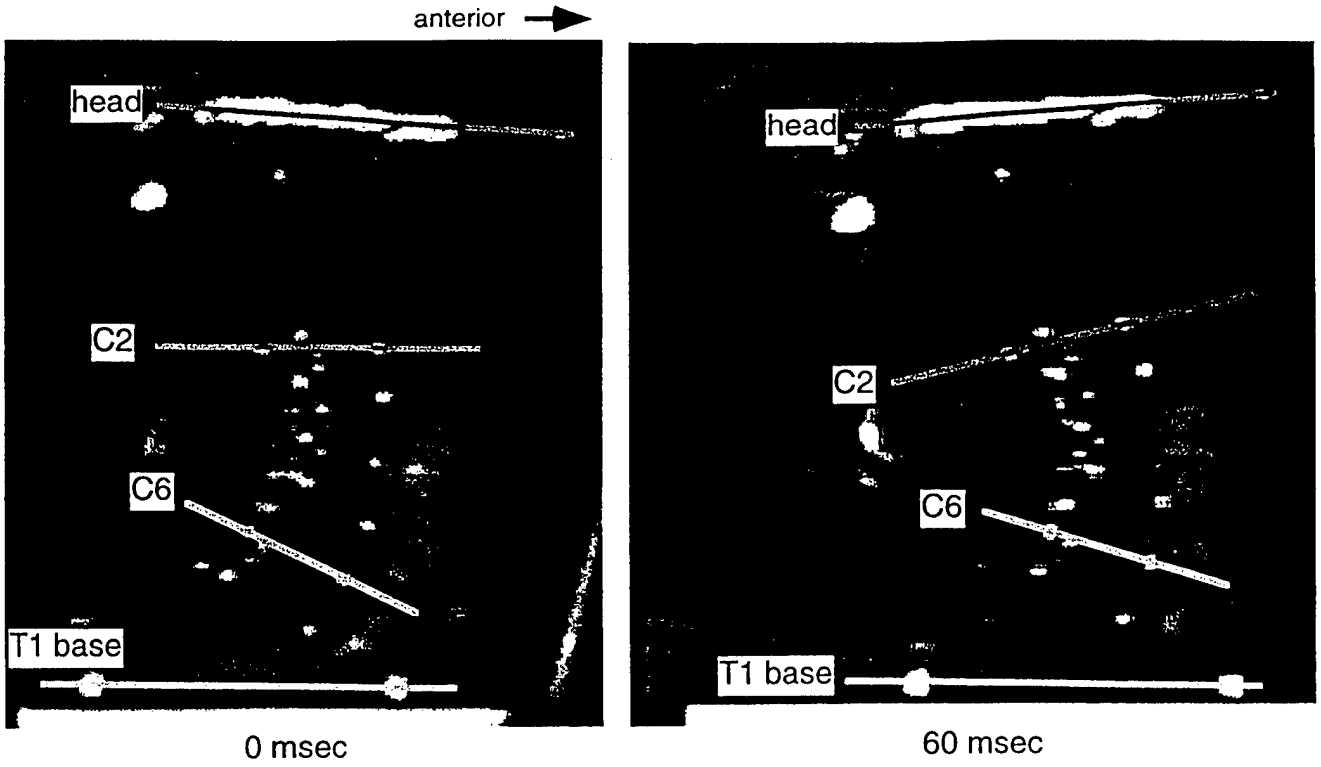
anterior
head
C2
C6
T1 base
0 msec
head
C2
C6
T1 base
60 msec

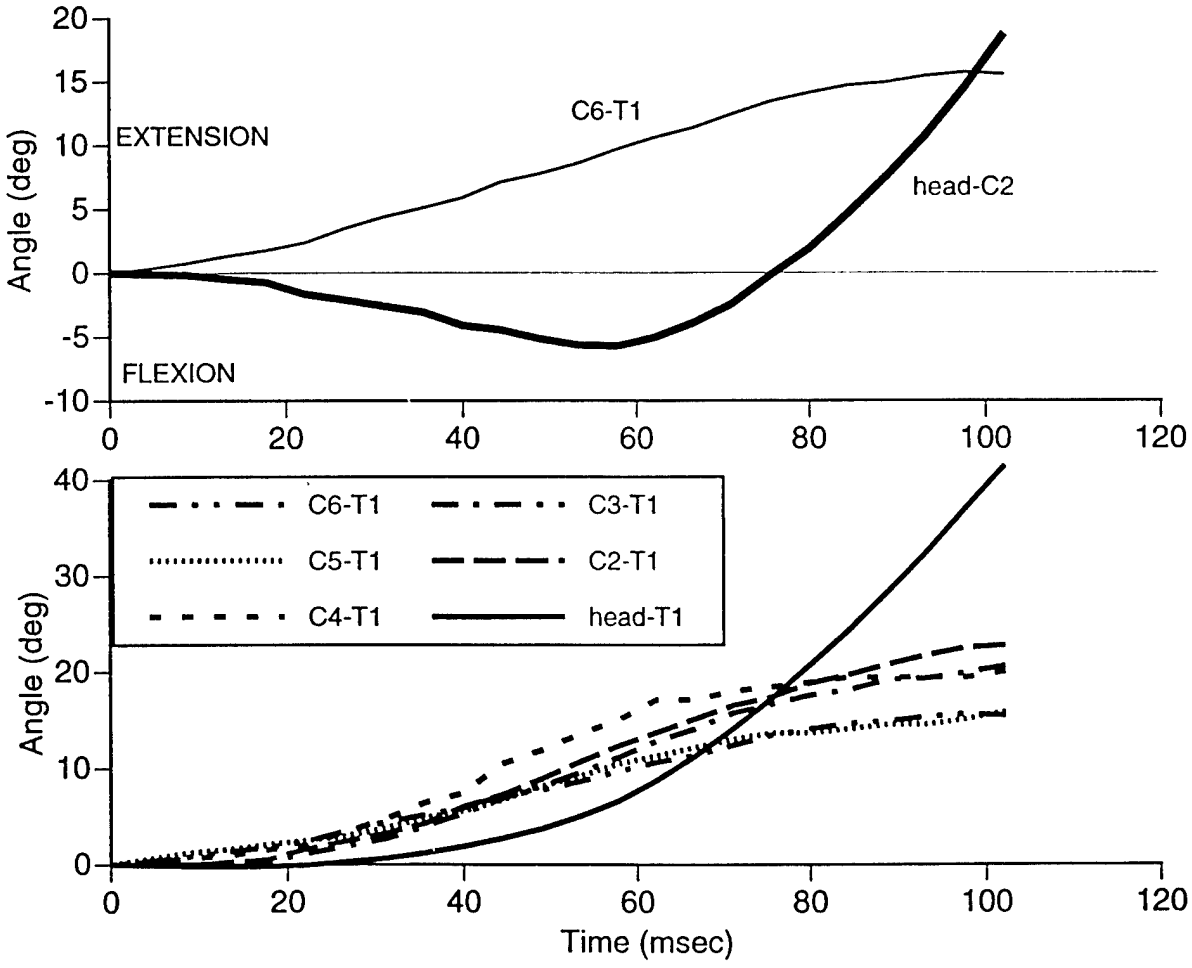
Angle (deg)
EXTENSION
FLEXION
C6-T1
head-C2
20
15
10
5
0
-5
-10
0
20
40
60
80
100
120
C6-T1
C3-T1
C5-T1
C2-T1
C4-T1
head-T1
Angle (deg)
Time (msec)

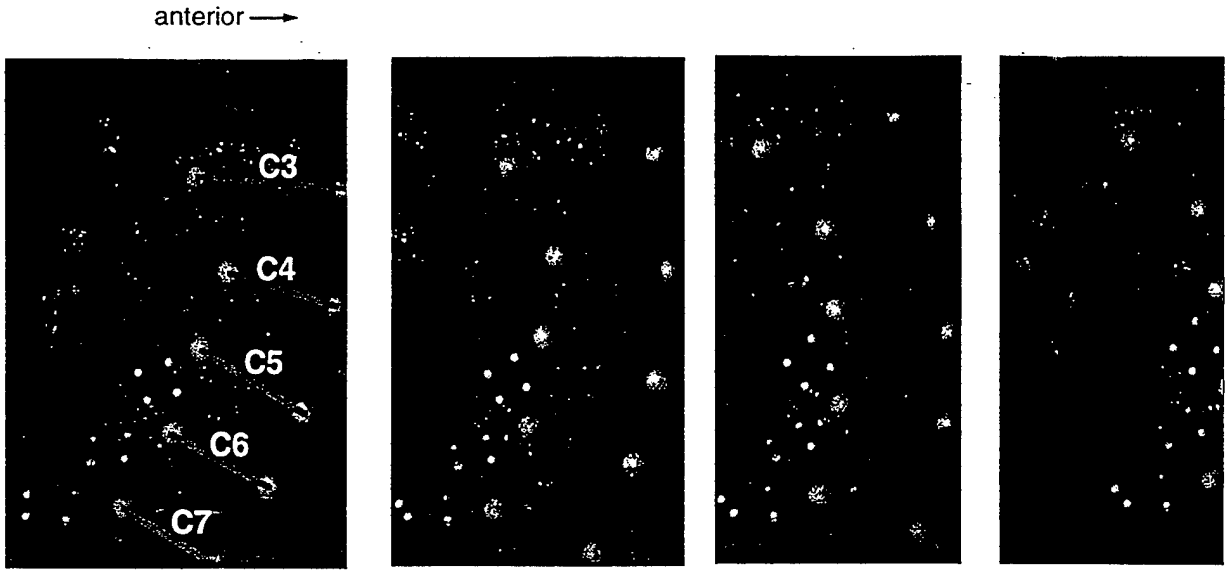
anterior
C3
C4
C5
C6
C7
0 msec
40 msec
60 msec
78 msec

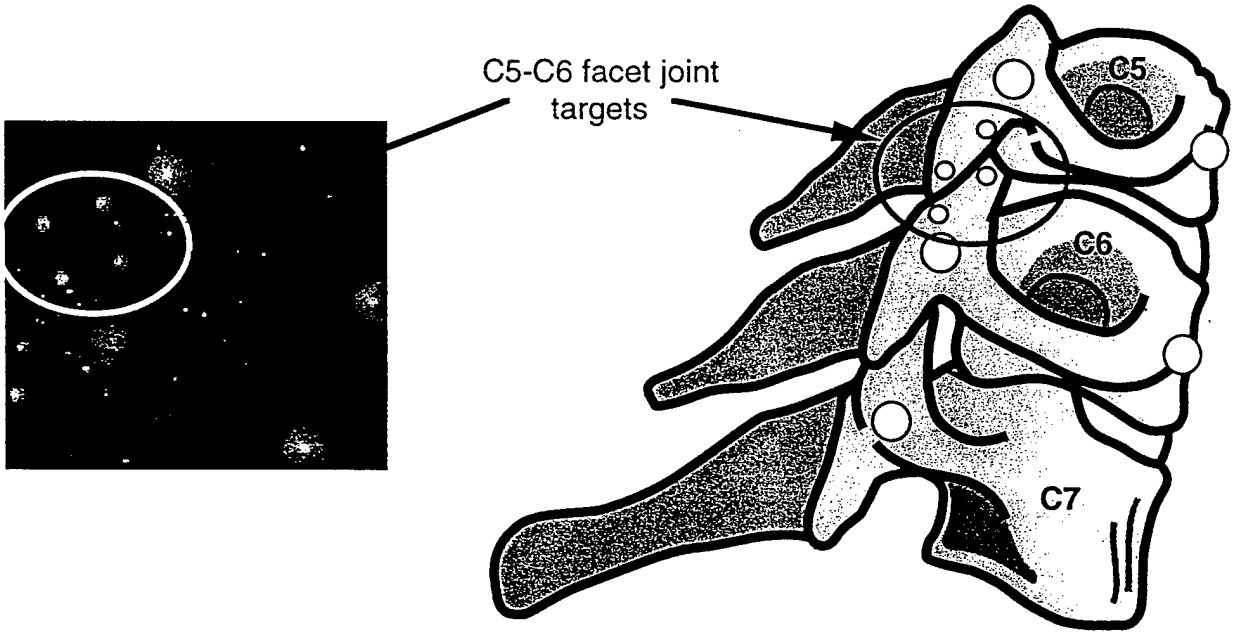
C5-C6 facet joint
targets
C5
C6
C7

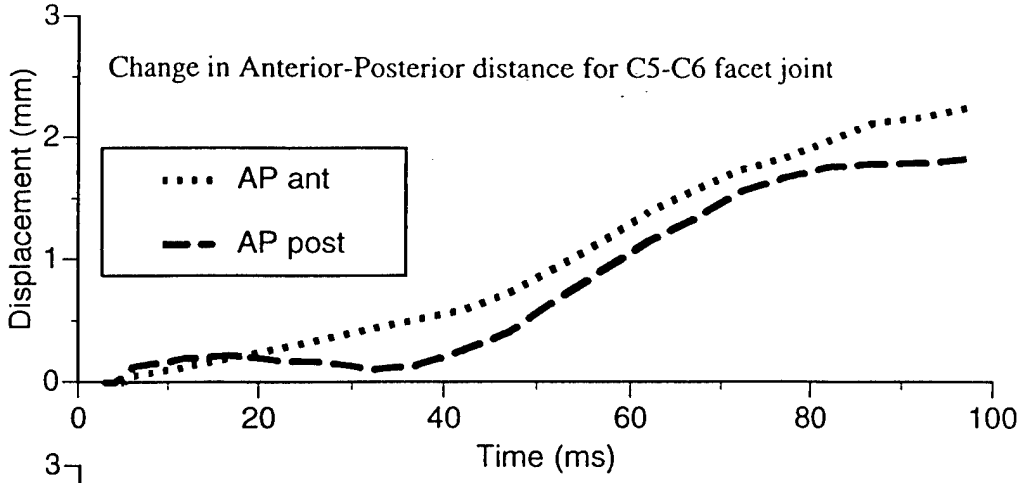
Change in Anterior-Posterior distance for C5-C6 facet joint
AP ant
AP post
Displacement (mm)
Time (ms)
0
1
2
3
0
20
40
60
80
100

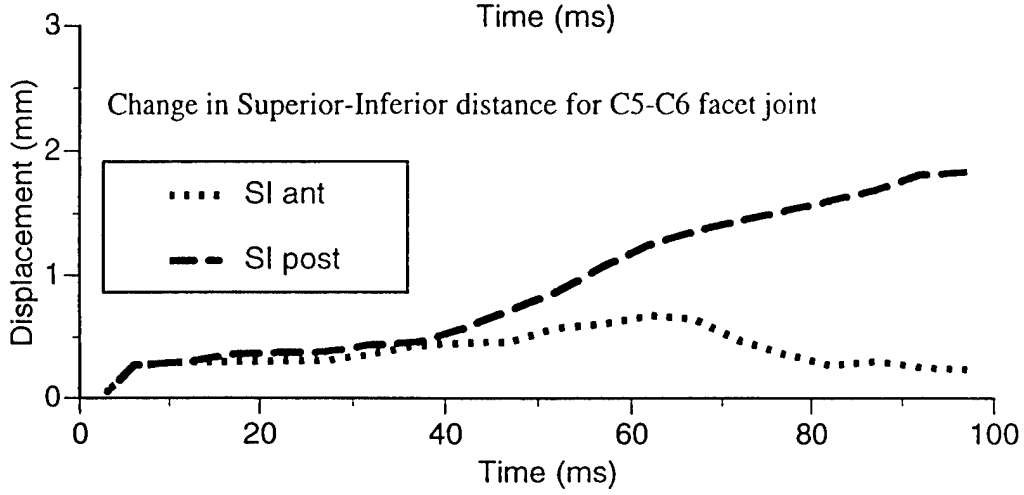
Change in Superior-Inferior distance for C5-C6 facet joint
SI ant
SI post
Displacement (mm)
Time (ms)
0
1
2
3
0
20
40
60
80
100

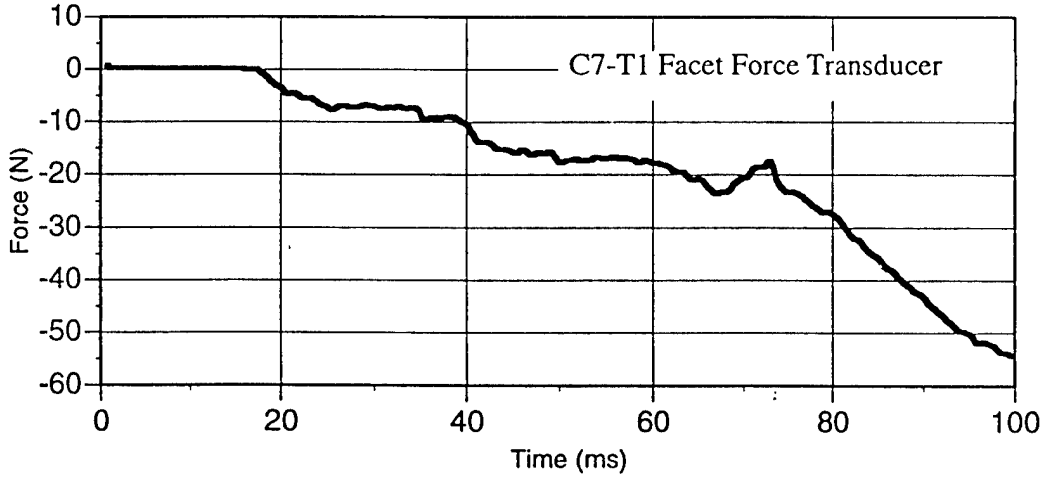
C7-T1 Facet Force Transducer
Force (N)
Time (ms)
10
0
-10
-20
-30
-40
-50
-60
0
20
40
60
80
100

SEGMENTED COLUMN MODEL TO PREDICT HUMAN CERVICAL SPINE BUCKLING

Liming Voo, Y. King Liu

Abstract

The response of the human cervical spine to external loads is influenced by stiffness of the cervical intervertebral joints and boundary conditions in addition to loading conditions. This study examines the influence of boundary conditions and intervertebral joint stiffnesses on the buckling responses of the straightened cervical spine in the sagittal plane. The straightened cervical spine was modeled as a segmented column with intersegmental joint stiffnesses in axial compression, shear and bending. Experimental stiffness data of the cadaver cervical intervertebral joints were used for the model intersegmental joint. Fixed-free, fixed-pinned, fixed-slide and fixed-fixed end-conditions were simulated. The column buckling responses were calculated by a computer software using principles of eigenvalue buckling analysis. The computed critical loads agreed with *in vitro* experimental results. The end-condition appeared to be the most influential factor for the magnitude of the critical loads and buckling mode shapes of the column. Compressive stiffness was not significant for column buckling. Bending and shear stiffnesses considerably affected the critical loads and the buckling mode shapes. Buckling response included joint dislocation modes unique for the segmented column. The segmented column is a better model for quantitative analysis of the cervical spine buckling response than a homogenous column.

1. Introduction

Cervical spinal injury occurs in motor vehicle crashes, falls, diving, tackle football, hockey and other contact sports. Consequences of severe neck injuries range from fatality to complete or incomplete quadriplegia [1-4]. The design of protective equipment requires an understanding of the mechanisms of cervical spine injury.

Epidemiological studies have shown that the majority of severe neck injuries occur due to compression-related loading resulting in vertebral body fractures and/or intervertebral joint dislocations [1-4]. Column buckling has been suggested as a potential mechanism associated with compression and compression-flexion types of cervical spine injuries [5-7].

This chapter discusses the characteristics of a segmented column model suitable for simulating the potential buckling responses of the straightened cervical spine under axial compression. A brief description about the evolution of this idea and definition of the terminology is provided first. A section is devoted to the methodology and results of the segmented column model analysis, followed by two sections on the equivalent homogeneous column model and a comparison of the two modeling approaches. The limitation, extension, relevance, and application of a segmented column model for the study of human cervical spine injuries are also discussed.

2. Background

The human cervical column in its naturally lordotic configuration does not exhibit buckling behavior because a compressive load would continually alter the pre-existing lordosis of the cervical spine, and buckling as defined by Euler in 1944, would not occur. However, qualitative analysis of severe neck injuries of compression-flexion types (vertebral body fracture and/or dislocation) in football athletes observed that straightened cervical spine and crown loading are the consistent factors associated with such injuries [5]. *In vitro* experimental production of cervical vertebral burst or compression fractures under longitudinal compression also necessitated a straightened cervical pre-alignment configuration [8,9]. This suggested that the straightened cervical column buckling in the sagittal plane is a potential mechanism of such injurious responses.

Liu and Dai proposed the concept of the stiffest axis and second stiffest axis of the cervical spine along which an impact load may induce buckling of the cervical column [7]. Idealizing the straightened human neck to be a homogeneous beam-column, the stiffest axis and the second stiffest axis concept provided insight into the possible underlining mechanisms and predicted that the cervical column pre-alignment (unloaded configuration, load alignment) was the key parameter for the production of the compression-related type of cervical injuries. A later work mapped out the potential column failure surfaces of a beam-column [6]. The stiffness variation of a beam-column due to change in loading angle and eccentricity was explored by the same authors (see proceeding chapter). The methodology of determining the stiffness matrix of a beam-column under the loading along the second stiffest axis was also presented. However, because of the homogeneity assumption, a direct application of their results to the inherently inhomogeneous cervical column is difficult. A model for the cervical spine should account for the inhomogeneity in the material, discontinuity in the deformation field, and bending and shear stiffness parameters. This can be achieved by treating the ligamentous human cervical spine as a segmented column.

There is a wide range of variation in the stiffness of the lower cervical spine (Table 1). Some studies have found that the lower cervical joints are stiffer than the mid cervical joints [10,11]. In contrast, others have found no significant differences among the cervical spinal levels between C2 and T1 [12,13]. Buckling responses of the cervical spinal column may not be sensitive to all of the intersegmental stiffness parameters. The boundary conditions have been shown to significantly affect the behavior of the ligamentous cadaver cervical spine under compressive load [14]. The buckling responses of the cervical column may also be affected by the boundary conditions. The terms defined below are used extensively in this chapter.

Homogeneous column	structure which has the same material throughout its entire column;
Segmented column	inhomogeneous structure which has a set of rigid segments jointed by elastic elements in series;
Bending	in-plane rotation of one segment with respect to the adjacent one;
Buckling	geometric change from one equilibrium configuration to another due to an applied load;
Buckling mode shape	describes a buckled column configuration with respect to geometry, without regard to load;
Critical load	maximum load that the column can carry in its initially unbuckled configuration;
Buckling mode	describes a buckled column with respect to shape and load;

End-condition boundary conditions at the end of the column.

Buckling response of a column is represented by buckling mode shapes and their corresponding critical loads. Each buckling mode shape represents a possible equilibrium configuration while its corresponding critical load is the magnitude at which the previous equilibrium configuration starts to change into this configuration. Therefore, the buckling mode shapes relate to the possible buckled equilibrium configurations of the initially straightened cervical column while the critical loads provide estimated load magnitudes sustained by the structure.

3. Buckling of a Segmented Column Model

The straightened cervical spine was idealized as a segmented column model consisting of eight rigid segments (cylinders) connected by elastic joints (Figure 1). The differences in the spinal level and asymmetry were neglected for simplicity and easy comparison to a homogeneous model. The height of each segment was 15 mm for each vertebra based on literature data [15]. Each joint permitted the adjacent segments to have three degrees-of-freedom with their associated stiffness values, i.e., axial (longitudinal) and shear (lateral) translations, and lateral rotations (bending). The three stiffness parameters (axial, shear, bending) used values obtained from the literature of cadaver experimental data that included axial compression, anteroposterior shear, and flexion-extension bending of a typical lower cervical intervertebral joint [10-13].

Three sets of stiffness values were used in each direction to evaluate the effects of joint stiffness on buckling: the low and high values encompassing the range in the actual experimental data (Table 1) and a mean value (Table 2). One stiffness parameter was varied (low, high, mean) while the other two were held constant at their mean level. This resulted in a total of seven models for the three parameters (Table 3). Model 1 was used as the control with all three mean stiffness values; models 2 and 3 were used to test the effects of axial (compressive) stiffness variation; models 4 and 5 were used to test effects of shear stiffness variation; and models 6 and 7 were used to test the effects of bending stiffness variation.

Table 1: Stiffnesses of the Lower Cervical Intervertebral Joints

		Comp	Tension	+Shear	-Shear	Lat Shear	Flex	Ext	Lat Bend	Torsion
Author	Region			(N/mm)				(Nm/rad)		
Liu	middle	3690	590	n/a	n/a	n/a	29	71	158	176
	lower	4120	580	n/a	n/a	n/a	169	148	219	225
Coffee	middle	5180	900	580	220	n/a	86	n/a	n/a	n/a
	lower	1360	200	104	130	n/a	166	191	n/a	n/a
Moroney	all	1080	390	140	50	120	152	186	172	149
Panjabi*		140	52	34	52	52	n/a	n/a	n/a	n/a

* Measured at 25-N force

Table 2: Stiffness Data Used in the Study

Description	Low	High	Mean
Axial Compressive (N/mm)	140	5180	3500
Anteroposterior shear (N/mm)	34	580	200
Flexion-extension bending (Nm/rad)	29	169	99

Table 3: Parametric Matrix for the Stiffness Variation

Model	Compression (N/mm)	Shear (N/mm)	Bending (Nm/rad)
1	3500	200	99
2	140	200	99
3	5180	200	99
4	3500	34	99
5	3500	580	99
6	3500	200	29
7	3500	200	169

Model 1: Control
Models 2 & 3: Effect of compressive stiffness variation
Models 4 & 5: Effect of shear stiffness variation
Models 6 & 7: Effect of bending stiffness variation

To evaluate the effects of boundary conditions, the following four typical end-conditions of a column were considered: fixed-free (FR), fixed-slide (FS), fixed-pinned (FP), and fixed-fixed (FF) (Figure 2). It was assumed that the lower end of the cervical spinal column was fixed while the upper end was allowed to move at least axially. The FR condition assumed that the upper end of the cervical column was free to move in any direction. The FS condition assumed that the upper end was also free in lateral (anteroposterior shear) translation. The FP condition assumed that the upper end was also free to rotate in the sagittal plane. The FF condition assumed that the upper end was allowed to translate only axially.

A total of 28 model simulations (7 models, 4 boundary conditions) were conducted. Linear eigenvalue buckling analysis was performed using a general purpose finite element analysis software, ANSYS®. The equation to be solved was:

$$([K] + \mu_i[S])\{u\}_i = \{0\} \quad (1)$$

where [K] = elastic stiffness matrix; [S] = stress stiffness matrix (based on a preload); μ_i = ith eigenvalue or critical load; $\{u\}_i$ = ith eigenvector of nodal displacements (used to construct buckling mode shapes). Each numerical solution provided the critical loads and corresponding buckling mode shapes. To keep the context of this chapter within the material related to cervical spine injury, only the first three buckling modes were included in each of the 28 simulations.

3.1 Mode Shapes

The segmented column exhibited complex buckling mode shapes. The mode shapes were generally mixtures of bending and joint dislocation (shear translation) patterns. To simplify the presentation however, the resulting shapes from the first three buckling modes were grouped into the following eight distinct sets (Figure 3).

A. load-end free deflection and rotation (first buckling mode for FR);
B. load-end lateral deflection without rotation (first buckling mode for FS);
C. joint (shear) dislocation with slight bending (first buckling mode for FP and FF with slight variations in each case);
D. single bending curve (second buckling mode for FR, and first or second buckling mode for FP with slight variations in each case);
E. stiffer single bending curve (second buckling mode for FS, and the first or second buckling mode for FF with slight variations in each case);
F. joint dislocation with double-curve (second or third buckling mode for FP, and first, second or third buckling mode for FF with slight variations in each case);
G. double-bending-curve with varying degree of joint dislocation (third buckling mode for FR and FP, and second buckling mode for FP with some variations in each case);
H. stiffer double-bending-curve with varying degree of joint dislocation (third buckling mode for FS and FF, and second buckling mode for FF with some variations in each case).

Similar mode shapes were grouped together in the above sets if their differences were small. For example, shape (C) was mainly a joint dislocation with varying degrees of bending curvature depending upon the end-conditions and stiffnesses: first mode with low shear stiffness in FP and FF conditions, and first mode with high bending stiffness and mean shear stiffness in FP condition. When the joint dislocation was less prominent than bending, the mode shapes were either grouped into shape (D) for FP condition or (E) for FF condition. Similarly, shape (F) is essentially a joint dislocation with varying degree of higher order bending curvature: the upper section of the column was on the opposite side of the lower section with respect to the longitudinal axis of the column (S curve). This shape included: 1) first mode with mean shear and mean or high bending stiffness in FF condition; 2) second mode with mean shear and bending stiffness in FP condition; 3) third mode with mean bending stiffness and high shear stiffness or mean shear stiffness and low bending stiffness in FP condition; 4) second mode with mean bending stiffness and high shear stiffness in FF condition; 5) third mode with mean shear stiffness and low bending stiffness in FF condition. Other S-curved mode shapes with less prominent joint dislocation were grouped either into shape (G) for FR and FP conditions or shape (H) for FS and FF conditions.

3.2 Effects of Stiffness

The intersegmental axial compressive stiffness had no influence on the buckling mode shapes or critical loads in any of the four end-conditions examined when the stiffness varied from 140 N/mm to 5180 N/mm while keeping the stiffnesses in shear and bending constant. The critical loads and buckling mode shapes for the mean stiffness values are presented in Table 4. Note that the second buckling mode for FP and the first buckling mode for FF have the same joint dislocation mode shape with a double-bending curve (shape F) and their critical loads are nearly equal (Table 4).

Table 4: Critical Loads (N) and Mode Shapes with Mean Stiffness

Buckling Modes	End-Conditions			
	Fixed-Free	Fixed-Slide	Fixed-Pinned	Fixed-Fixed
	Critical Loads			
1	288	1306	1982	3588
2	2520	4967	3594	4967
3	6597	10258	6755	10516
	Mode Shapes			
1	A	B	D	F
2	D	E	F	E
3	G	H	G	H

Note: Mean shear stiffness K_S = 200 N/mm; mean bending stiffness Kb = 99 Nm/rad;
The letters A, B, D, E, F, G, and H refer to the mode shape shown in Figure 3.

The bending stiffness between the segments affected the response for all the four end-conditions (Table 5). The critical loads were proportional to the stiffness. The order of the second and third modes in the FP condition was reversed for the decreased bending stiffness of 29 Nm/rad compared to those with the mean stiffness (Tables 4, 5). This resulted in the dislocation shape to be in the third mode (shape F). Similarly, the decreased stiffness also resulted in a shift of the dislocation shape from the first to the third mode for the FF condition (Tables 4, 5). However, for the FP condition, the higher bending stiffness of 169 Nm/rad resulted in the first buckling mode to be of the joint dislocation type with a single-bending curve (shape C); the second and third buckling modes were the usual single and double-bending curves. For the FF condition, the higher bending stiffness increased the critical loads without changing the shapes.

Table 5: Effect of Bending Stiffness Kb on Critical Loads (N) and Mode Shapes

Buckling	Fixed-Free		Fixed-Slide		Fixed-Pinned		Fixed-Fixed	
Modes	Low K_b	High K_b	Low K_b	High K_b	Low K_b	High K_b	Low K_b	High K_b
	Critical Loads							
1	84	492	383	2229	659	2683	1456	4544
2	738	4300	1456	8477	1814	4925	2247	8477
3	1933	11259	3006	17507	3003	11376	3661	17733
	Mode Shapes							
1	A	A	B	B	D	C	E	F
2	D	D	E	E	G	D	H	E
3	G	G	H	H	F	G	F	H

Note: Low K_b = 29 Nm/rad, High K_b = 169 Nm/rad; K_c = 3500 N/mm; K_S = 200 N/mm;
The letters A, B, C, ..., H refer to the mode shape shown in Figure 3

The shear stiffness also influenced the buckling mode shapes and their corresponding critical loads depending on the end-condition (Table 6). The critical load and buckling mode shapes with FR and FS conditions did not change when the shear stiffness varied from 34 N/mm to 580 N/mm. For the FP condition, the low shear stiffness

in the first buckling mode corresponded to the joint dislocation shape (shape C) while the second buckling mode became the single-bending curve shape (shape D); the high shear stiffness increased the first critical load while reversing the order of the second and third buckling modes with a much higher load for the secondary joint dislocation shape (shape F). For the FF condition, the lower shear stiffness changed the first buckling mode from the secondary joint dislocation with a double-bending curve (shape F) to the joint dislocation with a single-bending curve (shape C) and a correspondingly lower critical load; the higher shear stiffness reversed the order of the first and second buckling modes and increased loads in the second (shape F) and third (shape H) modes.

Table 6: Effect of Shear Stiffness Ks on Critical Loads (N) and Mode Shapes

Buckling	Fixed-Free		Fixed-Slide		Fixed-Pinned		Fixed-Fixed	
Modes	Low K_S	High K_S	Low K_S	High K_S	Low K_S	High K_S	Low K_S	High K_S
				Critical Loads				
1	288	288	1306	1306	716	2237	1704	4967
2	2520	2520	4967	4967	2576	6090	4967	7077
3	6597	6597	10258	10258	6613	9253	10293	11811
				Mode Shapes				
1	A	A	B	B	C	D	C	E
2	D	D	E	E	D	G	E	F
3	G	G	H	H	G	F	H	H

Note: Low K_S = 34 N/mm, High K_S = 580 N/mm; K_C = 3500 N/mm; K_b = 99 Nm/rad;
The letters A, B, C, ..., H refer to the mode shape shown in Figure 3.

4. Buckling of an Equivalent Homogeneous Column Model

For the purpose of comparison, the closed-form solutions of the equivalent homogeneous models were obtained using the procedures described below. The critical loads of an idealized continuous and homogeneous column [16] are given by:

$$P = EI\left[\frac{2n-1}{n}\right]^2\left[\frac{\pi}{L}\right]^2 \tag{2}$$

where n = 1,2,3, ... for FR condition and n = 2,3,4, ... for FP condition;
or:

$$P = EIn^2\left[\frac{\pi}{L}\right]^2 \tag{3}$$

where n = 1,2,3, ... for FS condition and n = 2,3,4, ... for FF condition; E is the Young's modulus of elasticity; I is the area moment of inertia of the column cross-section; and L is the total length of the column.

When n = 1 in equation (2), $P = EI\pi^2/L^2$ is the original Euler's buckling load. The quantity EI in equations (2) and (3) is directly proportional to the bending stiffness (K_{tb}) of the structure. The critical load of a homogeneous column is directly proportional to its bending stiffness K_{tb}. The equivalent bending stiffness K_{tb} of the whole column, which has seven joints and eight segments, can be approximated in terms of bending stiffness K_b of individual joints as if they were seven springs connected in series [17]. Thus, the overall stiffness K_{tb} is one-

seventh of K_b. A cantilevered homogeneous beam loaded by a moment M at the free-end has free-end rotation R = ML/EI = M/K_{tb}. Hence, we have the following relation:

$$\frac{EI}{L} = K_{tb} = \frac{K_b}{7} \tag{4}$$

Dividing both sides of (4) by L = 15 mm, we have

$$\frac{EI}{L^2} = \frac{K_b}{735} \tag{5}$$

Applying (5) to equations (2) and (3) we then have

$$P = \left[\pi \frac{2n-1}{n}\right]^2 \left[\frac{K_b}{735}\right] \tag{6}$$

$$P = [\pi n]^2 \left[\frac{K_b}{735}\right] \tag{7}$$

Since the continuous homogeneous column has infinite degrees-of-freedom, it theoretically has an infinite number of possible buckling mode shapes. Only the first three modes were examined in this text for the purpose of comparison with the segmented column. The first buckling mode shapes of the homogeneous column for the four end-conditions are shown in Figure 2. The homogeneous column had only bending stiffness as the variable. Hence, there were only three homogeneous models with low, mean and high bending stiffness values, respectively. The critical loads change with variation of the bending stiffness (Table 7). Critical loads of an equivalent homogeneous column for the mean (K_b = 99 Nm/rad), low (K_b = 29 Nm/rad), and high bending stiffnesses (K_b = 169 Nm/rad), were slightly higher than the inhomogeneous segmented column for all the four end-conditions (Table 7).

Table 7: Critical Loads (N) -- Homogeneous Column vs. Segmented Column

Buckling	Fixed-Free		Fixed-Slide		Fixed-Pinned		Fixed-Fixed	
Modes	Homog.	Seg.	Homog.	Seg.	Homog.	Seg.	Homog.	Seg.
Low K_b = 29 Nm/rad								
1	97† (A)	84 (A)	389 (B)	383 (B)	876 (D)	659 (D)	1558 (E)	1456 (E)
2	876 (D)	738 (D)	1558 (E)	1456 (E)	2434 (G)	1814 (G)	3506 (H)	2247 (H)
3	2434 (G)	1933 (G)	3506 (H)	3006 (H)	4770 @	3003 (F)	6232 @	3661 (F)
Mean K_b = 99 Nm/rad								
1	332 (A)	288 (A)	1329 (B)	1306 (B)	2991 (D)	1982 (D)	5318 (E)	3588 (F)
2	2991 (D)	2520 (D)	5318 (E)	4967 (E)	8300 (G)	3594 (F)	11964 (H)	4967 (E)
3	8300 (G)	6597 (G)	11964 (H)	10258 (H)	16268 @	6755 (G)	21264 @	10516 (H)
High K_b = 169 Nm/rad								
1	567 (A)	492 (A)	2269 (B)	2229 (B)	5106 (D)	2683 (C)	9077 (E)	4544 (F)
2	5106 (D)	4300 (D)	9077 (E)	8477 (E)	14183 (G)	4925 (D)	20424 (H)	8477 (E)
3	14183 (G)	11259 (G)	20424 (H)	17507 (H)	27799 @	11376 (G)	36309 @	17733 (H)

* K_c = 3500 N/mm; K_s = 200 N/mm; Seg = Segmented; Homog = Homogeneous.

† The letter in parenthesis after each number refers to the mode shape in Figure 3

@ Higher order mode shape

5. Homogeneous Column versus Segmented Column

The following characteristics in the buckling response are true for both the homogeneous and the segmented columns: 1) the end-condition is the most influential factor; 2) bending is the primary type of buckling deformation; 3) critical loads are directly proportional to the bending (flexural) stiffness of the column; and 4) compressive stiffness does not affect the critical loads or the mode shapes. Unlike the homogeneous column however, the inhomogeneous segmented column indicated additional characteristics: 1) joint dislocations are also primary mode shapes and often accompany bending mode shapes in the FP and FF end-conditions; 2) shear stiffness influences the critical loads and is associated with most of the shapes in the FP and FF conditions where joint dislocation accompanies bending; and 3) varying the magnitude of shear or bending stiffness changes the relative order of dislocation and bending mode shapes.

As expected, the critical loads of the segmented column were slightly lower than the homogeneous column associated with similar bending modes. The segmented column allows additional discontinuity at each joint which is lacking in the homogeneous column. This characteristic of the segmented column makes it more flexible than a homogeneous column. The finding that the compressive stiffness does not influence the critical loads and mode

shapes of a segmented column agrees with the theoretical results of linear and nonlinear buckling analysis of a homogeneous column [16]. The segmented column model predicted joint dislocation mode shapes that do not appear in the buckling of a homogeneous column. This unique characteristic may be attributed to the intersegmental joints which cause discontinuity of stiffness and deformation and additional kinematic freedom on shear in a segmented column. Joint dislocation is a common failure mode seen in human cervical spine injury, which is clinically termed vertebral subluxation or unilateral/bilateral facet dislocation. Such injuries can have serious neurologic damage because the spinal cord is subjected to high shearing and stretching forces.

The ligamentous cervical spine consists of vertebrae connected by soft tissues making up complex joints. Between any two adjacent vertebrae, three relative translations (longitudinal tension-compression, A-P shear, lateral shear) and three rotations (flexion-extension, lateral bending, torsion) are possible. A homogeneous column model does not account for the kinematic flexibility of the intervertebral joints in the cervical column. A segmented ligamentous column model is a better approximation and an improvement over the homogeneous column model.

6. Limitation and Potential Extension of the Segmented Model

The upper cervical spinal joint (occipito-atlanto-axial complex) is substantially different from those of the mid to lower cervical spine and is not simulated in this parametric study. The level dependence of the stiffness between the mid and lower cervical joints is still not clear in the literature and therefore ignored in the present model. However, the ranges in these values adopted in this study may encompass, in a qualitative sense, the expected difference in the stiffness magnitudes and resulting critical loads. It is possible to extend the present model by merely assigning different numerics for these parameters when such experimental data become available.

The present model assumed axisymmetry for the sagittal buckling analysis. The anteroposterior shear and postero-anterior shear stiffnesses were assumed identical; the bending stiffnesses were also assumed identical under flexion and extension. The symmetry in stiffness was adapted for the simplicity of parametric analysis. The model can be extended to include the asymmetry characteristics of the cervical column in the sagittal plane. Since the linear eigenvalue analysis requires the initial column geometry to be straight and symmetric, the load vector was aligned along the longitudinal axis of the structure and the load-deformation relations were assumed linearly elastic.

The parametric analysis did not explicitly consider the role of neck muscles. Muscle actions are required *in vivo* to align the cervical spine into the straight configuration, a feature shown to be a necessary and sufficient condition to produce clinical cervical spine injuries. The column model in this study was used to simulate the probable behavior of the cervical spine subjected to high-speed axial compression in such incidences as motor vehicle crashes and head-on impact in contact sports. Crashes like these produce trauma to the cervical spine within the first few milliseconds of loading during which time muscle activation is questionable [18]. Foust et al., have found that the average neck muscle reflex times range from 56-92 milliseconds for flexors and 54-87 milliseconds for extensors [19]. The model can be extended to include the effects of neck muscles by appropriately adding structural elements. Such an extended model may be able to predict certain *in vivo* neck responses where muscle actions are important.

7. Relevance to Cervical Spine Injury

The cervical column in its naturally lordotic configuration does not exhibit buckling behavior in the sagittal plane because a compressive load would continually increase the pre-existing lordosis of the cervical spine, and buckling as defined by Euler, would not occur. When its natural lordosis is eliminated however, the cervical spinal column is in its stiffest configuration and buckles in the sagittal plane under longitudinal compression. Liu and Dai, based on an idealized homogeneous beam-column model, predicted that for a straightened cervical spinal column, there exist unique stiffest and second stiffest axes along which a compressive force may cause buckling with or without material damage of the column [6,7].

The critical loads associated with the corresponding mode shapes and end-conditions (using the mean stiffness values) agree with earlier *in vitro* experimental tests. For example, the average peak compressive loads sustained by the cervical column were 289 N for FR, 1720 N for FS, and 4810 N for FF end-conditions in static *in vitro* experiments on human cadavers [14]. The present model predicted the critical loads to be 288 N for FR, 1306 N for FS, and 4967 N for FF conditions, respectively, for the similar mode shapes (Table 4). The peak compressive force of 1355-3613 N for facet-joint dislocation in the Pintar et al., study compares favorably with the present

critical load of 3588 N for mean shear stiffness (Table 4), and 1704 N for low shear stiffness with similar joint dislocation buckling mode shapes (Table 6) [20]. The end-conditions in Pintar et al., were similar to the FF condition in the present study [20]. The slightly lower compressive failure load in their experiments is probably due to the inherent imperfections in the cervical column, e.g., residual lordosis, loading eccentricity, and/or material inhomogeneity; or material failure occurred before the buckling. In dynamic cadaver head-neck vertical impact experiments, Pintar et al., found the mean force at failure to be 3326 N with a range of 744-6431 N when the boundary conditions were similar to that of FF in the present modal analysis [9]. In comparison, the model predicted a mean critical load of 3588 N for dislocation or 4967 N for bending, both higher than the mean experimental failure load. This implies that local material failure (fracture) might have occurred before the compressive force reaching the level of critical load for buckling in the dynamic experiment. The fact that the majority of the injuries were of the compression type supports this observation.

There are generally two types of column failure: material (material fracture or plastic yielding) and geometric (instability due to buckling) when the critical load is reached. Buckling behavior may also lead to material failure. The human cervical column possesses these two types of failure [6]. The type of failure *in vivo* depends on tolerance. In FR condition, the critical load for buckling is generally exceeded first, resulting in a buckled cervical column with no material failure [14]. In the FF condition, the cervical column may reach the joint dislocation buckling limit first as in the Pintar et al., static study or vertebral fracture tolerance first as in the Pintar et al., dynamic study [9,20]. The difference between the two results may be due to the structural response to the variations in rates of loading (static vs. dynamic).

The segmented column model has extended the earlier concept of stiffest axis of the cervical column and provided quantitative and experimentally verifiable results [7]. Previously reported results based on a homogeneous column model can only provide a conceptual framework. By using experimental data of isolated cervical motion segments, the present model has successfully predicted experimental failure loads (critical loads) of the whole ligamentous cervical spine. It has demonstrated that column buckling is a probable mechanism of cervical spine injury, which is an aspect of pathomechanics not understood before. This study shows the potential buckling mode shapes the cervical column can undergo depending on the boundary conditions. These mode shapes, corresponding to clinical injury types, have not yet been identified experimentally. Experimental studies that correlate the injury type, injury location and the curvature of the cervical column before and at the time of injury, will shed some light in the mechanisms of injury. The relationship between the boundary conditions and critical loads suggests that less degree of constraint on the head at the time of impact reduces the load in the cervical spine and the risk of serious injury. This knowledge may help improve the potential impact environment of the head and neck for the safety of cervical spine in contact sports and motor vehicle crashes.

8. Conclusion

In summary, a segmented column (conceptually, numerically) is a better approximation of the buckling response of the human cervical spine compared to a homogeneous column. The critical load is principally determined by end-conditions, bending and shear stiffnesses, and buckling mode shapes. Higher degrees of end-constraints, higher magnitudes of bending or shear stiffness, and/or higher orders of the buckled mode result in a higher critical load. The end-condition is the most influential factor for the buckling mode shape and the critical load of the column. Compressive stiffness has negligible influence on the critical loads or buckling mode shapes. Bending stiffness influences the critical loads as well as the order of buckling mode shapes under all the four investigated end-conditions. Critical loads are directly proportional to the bending stiffness. Shear stiffness influences the critical loads and is associated with most of the buckling mode shapes in the FF and FP conditions where joint dislocation accompanies bending. Joint dislocation buckling mode shapes are unique to the segmented column and occur only in the FP and FF conditions. Varying the magnitude of shear or bending stiffness changes the relative order of joint dislocation and bending buckling modes.

Acknowledgment: This research was supported in part by the Helen Streiffer Fund at the University of Iowa Foundation, PHS CDC Grants R49CCR-507370, and the Department of Veterans Affairs Medical Research Service.

References

[1] McElhaney J, Roberts V, Paver J, Maxwell M, Etiology of Trauma to the Cervical Spine. In: *Impact Injury of the Head and Spine.* Ewing CL, Thomas DJ, Sances A Jr., Larson SJ (eds). CC Thomas, Springfield, IL 1983: 41-71.

[2] Tator CH, Edmonds VE. National survey of spinal injuries in hockey players. *Can Med Assoc J* 1984:130: 875-880.

[3] Torg JS, Vegso JJ, Oneill MJ, Sennett B. The epidemiologic, pathologic, biomechanical, and cinematographic analysis of football-induced cervical spine trauma. *American J Sports Medicine* 1990:18(1): 50-57.

[4] Yoganandan N, Haffner M, Maiman DJ, Nichols H, Pintar FA, Jentzen J, Weinshel S, Larson SJ, Sances A. Epidemiology and injury biomechanics of motor vehicle related trauma to the human spine. *SAE Transactions* 1990:98(6): 1790-1807.

[5] Burstein AH, Otis JC, Torg JS. Mechanisms and Pathomechanics of Athletic Injuries to the Cervical Spine. In: *Athletic Injuries to the Head, Neck and Face.* JS Torg (ed). Lea and Febiger, Philadelphia 1982: 139-154.

[6] Dai QG, Liu YK. Failure analysis of a beam-column under oblique-eccentric loading: Potential failure surfaces for cervical spine trauma. *J Biomech Eng* 1992:114: 119-128.

[7] Liu YK, Dai QG. The second stiffest axis of a beam-column: Implications for cervical spine trauma. *J Biomech Eng* 1989:111(2): 122-127.

[8] Pintar FA, Sances A Jr, Yoganandan N, Reinartz JM, Maiman DJ, Suh JK, Unger G, Cusick JF, Larson SJ. Biodynamics of the total human cadaver cervical spine. In: *Proceedings 34th Stapp Car Crash Conference*, Orlando, FL, Society of Automotive Engineers 1990, pp 55-72.

[9] Pintar FA, Yoganandan N, Voo L, Cusick JF, Maiman DJ, Sances A Jr. Dynamic characteristics of the human cervical spine. *SAE Transactions* 1995:104(6): 3087-3094.

[10] Coffee MS, Edwards WT, Hayes WC, White AA III. Biomechanical properties and strength of the human cervical spine. *Trans ASME Bioengineering Div* 1987:3: 71-72.

[11] Liu YK, Krieger KW, Njus G, Ueno K, Connors M, Wakano K, Thies D. Cervical spine stiffness and geometry of the young human male. Wright-Patterson AFB, AFAMRL-TR-80-138, Dayton, OH, 1981.

[12] Moroney SP, Schultz AB, Miller JA, Andersson GB. Load-displacement properties of lower cervical spine motion segments. *J Biomechanics* 1988:21(9): 769-779.

[13] Panjabi MM, Summers DJ, Pelker RR, Videman T, Friedlaender GE, Southwick WO. Three-dimensional load-displacement curves due to forces on the cervical spine. *J Orthopaedic Res* 1986:4: 152-161.

[14] Myers BS, McElhaney JH, Richardson WJ, Nightingale RW, Doherty BJ. The influence of end condition on human cervical spine injury mechanism. In: *Proceedings 35th Stapp Car Crash Conference,* San Diego, CA, Society of Automotive Engineers, Inc. 1991, pp 391-399.

[15] Sherk HH, Dunn EJ, Eismont FJ, Fielding JW, Long DM, Ono K, Penning L, Raynor R. *The Cervical Spine.* Second Edition. JB Lippincott Co., Philadelphia, PA, 1989: 881 pp.

[16] Chen W, Atsuta T. *Theory of Beam-Columns.* Volume 1. McGraw-Hill, Inc., 1976.

[17] Lucas DB, Bresler B. Stability of the Ligamentous Spine. Univ. of California, San Francisco, 1961.

[18] Yoganandan N, Pintar FA, Sances A Jr, Maiman DJ. Strength and motion analysis of the human head-neck complex. *J Spinal Disord* 1991:4(1): 73-85.

[19] Foust DR, Chaffin DB, Snyder RG, Baum JK. Cervical range of motion and dynamic response and strength of cervical muscles. In: *Proceedings 17th Stapp Car Crash Conference*, Oklahoma City, OK., Society of Automotive Engineers, Inc., 1973:39: 285-308.

[20] Pintar FA, Yoganandan N, Sances A Jr, Reinartz J, Harris G, Larson SJ. Kinematic and anatomical analysis of the human cervical spinal column under axial loading. *SAE Transactions* 1990:98(6): 1766-1789.

Figure Captions

Figure 1: Segmented column model and the specific stiffness parameters for the intersegmental joints.

Figure 2: Shapes of the first buckling mode for the homogeneous column under the four end-conditions: (a) fixed-free; (b) fixed-slide; (c) fixed-pinned; and (d) fixed-fixed

Figure 3: General buckled shapes of the inhomogeneous segmented column (A) load-end free deflection; (B) load-end slide; (C) joint dislocation; (D) single curve bending; (E) stiffer single-curve; (F) joint dislocation with double-curve; (G) and (H) double-curve bending.

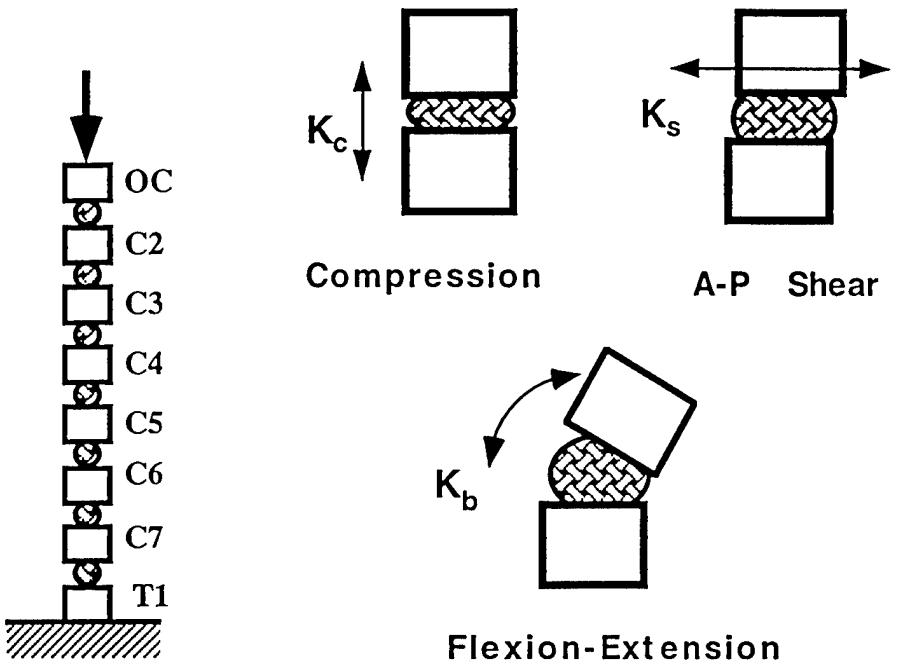

Figure 1: Segmented column model and the specific stiffness parameters for the intersegmental joints.

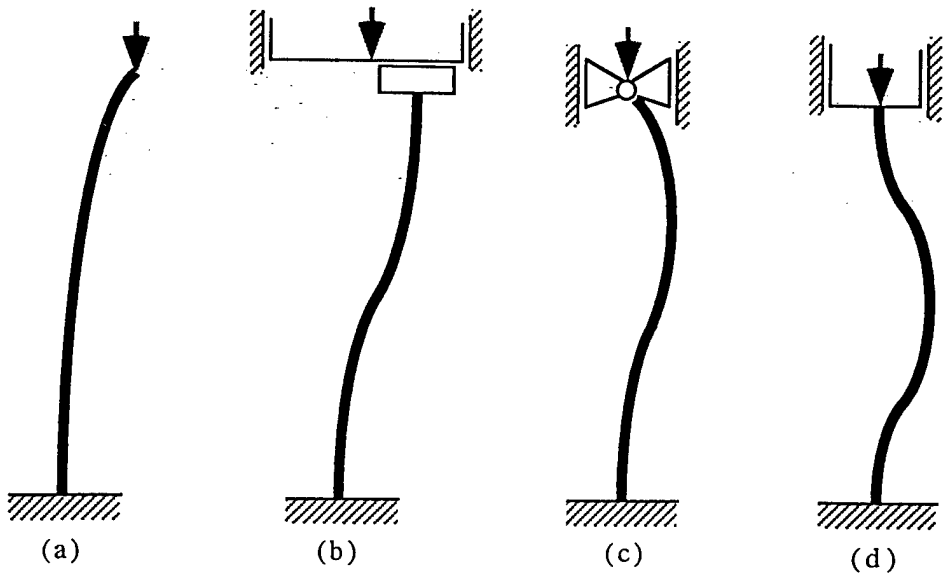

Figure 2: Shapes of the first buckling mode for the homogeneous column under the four end-conditions: (a) fixed-free; (b) fixed-slide; (c) fixed-pinned; and (d) fixed-fixed

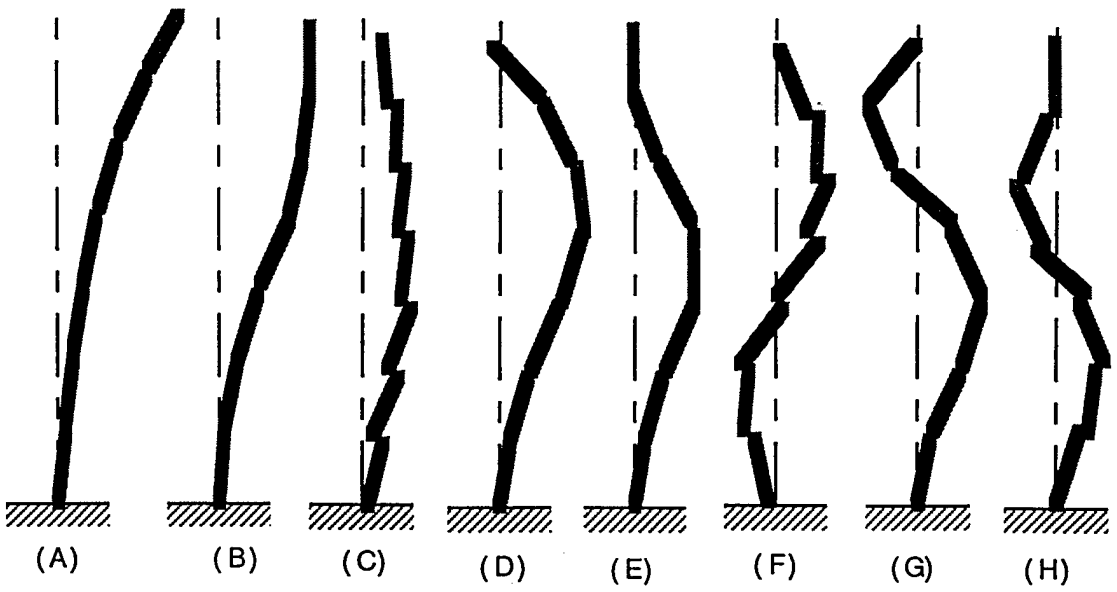

Figure 3: General buckled shapes of the inhomogeneous segmented column (A) load-end free deflection; (B) load-end slide; (C) joint dislocation; (D) single curve bending; (E) stiffer single-curve; (F) joint dislocation with double-curve; (G) and (H) double-curve bending.

LOWER CERVICAL SPINE FINITE ELEMENT ANALYSIS

Narayan Yoganandan, Srirangam Kumaresan, Frank A. Pintar

Abstract

This chapter describes the current finite element modeling approaches to study the biomechanics of the human lower cervical spine. These include the C4 isolated vertebra, C4-C5 one-motion segment and C4-C5-C6 two-motion segment models. The isolated model was used to study the mechanism of failure in the vertebra and the one-motion segment model studied the load sharing among the spinal components. The results from these two models are restricted by their end effects. The need to accurately incorporate the three-dimensional geometry, accurate definitions of the joints and the associated soft tissue structures, and experimental validation in as many physiologically relevant modes of loading as possible is emphasized in this chapter. Our efforts of systematically developing and exercising an anatomically accurate and materially comprehensive detailed finite element model are described. The results are discussed from this fully three-dimensional two-motion segment, geometrically and materially nonlinear, finite element model. The model output parameters have been exhaustively validated under various physiologic, simple and complex loading modalities using experimental information. Information is presented from the linear model for clinical applications such as laminectomy, facetectomy and fusion. Results from the nonlinear model with regard to spinal degeneration effects and extensions into the pediatric domain are also given in this chapter. The relative contributions and the importance of the external (e.g., flexural stiffness) and internal responses (e.g., load-sharing, stresses) on the clinical biomechanics of the cervical spine are delineated.

1. Introduction

1.1 Need for the Computer Finite Element Model

Computer driven stress analysis based finite element (FE) models are an important adjunct to clinical and laboratory experimental research. While clinical studies can address treatment outcome and human cadaver experimental biomechanical studies can determine the external response (e.g., sagittal rotation under physiologic flexion loading), computer models offer complimentary and unique perspective on the biomechanical behavior of the human cervical spine under normal, degenerated and iatrogenically altered/surgical conditions. Many of the problems that eventually alter the spine structurally originate because the internal components change materially. For example, the disc nucleus may lose water content altering the way the joint distributes the load. The long-term changes that result because of an altered internal load distribution may eventually lead to spondylotic changes in the spine. A highly accurate FE model is necessary to study the internal changes. Finite element models provide additional insight in terms of delineating the stress distributions in the various components of the spine, that may serve as a basis to evaluate the response of the normal spine and the effects of degeneration and surgical interventions. Because of the absolute reproducibility and repeatability of these models, detailed parametric analyses with regard to the geometrical conditions and material property changes (simulating for example, degenerated conditions) can be easily performed and biomechanical responses can be assessed using this technique [1]. In fact, this principle is routinely used to study lumbar spine mechanics. However, relatively little information is available on the human cervical spine [2]. The salient features and the details of the existing finite element models emphasizing the human lower cervical spine, the focus of this chapter, are summarized in Table 1.

Table 1: Finite Element Models of Lower Cervical Spine

	Bozic et al (1994)	Yoganandan et al (1995)	Clausen (1996)	Kumaresan et al (1997)
Model	C4 vertebra	C4-C5-C6 motion segment	C5-C6 motion segment	C4-C5-C6 motion segment
Component	Cortical + cancellous bone	Vertebra, discs, posterior elements, endplates, all ligaments	Vertebra, discs, posterior elements, endplates, ligaments, Luschka joint	Vertebra, discs, posterior elements, endplates, all ligaments, facet joint capsule, uncovertebral joint
Geometry	Actual - 1.5 mm, axial scans for hard tissue definition	Actual - 1.0 mm, sagittal, coronal, and axial CT scans combined with cryomicrotome anatomic sections	Actual - 1.5 mm, axial CT scans for hard tissue definition	Actual - 1.0 mm, sagittal, coronal & axial CT scans combined with cryomicrotome anatomic sections for soft tissue definition e.g, disc details, ligament origin, insertion, uncovertebral joint anatomy
Loading	4 mm axial compression (3400 N)	1 mm axial comp., 1.8 Nm flexion, extension, lateral bending and axial torsion	74 N comp., 1.8 Nm flexion, extension, lateral bending and axial torsion	500 N complex anterior, midline and posterior eccentric loads, 800 N pure compression, 3 Nm flexion, extension
Boundary Condition	Fixed at inferior surface through linear springs	Fixed at C6 and loading on C4 vertebra	Fixed at C6, loading on C5 vertebral body	Fixed at C6 and used simulated boundaries at C4 vertebra with experiment set-up
Model Detail	8590 eight-noded solid elements	9178 solid, 1193 thin shell, 592 two-noded elements	total 5577 elements	10863 solid, 984 incompressible fluid, 1410 disc composite rebar, 149 membrane, 517 cable elements
Type Analysis Software	3-D Linear, static ABAQUS	3-D Linear static I-DEAS, NASTRAN	3-D Nonlinear static ABAQUS	3-D Nonlinear static I-DEAS, ABAQUS

Validation	None	Shea et al., Moroney et al., Liu et al., results F-Δ, M-q data	Moroney et al., results M-q data	Pintar et al., Shea et al., results F-Δ, M-q and micro strain data
Application	Burst fracture modeling	Stress analysis of intact spine, laminectomy, facetectomy, interbody fusion	Load sharing	Pediatric spine biomechanics, intervertebral load bearing characteristics

Note: 3-D = Three-dimensional, θ = Rotation, Δ = Deflection

In 1994 Bozic et al., created a finite element model of the mid-cervical vertebra based on computed tomography (CT) images [3]. The actual geometry of C4 was represented by 8,590 isoparametric eight-noded brick elements. The modulus of the elasticity was based on CT density. Traumatic loading was simulated by applying an axial compressive displacement of 4 mm through the 221 linear spring elements attached to the superior vertebral body surface. The resulting force was 3,400 N. Two hundred and forty-one linear spring elements in the inferior direction provided the restraint boundary. The total stiffness of the springs at the superior and inferior directions approximated the stiffness of the intervertebral disc. In addition, restraints were applied in the medial, lateral and anteroposterior directions by using springs of low stiffnesses. The internal shear stress response was correlated to the initiation of failure in the central cancellous core. The model predicted the initiation of failure (maximum shear stress theory) in the central cancellous core. Despite the detailed finite element modeling, the isolated vertebra model limits the applicability of the results due to lack of adjacent soft tissues.

In 1995, Yoganandan et al., reported the first ever detailed anatomically accurate three-dimensional finite element model of the C4-C5-C6 region of the human lower cervical spine. The developmental procedure, the need for such a methodology, experimental validation under physiologic flexion, extension, lateral bending, axial rotation and compression, as well as complex loadings, together with the effects of surgical alteration, material property sensitivity analyses, and recent advancements into the nonlinear pediatric domain are discussed in the next section. These efforts have been advanced since 1992 [4-13].

In 1996, Clausen developed a one-motion segment cervical spine (C5-C6) finite element model [14]. The bony geometrical details were obtained by mirror-imaging the 1.5 mm axial CT scans and adopting manual digitizing procedures. The facet articulating surfaces were assumed flat. The soft tissue anatomy structures such as intervertebral discs, facet joints, ligaments and the uncovertebral joints were incorporated using the bony images. While disc modeling included the fibers and the ground substance, facet joint modeling did not accurately depict the synovial fluid and synovial membrane [7]. The model consisted of 5577 elements. Pure compression (73.6 N) and moment (1.8 Nm) with preload (73.6 N) were applied to the C5 endplate. The boundary condition was simulated by fixing the inferior surface of the inferior-most vertebrae. The model was validated under compression, flexion, extension, lateral bending and axial torsion. Load sharing among the spinal components was determined. Being a one-motion segment model, the end-effects from the loading and boundary conditions on superior and inferior vertebrae may restrict the model applicability. In addition, validation efforts were advanced only to match the external response (e.g., moment-rotation). Validation efforts such as the strains in the vertebral bodies were not conducted. Furthermore, since the CT scans were used to create the model that can only define the bony components, the addition of the soft tissue details such as the attachment of the ligament points and the definition of the uncovertebral joints appears to be somewhat arbitrary. Consequently, the biomechanical output from this "assumed" geometry single-motion segment model should be weighed with caution.

2. Model Development

2.1 Geometry and Material Property

For a finite element model to be of value in a clinical environment, the following factors must be considered: geometry, material properties, loading, boundary conditions and validation [2]. Since the model is stress analysis based (in contrast to lumped parameter simulation), these factors may have a significant effect on the

results. Because of the anatomic-structural differences in the various components of the spine (facet, disc, uncovertebral joints), it is important to incorporate these structures in a three-dimensional configuration to study the biomechanics. Furthermore, the geometry of the adjacent structures including the vertebrae and the surrounding ligament complex must be included. To predict realistic biomechanical responses (external and internal in terms of component load sharing, stress distributions), assuming regular geometries for the cervical spine components will only result in rudimentary approximations of the behavior. Consequently, both hard (CT scans of cervical spine at 1 mm intervals in the axial, sagittal, and coronal planes) and soft (using sequential cryomicrotome sections at 200 to 1000 micron intervals) tissue anatomic details are necessary to completely describe the three-dimensional architecture of the human cervical spine. Recognizing these necessities, we developed an anatomically accurate three-dimensional finite element model of the human lower cervical spine using CT and cryomicrotome sections.

To obtain the geometrical data required for the finite element model, the cervical spine (occiput to T1) was isolated from a 33 year old unembalmed human cadaver. Medical records were checked and pre-radiography was performed to ensure the absence of bony abnormalities, spine disease or trauma. Radiographs were taken in the anteroposterior, lateral and oblique planes. The specimen was positioned in a Styrofoam container. The specimen was aligned along the anatomical axes with respect to the exterior surfaces of the container. Carboxy-methyl-cellulose-gel was poured around the specimen. The specimen was frozen. High resolution CT scans (General Electric, High Speed Advantage, Waukesha, WI) were obtained in the three anatomic planes at 1.0 mm intervals. Figures 1a and 1b show coronal and sagittal CT sections. Sequential anatomic sections of the specimen were obtained using cryomicrotomy procedures. For this purpose, a heavy-duty cryomicrotome was used. The frozen specimen was placed on the bench of the cryomicrotome and prepositioning procedures were used to align the specimen. Actual cross-sectional anatomical features were obtained at 0.2 to 1.0 mm intervals. Soft tissue details such as the insertion points of the various cervical spinal ligaments and the relative geometry of the intervertebral discs were determined.

Each two-dimensional sagittal and coronal CT image was translated into a rasterized computer graphics image and processed using an edge-detection algorithm to extract accurate outlines of the vertebral cross-sections (Figure 2). For this purpose, the NIH computer software (public domain) was used. Using a graphics software, these two-dimensional geometric bony boundary data files were converted into a universal graphics data format. The relative spatial positions and the complex shape of all the cervical vertebrae were maintained during the computer reconstruction. The solid model development included the "wire-mesh" generation, surface creation, and solid's definition (Figure 3). The wire-mesh forms the basic unit in the solid model development. A three-dimensional wire-mesh geometry was constructed by stacking the sequential two-dimensional cross-section outlines from the imported geometric data files. By defining a series of four closed-loop boundary curves using the wire-mesh line segments, a series of surfaces was created for the entire model. They were carefully re-examined against the CT scans and the cryosection anatomy for geometrical accuracy. Each solid was then formed by filling the volume defined by a group of six surfaces. The surfaces and solids for the intervertebral discs were constructed in a similar fashion with the help of sequential cryosection anatomy. The solid model for the entire cervical spine structure was thus developed following these methods.

A mapped-mesh technique was used to obtain the finite element mesh (Figure 4). This method allows for the semi-automatic creation of finite elements that conform precisely to the shape of the defined volume. The completed finite element mesh is shown in Figure 5. At this stage, the number of elements, element type and element size were chosen. The solids representing the cancellous bone, transverse processes, pedicles, laminae and spinous processes were discretized after the number of elements per edge were specified for the appropriate mapped-mesh volumes. The facet joint articulation anatomy was defined using cryosections. The articular cartilage, synovial fluid, synovial membrane and capsular ligament were included in the facet joints at C4-C5 and C5-C6 levels. Based on our earlier study, the bilateral facet joints were modeled using the fluid model approach, i.e., the synovial fluid was idealized using incompressible fluid elements, articular cartilages were defined by eight-noded solid elements, the synovial membrane was modeled with four-noded membrane elements, and capsular ligaments were modeled with three-dimensional nonlinear tension active cable elements. The anulus fibrosus and nucleus pulposus of the intervertebral discs were included in the model at the superior (C4-C5) and inferior (C5-C6) levels. The anulus fibers were defined using fiber-reinforced concrete element approach, i.e., the collagenous fibers were modeled using rebar elements embedded in the matrix of ground substance that was defined using isoparametric solid element. The rebar elements were allowed to carry only the tensile forces, i.e., no-compression option was used. The fiber content was defined as approximately 20 percent of the anulus volume and arranged in alternating criss-cross fiber angles of 25 degrees [15-16]. The nucleus pulposus bounded by the anulus fibrosus and endplates was modeled using

incompressible fluid element. The anatomy of the uncovertebral joints was defined based on three-dimensional geometrical data obtained using cryomicrotome sections. They were defined bilaterally at the C4-C5 and C5-C6 levels. The joint space was modeled using an incompressible fluid element with geometry dimensions which included their location, length, depth and height. The synovial membrane enclosing the joint space was modeled using the membrane elements. The ligament insertion points were identified using cryosection anatomy. All of the ligaments were simulated by nonlinear cable elements. The nonlinear material values of the ligaments (anterior longitudinal ligament, posterior longitudinal ligament, interspinous ligament, capsular ligament and ligamentum flavum) were obtained by analyzing the data from experimental work conducted in our laboratory [17-18]. The ligaments were modeled using the no-compression cable elements to simulate the tension-active characteristics with material nonlinearity.

Thus, the detailed anatomically accurate three-dimensional finite element model included: cortical shell, cancellous core and end plates of the vertebral bodies, nucleus pulposus, anulus fibers and ground substance of the intervertebral discs, posterior parts of the vertebrae including the facet pillars, vertebral arches, laminae and spinous processes, facet joint components comprising of the capsular ligaments, synovial fluid, synovial membrane and articular cartilages, spinal ligaments including the anterior and posterior longitudinal ligament, ligamentum flavum and interspinous ligaments, and the uncovertebral, neurocentral or Luschka's joints. All these load bearing structural components of the cervical spine were simulated in the three-dimensional finite element model. To the best of our knowledge, this is the most comprehensive and anatomically accurate three-dimensional finite element model of the human cervical spine. Because of the inclusion of all the above described components, it is possible to determine the biomechanical response in terms of stresses and stress distributions in these components secondary to physiologic loads simulating a variety of spinal configurations including normal, degenerated and iatrogenically/surgically altered conditions. A total of 12,722 finite elements were used to describe the materially and geometrically nonlinear finite element model of the cervical spine.

2.2 *Physiologic Loading*

To exercise the model under physiologic force vectors, appropriate loading and boundary conditions were specified. In the initial analysis, physiologic compression, flexion, extension, lateral bending and axial torsion pure moment force vectors were used. In the subsequent analysis, combined complex vectors including varying degrees of compression-flexion and compression-extension loads were analyzed. These external load vectors were applied to the top surface of the model and the boundary conditions were such that the bottom surface of the inferior-most vertebra was constrained in all degrees-of-freedom. The three-dimensional anatomically accurate finite element model was developed using the I-DEAS software, the initial linear analyses were conducted using the NASTRAN software and the nonlinear analyses were done using the ABAQUS software (Table 1).

2.3 *Validation*

Despite the accurate replication of the three-dimensional spinal anatomy and specification of the material properties, loading and boundary conditions, to have confidence in the finite element model, validation is imperative. This was accomplished by comparing the finite element response with experimental data under each of the above cited multiple load vectors. In general, the confidence in the model output increases with increasing number of parameters for validation and increasing ranges/types of load vectors. It should be noted that the experimental responses are often limited to external recordings such as forces, displacements, moments, rotations or surface strains. As is done in lumbar spine studies, the external response in terms of force-deformation relationships or moment-rotation relationships of the finite element model under compression and pure moment loading (flexion, extension, lateral bending, axial torsion) was compared with experimental data. An excellent match was found in the force-displacement response under compression with experimental results, and the validation of the finite element model moment-rotation response under flexion, extension, lateral bending and axial torsion was also excellent [5,10,12-13].

The following five different types and levels of complex loadings were applied to further validate the finite element model. Compression-flexion loadings were applied at 1 and 2 cm anterior from the line of traverse of the posterior longitudinal ligament that was taken as the reference line, i.e., anterior eccentricity loadings. Midline compression loading was applied on the reference line. Compression-extension loadings were applied at 1 and 2 cm posterior from the reference line, i.e., posterior eccentricity loadings. All loading and boundary conditions simulated

in the model followed the experimental setup that was used in validation. The analysis included the effect of geometric (large deformation and strain) and material nonlinearities. The force-displacement response and the localized strain data in the anterior aspect of the vertebral body and in the lateral masses of the C5 vertebra computed from the finite element model were compared with experimental results under uniform compression and complex eccentric loadings [19]. The moment-rotation responses of the finite element model were also validated with experimental data under pure flexion and extension loadings [20].

The FE model force-displacement response (external) matched well with the experimental results under uniform compression (Figure 6a). The initial toe region of low stiffness and the remaining high stiffness characteristics of the cervical spine were observed in the finite element response. The internal microstrain response in the vertebral body and the lateral masses computed from the finite element model matched well with the experimental results (Figure 6b). Strain data from the finite element model were obtained over a region of the anterior portion of the vertebral body and lateral facet masses, and the mean and range of strains were compared with experimental results. This procedure was adopted to account for the strain measurement variability in different specimens used in the experimental studies. Under compression-flexion (anterior eccentric loads, i.e., 1 and 2 cm from reference line), compression-extension (posterior eccentric loads, i.e., 1 and 2 cm from reference line), and compression loading, the model response correlated well with experimental data. In addition, the model response matched well with experimental results under flexion and extension [21]. Because of these extensive multiple validations under a variety of load vectors, the finite element model is considered to be reasonable and has the potential to delineate the internal responses in terms of the stresses and stress distributions under physiologic and complex load vectors and under a variety of structural configurations.

3. Application

3.1 Parametric Analysis: Material Property Sensitivity

One of the principal advantages of using a computer based finite element model of the human cervical spine lies in the exploitation of its reproducibility and repeatability characteristics. Towards this end, several initial investigations were conducted to determine the significance of the changes in the material properties of one or more components representing the effect of spinal degeneration on the internal and external responses under physiologic loads [12-13,22]. In the initial material property sensitivity study, the properties of the spinal components were assumed to be linear, homogeneous and isotropic. Therefore, the Young's modulus of elasticity and Poisson's ratio values were assigned to each individual spinal element. Because of the general relative insignificance of the Poisson's ratio with respect to the biomechanical response of the spinal elements, this property was chosen to be invariant. In contrast, for each spinal component, three sets of Young's modulus values were used: low, basic and high. The basic value corresponded to the magnitudes used during the FE model validation. The low and high values encompassed the range in the parameters used/reported in previous studies. In addition, these values are representative of the degenerated spine material characteristics. The sensitivity analysis of different material properties under compression, flexion, extension, lateral bending and axial torsion was conducted by varying each input material property independently from the basic model values. A two- to four-fold increase in the material property values was chosen for the hard tissue structures (representing the low and high cases). For the soft tissue structures, the low and high values were 50 and 200 percent of the basic model parameters. A total of 432 output parameters were evaluated. Because of these numerous data, the results were normalized with respect to the basic model output highlighting the differences between the hard and soft tissue changes on the biomechanical responses. From an external response characteristic point of view (angular motion change under pure moment loading), variations in material properties of the hard tissue structures (cancellous core, cortical shell, end plates, posterior elements) did not considerably affect the external angular motion. In contrast, the variations in the material properties of the intervertebral discs and ligaments representing the soft tissue structures significantly altered the angular motion. The angular motions increased with a decrease in the disc and the ligament moduli, and decreased with an increase in the corresponding values. The disc material property variations were found to have a larger effect under all loading modes than the changes in the material properties of the spinal ligaments. Since spinal degeneration often initiates from the material property changes in the intervertebral disc structures, it can be surmised that the external biomechanical response of the spine is most sensitive to the status and the integrity of the intervertebral disc structure.

As indicated earlier, finite element model has the ability to provide additional biomechanical details such as internal stress values and stress distributions in the various components of the human cervical spine. It should be reemphasized that this type of response cannot be obtained from any clinical, epidemiological or experimental biomechanical research. While the variations in the modulus of the hard tissue structures had little effect on the internal stress distributions of the inferior and superior intervertebral discs, the variations in the properties of the soft tissue structures (disc and ligaments) affected the stresses in both the intervertebral discs. The changes in the internal stress magnitudes were considerably higher compared to the changes in the external angular response (previous paragraph) suggesting a higher role of the internal biomechanical variables compared to the traditionally obtainable external response from experimental studies. In other words, while the soft tissues changes alter the internal and external responses of both the hard and the soft tissue structures, bony changes accounted for stress alterations only in the hard tissues, emphasizing the relative role of these components on spinal strength. An increase in load sharing implies an added role to the vertebral bodies secondary to disc degeneration. Changes in the constituents of the spinal components induce alterations in the biomechanical properties. For example, the properties of the soft tissue structures are a function of their composition, level of hydration and age. It is well known that the aging process affects degeneration resulting in altered biomechanical characteristics including the formation of osteophytes compromising the integrity of spinal structures. A systematic biomechanical analysis can be done if these variations in terms of the mechanical properties can be quantified and used as input into finite element models. The results from this initial investigation emphasizing the overriding influence in the role of the changes in the material properties of the soft tissues on both the external and internal responses have the potential to shed light on the effects of age-related degenerative changes of the human cervical spine.

3.2 Surgical Alterations

3.2.1 Facetectomy

The next step in highlighting the potential of this finite element model was to evaluate the biomechanical effects of surgical procedures such as unilateral and bilateral facetectomy (grades: 25, 50, 75 and 100%). Again, the biomechanical effects of these iatrogenically altered conditions were evaluated under physiologic flexion, extension, lateral bending and axial torsion; this was accomplished using our earlier (Table 1) three-dimensional FE model incorporating the principles of linear analysis [10]. Both external angular rotation versus moment response that can be correlated with experimental data and the internal stress distributions and stress levels, were obtained to delineate the effects of these procedures on the types of biomechanical variables (external, internal). The gross overall angular rotation versus moment external responses correlated with experimental data. These correlations served as baseline data to further analyze the internal response variables. Considerably greater increase in the angular rotation was found when facet resection was increased from 50 to 75 percent for bilateral facetectomy. While similar trends in the internal stress (distribution) variables in the discs and in the vertebral bodies occurred due to graded facetectomy, the actual magnitudes of the stress changes with respect to the intact specimen were considerably higher compared to the change in the magnitudes of the external angular rotation versus moment responses. Again, these findings suggest an accentuated role for the internal biomechanical variables to be more sensitive and better characterize the response of the cervical spine under iatrogenically altered conditions. This increase in the stress magnitude in the intervertebral disc anulus may lead to degenerative changes at the facetectomized spinal level. It is known that the bone remodeling is the response of bone tissue to mechanical stress. Soft tissues may also change structural properties as an adaptation to higher stress environment. The above internal biomechanical response variations in terms of the soft and hard tissue stresses before and after facetectomy may better reveal the true nature of the accelerated degenerative process in the cervical column.

3.2.2 Laminectomy with Graded Facetectomy

The finite element analysis of graded facetectomy combined with laminectomy also indicated similar overriding influence of the internal stresses and the stress distributions in the intervertebral structures; this was accomplished using our earlier (Table 1) three-dimensional FE model incorporating the principles of linear analysis [5,23]. Again, clinically, hypermobility may lead to cervical spinal curvature alterations following laminectomy, and excessive disc loading represented by accentuated levels in the disc stresses may accelerate the degenerative changes in the disc. This may result in further formation of osteophytes and a progressive deterioration in the

biomechanical load carrying capacity of the human cervical spine. The finite element model stress analysis response therefore, provides an additional facet to the understanding of the extrinsic as well as the intrinsic responses. These issues are described in detail in a subsequent chapter.

3.2.3 Discectomy and Fusion

Additional studies to demonstrate the feasibility of using this accurate finite element model of the human cervical spine were carried out to study the effects of anterior cervical discectomy and fusion; this was done using our earlier (Table 1) three-dimensional FE model incorporating the principles of linear analysis [8]. Smith-Robinson and Bailey-Badgley procedures were simulated according to accepted techniques. Five different types of graft materials were used. These included a tricortical iliac crest graft that consists of the outer cortical bone surrounding the cancellous core on the anterior and bilateral sides, titanium core, titanium cage surrounding a central cancellous core, tantalum core and a tantalum cage surrounding a central cancellous core. The response of these five graft materials used in the two surgical procedures were evaluated with respect to the intact spine under compression and flexion, extension, lateral bending and axial torsion. Again, both the external response in terms of the force-displacement stiffness for compression loading and angular rotation-moment stiffness for flexion, extension, lateral bending and axial torsion were evaluated. While the Smith-Robinson technique resulted in the highest increase in the external response under all modes of loading for all materials, the Bailey-Badgley procedure technique produced a higher increase in the disc and the vertebral body stresses and stress distributions. The higher change in the internal vertebral body stresses and stress distributions in the Bailey-Badgley model may be due to the inclusion of the fusion material into the adjacent vertebrae. Because of these added stresses in the intervertebral components, a higher demand is placed on these local structures due to surgery. For both surgical procedures, the external stiffness was the highest in the titanium core and least in the tantalum cage. This may be attributed to the material property magnitudes of the different graft materials. Consequently, if the objective is to achieve a maximum overall strength *in vivo*, a material with the highest strength is potentially desirable. These issues are further covered in a subsequent chapter.

3.3 Normal versus Degenerated Spine Conditions: Stress Distribution

The internal component stresses were predicted under normal and degenerated conditions of the spine. This was accomplished using our subsequent three-dimensional FE model incorporating the principles of geometrically and materially nonlinear analysis (Table 1). For this purpose, as an example, the von Misses stresses in the C5 vertebral body were obtained under axial compression. Degenerated characteristics were simulated by altering the material properties of the intervertebral nucleus (dehydration) and anulus fiber slackening. For the normal spine the maximum stress in the C5 body was 99 MPa, and for the degenerated spine the stress was 113 MPa. The stress distributions are shown in figure 7. Not only the stress magnitudes have increased (99 to 113 MPa), but also the stress patterns have altered. Any increase in the local stresses secondary to the structural component alterations such as disc material property changes accentuates the stress/load on the vertebral body that may lead to further degenerative changes. Using this approach it is therefore, possible to isolate on a local component basis and predict regions of high stress concentration that may be indicative of future cervical spine symptomatology.

3.4 Pediatric Spine Responses

The anatomically accurate and experimentally validated nonlinear finite element model of the adult spine structure was modified to create the one, three and six year old pediatric spine models by incorporating the local geometrical and material characteristics of the developmental anatomy. All nonlinear models were exercised using the ABAQUS software. The models adopted the principles of structural scaling, and geometrical and material modifications to represent the developmental anatomy of the age-specific pediatric populations. The nonlinear responses of the pediatric structures were compared to the nonlinear responses of the well-developed adult spine structure. Briefly, results indicated the following: local age-related changes in the anatomy together with the changes in the material properties of the various spinal components are critical factors that contribute to the differences between the one, three and six year old pediatric and adult spines. A mere overall structural scaling of the responses from an adult spine is a less accurate representation of the pediatric behavior. Additional details of the construction,

development and comparison of the responses with the adult spine under compression, flexion and extension are given in a subsequent chapter.

4. Conclusions

These computer finite element modeling studies of the human cervical spine conducted by our group are based on actual three-dimensional anatomy; detailed representation and incorporation of all the load bearing elements of the spine; normal and degenerated material properties of the intervertebral components; incorporation of the appropriate physiologic load vectors associated with the different loading modalities; and, exhaustive validation studies by comparing with numerous experimental studies. They have clearly opened new avenues to better describe the biomechanical behavior of the cervical spine. Because of the estimation of the internal stresses and stress distributions in the intervertebral components secondary to different types of load vectors and under different types of anatomic/structural configurations, it is now possible to address not only the differences in the external responses and the internal stress distributions, but also it is possible to provide quantitative biomechanical measures that may be more appropriate and sensitive to describe the load carrying capacity, strength and stability of this structure. The biomechanical community is well poised to undertake the challenges ahead with regard to a better understanding of the human cervical spine behavior.

References

[1] Yoganandan N, Myklebust JB, Ray G, Sances A Jr. Mathematical and finite element analysis of spinal injuries. *CRC Review Biomed Eng* 1987:15(1): 29-93.

[2] Yoganandan N, Kumaresan S, Voo L, Pintar F. Finite element applications in human cervical spine modeling. *Spine* 1996:21(15): 1824-1834.

[3] Bozic KJ, Keyak JH, Skinner HB, Bueff HU, Bradford DS. Three-dimensional finite element modeling of a cervical vertebra: An investigation of burst fracture mechanism. *J Spinal Disorders* 1994:7(2): 102-110.

[4] Denman JA. Development and validation of a three-dimensional nonlinear finite element model of the C4-C6 cervical spine unit, in M.S. Thesis. 1995, Marquette University: Milwaukee, WI, 110 pp.

[5] Kumaresan S, Yoganandan N, Pintar F, Voo L, Cusick J, Larson S. Finite element modeling of cervical laminectomy with graded facetectomy. *J Spinal Disord* 1997:10(1): 40-47.

[6] Kumaresan S, Yoganandan N, Pintar FA. Adult and pediatric human cervical spine finite element analyses. In: *ASME Summer Bioengineering Conference,* Sun River, OR, 1997.

[7] Kumaresan S, Yoganandan N, Pintar FA. Nonlinear finite element analysis of human cervical spine facet joint. In: *ASME Summer Bioengineering Conference*, Sun River, OR, 1997.

[8] Kumaresan S, Yoganandan N, Pintar F. Finite element analysis of anterior cervical spine interbody fusion. *Biomed Mat & Eng* 1997 (In Press).

[9] Voo L, Denman J, Kumaresan S, Yoganandan N, Pintar FA, Cusick JF. Development of 3-D finite element model of the cervical spine. *Adv Bioeng* 1995:31: 13-14.

[10] Voo LM, Kumaresan S, Yoganandan N, Pintar FA, Cusick JF. Finite element analysis of cervical facetectomy. *Spine* 1997:22(9): 964-969.

[11] Yoganandan N, Voo L, Pintar FA, Kumaresan S, Cusick JF, Sances A Jr. Finite element analysis of the cervical spine. In: *CDC Injury Prevention Through Biomechanics*, Detroit, MI, 1995, pp 149-155.

[12] Yoganandan N, Kumaresan S, Voo L, Pintar F, Larson S. Finite element modeling of the C4-C6 cervical spine unit. *Med Eng Phy* 1996:18(7): 569-574.

[13] Yoganandan N, Kumaresan S, Voo L, Pintar F. Finite element model of the human lower cervical spine. *J Biomech Eng* 1997:119(1): 87-92.

[14] Clausen JD, Goel VK, Traynelis VC, Wilder DG. Cervical spine biomechanical investigation using an experimentally validated FE model of the C5-C6 motion segment. In: *Proceedings Orthopedic Research Society,* Atlanta, GA, 1996 (In Press).

[15] Pooni JS, Hukins DW, Harris PF, Hilton RC, Davies KE. Comparison of the structure of human intervertebral discs in the cervical, thoracic and lumbar regions of the spine. *Surg Radiol Anat* 1986:8: 175-182.

[16] Ghosh P. *Biology of the Intervertebral Disc*, CRC Press, Inc., Boca Raton, FL, 1988.
[17] Pintar FA. Biomechanics of Spinal Elements, Marquette University, Milwaukee, WI, 1986, 222 pp.
[18] Grossheim L. Morphology of the human cervical spine. In: Biomedical Engineering, Marquette University, Milwaukee, WI, 1989, 183 pp.
[19] Pesigan MF. Measurement of cervical vertebrae strain for assessment of injury mechanisms, in Biomedical Engineering, Marquette University, Milwaukee, WI, 1989.
[20] Shea M, Edwards WT, White AA III, Hayes WC. Variations of stiffness and strength along the human cervical spine. *J Biomech* 1991:24(2): 95-107.
[21] Kumaresan S, Yoganandan N, Pintar FA. Validation of nonlinear finite element model of human lower cervical spine. In: *ASME Bioengineering Conference,* Dallas, TX, 1997.
[22] Kumaresan S, Yoganandan N, Pintar FA. Importance of material properties on spinal components load sharing. *Mathematical Computer Modelling and Scientific Computing* 1997 (In Press).
[23] Kumaresan S, Yoganandan N, Voo L, Pintar FA, Cusick J. Finite element analysis of cervical laminectomy. In: *11th Annual North American Spine Society*, Vancouver, Canada, 1996, pp 271-272.

Figure Captions

Figure 1a: Coronal CT section of the human cervical spine.

Figure 1b: Sagittal CT section of the human cervical spine.

Figure 2: Rasterized images of Sagittal CT section (top) and Coronal CT section (bottom).

Figure 3: Solid model of a single vertebrae.

Figure 4: Finite element mesh of a single vertebrae.

Figure 5: Finite element mesh of C4-C5-C6 structure.

Figure 6a: Comparison of finite element model force-displacement response with experimental data under compression

Figure 6b: Comparison of finite element model strain response with experimental data under compression

Figure 7: Stress distribution in C5 vertebra under compression. Top: normal spine. Bottom: degenerated spine.

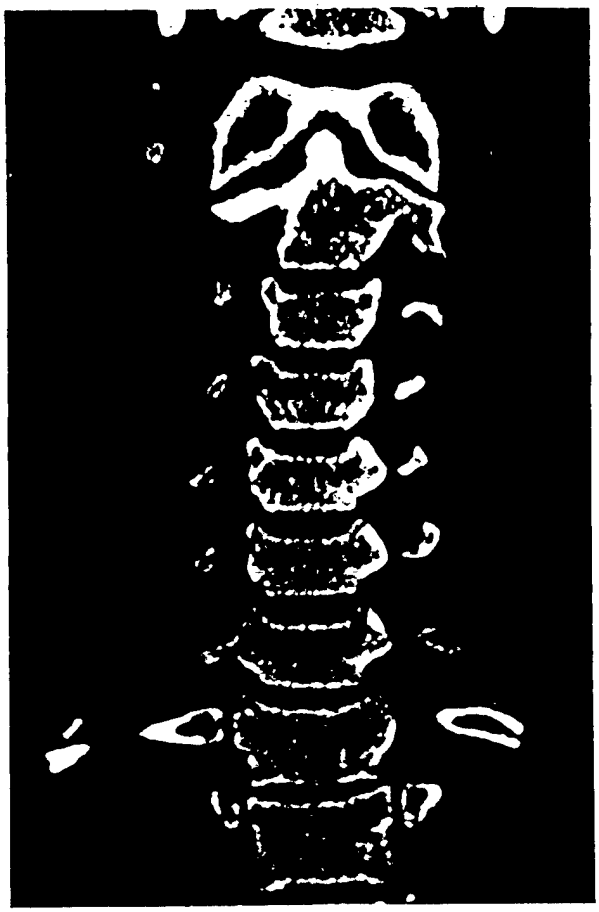

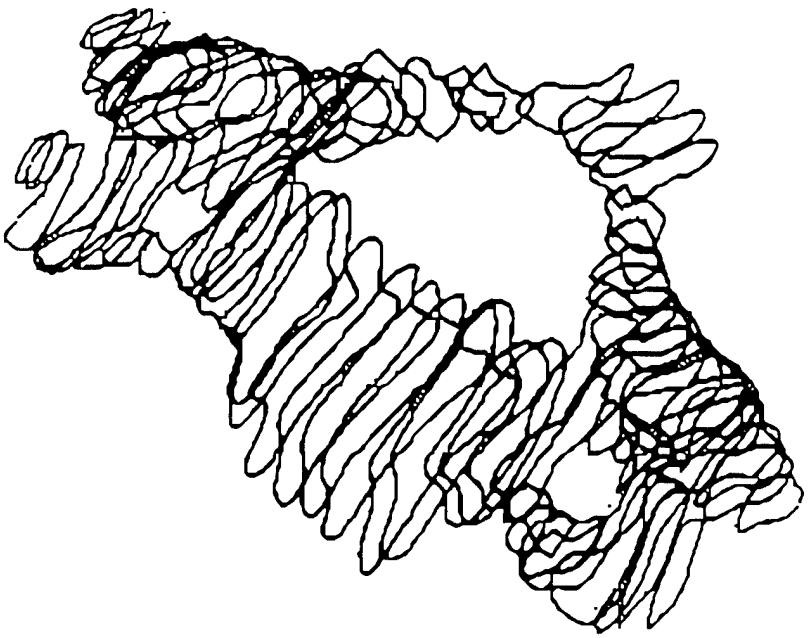

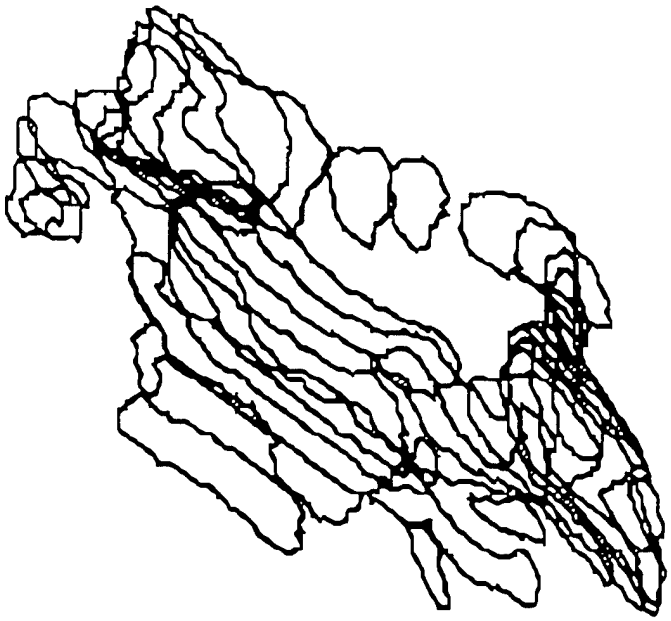

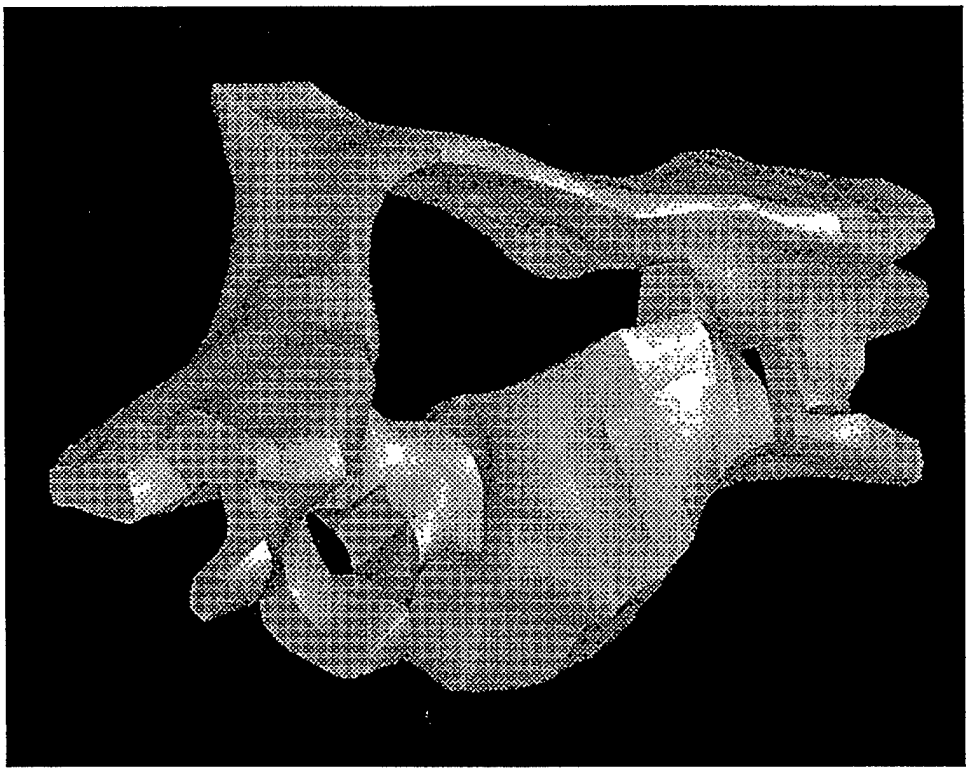

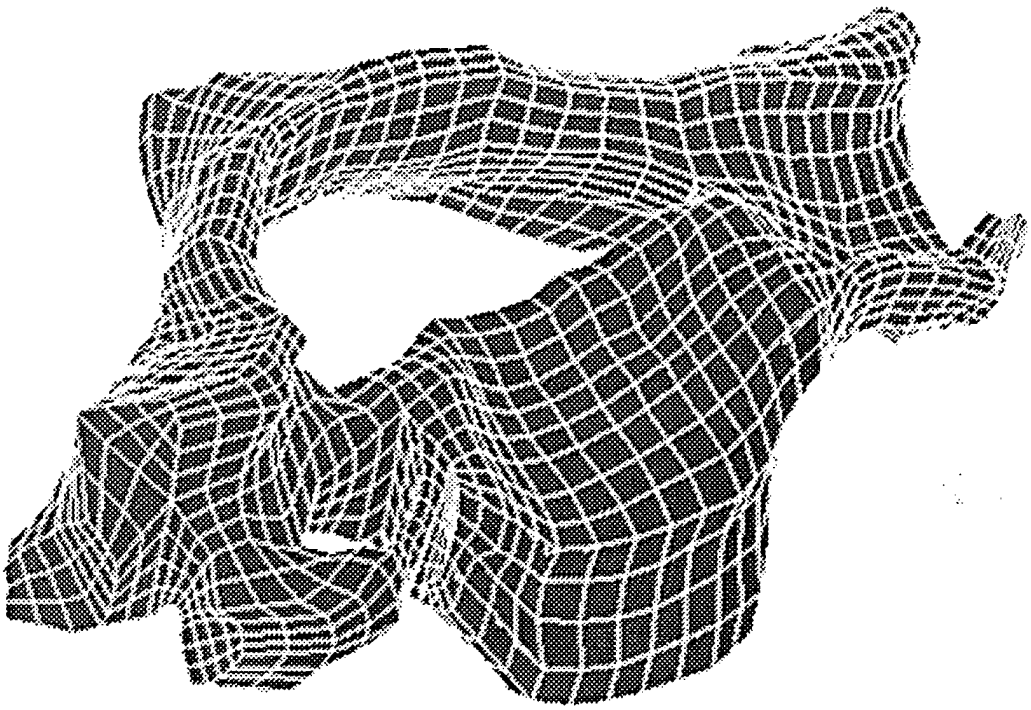

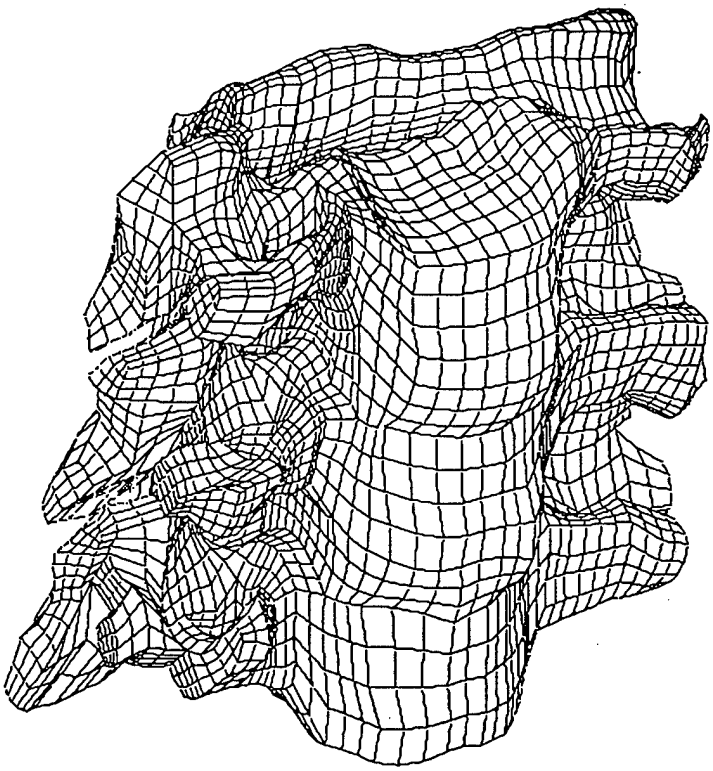

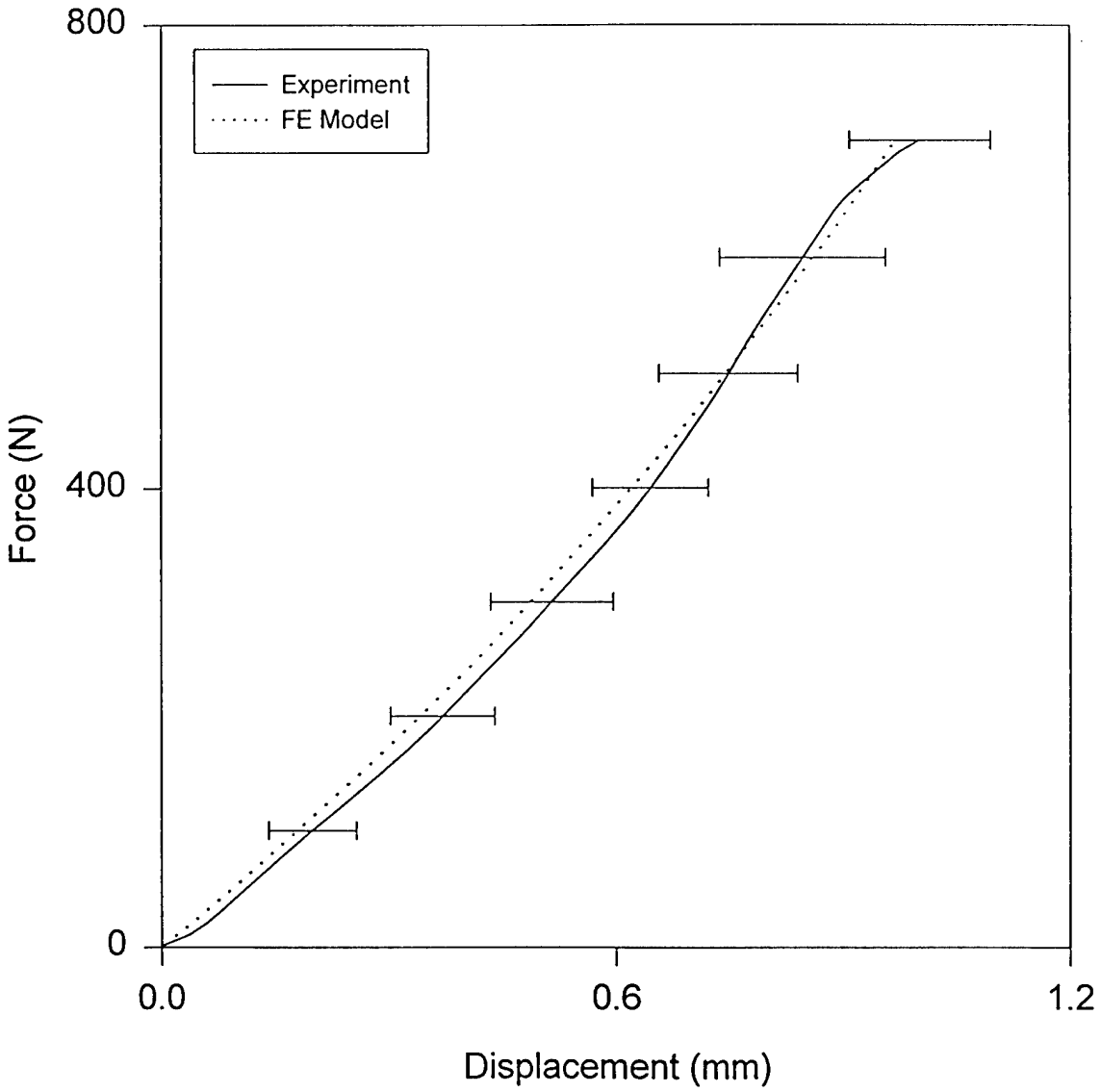
800
400
0
Force (N)
Experiment
FE Model
0.0
0.6
1.2
Displacement (mm)

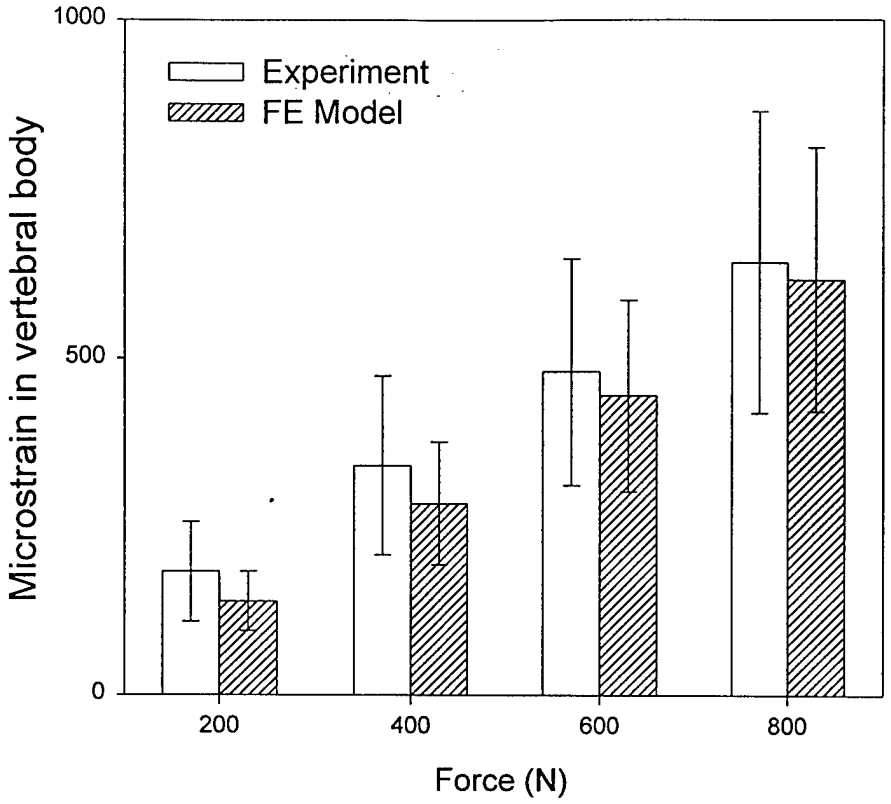
1000
500
0
Experiment
FE Model
Microstrain in vertebral body
200
400
600
800
Force (N)

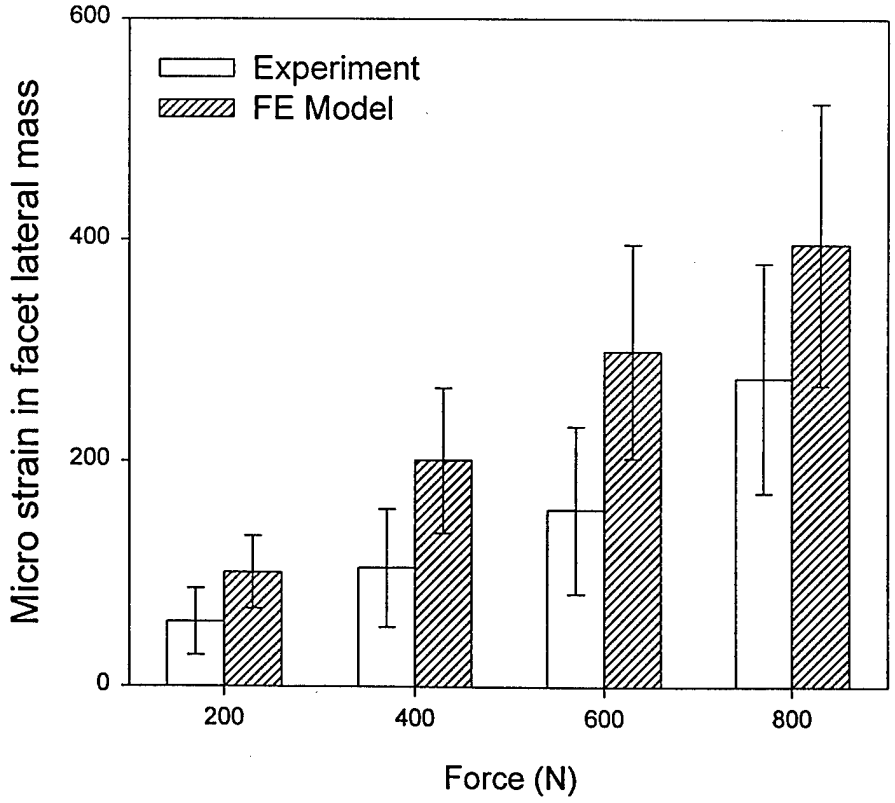
600
400
200
0
Experiment
FE Model
Micro strain in facet lateral mass
200
400
600
800
Force (N)

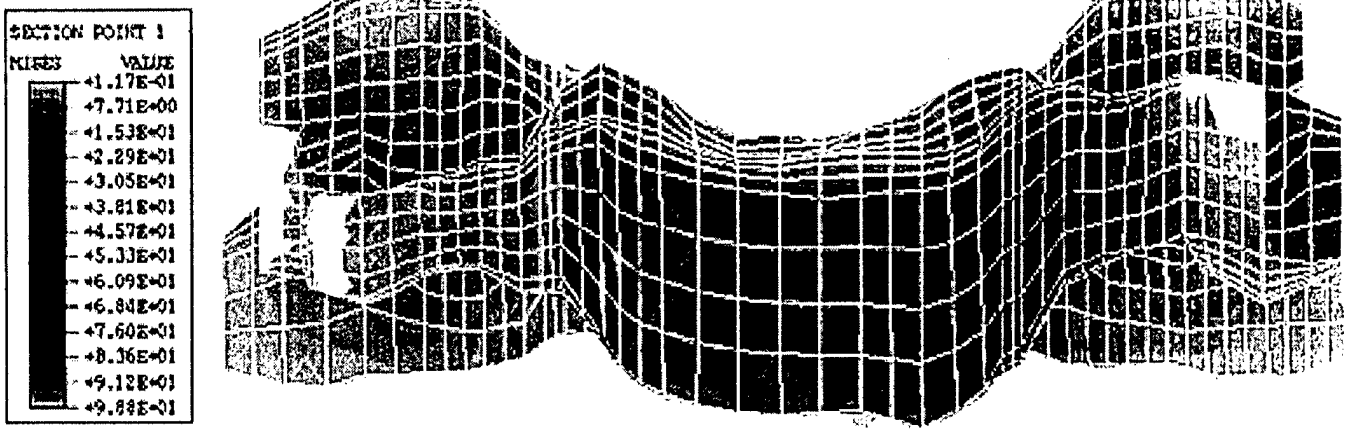

NORMAL

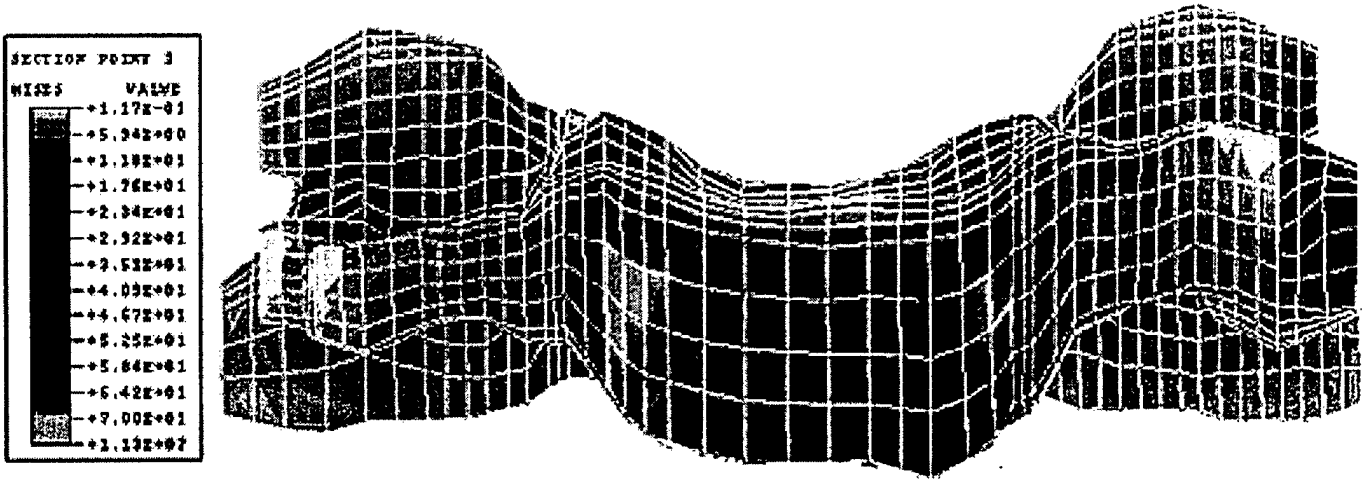

DEGENERATED

ONE, THREE AND SIX YEAR OLD PEDIATRIC CERVICAL SPINE FINITE ELEMENT MODELS

Srirangam Kumaresan, Narayan Yoganandan
Frank A. Pintar, Wade Mueller

Abstract

Because of a paucity of information on the biomechanical responses of the pediatric human neck and the recent awareness on the importance of understanding the pediatric neck biomechanics, our group advanced an initial study to quantify the responses as a function of age. In particular, the biomechanical responses of the one, three and six year old pediatric human cervical spine structures under different physiologic loading modes are described. The anatomically accurate and experimentally validated finite element model of the adult spine structure was modified to create the one, three and six year old pediatric spine models by incorporating the local geometrical and material characteristics of the developmental anatomy. The responses of the pediatric structures under different load vectors and the use of different methodologies were compared to the mature adult cervical spine. An important finding from this detailed three-dimensional nonlinear finite element study is: local age-related changes in the anatomy together with the changes in the material properties of the various spinal components are critical factors that contribute to the differences between the one, three and six year old pediatric and adult spines. A mere overall structural scaling of the adult responses is a less accurate representation of the pediatric behavior.

1. Introduction

Advances made in cervical spine biomechanics research enhanced our understanding of the behavior of this region of the human vertebral column [1-24]. These data are only applicable to the population beyond the second

decade of life. There remains however, a paucity of these types of quantified information for the pediatric human. This topic of pediatric neck biomechanics is gaining more importance in the clinical arena and vehicular crashworthiness environment. A mere overall scaling from the adult cervical spine may not be accurate enough to obtain the actual pediatric human cervical spine response. This is because developmental changes in the anatomy and geometry and material property characteristics affect the spinal response. The effects are different not only at different age groups but also under different types of forces. Systematically deduced data on the response of the pediatric spine to address the above factors are clearly needed. In this chapter, anatomically relevant finite element models of the one, three and six year old pediatric human cervical spines are developed and exercised using the principles of geometrical and material nonlinear analysis under compression, flexion and extension forces. The responses were compared with the adult human cervical spine model [25].

2. Biomechanically Relevant Developmental Anatomy

2.1 Vertebrae

From birth to adulthood, the cervical vertebrae continuously ossify to attain skeletal maturity. The ossified vertebrae develop from the cartilaginous structures formed during fetal life [20]. At the age of one year, the typical vertebrae consist of three ossified bony structures connected by the soft cartilages [26]. Figure 1 shows a schematic of a typical cervical vertebra of a one year old human. The nearly flat vertebral centrum and the two neural arches constitute the ossified bony elements that are connected by the cartilages of the spinous processes, bilateral costal cartilages of the transverse processes and bilateral neurocentral cartilages. As development occurs, bony ossification centers fuse to gain structural strength. At three years of age, the neural arches fuse posteriorly at the spinous process (Figure 2). By the age of six, the neural arch completely fuses with the vertebral centrum. However, the growth plates remain intact on the vertebral centrum and the vertebral body retains its flat superior and inferior surfaces (Figure 3).

2.2 Intervertebral Disc

At one year, the disc is characterized by a large nucleus pulposus relative to the total area of the whole disc and loosely embedded fibers in the anulus making a lack of clear demarcation of the anulus with the nucleus pulposus (Figure 4) [27, 28]. In the three year old, the disc shows better demarcation of the anulus and nucleus pulposus due to increased formation of fibers in the anulus. However, the nucleus pulposus still occupies a larger area of the disc volume (Figure 5). At six years of age, the fibers in the anulus become coarse and stiff making a more clear demarcation between the nucleus pulposus and anulus (Figure 6).

2.3 Facet Joint

The postero-laterally placed facet joint undergoes changes with growth of the spine [26, 29]. The facet joint is composed of articular cartilages, synovial fluid, synovial membrane and capsular ligament (Figure 7). During early childhood, the facet joint orientation with respect to the sagittal plane is more horizontal, i.e., towards the axial plane [29]. Specifically, at one year, the facet orientation of the vertebrae is almost horizontal. Between the one year old and the adult spine, a 15 degree difference in the facet orientation occurs. As the cervical vertebrae grow, the facet orientation is more towards the transverse plane (Figure 8).

2.4 Uncovertebral Joint

The bilateral uncovertebral joints are formed between the disc and the vertebral body in the adult spine [30]. This joint develops after the formation of the uncinate processes. In the pediatric spine, the uncovertebral joints are not developed. In the first twenty years, the joints appear as a fibrocartilage like the intervertebral discs, and after this period they transform into diarthrosis [31].

3. Pediatric Cervical Spine Model Development

The details of the adult cervical spine (C4-C5-C6) model development are presented in a previous chapter. Briefly, the adult model was constructed based on actual geometry obtained from close-up computed tomography and cryomicrotomy sections. The model included the cortical bone, cancellous core, endplate and uncinate processes of the vertebral body, posterior elements of the vertebrae which include the laminae, pedicles, transverse and spinous processes, anulus fibrosus and nucleus pulposus of the intervertebral discs, uncovertebral or neurocentral or Luschka's joints located bilaterally around the uncinate processes, joint capsule consisting of the articular cartilage, synovial fluid and synovial membrane forming the boundaries of the facet bones, and the spinal ligaments that include the anterior and posterior longitudinal ligaments, interspinous ligaments, capsular ligaments and ligamentum flavum [1, 32]. This adult model was validated with experimental data in terms of external and internal responses under loading modes such as compression, flexion, extension, compression-flexion and compression-extension loadings. A good agreement between the model output and the experimental data has provided confidence in the further use of this anatomically accurate, three-dimensional nonlinear finite element model to create the pediatric spine models [25, 33-39].

This experimentally validated adult spine model was modified to incorporate the characteristic anatomical local component geometry and material property differences to develop the one, three and six year old pediatric models [26-29, 40-46]. The following local spinal components were simulated in the adult model to create the one year old pediatric finite element model: cartilages of the spinous processes, bilateral costal cartilages of the transverse processes, bilateral neurocentral cartilages, and superior and inferior growth plates on the vertebral centrum. These modifications to the cervical vertebrae resulted in reduced height of the vertebral centrum leading to approximately equal heights between the centrum and intervertebral disc. In addition, the nearly horizontal vertebral centrum was devoid of the local uncovertebral and the uncinate anatomy. The larger nucleus pulposus and the loosely embedded anulus fibers in the ground matrix of the intervertebral disc were also modeled. The more horizontal (increased by 15 degrees) facet joint orientation angle compared to the adult spine was modeled in this one year old pediatric spine. The other components of the facet joint anatomy remained the same. The cartilages of the one year old pediatric spine vertebrae were idealized as isoparametric solid elements. The finite element definitions for the other components remained the same as in the adult model. The material properties for the cartilages of the pediatric spine models were adopted from literature [47, 48]. The material properties of the ligaments for the one year old group were 80 percent of the adult model values [25, 49, 50]. The Young's modulus of the anulus fibers were assumed to be 20 percent less than the adult model, and the volume was reduced to ten percent as compared to the 20 percent volume in the adult model. The material properties of the vertebral centrum and neural arches were assigned softer material properties than the adult counterparts to represent the initial ossified nature of the vertebrae [25, 49]. Table 1 lists the material properties used in the one year old pediatric spine.

Table 1: Material Properties Used in the One Year Old Pediatric Finite Element Model

Components	Young's Modulus (MPa)	Poisson's Ratio	Source
Vertebral centrum	75.0	0.29	[49]
Growth plate	25.0	0.40	[47,48]
Costal cartilage	25.0	0.40	[47,48]
Neural arches	200.0	0.25	[49]
Posterior synchondrosis	25.0	0.40	[47,48]
Neurocentral cartilage	25.0	0.40	[47,48]
Disc anulus ground substance	4.2	0.45	[50-53]
Disc anulus fibers	400 (10%)	0.30	[50-53]
Articular cartilages	10.4	0.40	[54]
Synovial fluid	1666.7 *		[52]
Uncovertebral joint	1666.7 *		[52]
Synovial membrane	12.0	0.40	[48]
Ligaments			[1,55]

Anterior Longitudinal		Posterior Longitudinal		Interspinous		Ligamentum Flavum		Capsular	
def.	force	def.	force	def.	force	def.	force	def.	force
1.4	28.4	1.0	23.2	1.3	13.5	1.9	36.7	1.8	42.9
2.7	51.9	2.0	41.1	2.7	19.5	3.7	65.9	3.9	70.3
4.1	71.8	3.0	57.0	4.0	23.6	5.6	95.7	5.8	87.5
5.4	86.9	4.0	68.6	5.4	26.3	7.5	106.9	7.7	100.6
6.8	95.7	5.0	75.8	6.7	27.9	9.4	117.8	9.7	107.8

* - Bulk modulus (Mpa)

Using this one year old pediatric spine model, the following developmental changes were incorporated to create the three year old pediatric finite element model: fusion of the posterior synchondrosis, an increase in the volume of the anulus fibers in the intervertebral discs, and a decrease in the facet joint orientation by approximately seven degrees. The material properties of the ligaments for the three year pediatric group were 15 percent less than the adult model value [25]. The Young's modulus of the anulus fibers were assumed to be 15 percent less than the adult model and the volume was reduced to 15 percent [25]. Table 2 lists the material properties used in the three year old pediatric spine.

Table 2: Material Properties Used in the Three Year Old Pediatric Finite Element Model

Components	Young's Modulus (MPa)	Poisson's Ratio	Source
Vertebral centrum	75.0	0.29	[25]
Growth plate	25.0	0.40	[47,48]
Costal cartilage	25.0	0.40	[47,48]
Neural arches	200.0	0.25	[25]
Neurocentral cartilage	25.0	0.40	[47,48]
Disc anulus ground substance	4.2	0.45	[50-53]
Disc anulus fibers	425 (15%)	0.30	[50-53]
Articular cartilages	10.4	0.40	[54]
Synovial fluid	1666.7 *		[52]
Uncovertebral joint	1666.7 *		[52]
Synovial membrane	12.0	0.40	[48]
Ligaments			[1,55]

Anterior Longitudinal		Posterior Longitudinal		Interspinous		Ligamentum Flavum		Capsular	
def.	force	def.	force	def.	force	def.	force	def.	force
1.4	30.2	1.0	24.7	1.3	14.4	1.9	39.1	1.8	45.6
2.7	55.2	2.0	43.7	2.7	20.7	3.7	70.1	3.9	74.7
4.1	76.3	3.0	60.6	4.0	25.1	5.6	101.7	5.8	92.9
5.4	92.3	4.0	72.9	5.4	27.9	7.5	113.6	7.7	106.9
6.8	101.7	5.0	80.5	6.7	29.7	9.4	125.1	9.7	114.6

* - Bulk modulus (Mpa)

The six year old pediatric finite element model was developed by incorporating the following developmental changes to the three year old model: fusion in the costal cartilages of transverse processes and the neurocentral cartilages of the vertebral centrum, further increase in the volume of the anulus fibers in the intervertebral discs, and a further decrease in the facet orientation by approximately five degrees. The material properties of the ligaments for the three year pediatric group were ten percent less than the adult model [25]. The Young's modulus of the anulus fibers were assumed to be 10 percent less than the adult model and the same volume of fiber in the adult model was used for the six year old pediatric spine. Table 3 lists the material properties used in the six year old pediatric spine.

Table 3: Material Properties Used in the Six Year Old Pediatric Finite Element Model

Components	Young's Modulus (MPa)	Poisson's Ratio	Source
Vertebral centrum	75.0	0.29	[25]
Growth plate	25.0	0.40	[47,48]
Neural arches	200.0	0.25	[25]
Disc anulus ground substance	4.2	0.45	[50-53]
Disc anulus fibers	450 (20%)	0.30	[50-53]
Articular cartilages	10.4	0.40	[54]
Synovial fluid	1666.7 *		[52]
Uncovertebral joint	1666.7 *		[52]
Synovial membrane	12.0	0.40	[48]
Ligaments			[1,55]

Anterior Longitudinal		Posterior Longitudinal		Interspinous		Ligamentum Flavum		Capsular	
def.	force	def.	force	def.	force	def.	force	def.	force
1.4	31.9	1.0	26.1	1.3	15.2	1.9	41.3	1.8	48.2
2.7	58.4	2.0	46.3	2.7	21.9	3.7	74.2	3.9	79.1
4.1	80.7	3.0	64.2	4.0	26.6	5.6	107.6	5.8	98.5
5.4	97.7	4.0	77.2	5.4	29.6	7.5	120.3	7.7	113.2
6.8	107.6	5.0	85.2	6.7	31.4	9.4	132.5	9.7	121.3

* - Bulk modulus (Mpa)

To these three separate age-specific pediatric cervical spine models, material properties (described above) and loading and boundary conditions were specified so that the structures could be exercised using the principles of nonlinear (geometric, material) finite element analysis. Compression, flexion and extension load vectors were applied as done in the adult model and the resulting deformations were obtained in the nonlinear domain. The biomechanical responses of the pediatric responses were compared using the following three methods.

4. Pediatric Responses

4.1 Method 1 - Child Responses Using Overall Structural Scaling of the Adult Model (CROS)

Structural scaling is defined as the overall pure scaling (reducing size) of the adult model without incorporating the characteristic anatomical features of the pediatric spine. Thus, the output from the basic adult model was investigated from an overall structural (geometric) scaling viewpoint. Parametric studies were conducted by varying the overall adult structure from its basic value (termed as 100%) up to 180 percent size, and the responses were compared in a nondimensionalized manner with respect to the basic model. This was accomplished for each load vector, i.e., compression, flexion and extension. The normalized response representing the peak change/deviation in the flexibility from the basic model for each of the above increased cervical spine sizes was determined using the following equation. Principles of linear regression were applied and the responses were determined from the regression line using the geometric scaling factors to the three age-specific (individual) pediatric spine structures [47]. The reduction of the overall size of the adult model was not possible as the already fine finite

element size caused the solution to diverge. The scaled-up adult model was extrapolated to obtain the scaled-down child response using the regression equation.

$$(NR)_j = \frac{(R)_{i,j} - (R)_{b,j}}{(R)_{b,j}}$$

Where

NR = normalized response under load j
R = response from the particular model
R_b = response from the basic model (100%)
j = load (compression, flexion and extension)
i = overall structural size (120, 140, 160, 180%)

4.2 Method 2 - Child Responses Using Anatomically and Materially Modified Pediatric Models (CRAM)

The one, three and six year old pediatric models developed using the appropriate local component geometry and material property modifications were exercised under the same external load vectors, i.e., compression, flexion and extension. The biomechanical responses obtained were similar to the adult model (e.g., nonlinear moment-rotation characteristics). The peak changes in the flexibilities in these pediatric responses compared to the basic adult response were determined. This methodology described the pediatric behavior based on the inclusion of the local component geometry and material changes. The following equation was used to determine the peak changes in the responses.

$$(NR)_{p,j} = \frac{(R)_{p,j} - (R)_{b,j}}{(R)_{b,j}}$$

Where

NR = normalized response under load j
p = the three pediatric models
R_p = response from the particular pediatric model
R_b = response from the basic adult model
j = load (compression, flexion and extension)

4.3 Method 3 -Child Responses Using Anatomically and Materially Modified, and Structurally Scaled Pediatric Models (CRAMS)

The first method (CROS) resulted in an estimation of the representative pediatric biomechanical responses obtained from the adult model by adopting the principles of structural scaling. The second method (CRAM) resulted in an estimation of the pediatric biomechanical responses using the age-specific finite element models that incorporated the effects of local geometry and material property changes. The overall size of the pediatric spine finite element models remained the same as that of the adult spine in this method. In contrast, the third method (CRAMS) incorporated the overall structural scaling on the age-specific pediatric models with the local component geometry and material property changes. Using the response obtained in the CRAM method and the scaling factors described in the CROS method, the responses for each of the three pediatric models under each of the three forces were determined. The peak changes in the responses were compared to the basic adult model using the following equation.

$$(NR)_{q,j} = \frac{(R)_{q,j} - (R)_{b,j}}{(R)_{b,j}}$$

Where

NR	=	normalized response under load j
q	=	the three scaled pediatric models
R_q	=	response from the particular pediatric model
R_b	=	response from the basic adult model
j	=	load (compression, flexion and extension)

5. Results and discussion

The biomechanical force-deflection and moment rotation responses were nonlinear for all the three age groups. The reader is referred to a recent publication for additional details [25]. The comparison of the change in the flexibility biomechanical responses at peak load/moment levels (Figure 9) of the three age groups with the adult model using all three methods, indicated that the values obtained using the CROS method (pure overall structural scaling of the adult model) were significantly lower than the CRAM method (adult model incorporating the local anatomical and material property changes). When the overall structural scaling was added to the model with anatomical and material property changes (CRAMS), the magnitudes in the biomechanical responses further increased. However, the increase due to the addition of this overall structural scaling was smaller compared to the increases in the responses from method 1 to the second method. In other words, incorporation of the local component anatomy and material property variations considerably affected the biomechanical response. This was found to be true irrespective of the loading mode, load levels and age categories.

In addition, results indicated that considerable changes exist among the various ages in the pediatric group and also between any pediatric group and the adult spine. These differences could be primarily attributed to the anatomy, geometry and material property variations of the human neck. For example, the uncovertebral joints begin to develop only during the first and second decade of life; uncinate processes develop just prior to the uncovertebral anatomy; flat vertebral bodies persist even at the end of the first decade; facet joint orientations are more flat during the first two to three years of life and gradually reach the adult orientation after approximately six years; the nucleus to anulus ratio decreases from birth to six years, and the ossifications to the vertebrae occur both in the anterior and posterior regions with increasing age. Consequently, to accurately delineate the age-related pediatric cervical spine biomechanics, it would be necessary to incorporate these characteristic developmental features in the modeling process. Although it would be ideal to conduct cervical spine experiments using the respective age-related pediatric human cadavers, such information is not available. In the present study, an indirect method was used. The method consisted of constructing an anatomically accurate three-dimensional finite element model of the adult cervical spine and using this model to create the one, three and six year old pediatric spine models by incorporating the local component anatomical and material features.

Three different methods were adopted to compare the biomechanical responses of three different pediatric cervical spine models. The first, termed as the overall structural scaling, the CROS method incorporated overall reduction in the geometry of the adult spine to represent the pediatric spine. This structural scaling methodology precluded the local component anatomy and material property variations to this group of the population. Our results clearly indicated that the response with regard to this type of scaling method is linear, and the pediatric one, three and six year old models differ from the adult by a maximum of 118 percent under the three types of loads (Figure 9) [25]. The anatomically and materially modified method included systematic modifications to the adult model to obtain the three pediatric models (CRAM). The results were found to be distinctly different compared to the results from the CROS method (Figure 9). The differences mainly stem from the local component anatomy and the material property alterations that were modeled as part of the developmental process. While these results are an improvement over the pure overall structurally scaled responses, the effective reductions in the pediatric geometry were not included in these

evaluations. The anatomically and materially modified, and structurally scaled method (CRAMS) included the effects of the first and second methods (CROS and CRAM). The behavior of the three pediatric models under flexion and extension was similar, i.e., the one year old model was the most flexible followed by the three and six year old models [25]. In contrast, under compression, the three year old was the most flexible, followed by the six and one year old pediatric groups. The flat facet joint orientation present in the one year old group may provide an additional resistance to the compressive load and may thus decrease the flexibility of the spine under this force. In addition, the other local anatomical features such as the presence of the bilateral neurocentral cartilages together with the posterior synchondrosis may also add to the structural response. A characteristic feature in the compression and extension responses is that the change in flexibility decreases with increasing load levels and this is true for all the three pediatric models [25]. In contrast, the change in flexion response was almost independent of the moment level for all the three groups indicating the possible existence of linear scaling [25]. It should be noted that these identifications could only be made because of the systematic incorporation of the local component anatomy and material property changes that occur to the different age groups in the pediatric human, and the inclusion of the appropriate overall structural scaling in the nonlinear finite element models.

Pediatric spine responses obtained from pure overall structural scaling of the adult model without incorporating the local component anatomy and material property changes (CROS) are significantly different from pediatric models that included these local component anatomy and material property modifications (CRAM). In other words, the local component anatomy and material properties of the individual spinal elements appear to have a predominant effect on the biomechanical response. Consequently, it can be surmised that it is imperative to include the developmental anatomical changes to the pediatric population to describe their biomechanical responses and to develop more appropriate scaling factors for this group. These data may be of value not only to the treatment of pediatric disorders but also to design and develop anthropometric child dummies with improved biofidelity so that injury can be predicted in crash environments. Such an approach will assist in the development of child restraint systems and safer vehicular interior components.

Acknowledgment: This study was supported in part by PHS CDC Grant R49CCR 507370 and the Department of Veterans Affairs Medical Research.

References

[1] Pintar FA. *Biomechanics of Spinal Elements*. Marquette University, Milwaukee, WI, 1986: 222 pp.

[2] Pintar FA, Myklebust JB, Yoganandan N, Maiman DJ, Sances A Jr. Biomechanics of human spinal ligaments. In: *Mechanisms of Head and Spine Trauma*. Sances A Jr, Thomas DJ, Ewing CL, Larson SJ, Unterharnscheidt F (eds). Aloray Publisher, Goshen, NY, 1986: 505-527.

[3] Pintar FA, Yoganandan N, Sances A Jr, Reinartz J, Harris G, Larson SJ. Kinematic and anatomical analysis of the human cervical spinal column under axial loading. *SAE Transactions* 1990:98(6): 1766-1789.

[4] Pintar FA, Sances A Jr, Yoganandan N, Reinartz JM, Maiman DJ, Suh JK, Unger G, Cusick JF, Larson SJ. Biodynamics of the total human cadaver cervical spine. In: *Proceedings 34th Stapp Car Crash Conference*, Orlando, FL, 1990, pp 55-72.

[5] Pintar FA, Yoganandan N, Pesigan M, Reinartz J, Sances A Jr. Experimental measurement of cervical vertebral strain to assess load transfer. *Adv Bioeng* 1991:20: 127-128.

[6] Pintar FA, Yoganandan N, Maiman DJ, Sances A Jr. Cervical spinal bony injury and the potential for cord injury. In: *5th Symposium on Injury Prevention Through Biomechanics*, Detroit, MI, 1995, pp 161-169.

[7] Pintar FA, Schlick MB, Yoganandan N, Maiman DJ. Instrumented artificial spinal cord for human cervical pressure measurement. *Bio-Med Mat & Eng* 1996:6(2): 219-229.

[8] Yoganandan N, Sances A Jr, Maiman DJ, Myklebust JB, Pech P, Larson SJ. Experimental spinal injuries with vertical impact. *Spine* 1986:11(9): 855-860.

[9] Yoganandan N, Myklebust JB, Ray G, Sances A Jr. Mathematical and finite element analysis of spinal injuries. *CRC Review Biomed Eng* 1987:15(1): 29-93.

[10] Yoganandan N, Pintar FA, Butler J, Reinartz J, Sances A Jr, Larson SJ. Dynamic response of human cervical spine ligaments. *Spine* 1989:14(10): 1102-1110.

[11] Yoganandan N, Pintar FA, Wilson CR, Sances A Jr. In vitro biomechanical study of female geriatric cervical vertebral bodies. *J Biomed Eng* 1990:12(2): 97-101.

[12] Yoganandan N, Sances A Jr, Pintar FA, Maiman DJ, Reinartz J, Cusick JF, Larson SJ. Injury biomechanics of the human cervical column. *Spine* 1990:15(10): 1031-1039.

[13] Yoganandan N, Maiman DJ, Pintar FA, Sances A Jr, Chintapalli K, Unger GF. Cervical spine injuries from motor vehicle accidents. *J Clin Eng* 1990:15(6): 505-513.

[14] Yoganandan N, Pintar FA, Sances A Jr, Maiman DJ. Strength and motion analysis of the human head-neck complex. *J Spinal Disord* 1991:4(1): 73-85.

[15] Yoganandan N, Pintar FA, Sances A Jr, Reinartz J, Larson SJ. Strength and kinematic response of dynamic cervical spine injuries. *Spine* 1991:16(10): 511-517.

[16] Yoganandan N, Pintar FA, Arnold P, Reinartz J, Cusick JF, Maiman DJ, Sances A Jr. Continuous motion analysis of the head-neck complex under impact. *J Spinal Disord* 1994:7(3): 420-428.

[17] Yoganandan N, Pintar FA, Cusick JF, Reinartz J, Sances A Jr, Maiman DJ. Cervical spine injury mechanism under vertical impact. *ASME - BED* 1994:28: 339-340.

[18] Yoganandan N, Pintar FA. Inertial loading of the human cervical spine. *J Biomech Eng* 1997:119(3): 237-240.

[19] Yoganandan N, Pintar FA, Kleinberger M. Cervical vertebral and facet joint kinematics under whiplash loading. *J Biomech Eng* (In Press)

[20] Sherk HH, Dunn EJ, Eismont FJ, Fielding JW, Long DM, Ono K, Penning L, Raynor R. *The Cervical Spine*. Second Edition, JB Lippincott Co., Philadelphia, PA, 1989: 881.

[21] Cusick JF, Yoganandan N, Pintar FA, Gardon M. Cervical spine injuries from high velocity forces: A pathoanatomical and radiological study. *J Spinal Disords* 1996:9(1): 1-7.

[22] Cusick JF, Pintar FA, Yoganandan N, Reinartz JM. Biomechanical alterations induced by multilevel cervical laminectomy. *Spine* 1995:20(22): 2393-2399.

[23] Cusick JF. Pathophysiology and treatment of cervical spondylotic myelopathy. *Clin Neurosurg* 1991:37: 661-681.

[24] Cusick JF, Yoganandan N, Pintar FA, Myklebust JB, Hussain H. Biomechanics of cervical spine facetectomy and fixation techniques. *Spine* 1988:13(7): 808-812.

[25] Kumaresan S, Yoganandan N, Pintar F. Age-specific pediatric cervical spine biomechanical responses: Three-dimensional nonlinear finite element models. In: Proceedings *41st Stapp Car Crash Conference*, Orlando, FL, 1997.

[26] Bailey D. The normal cervical spine in infants and children. *Radiology* 1952:59: 712-719.

[27] Peacock A. Observations on the postnatal structure of the intervertebral disc in man. *J Anat* 1956:86(Part 2): 162-179.

[28] Taylor JR. Growth of human intervertebral discs and vertebral bodies. *J Anat* 1975:120(1): 49-68.

[29] Kasai T, Ikata T, Katoh S, Miyake R, Tsubo M. Growth of the cervical spine with special reference to its lordosis and mobility. *Spine* 1996:21(18): 2067-2073.

[30] Hall MC. *Luschka's Joint*. CC Thomas, Springfield, IL, 1965: 141.

[31] Penning L. Functional anatomy of joints and discs. In: *The Cervical Spine*. HH Sherk, EJ Dunn, FJ Eismont, JW Fielding, DM Long, K Ono, L Penning, R Raynor (eds). JB Lippincott Company, Philadelphia, PA, 1989: 33-56.

[32] Kumaresan S, Yoganandan N, Pintar FA. Validation of nonlinear finite element model of human lower cervical spine. In: *ASME Bioeng*, Dallas, TX, 1997.

[33] Kumaresan S, Yoganandan N, Pintar F, Voo L, Cusick J, Larson S. Finite element modeling of cervical laminectomy with graded facetectomy. *J Spinal Disord* 1997:10(1): 40-47.

[34] Kumaresan S, Yoganandan N, Pintar F. Finite element analysis of anterior cervical spine interbody fusion. *Biomed Mat & Eng* 1997 (In Press)

[35] Voo L, Denman J, Kumaresan S, Yoganandan N, Pintar FA, Cusick JF. Development of 3-D finite element model of the cervical spine. *Adv Bioeng* 1995:31: 13-14.

[36] Voo LM, Kumaresan S, Yoganandan N, Pintar FA, Cusick JF. Finite element analysis of cervical facetectomy. *Spine* 1997:22(9): 964-969.

[37] Yoganandan N, Kumaresan S, Voo L, Pintar F, Larson S. Finite element modeling of the C4-C6 cervical spine unit. *Med Eng Phy* 1996:18(7): 569-574.

[38] Yoganandan N, Kumaresan S, Voo L, Pintar F. Finite element applications in human cervical spine modeling. *Spine* 1996:21(15): 1824-1834.
[39] Yoganandan N, Kumaresan S, Voo L, Pintar F. Finite element model of the human lower cervical spine. *J Biomech Eng* 1997:119(1): 87-92.
[40] Bonadio WA. Cervical spine trauma in children: Part I: General concepts, normal anatomy, radiographic evaluation. *Am J Emergency Med* 1993:11(2): 158-165.
[41] Hindman BW, Poole CA. Early appearance of the secondary vertebral ossification centers. *Radiology* 1970:95: 359-361.
[42] Knutsson F. Growth and differentiation of the postnatal vertebra. *Acta Radiologica* 1961:55: 401-408.
[43] O'Rahilly R, Benson DR. The development of the vertebral column. In: *The Pediatric Spine.* DS Bradford, RN Hensinger (eds). Thieme Inc., New York, 1985: 3-17.
[44] Roaf R. Vertebral growth and its mechanical control. *J Bone Joint Surg* 1960:42B: 40-59.
[45] Tulsi RS. Growth of the human vertebral column: An osteological study. *Acta Anat* 1971:79: 570-580.
[46] Veldhuizen AG, Baas P, Webb PJ. Observations on the growth of the adolescent spine. *J Bone Joint Surg Br* 1986:68-B(5): 724-728.
[47] Melvin JW. Injury assessment reference values for the CRABI 6-month infant dummy in a rear-facing infant restraint with airbag deployment. In: *SAE Congress and Exposition*, Detroit, MI, 1995, pp 1-12.
[48] Yamada H. *Strength of Biological Materials.* FG Evans (ed). Williams & Wilkins, Baltimore, MD, 1970: 297 pp.
[49] Kumaresan S, Yoganandan N, Pintar FA. Adult and pediatric human cervical spine finite element analyses. In: *ASME Summer Bioengineering Conference*, Sun River, OR, 1997.
[50] Saito T, Yamamuro T, Shikata J, Oka M, Tsutsumi S. Analysis and prevention of spinal column deformity following cervical laminectomy I. Pathogenetic analysis of postlaminectomy deformities. *Spine* 1991:16: 494-502.
[51] Galante JO. Tensile properties of the human lumbar anulus fibrosus. *Acta Ortho Scand (suupl)* 1967: 100.
[52] Ueno K, Liu YK. A three-dimensional nonlinear finite element model of lumbar intervertebral joint in torsion. *Biomech Eng* 1987:109: 200-209.
[53] Wu HC, Yao RF. Mechanical behavior of the human anulus fibrosus. *J Biomech* 1976:9: 1-7.
[54] Kempson GE. Mechanical properties of articular cartilage. In: *Adult Articular Cartilage.* Pitman, Kent, England. 1979: 333-414.
[55] Grossheim L. *Morphology of the Human Cervical Spine.* In: *Biomedical Engineering*, 1989, Marquette University, Milwaukee, WI. 183 pp.

Figure Captions

Figure 1: Left: superior view of the one year old human cervical vertebra. Right: anterior view of one year old cervical spine functional unit. Note the bilateral costal cartilages, bilateral neurocentral cartilages, spinous cartilage and growth plate, and vertebral centrum and neural arches.

Figure 2: Left: superior view of the three year old human cervical vertebra. Right: anterior view of the three year old cervical spine functional unit. Note the fused posterior cartilages.

Figure 3: Left: superior view of the six year old human cervical vertebra. Right: anterior view of the six year old cervical spine functional unit. Except for the growth plates other cartilages are merged with the hard tissues.

Figure 4: Left: schematic of a sagittal section of the intervertebral disc of the one year old human cervical spine. Right: magnified view of the anulus laminates showing the arrangement of the fibers in the anulus ground substance. The soft fibers occupy 10% volume of the anulus.

Figure 5: Left: schematic of a sagittal section of the intervertebral disc of the three year old human cervical spine. Right: magnified view of the anulus laminates showing the arrangement of the fibers in the

anulus ground substance. The fibers with moderately increased stiffness occupy 15% volume of the anulus.

Figure 6: Left: schematic of a sagittal (anterior to posterior) section of the intervertebral disc of the six year old human cervical spine. Right: magnified view of the anulus laminates showing the arrangement of fibers in the anulus ground substance. The fibers with increased stiffness occupy 20% volume of the anulus.

Figure 7: Magnified view of the cervical facet joint.

Figure 8: Top: schematic of a sagittal view of cervical spine functional unit. Bottom: magnified view of the facet joint orientation in the one, three and six year old and adult cervical spine structures.

Figure 9: Comparison of the biomechanical responses of one, three and six year old pediatric spine models with adult model response under compression (top), flexion (middle), extension (bottom). CROS: Child responses using overall structural scaling. CRAM: Child responses using anatomical and material scaling. CRAMS: Child responses using anatomical and material, and structural scaling.

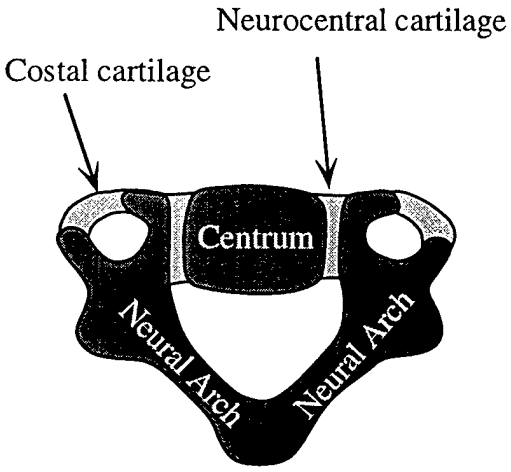
Neurocentral cartilage
Costal cartilage
Centrum
Neural Arch
Neural Arch

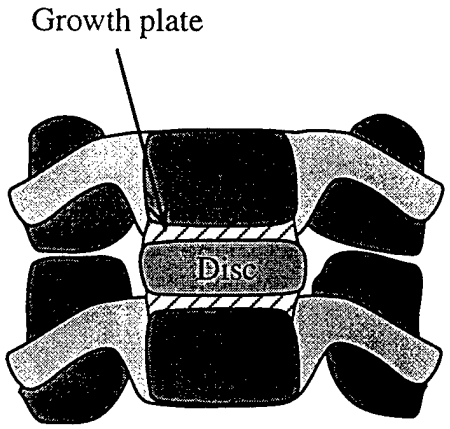
Growth plate
Disc

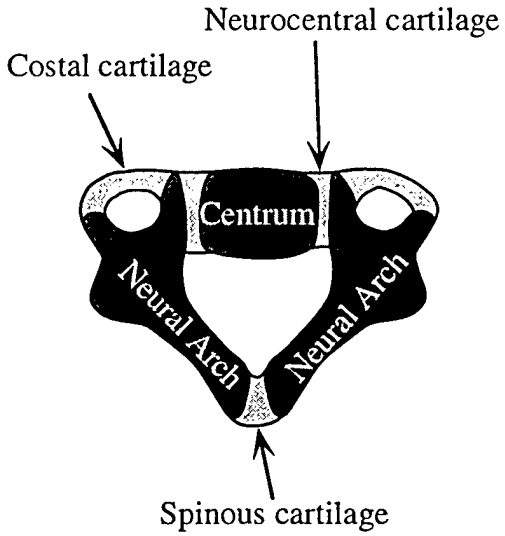
Neurocentral cartilage
Costal cartilage
Centrum
Neural Arch
Neural Arch
Spinous cartilage

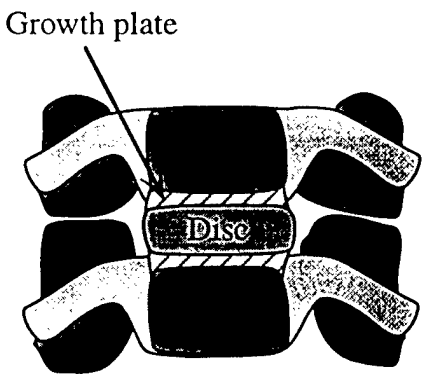
Growth plate
Disc

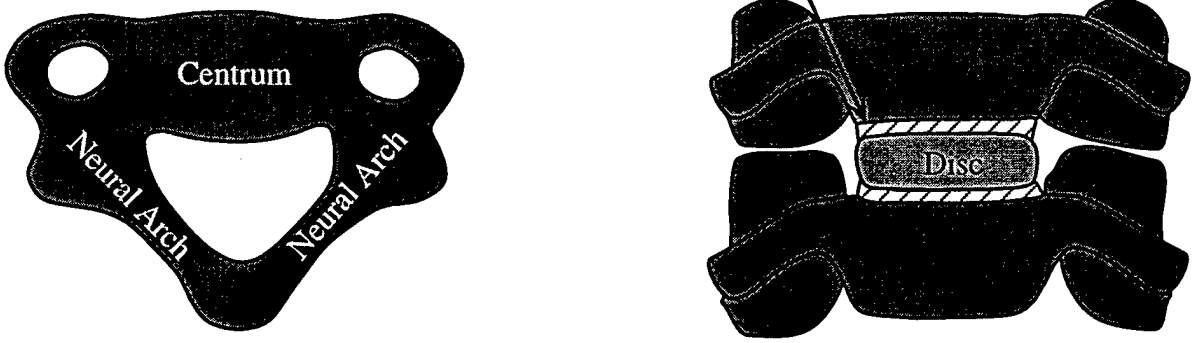
Growth plate
Centrum
Neural Arch
Neural Arch
Disc

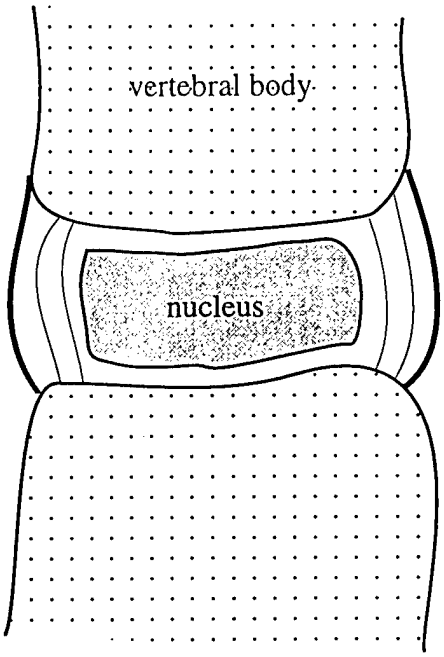
vertebral body
nucleus

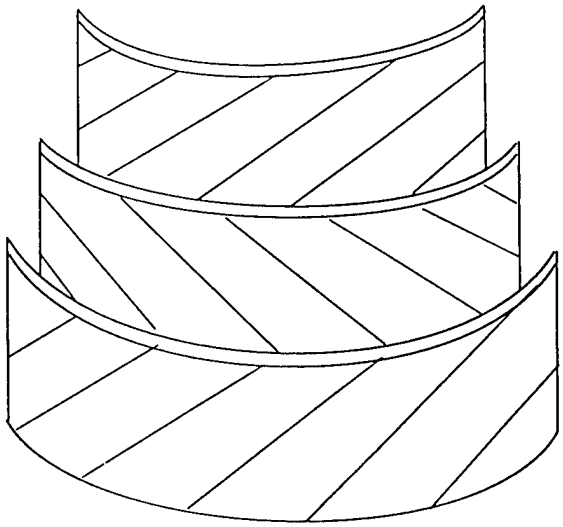

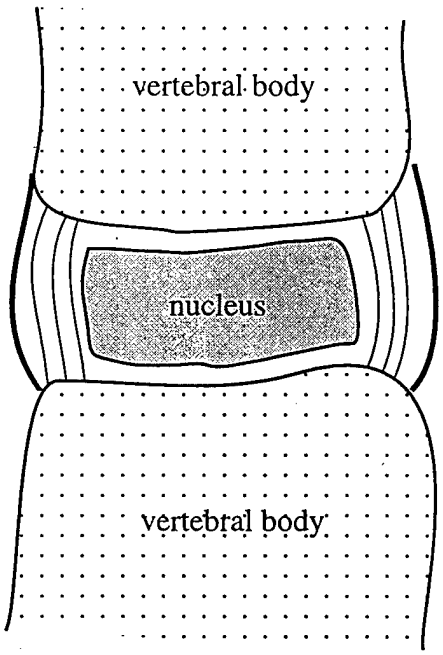
vertebral body
nucleus
vertebral body

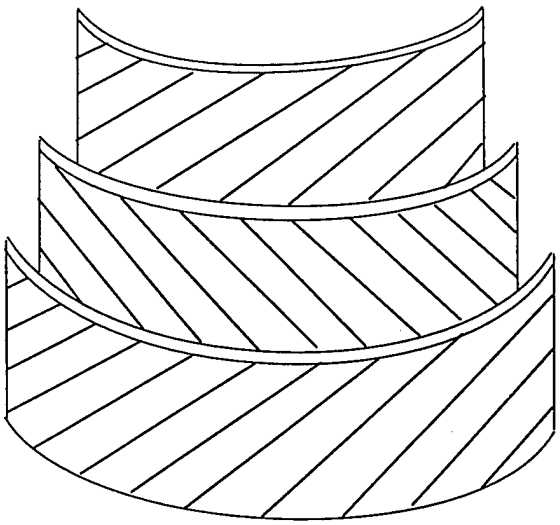

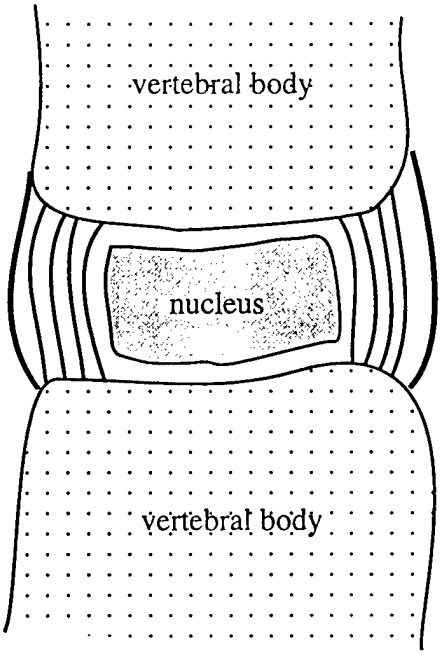
vertebral body
nucleus
vertebral body

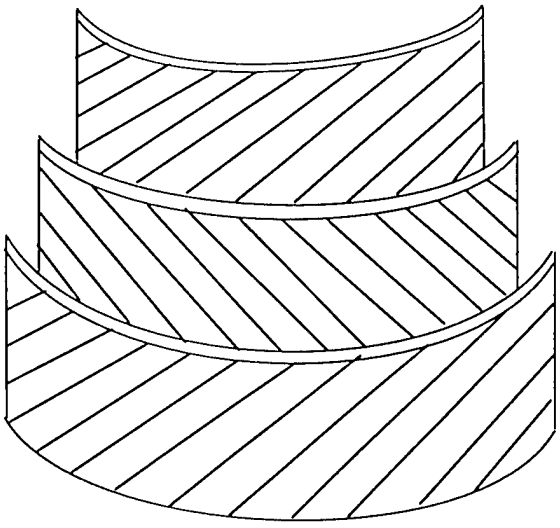

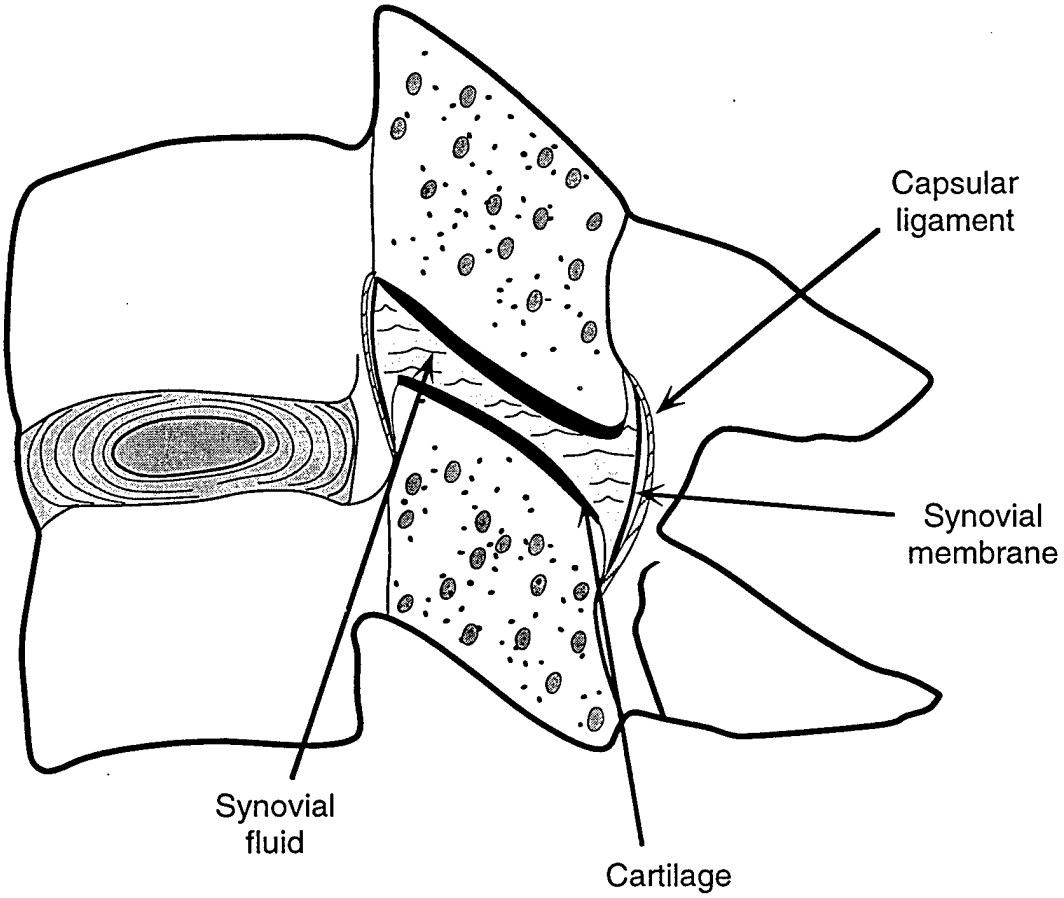
Capsular
ligament
Synovial
membrane
Synovial
fluid
Cartilage

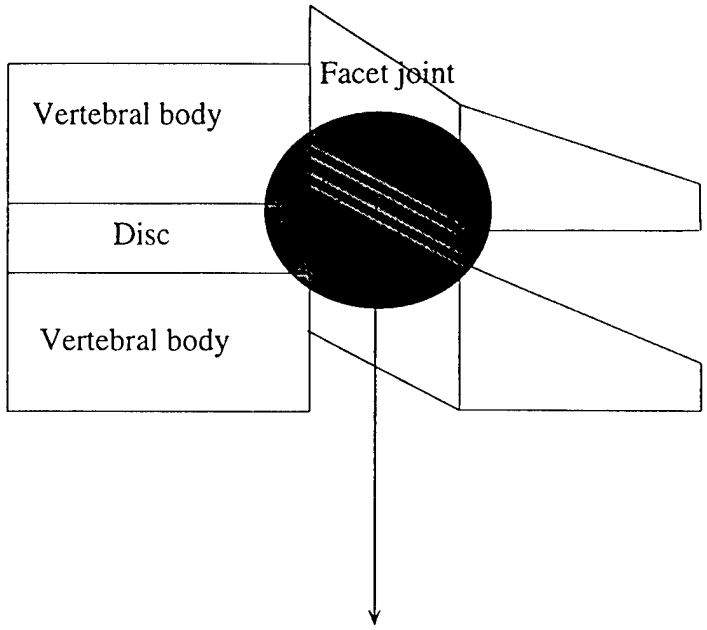

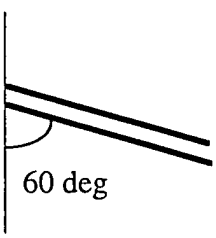

1 Year

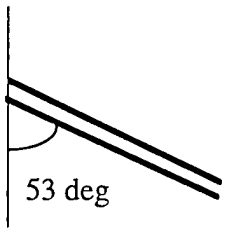

3 Year

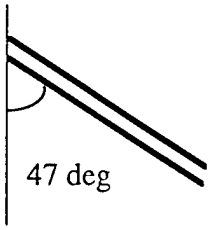

6 Year

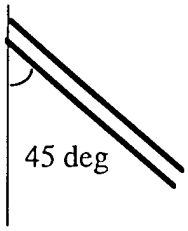

Adult

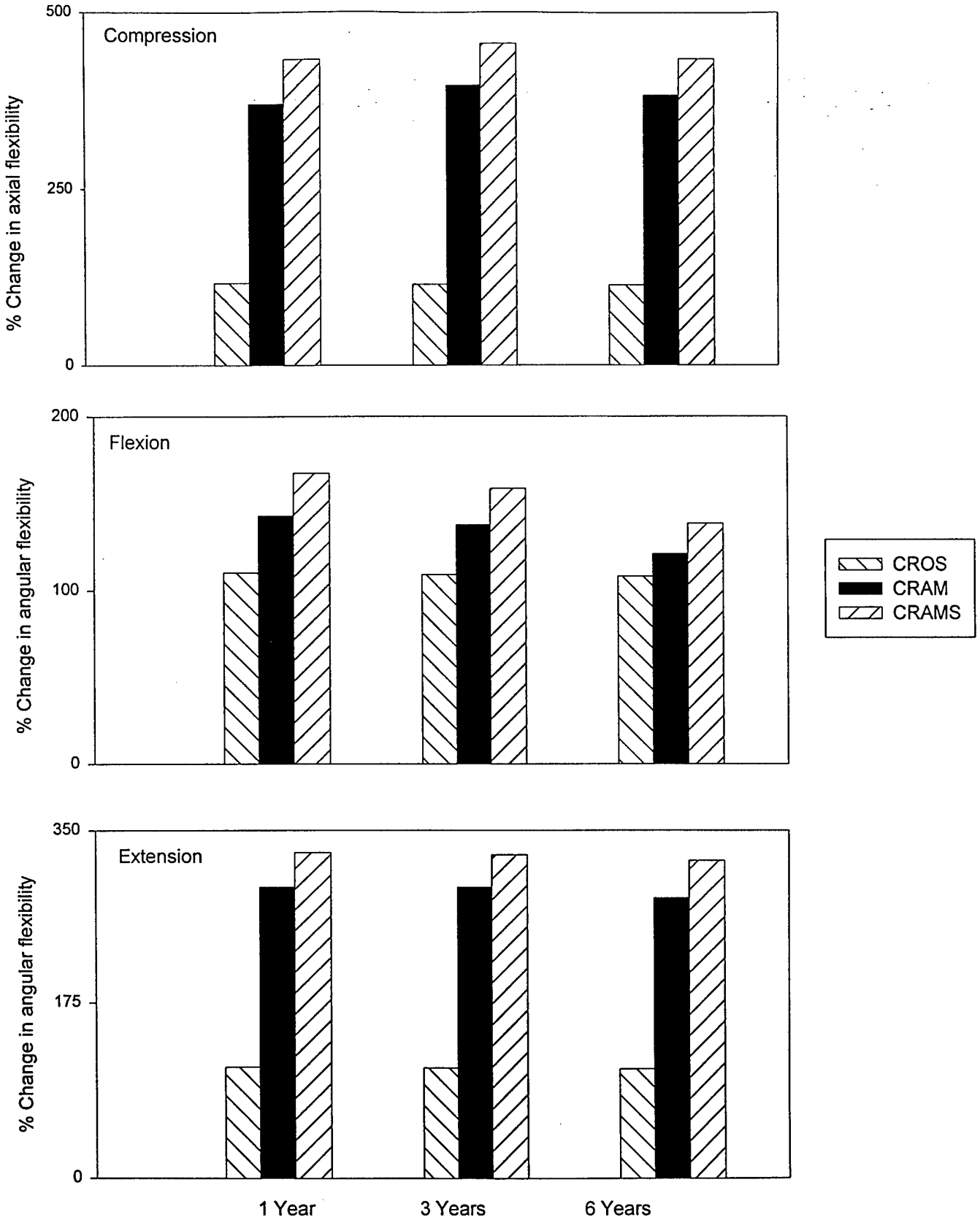
Compression
% Change in axial flexibility
500
250
0
Flexion
% Change in angular flexibility
200
100
0
Extension
% Change in angular flexibility
350
175
0
1 Year
3 Years
6 Years
CROS
CRAM
CRAMS

NEUROSURGICAL STRATEGIES IN ADULT AND PEDIATRIC HEAD INJURY

Patrick R. Walsh, Brian P. Walsh

Abstract

Epidemiologic studies bear witness to the frequency of traumatic dysfunction of the nervous system but only hint at the associated human costs which have led to efforts to prevent trauma and to prevent or ameliorate injury and resultant morbidity and mortality. To this end, a variety of animal models have been developed and clinical investigations of craniocerebral trauma have been undertaken.

1. Introduction

A challenge to investigators and clinicians arose from the review of Langfet of statistical analysis of the outcome of severe head injuries; mortality rates reported demonstrated no more than a 10-15 percent improvement from a level of approximately 65 percent between 1909 and the mid 1970s [1-6]. No difference in outcome was apparent in studies published by centers throughout the World despite marked differences in treatment protocols. These findings prompted many to question the validity of treatment, protocols and to consider the possibility that poor outcome and a possibly fixed percentage of the severely injured should be considered inevitable. Substantial reduction in mortality rate was reported in a series of studies by Becker and co-workers who employed a multi-modal monitoring system in a critical care unit in a formal treatment protocol directed toward the secondary events which follow craniocerebral trauma [7-8]. In addition to reduction of crude motality rates, investigational efforts have been directed towards improvement in the quality of survival and have involved the quest for evaluation of indices of

potential value in guidance of therapy and with reliability and accuracy for prediction of both short-term neurologic change for guidance of accute treatment, and a final outcom [7-13].

Neurosurgical strategies in the manangement of craniocerebral trauma include nonsurgical treatment and specific surgical intervention. Indications for surgery typically arise from elements of clinical status, physiologic parameters and radiologic findings [14-15]. Surgical procedures primarily address static deforming forces generated by displaced osseus structures, contusions or hematomas. Such procedures have undergone evolutionary refinement however, the principles espoused by Cushing have not been fundamentally altered [16]. Closure of scalp lacerations, debridement of displaced and potentially contaminated fragments of skull, dural closure and debridement of brain and evacuation of hematomas are essentially universally accepted surgical principles. Details of surgical procedures have been summarized and are available from multiple sources. The interested reader is referred to the comprehensive historical review of head injury by Gurdjian [17].

Controversy continues however, to surround issues of timing and of specific indications for surgical intervention. A spectrum exists regarding timing of surgical intervention; treatment by immediate placement of burr or twist drill holes at prescribed sites has been advocated in dire clinical situations, formal neuroradiologic evaluation prior to intervention has been suggested for more stable injured patients [18-19]. The yield from single burr holes without radiographic guidance has been relatively low; only a small portion of a hematoma may be evacuated without substantial enlargement of the surgical defect however, positive findings were reported in 56 percent of patients who underwent bilateral frontal, temporal, and parietal burr holes with clinical findings compatible with transtentorial herniation, a clinical situation associated with extremely poor prognosis [19-22].

Although little debate attends the decision for surgical decompression in the patient with rapidly deteriorating neurologic status due to an expanding hematoma, other minimally symptomatic patients may present immediately or several weeks after development of hematoma [24-26]. Nonsurgical management may be appropriate for many patients in this latter group and small hematomas are often managed without surgical intervention [14-15,23,26,40-42]. Primary cortical injury may be less significant with the epidural hematoma, which typically arises from arterial sources of hemmorhage and is limited in size by dural adhesion to the inner table of the skull, than with subdural hematoma, which may be generated by hemmorage from the injured pial surface of the brain. Delayed decompression would be expected to generate a deleterious effect on outcome; however, this has not been proven in the manangement of subdural hematoma. Reduction in mortality rate related to surgery within four hours reported by Selig et al., was not confirmed by the more recent studies in which prognostic factors of value included patient age, neurologic status, elevation of intracranial pressure and parenchymal injury [27]. Perhaps subdural hematomas generated by cortical sources of hemmorhage may behave differently from those related to shearing of draining veins. In any case, in most centers, time required for transport, stabilization of nonneural injuries, and clinical and neuroradiologic evaluation dictates a substantial delay in timing of such decompressive procedures.

The role of operative treatment of cerebral contusions and edematous states is more difficult to define than in the case for hematomas [14-15]. This parenchymal injury may occur in isolation or in association with hematoma, and findings of brainstem compression may develop abruptly in the first days of the injury. Decompression craniectomy and parenchymal resections are typically considered on the basis of neurologic status, mass effect and intracranial pressure, as nonoperative management directed by principles of critical care outlined below [28-30,34-43].

Of far greater general interest than details of surgical procedures is aspects of the nonoperative manangement of craniocerebral trauma. Priciples of critical care management and multi-modal monitoring espoused by Becker have been advanced by Rosner and others [7-8]. Elevation of the blood pressure threshold for maintainence of cerebral perfusion pressure in the setting of brain injury was indentified by Rosner et al., and others and constitutes a central tenet of treatment in this patient population [24,44-45]. The utility of hyperventilation and of osmotic diuretics has been redefined from fundamentals of treatment to a lesser role with improved appreciation of physiologic mechanisms. Formal courses in neurosurgical critical care have been sponsored by the Amercian Association of Neurological Surgeons and have stressed this concept and have mandated attention to multiple physiologic systems [46-47].

Four primary families of indices have emerged in the nonoperative management of acute head injury; these include measures of clinical neurologic status, neuroradiologic or anatomic diagnostic categories, physical properties of the nervous system (intracranial pressure, compliance) and electrophysiologic indices (electroencephalograms, evoked potentials). Clinical examination remains the cornerstone of evaluation of the nervous system injury; however, few studies of central nervous system trauma prior to the mid 1970s reported outcome as a function of initial neurologic status [6]. A variety of coma scales have been proposed; widespread adoption of the Glasgow

Coma Scale has established uniformity between centers [31-33,48-51]. This scale has been shown to be a useful prognostic instrument; however, confidence intervals are lower than for other combinations of clinical indicants [52-54]. Approximately two-thirds of the scale are occupied by eye opening and verbal response, and relatively little separation of patients at the lower end of the scale (less than or equal to seven) has been reported despite nearly equal frequencies of "good" and "poor" outcomes within this group [11]. The utility of the scale for sensitive, serial evaluation has been questioned, and addition of brainstem reflexes, known to be useful predictors in both traumatic and nontraumatic coma, to a scale suitable for serial tracking and treatment evaluation has been proposed [53]. Content and Narayan have provided a detailed review of multi-variate predictive models proposed by Narayan et al., Choi et al., and Klauber et al [55-58]. The pattern of multi-modal evoked potential changes has been correlated with final outcome in head injury; however, nonstationarity of the evoked potential has been identified in a computer-based system for automated serial tracking of the evoked potential which may compromise long-term predictive strength of single studies [59]. Neuroradiologic (CT) findings of predictive strength have included cisternal configuration, volume and configuration of hematoma, and mass effect with abnormal parenchymal density [60-61].

These findings suggest limiting intracranial pressure monitoring to specific patterns of injury, and tracking of neurologic examination and physiologic parameters and sequential CT scanning constitute current practice. Many centers have devised flow sheets for these data; the form developed in our center permits generation of various published coma scales. A model coma scale with adaptation for entry with a computer-based automated monitoring system; copies available upon request [65]. Various biochemical predictors have been proposed.

Treatment protocols arising from animal experimentation are critically dependent upon the "validity" of animal models. In general, as the "accuracy" of reproduction of the complex picture of clinical trauma is improved, quantification and isolation of both manipulated and measured variables becomes increasingly problematic. In this setting, each of the models currently in use may be seen to mirror only selected facets of the human situation, thus the strength of direct correlation and prediction is limited. Multiple lines of investigation in animals have generated interest in pharmacological management of head injuries; in view of the complexities of modelling with limitations as noted above, it is perhaps not surprising that no pharmacologic treatment has, as of yet, been introduced to clinical practice on the basis of statistical effect on outcome [35-39]. Pharmacologic protocols proposed for the treatment of head injury have been directed toward amelioration of ischemia and stabilization and salvage of damaged membranes. Ischemia has been proposed as a secondary effect of trauma in reflection of primary vascular injury. These are discussed in the next chapter. The delay of development of axonal retraction balls in diffuse axonal injury has generated enthusiasm that reversability of pathologic and biochemical cascades may be feasible with the appropriate pharmacologic agent.

Laboratory and clinical trials have addressed generation of free radicals, effects of cytokines, NO, NMDA receptors, toxicity of neurotransmitters and amino acids, and gangliosides as well as potential utility of calcium channel blockade, hypothermia, iron, barbiturates and steroids [62-63]. A fundamental question surrounds the issue of the biochemical and anatomic cascades identified; are these inevitable sequelae of injury or causation events, which may be reversed? These areas constitute potentially valuable fields for future research. Despite earlier enthusiasm for these agents, the use of glucocorticoids was not recommended by the task force which developed guidelines for the management of severe head injury for the Brain Trauma Foundation [64]. The task force found insufficient data to support treatment standards in multiple areas of management of severe head injury, attesting to the controversy surrounding various treatment regimines.

The lack of standardized outcome parameters hinders direct comparison of studies; validation of outcome parameters should constitute an area for additional study to confirm presumed beneficial effects of both specific treatments of head injury in the acute phase and of rehabilitative programs.

References

[1] National Center for Health Statistics. Advance report of final mortality statistics 1985. Washington D.C., US Government Accounting Office.

[2] National Center for Health Statistics. Current estimates for the National Health Interview Survey, United States, 1985. Washington D.C., US Government Printing Office, 1986.

[3] National Highway Safety Administration, Fatal Accident Reporting System, 1987, Washington D.C., US Department of Transportation, 1988.

[4] Interagency Head Injury Task Force Reports. National Institute of Neurological Disorders and Stroke. National Institute of Health, Bethesda, MD, 1989.
[5] Caveness, WF. Incidence of craniocerebral trauma in the United States in 1976 and the trend from 1970 to 1975. *Adv. Neurol* 1979:22: 1-3.
[6] Langfitt, TW. Measuring the outcome from head injuries. *J Neurosurg* 1978:48: 673-678.
[7] Becker DP, Miller JD, Ward JD, Greenberg RP, Young HF, Sakalas R. The outcome from severe head injury with early diagnosis and intensive manangement. *J Neurosurg* 1977:47: 491-502.
[8] Griffith RL, Becker DP. Physiological monitoring of the head injury patient. *Adv Neurol* 1979:22: 51-55.
[9] Levati A, Farina ML, Vecchi G, Rossanda M, Marrubini MB. Prognosis of severe head injuries. *J Neurosurg* 1982:57: 779-783.
[10] Narayan RK, Greenberg RP, Miller JD, Enas GG, Choi SC, Kishore PRS, Selhorst JB, Lutz HA, Becker DP: Improved confidence of outcome prediction in severe head injury. *J Neurosurg* 1981:54: 751-762.
[11] Salcman M, Schepp RS, Ducker TB. Calculated recovery rates in severe head trauma. *Neurosurgery* 1981:8(3): 301-308.
[12] Stablein DM, Miller JD, Choi SC, Becker DP. Statistical methods for determining prognosis in severe head injury. *Neurosurgery* 1980:6(3): 243-248.
[13] Young B, Rapp RP, Pharm D, Norton JA, Haack D, Tibbs PA, Bean JR. Early prediction of outcome in head-injured patients. *J Neurosurg* 1981:54: 300-303.
[14] Kelly DF, Nikas DL, Becker DP. Diagnosis and treatment of moderate and severe head injuries in adults. Fourth Edition. *Youman's Neurological Surgery* 1996(3): 1618-1718.
[15] Samudrala S, Cooper PR. Traumatic intracranial hematomas. 2nd Edition. Wilkins RH, Rengachary SS (eds). *Neurosurgery* 1996(2): 2797-2807.
[16] Cushing H. Notes on penetrating wounds of the brain. *Brit Med J* 1918:1: 221-226.
[17] Gurdjian ES. Head injury from antiquity to the present with special reference to penetrating head wounds, 1973.
[18] Mahoney BD, Rockswold GL, Ruiz E, et al. Emergency twist drill trephination. *Neurosurgery* 1981:8: 551-554.
[19] Andrews BT, Pitts LH, Lovely MP, et al. Is CT scanning necessary in patients with tentorial herniation? *Neurosurgery* 1986:19: 408-414.
[20] Samudrala, S, Cooper PR. Traumatic intracranial hematomas. 2nd Edition. Wilkins RH, Rengachary SS (eds). *Neurosurgery* 1996(2): 2797-2807.
[21] Fell DA, Fitzgerald S, Moiel RH, Caram P. Acute subdural hematomas: review of 144 cases. *J Neurosurg* 1975:42: 37-42.
[22] Jamieson KG, Yelland JDN. Surgically treated traumatic subdural hematomas. *J Neurosurg* 1972:37: 137-149.
[23] Bender MB, Christoff N. Nonsurgical treatment of subdural hematomas. *Arch Neurol* 1974:31: 73-79.
[24] Poon WS, Rehman SU, Poon CYF, Li AKC. Traumatic extradural hematoma of delayed onset is not a rarity. *Neurosurgery* 1992:30: 681-686.
[25] Borovich B, Braun J, Guilburd JN, et al. Delayed onset of traumatic extradural hematoma. *J Neurosurg* 1985:63: 30-34.
[26] McKissock W, Lond MS, Richardson A, et al. Subdural hematoma: a review of 389 cases. *Lancet* 1960:1: 1365-1369.
[27] Seelig JM, Becker DP, Miller JD, et al. Traumatic acute subdural hematoma: Major mortality reduction in comatose patients treated within four hours. *N Eng J Med* 1981:304: 1511-1518.
[28] Wilberger JE Jr, Harris M, Diamond DL. Acute subdural hematoma: morbidity, mortality, and operative timing. *J Neurosurg*1991:74: 212-218.
[29] Rosner MJ, Daughton S. Cerebral perfusion pressure management in head injury. *J Trauma* 1990:30: 933-941.
[30] Bouma GJ, Muizelaar JP, Bandoh K, et al. Blood pressure and intracranial pressure-volume dynamics in severe head injury: relationship with cerebral blood flow. *J Neurosurg* 1992:77:15-19.
[31] Benzer A, Mitterschiffthaler G, Marosi M, et al. Prediction of nonsurvival after trauma: Innsbruck Coma Scale. *Lancet* 1991:338: 977-978.
[32] Teasdale G, Jennet B. Assessment of coma and impaired consciousness: a practical scale. *Lancet* 1974:2: 81-84.

[33] Tesseris J, Pantazidis N, Routsi C, et al. A comparative study of the Reaction Level Scale (RLS85) with Glasgow Coma Scale (GCS) and Edinburgh-2 Coma Scale (modified) (E2CS(M). *Acta Neurochir* 1991:110: 65-76.

[34] Segatore M, Way C. The Glasgow Coma Scale: time for a change. *Heart Lung* 1992:21: 548-557.

[35] Mcintosh TK, Ving R, Smith DH, et al. Excitatory amino acids and traumatic nervous system injury in Meldrum. Meldrum BS, Morrini F, Simon RP (eds). In: *Excitatory Amino Acids*. Raven Press 1991: 695-701.

[36] Bailey I, Bell A, Gray J, et al. A trial of the effect of nimodipine on outcome after head injury. *Acta Neurochir* 1991:110: 97-105.

[37] Waxman K, Wilberger JE, et al. Report of the six month outcome of a clinical trial of PRG-SOD in severely head injured patients. *J Neurotrauma* 1995:12: 418-419.

[38] Chen MH, Bullock R, Graham DI, et al. Ischemic neuronal damage after acute subdural hematoma in the rat. Effects of pretreatment with a glutamate antagonist. *J Neurosurg* 1991:74: 944-950.

[39] Braughler JM, Hall ED. CNS trauma and stroke. Biochemical considerations for oxygen radical formation and lipid peroxidation. *Free Rad Biol Med* 1989:6: 289-301.

[40] Knuckey NW, Gelbards S, Epstein MH. The management of "asymptomatic" epidural hematomas: a prospective study. *J Neurosurg* 1989:70: 392-396.

[41] Hamilton M, Wallace C. Non operative manangement of acute epidural hematoma diagnosed by CT: The neuroradiologist's role. *Am J Neuroradiol*1992:13: 853-862.

[42] Servadei F, Faccini G, Seracchioli A, et al. Extradural hematoma: an analysis of the changing characterisics of patients admitted from 1980 to 1986. Diagnostic and therapeutic implications in 158 cases. *Brain Inj* 1988:2: 87-100.

[43] Ito H, Komai T, Yamato S. Fibrinolytic enzyme in the lining walls of chronic subdural hematoma. *J Neurosurg* 1978:48: 197-200.

[44] Wilberger JE Jr, Harris M, Diamond DL. Acute subdural hematoma: morbidity, mortality and operative timing. *J Neurosurg* 1991:74: 212-218.

[45] Haschberger K, Pucher R, Auer LM. Prognosis after acute subdural hemmorhage. *Acta Neurochirch* 1988:90: 111-116.

[46] Rossner MJ. Intracranial pressure: a critical examination of its physiology and pathophysiology. In: *Neurosurgical Critical Care*. Andrews B (ed). Mcgraw-Hill, New York, 1993: 57-112.

[47] Rossner MJ, Rossner SJ, Johnson, AH. Cerebral perfursion pressure manangement protocol and clinical results. *J Neurosurg* 1995:83: 949-962.

[48] Bouzarth WF, Lundermuth JR. Head injury watch sheet modified for a digital scale. *J Trauma* 1978:18(8): 571-579.

[49] Jennett B, Teasdale G, Brachman R, Munderhoud J, Knill-Jones R. Predicting outcome in patients after severe head injury. *Lancet* 1976: 1031-1034.

[50] Jennett B. Predictors of recovery in evaluation of patients in coma. *Adv Neurol* 1979:22: 129-135.

[51] Lundgren S, Holmgren E, Stalhammer D. Acute head injuries: cooperative efforts in clinical assessement. *J Neurosurg* 1981:55: 324.

[52] Greenberg RP, Newlon PG, Hyatt MS, Narayan RK, Becher DP. Prognostic implications of early multimodal evoked potentials in severely head injured patients: a prospective study. *J Neurosurg* 1981:55: 227-236.

[53] Born J, Albert A, Hans P, et al. Relative prognostic value of best motor response and brain stem reflexes in patients with severe head injury. *Neurosurgery* 1985:16: 595-601.

[54] Narayan RK, Greenberg RP, Ruller JD, Enas GG, Choi SC, Kushare PRS, Selhorst JB, Lutz HA, Becher DP. Improved confidence of outcome prediction in severe head injury. *J Neurosurg* 1981:54: 751-762.

[55] Constant CF, Narayan RK. Prognosis after head injury. In: *Youman's Neurological Surgery* 1996: 1792-1812.

[56] Narayan RK, Enas GG, Choi SC, et al. Practical technique for predicting outcome in severe head injury. In: *Textbook of Head Injury*. Becher DP, Gudeman SK (eds). WB Saunders, Philadelphia, 1989: 420-425.

[57] Choi SC, Narayan RK, Anderson RC, et al. Enhanced specificity in prognosis in severe head injury. *J Neurosurg* 1988:69: 381-385.

[58] Klauber MR, Marshfield LF, Luerssen TG, et al. Determination of head injury nonfatality: importance of the low risk patient. *J Neurosurg*1989:24: 31-36.

[59] Walsh, PR. Automated monitoring of the evoked potential in head injury. *American Assoc of Neurolog Surg* 1986: 118.

[60] Tousant SM, Klauber MR, Marshall LF, et al. Absent or compromised basal cisterns on first CT scan: Omnious predictors of outcome in severe head injury. *J Neurosurg* 1984:61: 691-694.

[61] Eisenberg HM, Gary HE, Aldrich ER, et al. Initial CT findings in 753 patients with severe head injury. *J Neurosurg* 1990:73: 688-698.

[62] Wilberger J. Molecular Basis of Head Injury. In: *The Molecular Basis of Neurosurgical Disease.* Raffel C, Harsch GR IV (eds). Williams and Wilkins, 1996:8: 296-303.

[63] Muizelaar JP. Secondary injury after severe traumatic brain injury: Mechanisms torward which clinical trials are tageted in impact head injury responses, mechanisms, tolerance, treatment and consequences. *AGAARD* CP-597, 1997:(15): 1-4.

[64] Bullock R, Chestnut RM, Clifton G, et al. Guidelines for the management of severe head injury. *The Brain Foundation, AANS, and Critical Care*, 1995.

[65] Ackmann JJ. A computer system for neurosurgical patient monitoring. *Computer Program Biomed* 1979:10: 81-88.

BASIC MECHANISMS IN CRANIOCEREBRAL TRAUMA-INTEGRATION OF BIOMECHANICS AND CLINICAL PATHOPHYSIOLOGY

Patrick R. Walsh, Brian P. Walsh

Abstract

No single chapter can hope to provide anything approaching a comprehensive review of the topics of brain injury and skull fracture; major neurosurgical compendia devote several hundred pages to these areas. Rather, it is the hope of the authors to provide an overview of major fields of import and to supply a bibliography with reviews and selected primary references. Although fracture of the skull may provide an indication of severity of trauma and require specific treatment in some circumstances, functional impairment which may follow brain injury mandates primary clinical and investigative interest in this component of craniocerebral trauma. Two major mechanistic schools of brain and spinal cord injury have arisen; the first emphasizes the vascular bed as a primary site of injury and views the ensuing "secondary injury" to neural elements as reflective of ischemic and chemical phenomena, whereas the second school has assigned the primary site of injury to neural elements. Despite historical division between proponents of these schools, appreciation has grown that the concepts need not be mutually exclusive and may play additional or complementary roles in specific clinical and experimental conditions.

1. Introduction

In no field of biomedical activity is the apparent chasm between the clinician and the engineer or basic scientist more dramatic. On contemplation of craniocerebral trauma the clinician addresses edema, ischemia and physiologic abnormalities, whereas the engineer focuses on parameters of energy transfer and dissipation. The late engineer, G. Snively, was fond of reiterating the position of Haddon that trauma should be defined succinctly in physical terms as uncontrolled transfer of energy to a biologic system [1-2]. Injury is therein defined as the state which follows if the energy buffering capacity of the organism has been exceeded. In this light, the primary events which attend trauma are seen to be mechanisms of energy dissipation. The engineer, charged by the epidemiologist with devising strategies and systems for prevention of trauma and amelioration of injury, must look to the clinician for guidance to establish human limitations of tolerance for trauma which establish thresholds for injury (defined and quantified by specific clinical, functional, morphologic, biochemical or electrophysiologic parameters). The clinician must correlate the secondary events addressed by treatment (primarily static deformation, ischemia and edema) with biomechanical data to meaningfully assist the engineer. The study of craniocerebral trauma clearly calls for intimate cooperation between disciplines if progress is to be made in the prevention of trauma and treatment of injury, which must emanate from appreciation of causation and primary pathophysiologic mechanisms operant. Treatment regimens emanate from results of clinical and animal studies; protocols are critically dependent on the validity of models. The attempt must be made to integrate biophysical and clinical data.

Uncontrolled mechanical energy transfer, which constitutes trauma, is defined mathematically for the organism by temporal characteristics and amplitude of energy applied and geometric factors; for a single neuron the net transfer is the result of a complex linkage of these parameters through geometric factors and tissue biophysical properties. Specific attributes of energy transfer correlate generally within broad limits with the nature of induced injury; i.e., skull fracture and focal or diffuse brain injury. A cogent review of this topic has been published [3]. The duration of transfer of mechanical energy is typically limited to a period of milliseconds in clinical trauma; in addition to these "transient" forces, which by definition have been terminated prior to presentation for treatment, static or plastic deforming forces may persist due to anatomic distortion induced by transient forces. In rare circumstances, static deforming forces (sustained crushing injuries) may occur independently of transient forces. Dynamic forces may include impulsive or inertial loading expressed through translational (linear), rotational or angular (translational and linear) acceleration in the presence or absence of a direct coup (contact) or impact. These forces generate tissue strains or deformation in a nervous system defined as an essentially noncompressible Newtonian fluid; a total of ten thousand metric tons would be necessary to compress the nervous system to one-half of its volume [4-5]. Tissue strain in the nervous system is therefore characterized by components of shear and tension to a far greater degree than compression. This low modulus of compressibility stands in contrast to a high modulus of deformation, and sustained shifts of components of the nervous system may be readily generated by static forces (mass effect) irrespective of the level of intracranial pressure (primarily a function of rate of expansion of mass and of intracranial compliance) and may aggravate injury by herniations or distortions induced by contact with nonneural rigid structures within the fixed volume of the cranium (falx, tentorium and foramen magnum depressed skull fractures or hematomas generated by transient forces) [6]. The contribution of shear stress to clinical impairment was analyzed by Stritch; these forces have been held responsible for both focused and diffuse axonal injury [3,7-14,16-17].

Patterns of injury associated with isolated inertial or impulsive loading tend to differ substantially from those generated by isolated impact (coup or contrecoup) [3,15]. Isolated inertial loading of the unrestrained craniocervical segment of the adult male Rhesus monkey has been generated in sled impact acceleration studies without cranial impact with restraint of the torso in a model of human "frontal crash" [19-20]. Brain and spinal injuries were identified with findings of contusion (typically associated with impact) [21]. Basal skull fracture and atlanto-occipital separation were observed at lethal levels of loading absent cranial impact [21]. The temporal course of induced electrophysiologic neural compromise, manifest in dose dependent attenuation and recovery of evoked potentials, was felt to be compatible with primary neural injury, independent of chemical and ischemic factors, based on previous studies in the subhuman primate [22-24]. Brief neurologic compromise defines the syndrome of concussion. Although angular acceleration has been assigned a major role in injury, these studies did not identify angular acceleration as a specifically injurious loading mechanism independent of translation and rotation, as levels well in excess of published injury thresholds were routinely induced in subjects without apparent injury.

Injuries due to isolated inertial loading seem to be relatively infrequent in civilian clinical practice as cranial contact often interrupts or initiates acceleration, and superficial evidence of contact phenomena are generally in

evidence at presentation. Isolated inertial loading at lower levels has been implicated in the development of concussion and diffuse axonal injury [3]. Although isolated inertial loading would be predicted to generate a diffuse pattern of injury, differences in biophysical characteristics of the brain and skull may additionally dictate differential motion of these structures with ensuing shear and tension strains and possible cavitation and impact of the brain with the skull [25]. These events may initiate biochemical and histopathologic cascades which culminate in parenchymal contusion, hemorrhage or laceration. Shearing of cortical bridging veins through this mechanism has been implicated in the pathogenesis of subdural hematoma; this injury pattern may be associated with substantial parenchymal injury, which may dictate profound neurologic impairment in the presence of a seemingly small hematoma or despite surgical evacuation of a hematoma.

In contrast to isolated inertial loading, local contact phenomena are associated with impact. Impact loading may generate scalp injury and deformation or penetration of the skull which differs dramatically from underlying brain in biophysical characteristics. Focal and resultant generalized deformations of the skull related to contact were eloquently demonstrated by Gurdjian [25]. Studies have indicated that force is a function of circumference, not area of the impactor. Osseus deformation is of clinical interest; recent review of skull fracture studies published prior to 1981 has been forwarded by Sances et al. Energy threshold for skull fracture was reported to be approximately 70 J in cadaver drop studies by Gurdjian; with an acceleration pulse of 5 ms, threshold was approximately 70 G and dropped to 50 G for duration equal to or greater than 30 ms [4]. More recently 980 to 1334 N produced parietal skull penetration by an impactor of 200-297 mm squared. Studies of impact biodynamics of the cadaver human skull have demonstrated deflection of 1.9 to 7.2 mm with quasi-static forces ranging from 1639 to 1702 N with return to initial position [30]. Fracture occurred with mean quasi-static force level of 6.4 kN and at a mean of 10.5 kN with dynamic loading [30]. Stiffness and energy absorbing characteristics of the skull may dictate substantial return toward initial configuration after fracture; i.e., deformation may be dramatically less at the time of presentation for treatment than at the time of energy loading [3]. Laceration of meningeal vessels by fracture of the inner table has been associated with formation of epidural hematoma, with size limited by dural adherence to the inner table of the skull, without substantial parenchymal injury. This provides an explanation for the better outcome of rapid evacuation of this hematoma than of subdural hematoma.

Relatively little interest in skull fracture is evident in neurosurgical texts which have focused primarily and appropriately on injuries to the brain. Specific fractures of clinical concern include those which involve the skull base or paranasal sinuses which may generate meningeal laceration and potential infection (meningitis or abscess), and fractures of the skull in the growing child which may continue to enlarge (leptomeningeal cyst). Displaced osseus fragments may generate static deformation of the nervous system; displacement of the inner table typically exceeds that of the outer table [25-27].

The signature parenchymal injury resulting from the coup of isolated impact loading is the focal contusion. Cavitation and shock wave propagation have been observed in experimental studies; finite element analysis has provided a valuable modeling technique. Contrecoup contusion may develop on the basis of transient configurational changes of the skull and mismatch of relative skull-brain motion in addition to phenomena of cavitation and shock wave propagation. In the absence of cranial fixation, inertial loading and cranial displacement may occur with the specific phenomena discussed in preceding paragraphs.

Diffuse axonal injury has been proposed by Generalli to account for approximately 40 percent of cases of traumatic coma; these present without apparent mass effect [3]. The potential contribution of axonal injury at the cervicomedullary junction in coma was explored by Friede. Biophysical behavior of elongation of neural structures due to circumferential constriction may be differentiated from that induced by axial tension. Clinical definition of injury may be made on morphologic grounds, neuroradiologic study, microscopic autoradiographic or functional evaluation of pathologic specimens, clinical evaluation, or physiologic parameters. Clinical evaluation has been traditionally focused on level of arousal and content of consciousness; a variety of coma scales and flow sheets have been devised and the Glasgow Coma Scale has become a standard form for depiction of neurologic status at presentation after brain injury. The classic study of Stupor and Coma by Posner provides an excellent review of mechanisms of unconsciousness. Neuroradiologic studies in recent years have primarily been limited to computed tomographic scanning as the utility of routine skull films has been questioned. Intracranial pressure and compliance are physical parameters routinely monitored in head injured patients rather than a specific injury, and have been analyzed. Pressures may reach markedly elevated levels absent parenchymal injury as in pseudotumor cerebri; however, similar levels in traumatic coma are ominous. The guidelines for management of severe head injury observed that no prospective randomized multi-center trial had addressed the efficacy and safety of monitoring intracranial pressure in craniocerebral trauma, therefore no standard could be established. However, as noted in the

earlier chapter, multi-modal monitoring, including monitoring of intracranial pressure, appeared to reduce mortality; this observation has been confirmed by multiple centers and the procedure has become commonplace. Specific guidelines for monitoring and treating intracranial pressure elevation were forwarded [28]. Physiologic definitions of injury have included electrophysiologic abnormalities (EEGs, EPs) or functional abnormalities estimated by MR spectroscopy or PET scanning in clinical injury or autoradiography in experimental studies.

Energy transfer involves the vascular system and skull as well as the brain in craniocerebral trauma. Ischemia and vasogenic, cytotoxic and hypoxic edema have been indicated as features of a cascade which follows vascular damage in cranial injury. An additional deleterious cascade has been identified morphologically in diffuse axonal injury; reversibility of each of these progressive sequences constitutes a fundamental research question. The apparent import of axonal injury at the level of the cervicomedullary junction was stressed by Friede and others; attention to this potential mechanism has been limited perhaps in reflection of difficulties in imaging this region neuroradiologically [18].

Classification of craniocerebral trauma and ensuing injury may be validly carried out on other than mechanistic grounds, most commonly severity, anatomy and etiology. On clinical grounds, the scalp, skull and brain may be injured in combination or isolation, and injuries may be identified as penetrating or closed. Etiologic classification is of interest to both clinician and epidemiologist and generates categories such as missile wound, motor vehicle crash, beatings and falls. Classification of head injury on the basis of severity must generate a spectrum for even the most subtle, transient neurologic deficit may lead to mortality in threatening circumstances, and neuropsychiatric abnormalities have been identified in patients without loss of consciousness. Classification on the basis of severity has also been addressed by degree of disruption of level of consciousness and of duration of amnesia and by outcome. Pathologic classification of brain injury includes focal and diffuse patterns with concussion, contusion, laceration and hematoma formation [29-33].

References

[1] Snively GG. Head injury protection. In: *Impact Injury of the Head and Spine*. Ewing CL, Thomas DJ, Sances A Jr, Larson SJ (eds). CC Thomas, Springfield, IL, 1983: 539-548.

[2] Haddon W Jr. Energy damage as the ten countermeasure strategies. *J Trauma* 1973:13: 321-328.

[3] Gennarelli TA, Abel JM, Adams H, Graham DI. Differential tolerance of frontal and temporal lobes to contusion induced by angular acceleration. In: *Proceedings 23rd Stapp Car Crash Conference*, SAE, New York, 1979: 563-586.

[4] Holbourn AH, Edin MA, Oxed DP. Mechanics of head injuries. *Lancet* 1943: 438-441.

[5] Ommaya AK. Trauma to the nervous system. *Ann Royal Col Surg England* 1966:39: 317-347.

[6] Ommaya AK, Gennarelli TA. A physiologic basis for noninvasive diagnosis and prognosis of head injury severity. In: *Head Injuries*. McLauren RL (ed). Grune and Stratton, New York, 1976: 49-75.

[7] Strich SJ. Shearing of nerve stresses as a cause of brain damage. A pathological study of twenty cases. *Lancet* 1961: 443-448.

[8] Adams JH, Graham DI, Murray LS, et al. Diffuse axonal injury due to non missile head injury in humans: An analysis of 45 cases. *Ann Neurol* 1982:12: 357.

[9] Peerless SJ, Rewcastle WB. Shear injuries of the brain. *Can Med Assoc J* 1967:96: 577.

[10] Graham DI, Mclellan DR, Adams JH, et al. The neuropathology of the vegetative state and severe disability of non-missile head injuries. *Acta Neurochirg* 1983:32: 65-67.

[11] Jane JA, Seward O, Gennarelli TA. Axonal degeneration induced by experimental non-invasive head injury. *J Neurosurg* 1985:62: 96-100.

[12] Adams JH, Doyle D, et al. Diffuse axonal injury in head injury: Definition, diagnosis and grading. *Histopathology* 1989:15: 49-59.

[13] Gennarelli TA, Thibault LE. Biomechanics of acute subdural hematoma. *J Trauma* 1982:22: 680-686.

[14] Gennarelli TA, Thibault LE. Biological models of head injury. In: *Central Nervous System Trauma Status Report*. Becker DP, Povlishock JT (eds), 1985: 391-404.

[15] Graham DI, Adams JH, Gennarelli TA. Pathology of brain damage in head injury. Copper P (ed). In: *Head Injury*. Williams and Wilkins, Baltimore 1987: 72-88.

[16] Lundenberg R, Freytag E. Brainstem lesions characteristics of traumatic hyperextension of the head. *Arch Pathol* 1970:90: 509-515.

[17] Budzlovich GN. Pathogenesis of primary lesions in blunt head trauma with special reference to the brain stem injuries. In: *Head Injuries.* McClausin RL (ed). Grune and Stratton, New York, 1976.

[18] Friede RL. Specific cord damage at the level of the axis as a pathogenic mechanism in cerebral concussion. *J Neuropath Exp Neurol* 1960:19: 266-279.

[19] Thomas DJ, Jessop ME. Experimental head and neck injury. In: *Impact Injury of the Head and Spine*, 3rd Edition. Ewing CC, Thomas DJ, Sances A Jr, Larson SJ. CC Thomas, Springfield, IL, 1983: 177-220.

[20] Walsh PR, Jessop ME. The evoked potential in sled impact acceleration: Methodological and neurosurgical considerations. In: *Impact Injury of the Head and Spine*, 3rd Edition. Ewing CC, Thomas DJ, Sances A Jr, Larson SJ (eds). CC Thomas, Springfield, IL 1983: 302-309.

[21] Unterharnscheidt F. Neuropathology of Rhesus monkeys undergoing -Gx impact acceleration. In: *Impact Injury of the Head and Spine*, 3rd Edition. Ewing CC, Thomas DJ, Sances A Jr, Larson SJ (eds). CC Thomas, Springfield, IL 1983: 177-220.

[22] Saltzberg B, Barton WD Jr, Weiss MS, Berger MD, Ewing CL, Thomas DJ, Jessop ME, Sances A Jr, Larson SJ, Walsh PR, Myklebust JB. Dynamic tracking of evoked potential changes in studies of central nervous system injury during impact acceleration. In: *Impact Injury of the Head and Spine*, 3rd Edition. Ewing CC, Thomas DJ, Sances A Jr, Larson SJ (eds). CC Thomas, Springfield, IL 1983: 310-323.

[23] Beyer MD, Weiss MS. Effects of impact acceleration on somatosensory evoked potentials. In: *Impact Injury of the Head and Spine,* 3rd Edition. Ewing CC, Thomas DJ, Sances A Jr, Larson SJ (eds). CC Thomas, Springfield, IL, 1983: 324-380.

[24] Larson SJ, Walsh PR, Sances AJ, Cusick JF, Hemmy DC, Mahler H. Evoked potential in experimental myelopathy. *Spine* 1980:5(4): 299-302.

[25] Gurdjian ES. Mechanistic, clinical and prevention conclusions. In: *Impact head injury.* Springfield, IL, CC Thomas, 1975.

[26] Wilberger J. Molecular basis of head injury. In: *The Molecular Basis of Neurosurgical Disease*. Raffel C, Harsch GR IV (eds). Williams and Wilkins, 1996:8: 296-303.

[27] Muizelaar JP. Secondary injury after severe traumatic brain injury: Mechanisms toward which clinical trials are targeted in impact head injury responses, mechanisms, tolerance, treatment and consequences. *AGAARD* CP-597, 1997:(15): 1-4.

[28] Ward JD, Moulton RJ, Muizelaar JP, et al. Cerebral homeostasis and protection. In: *Concepts in Neurosurgery: Neurosurgical Critical Care.* Wirth FP, Ratcheson RA (eds). Williams and Wilkins, Baltimore MD, 1987: 187-213.

[29] Sances A Jr, Myklebust JB, Larson SJ, Cusick JF, Weber RC, Walsh PR. Biomechanical analysis of head and neck injuries. *CRC Crit Rev Bioeng* 1981:2(15) 1-79.

[30] Sances A Jr, Yoganandan N, Pintar FA, Kumaresan S, Walsh PR. Impact biodynamics of human skull fracture. In: Impact Head Injury. Responses, mechanisms, treatment and countermeasure. *AGAARD* CP-597 1996:(2) 1-5.

[31] Walsh PR, Curtis RL, Larson SJ, Ackmann JJ. Geometric alterations of feline spinal axons due to circumferential compression sufficient to elicit conductive blockade. In: *Proceedings 1st Meeting JC on Spinal Disorders.* AANS CNS 24, 1985.

[32] Thibault LE, Gennarelli TA. *Biomechanics and Craniocerebral Trauma in Central Nervous System Trauma Status Research Report.* Berker DP, Povlishock JT (eds). NINCDDS, NIH, Bethesda, MD, 1985: 379-38 .

[33] Guidelines for management for severe head injury.

ANALYSIS OF CERVICAL DISCECTOMY AND INTERBODY FUSION

Srirangam Kumaresan, Narayan Yoganandan, Frank A. Pintar
Dennis J. Maiman, Joseph F. Cusick

Abstract

The biomechanical responses of cervical discectomy with fusion were determined. Smith-Robinson and Bailey-Badgley surgical procedures with titanium cage, tricortical iliac crest, and tantalum cage materials were analyzed. A validated three-dimensional anatomically accurate three-segment C4-C5-C6 finite element model of the spine was exercised in compression, flexion, extension and lateral bending modes for the intact and for the two surgical procedures with three implant materials. The output included the external stiffness and angular rotation and the internal responses, i.e., disc and vertebral stresses. The highest increase in the external response under all modes of loading for all implant materials occurred in the Smith-Robinson technique. The increase was higher in the internal disc and vertebral body stresses in the Bailey-Badgley technique. These results in terms of external and internal responses provide a better understanding of the biomechanics of interbody fusion. Because of the inclusion of three-levels in the finite element model, it was possible to determine the internal mechanics of the various components at altered and unaltered adjacent intervertebral components secondary to these surgical procedures that may have clinical implications as accelerated changes have been observed at levels adjacent to fusion.

1. Introduction

Cervical discectomy is used to treat degenerative spinal disorders or trauma [1-5]. Discectomy is often accompanied with an additional procedure involving the insertion of graft material to enhance spinal strength and stability, and promote fusion. The graft materials used most often in fusion are tricortical bone, titanium and

tantalum [6-12]. These materials provide additional load bearing and strength characteristics to the fused spine based on its construction and type. *In vitro* experimental investigations provide insight into the behavior of the surgically altered spinal structures by evaluating the external response [13-18]. In contrast, the finite element model quantifies the internal responses (such as stresses) in the altered and unaltered adjacent intervertebral components secondary to these surgical procedures, in addition to the external response [19-24]. This chapter presents the application of the finite element method to determine the external and internal responses of cervical spine interbody fusion using three graft constructs under the Smith-Robinson and Bailey-Badgley procedures.

2. Model Development

The Smith-Robinson and Bailey-Badgley stabilization surgeries were simulated at the C4-C5 intervertebral disc level in our previously developed finite element model [25-28]. The details of the model construction, development and experimental validation are described in an earlier chapter. The Smith-Robinson technique included the following: the anterior longitudinal ligament was incised at the fused (C4-C5) level. The disc from the anterior edge to the posterior edge was transected leaving the disc material intact above the uncinate processes. The inferior endplate of C4 vertebral body and the superior endplate of C5 vertebral body were resected [4]. The graft material was placed in the intervertebral space simulating this surgical procedure. The posterior end of the graft was not in contact with the posterior longitudinal ligament. The three materials used for the graft are described later. The superior and inferior surfaces of the graft material connected the cancellous core of adjacent C4 and C5 vertebral bodies. Figure 1 illustrates the Smith Robinson procedure. The Bailey-Badgley procedure (Figure 2) was simulated in the following manner: the anterior longitudinal ligament at the fused level, the disc from the anterior edge to the posterior edge (leaving the larger portion of the disc laterally), and the anterior region of cortical shell of the C4 and C5 vertebral bodies were removed. The inferior endplate of the C4 vertebral body and the superior endplate of C5 vertebral body were partly resected. The graft material was filled between the removed anterior regions of the C4 and C5 vertebrae and the intervertebral disc [29]. Thus, the Bailey-Badgley procedure had a larger height compared to the Smith-Robinson procedure. The three different graft materials used were a tricortical iliac crest, a titanium cage surrounding a central cancellous core, and a tantalum cage surrounding a central cancellous core. The intact and the two surgically altered models were exercised under uniform compression and pure moment flexion, extension and lateral bending modes. The output included the external responses in the form of axial stiffness and angular rotation, and the internal responses in the form of intervertebral disc (C5-C6) and the cancellous core (C5) von Mises stresses.

3. Results and Discussion

Figure 3 shows the percentage increase in the axial and angular stiffnesses in the Smith-Robinson and Bailey-Badgley models. The stiffness was the highest with the titanium cage, followed by the iliac crest and the tantalum cage under all loading modes in both models. However, higher magnitudes were found in the Smith-Robinson simulation. The highest stiffness occurred in lateral bending and the lowest stiffness occurred under axial compression in both models. In addition, the increases in the stiffnesses were similar under flexion and extension loading modes. The highest stiffness with the titanium cage and the least with the tantalum cage may be attributed to the magnitude of the material properties of the different graft materials. Consequently, if the objective is to achieve the maximum overall strength *in vivo*, a material with the highest strength is desirable. A likely explanation for the increase in the stiffness in the Smith-Robinson model compared to the Bailey-Badgley model is that the structural replacement completely encompassed the excised disc rendering the cervical intervertebral joint to be intact from a spatial viewpoint. The changes in the unaltered C5-C6 disc stress are shown in figure 4. In both cases, the significant increase in the disc stress occurred under axial compression compared to the other loading modes. In the Smith-Robinson model, the disc stress decreased in flexion and extension with a higher magnitude for the stronger titanium cage. The stress changes however, remained positive under these load vectors in the Bailey-Badgley model. Figure 5 shows the change in the stress in the unaltered C5 cancellous core in the Smith-Robinson and the Bailey-Badgley models. In both cases, positive increases in the stresses occurred under axial compression, flexion and extension. However, the increases in the stress levels changed from a negative value for the titanium

cage and the iliac crest to a positive value for the tantalum cage in lateral bending. In contrast to the stiffness, the two procedures responded with considerably higher increases in the disc and the vertebral body stresses under compression. This suggests that the iatrogenic removal together with the graft material insertion has transformed the internal loading mechanics to the adjacent segmental components more than the external stiffness. The larger axial surface area of the fusion material in the Smith-Robinson model compared to the Bailey-Badgley model, together with the magnitudes in the material properties of the graft substance may explain the negative and positive changes in the intervertebral disc stresses under flexion and extension. In contrast, a consistent positive increase in the disc stresses under lateral bending for both the models may be due to the preservation of the uncinate processes in the simulations. The higher change in the vertebral body stresses in the Bailey-Badgley model than the Smith-Robinson model may be due to the inclusion of the fusion material into the adjacent vertebrae. This phenomenon was found to be true for all loading modes. These internal stress analyses indicate that the Bailey-Badgley model induces higher changes in the internal stresses in the intervertebral components compared to the Smith-Robinson technique.

4. Conclusion

A three-dimensional finite element modeling approach was used to quantitatively determine the external and internal biomechanics of the cervical discectomy with fusion. To have confidence in using such an approach, the finite element model must be based on accurate three-dimensional geometrical definition, appropriate material properties, loading and boundary condition incorporation, and finally, validation using experimental data [23-24]. The present finite element model was derived from actual human spine computed tomography and cryomicrotome images at very close intervals and therefore, the geometrical definition is accurate [21-30]. The material properties assigned to the components were obtained from literature [20-21,23,30-33]. The loading and boundary condition used in the present finite element analysis parallels the data from earlier studies [34-36]. Validation of the finite element model was carried out under compression, flexion, extension, lateral bending and axial torsion modes using literature [20-21,23,26,28,30,32-33]. These systematic model developments and validation provided the confidence to study the biomechanical effects of surgical procedure [19-21,23,25-26,30,32-33,37-39]. The Smith-Robinson technique resulted in the highest increase in external response under all modes of loading for all implant materials. The Bailey-Badgley technique produced a higher increase in the disc and the vertebral body stresses than the Smith-Robinson technique. These differences in the external and internal responses will assist in a better understanding of the biomechanics of the human cervical spine secondary to anterior interbody fusion. Further, it should be emphasized that the internal stress analysis using the finite element approach may offer an explanation to the subsequent changes in the spine following single-level fusion reported in clinical literature.

References

[1] Alemo-Hammad S. Use of acrylic in anterior cervical discectomy: Technical note. *Neurosurgery* 1985:17(1): 94-96.

[2] Gore DR. Technique of cervical interbody fusion. *Clin Orthop* 1984:188: 191-195.

[3] Simmons EH, Bhalla SK, Butt WP. Anterior cervical discectomy and fusion: A clinical and biomechanical study with eight-year follow-up. Discography: Technique and interpretation of results. *J Bone Joint Surg Br* 1969:51(2): 225-237.

[4] Smith GW, Robinson RA. The treatment of certain cervical spine disorders by anterior removal of the intervertebral disc and interbody fusion. *J Bone Joint Surg Am* 1958:40(3): 607-624.

[5] Stauffer ES, Kelly EG. Fracture-dislocations of the cervical spine: Instability and recurrent deformity following treatment by anterior interbody fusion. *J Bone Joint Surg Am* 1977:59(1): 45-48.

[6] Kaden B, Schramm J, Fuhrmann G, Hoffmann CH. Titanium intervertebral disc and instrumentation for fusion in anterior cervical discectomy. Technical note. *Neurosurg Rev* 1995:18(1): 25-29.

[7] Leong JC, Chow SP, Yau AC. Titanium-mesh block replacement of the intervertebral disk. *Clin Orthop* 1994:300: 52-63.

[8] Muhlbauer M, Saringer W, Aichholzer M, Sunder-Plassmann M. Microsurgical anterior decompression and internal fixation with iliac bone graft and titanium plates for treatment of cervical intervertebral disc herniation. *Acta Neurochir* 1995:134(3-4): 207-213.

[9] Smith MD, Cody DD. Load-bearing capacity of corticocancellous bone grafts in the spine. *J Bone Joint Surg Am* 1993:75-A(8): 1206-1213.

[10] Toth JM, Sandhu HS, Turner AS, Kabo JM, Pagedas MT, Kanim LEA. Porous tantalum composite as a spinal fixation material. SFB. New Orleans, LA, 1997.

[11] White AA, Hirsch C. An experimental study of the immediate load bearing capacity of some commonly used iliac bone grafts. *Acta Orthop Scandinav* 1971:42: 482-490.

[12] Zdeblick TA, Cooke ME, Wilson D, Kunz DN, McCabe R. Anterior cervical discectomy, fusion, and plating: A comparative animal study. *Spine* 1993:18(14): 1974-1983.

[13] Cusick JF, Yoganandan N, Pintar FA, Myklebust JB, Hussain H. Biomechanics of cervical spine facetectomy and fixation techniques. *Spine*. 1988:13(7): 808-812.

[14] Cusick JF, Yoganandan N, Pintar FA, Reinartz J. Biomechanics of sequential lumbar posterior surgical alteration. *J Neurosurg* 1992:76: 805-811.

[15] Maiman DJ, Sances A Jr, Myklebust JB, Larson SJ, Houterman C, Chilbert M, El-Ghatit AZ. Compression injuries of the cervical spine: A biomechanical analysis. *Neurosurgery* 1983:13(3): 254-260.

[16] Maiman DJ, Yoganandan N. Biomechanics of cervical spine trauma. In: *Clinical Neurosurg*ery. P Black (ed). Williams & Wilkins, Baltimore, MD, 1991: 543-570.

[17] Pintar FA, Yoganandan N, Voo LM, Cusick JF, Maiman DJ, Sances A Jr. Dynamic characteristics of the human cervical spine. *SAE Transactions* 1995:104(6): 3087-3094.

[18] Yoganandan N, Cusick JF, Pintar FA, Droese K, Voo L. An experimental technique to induce and quantify complex cyclic forces to the lumbar spine. *Neurosurgery* 1995:36(5): 956-964.

[19] Kumaresan S, Pintar FA, Yoganandan N. Finite element analysis of cervical laminectomy with graded facetectomy. *ASME Adv Bioeng* BED-Vol 33:1996: 27-28.

[20] Kumaresan S, Yoganandan N, Pintar F. Finite element analysis of anterior cervical spine interbody fusion. *Bio-Medical Materials & Engineering* 1997:(9): 1-10.

[21] Kumaresan S, Yoganandan N, Pintar F, Voo L, Cusick J, Larson S. Finite element modeling of cervical laminectomy with graded facetectomy. *J Spinal Disord* 1997:10(1): 40-47.

[22] Kumaresan S, Yoganandan N, Voo L, Pintar FA, Cusick J. Finite element analysis of cervical laminectomy. *11th Annual North American Spine Society*, Vancouver, Canada, 1996, pp 271-272.

[23] Yoganandan N, Kumaresan S, Voo L, Pintar F. Finite element applications in human cervical spine modeling. *Spine* 1996:21(15): 1824-1834.

[24] Yoganandan N, Myklebust JB, Ray G, Sances A Jr. Mathematical and finite element analysis of spinal injuries. *CRC Review Biomed Eng* 1987:15(1): 29-93.

[25] Kumaresan S, Voo LM, Yoganandan N, Pintar FA. Finite element biomechanics of the cervical spine. *6th Injury Prevention Through Biomechanics Symposium,* Wayne State University, Detroit, MI, Centers for Disease Control, 1996, pp 77-84.

[26] Kumaresan S, Yoganandan N, Pintar FA. Adult and pediatric human cervical spine finite element analyses. *ASME Adv Bioeng* BED-Vol 35:1997: 515-516.

[27] Kumaresan S, Yoganandan N, Pintar FA. Sensitivity of cervical spine finite element model to material property variations. *ASME Winter Bioengineering Conference,* Dallas, TX, November 16-21, 1997.

[28] Kumaresan S, Yoganandan N, Pintar FA. Importance of material properties on spinal components load sharing. *Mathematical Modelling and Scientific Computing* 1997:8: 6-10.

[29] Bailey RW, Badgley CE. Stabilization of the cervical spine by anterior fusion. *J Bone Joint Surg Am* 1960:42(4): 565-594.

[30] Yoganandan N, Kumaresan S, Voo L, Pintar F. Finite element model of the human lower cervical spine. *J Biomech Eng* 1997:19(1): 87-92.

[31] Pintar FA. Biomechanics of Spinal Elements [Doctoral Dissertation]. Marquette University, Milwaukee, WI, 1986, 222 pp.

[32] Yoganandan N, Kumaresan S, Voo L, Pintar F, Larson S. Finite element modeling of the C4-C6 cervical spine unit. *Med Eng Phy* 1996:18(7): 569-574.

[33] Yoganandan N, Voo L, Pintar FA, Kumaresan S, Cusick JF, Sances A Jr. Finite element analysis of the cervical spine. *CDC Injury Prevention Through Biomechanics,* Detroit, MI, 1995, pp 149-155.

[34] Liu YK, Krieger KW, Njus G, Ueno K, Connors M, Wakano K, Thies D. Cervical spine stiffness and geometry of the young human male. Wright-Patterson AFB, Dayton, OH, AFAMRL-TR-80-138, 1981.

[35] Moroney SP, Schultz AB, Miller JA, Andersson GB. Load-displacement properties of lower cervical spine motion segments. *J Biomech* 1988:21(9): 769-779.

[36] Kumaresan S, Pintar FA, Yoganandan N. Finite element idealization of uncovertebral joints in the cervical spine. *Mathematical Modelling and Scientific Computing* 1997:8: 1-5.

[37] Kumaresan S, Yoganandan N, Pintar FA. Nonlinear finite element analysis of human cervical spine facet joint. *ASME Adv Bioeng* BED-Vol 35:1997: 447-448.

[38] Kumaresan S, Yoganandan N, Pintar FA. Validation of nonlinear finite element model of human lower cervical spine. *ASME Winter Bioengineering Conference,* Dallas, TX, November 16-21, 1997.

[39] Voo LM, Kumaresan S, Yoganandan N, Pintar FA, Cusick JF. Finite element analysis of cervical facetectomy. *Spine* 1997:22(9): 964-969.

Figure Captions

Figure 1a: Illustration of the Smith-Robinson procedure. Left: graft material, middle: sagittal view of the spinal structure, and right: coronal view of the spinal segments.

Figure 1b: Smith-Robinson procedure simulated using the finite element model. The dark region is highlighted to show the graft material placement.

Figure 2a: Illustration of the Bailey-Badgley procedure. Left: graft material, middle: sagittal view of the spinal structure, and right: coronal view of the spinal segments.

Figure 2b: Bailey-Badgley procedure simulated using the finite element model. The dark region is highlighted to show the graft material placement.

Figure 3: Percentage change in stiffness (external response) of stabilized spine for the Smith-Robinson and Bailey-Badgley techniques. Data are normalized with respect to the intact spine. The three graft materials are shown in the legend. COM: compression; FLE: flexion; EXT: extension; LB: lateral bending.

Figure 4: Percentage change in C5-C6 disc stress (internal response) of stabilized spine for the Smith-Robinson and Bailey-Badgley techniques. Data are normalized with respect to the intact spine. The three graft materials are shown in the legend. COM: compression; FLE: flexion; EXT: extension; LB: lateral bending.

Figure 5: Percentage change in C5 vertebral stress (internal response) of stabilized spine for the Smith-Robinson and Bailey-Badgley techniques. Data are normalized with respect to the intact spine. The three graft materials are shown in the legend. COM: compression; FLE: flexion; EXT: extension; LB: lateral bending.

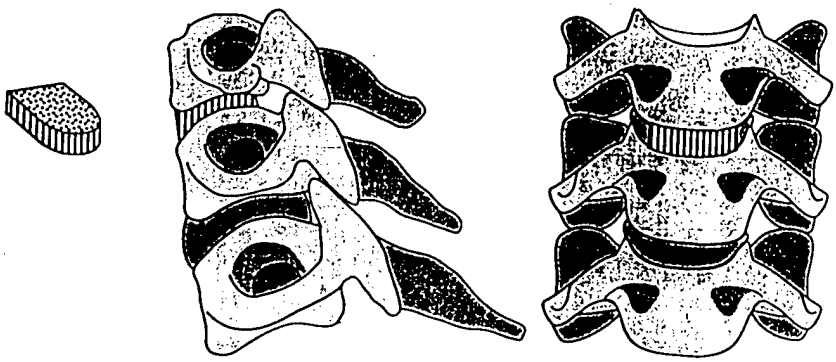

Figure 1a: Illustration of the Smith-Robinson procedure. Left: graft material, middle: sagittal view of the spinal structure, and right: coronal view of the spinal segments.

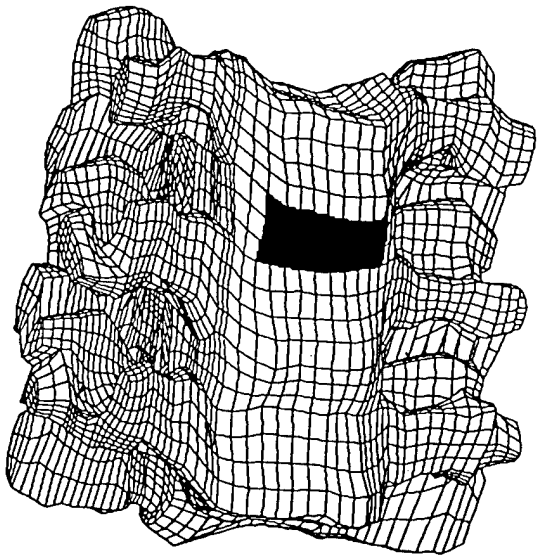

Figure1b: Smith-Robinson procedure simulated using the finite element model. The dark region is highlighted to show the graft material placement. .

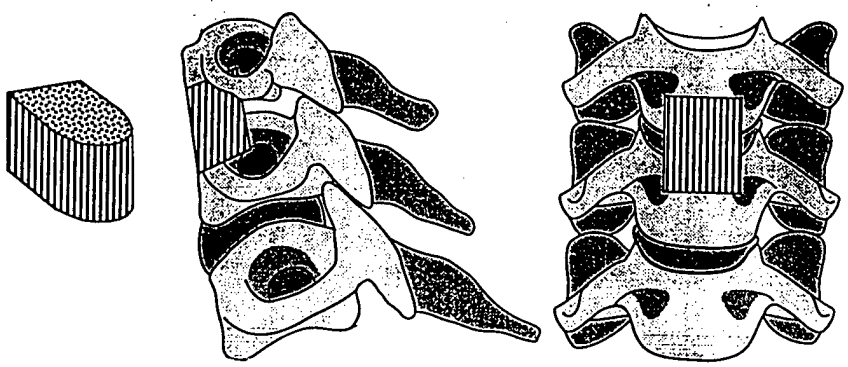

Figure 2a: Illustration of the Bailey-Badgley procedure. Left: graft material, middle: sagittal view of the spinal structure, and right: coronal view of the spinal segments.

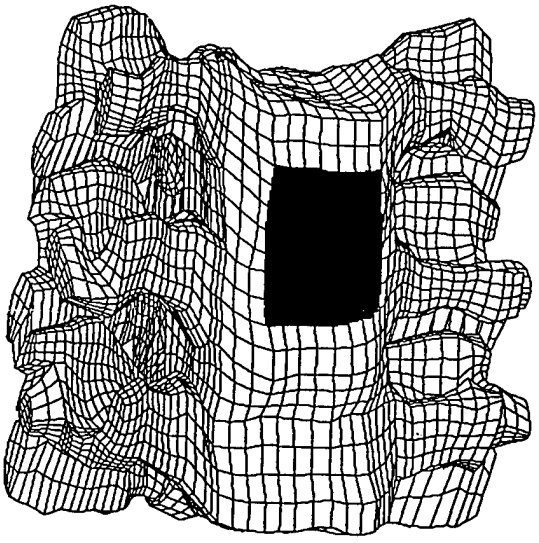

Figure 2b: Bailey-Badgley procedure simulated using the finite element model. The dark region is highlighted to show the graft material placement. .

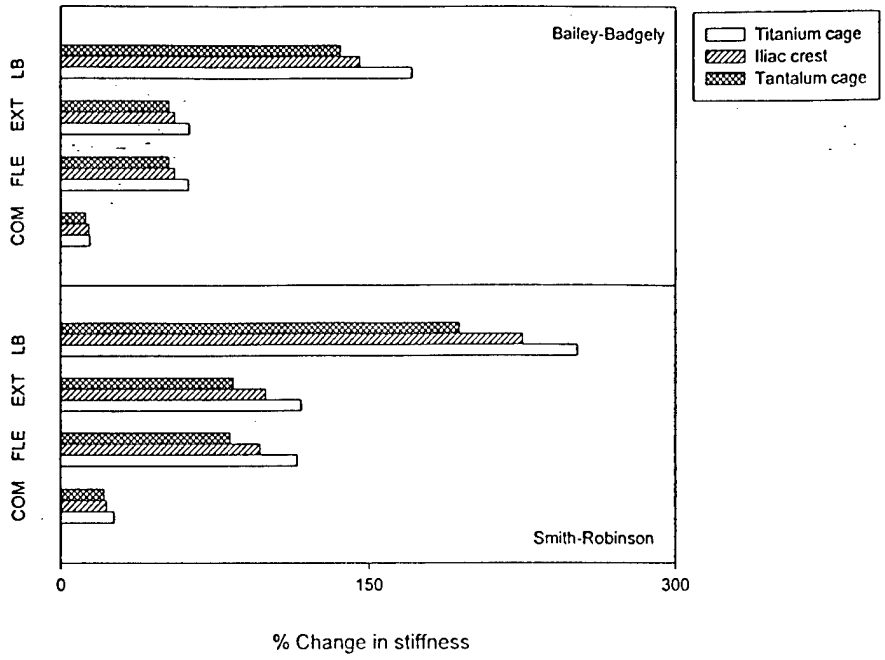

Figure 3: Percentage change in stiffness (external response) of stabilized spine for the Smith-Robinson and Bailey-Badgley techniques. Data are normalized with respect to the intact spine. The three graft materials are shown in the legend. COM: Compression; FLE: Flexion; EXT: Extension; LB: Lateral bending.

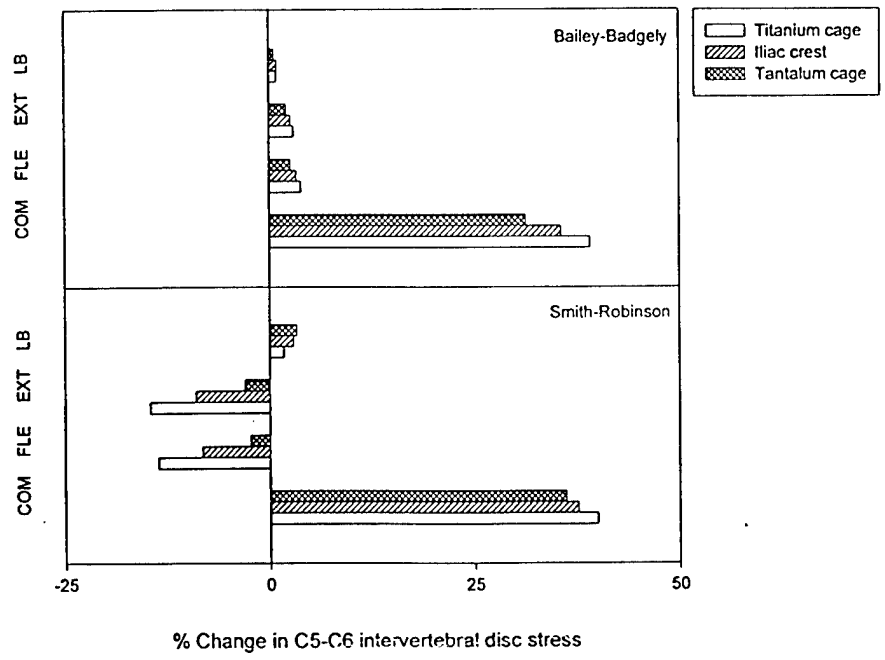

Figure 4: Percentage change in C5-C6 disc stress (internal response) of stabilized spine for the Smith-Robinson and Bailey-Badgley techniques. Data are normalized with respect to the intact spine. The three graft materials are shown in the legend. COM: Compression; FLE: Flexion; EXT: Extension; LB: Lateral bending.

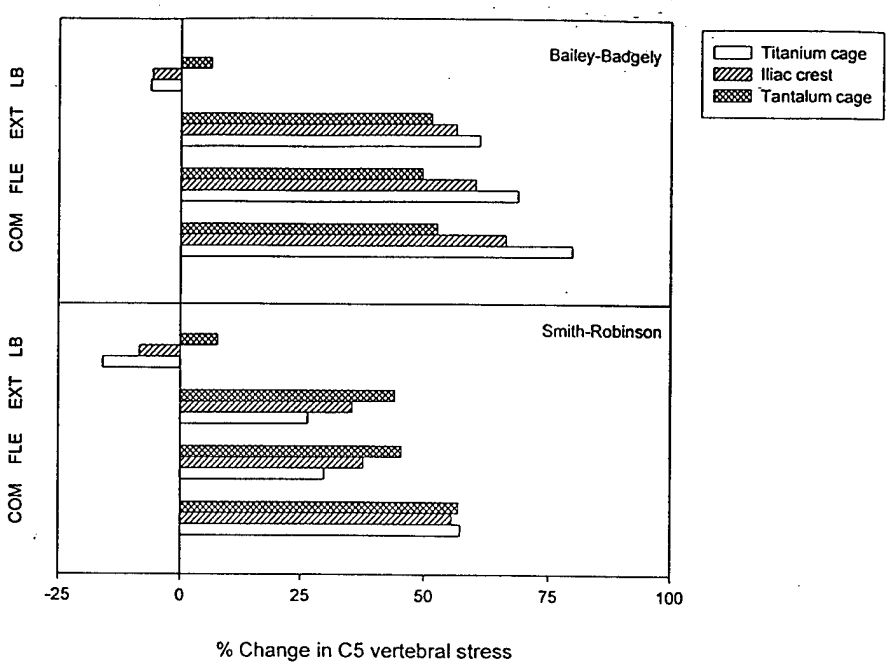

Figure 5: Percentage change in C5 vertebral stress (internal response) of stabilized spine for the Smith-Robinson and Bailey-Badgley techniques. Data are normalized with respect to the intact spine. The three graft materials are shown in the legend. COM: Compression; FLE: Flexion; EXT: Extension; LB: Lateral bending.

POSTERIOR CERVICAL SPINE INSTRUMENTATION: CRANIOCERVICAL FIXATION

Jamie Baisden, Joseph F. Cusick

Abstract

The craniocervical junction (C0-C1-C2) is a unique area of the spine due to the large range of motion compared to other areas of the spine. The two-motion segments, in essence, function as a single unit due to the high degree of coupling. This increased range of motion is due to the unique osseous geometry in conjunction with the additional ligamentous support and absence of intervertebral discs. The diversity of pathology observed at the craniocervical junction and the interactions between the osseous and ligamentous anatomy allow for both anterior and posterior surgical approaches to be successfully used. The mechanism of injury and/or the disrupted anatomy must be taken into account when choosing the stabilization technique. Other factors such as intraoperative degree of difficulty, immediate fixation and type of post-operative orthosis needed must be weighed with respect to risks and benefits when choosing the optimal operation for each patient.

1. Anatomy

The osseous anatomy of the craniocervical junction consists of two occipitoatlantal articulations, the bilateral occipital condyles articulating with the atlantal facets and four atlantoaxial joints. The median atlantoaxial joint acts as a double joint with two articular surfaces: anterior aspect of the dens articulating with the posterior aspect of the anterior arch of C1, and the posterior aspect of the dens articulates with the cartilaginous portion of the transverse atlantal ligament. The lateral atlantoaxial joints are the bilateral C1-C2 facets [1].

The ligamentous anatomy is more complex. The odontoid ligaments consist of the anterior atlanto-dental ligament, alar ligaments (atlantal and occipital) and apical ligament. The transverse ligament is key in determining stability of the atlantoaxial joint with respect to trauma and other craniocervical pathology [2-3]. Other ligamentous structures include the anterior longitudinal ligament, anterior atlanto-occipital membrane, posterior atlanto-occipital membrane, ligamentum flavum, the ligamentous nuchae and capsular ligaments (Figure 1) [1].

2. Biomechanics

The biomechanics of the atlanto-occipital and atlanto-axial joints are largely determined by their unique osseous geometry and ligamentous attachments. The primary movements of the occipito-atlanto-axial complex include rotation and flexion/extension with the atlanto-axial segment affecting the most predominant action of rotation (Table 1) [4-6]. The alar ligaments (atlantal and occipital) extend from the posterior and lateral aspects of the odontoid and insert on the medial aspect of the occipital condyles. Their primary function is to restrain rotation, but they also function in limiting flexion and lateral bending [6]. The transverse ligament is instrumental in limiting translation of C1-C2 and restraining flexion, and therefore, injury of this ligament may significantly increase instability in this mode. Capsular ligaments provide some protection from facet distraction, but provide little resistance to shear forces [6]. The tectorial membrane limits flexion/extension and distraction [5-6]. Simultaneous translation and rotation (coupling) at the C1-C2 articulation act to produce an associated upward movement of the dens in relation to the atlas. The normal distance from the basion to the odontoid process is approximately 5 mm and the normal translation between the clivus and the anterior arch of the atlas should be no more than 1-2 mm [7].

Table 1: Range of Motion of Occipito-Atlanto-Axial Complex [5]

C0-C1	Flexion-extension 25∞
	Lateral bending 5∞
	Rotation 5∞
C1-C2	Flexion-extension 20∞
	Lateral bending 5∞
	Rotation 40∞

3. Radiology

Plain skull films (AP, lateral, Towne's view) in conjunction with a cervical spine series (lateral, AP, right and left obliques, and open-mouth odontoid views) are good starting points to determine occipito-cervical pathology (bony or ligamentous injury) [7-8]. Panjabi and White have established criteria for C0-C1-C2 instability [6]:

>8∞ axial rotation C0-C1 to one side
>1 mm C0-C1 translation
>7 mm overlay C1-C2 (total right and left)
>45∞ axial rotation C1-C2 to one side
>4 mm C1-C2 translation
<13 mm posterior body C2 - posterior ring C1
Avulsed transverse ligament

Magnetic reasonance imaging (MRI) of the craniocervical spine with T1-T2 axial images including sagittal and coronal reconstructions provide more detailed soft tissue anatomy including ligamentous disruption (seen in atlanto-occipital dislocations and fractures) and evaluation of the cervicomedullary junction including pannus formation, epidural abscess, hematoma or tumor. Computed tomography (CT) scans of the C0-C1-C2 complex with fine (2 mm) cuts and sagittal and coronal reconstructions provide enhanced bony anatomy and bony involvement of infectious and tumor processes. Malalignment secondary to excessive rotation on CT may infer ligamentous injury but ligamentous injury is best identified on MRI. Flexion/extension views of the cervical spine either under fluoroscopy or plain films aid to establish the presence and degree of instability, but must be used with extreme caution in obtruded or sedated patients (Table 2).

Table 2: Pathology of the Craniocervical Junction

Developmental	Achondroplasia [9-12]	
	Chiari Malformation	
	Down's Syndrome [13]	
	Klippel-Feil Syndrome	
	Os odontium	
Infection		
Inflammatory	Rheumatoid Arthritis [14-18]	
Metabolic	Mucopolysaccharidoisis	- Hurler Syndrome
		- Morquio Syndrome
	Paget's Disease	
	Pseudotumor associated with chronic hemodialysis [19]	
Trauma - Bony	C0	- Occipital condyle fracture
	C1	- Jefferson/burst fracture
	C2	- Hangman fracture
		- Os odontium
		- Odontoid fractures (I, II, IIA, III)
Ligamentous	Atlanto-occipital dislocation [20-21]	
	Atlanto-axial instability	
Combined	Bony/ligamentous	
Tumor	Primary	
	Metastatic	
Iatrogenic [3]		

4. Surgery

The surgical approach to pathology of the craniocervical spine can best be guided following a thorough radiographic examination. This typically includes MRI, fine-cut CT with multidirectional reconstructions, and, if

indicated, dynamic flexion/extension views to access instability. Once fractures and ligamentous injuries are identified, the surgical approach for decompression and/or stabilization with fusion can be planned (Table 3). We limit our discussion to primarily pathology at C1 and C2. Surgical approaches to the clivus and foramen magnum are referred elsewhere [44-45].

Table 3. Surgery of the Craniocervical Spine

Anterior	Decompression:	- Transoral
		- Extrapharyngeal
Stabilization/Fusion	Odontoid Screw [22-31]	
	Anterolateral	
Posterior	Decompression:	- Suboccipital craniectomy
		- Laminectomy
Stabilization/Fusion	Occipitocervical	- Contoured loop/rod [32]
		- Occipitocervical plate [33-35]
		- Bone/wire/methylmethacrylate [36]
	Atlantoaxial	- C1-C2 transarticular screws [37-39]]
		- Interlaminar clamps [40]
		- Bone/wire/methylmethacrylate [40-43]

Once the pathology has been radiographically determined, proper alignment is maintained in cervical traction (2-5 kg), with or without a Philadelphia collar, or in a cervical halo. In cases of atlanto-occipital dislocation where the application of traction is "relatively" contraindicated, we use a cervical halo to provide pre-operative and post-operative stability, and to assist in safe intraoperative positioning. In cases of rheumatoid arthritis, in which the degree of reducibility is key, patients may be placed in cervical traction (up to 7-10 kg) for up to 5-7 days prior to operative intervention. Once reduced, the surgical approach may be only posterior, whereas, in cases that are nonreducible, an anterior decompression followed by a posterior stabilization may be required.

Intraoperative positioning can be accomplished more safely and easily after awake fiberoptic intubation, turning in a Philadelphia collar or halo orthosis, and with the aid of intraoperative fluoroscopy. This provides immediate feedback of neurologic function and decreases the delay to determine proper radiographic alignment during positioning. Electrophysiologic monitoring such as somatosensory evoked potentials may also provide an additional "safety net" during operative positioning and stabilization.

Posterior surgical approaches to the occipito-atlanto-axial complex have traditionally been more commonly used. We will review the basic approaches to surgery, in particular, stabilization of the craniocervical spine. Posterior surgical approaches to the craniovertebral junction are usually more focused on stabilization and fusion than decompression. A multitude of internal fixation devices such as plates, screws, contoured loops/rods and clamps have been combined with the more traditional bone and wire constructs to enhance stabilization and arthrodesis. Laminectomy and occasionally suboccipital craniectomy are performed for posterior decompression of the occipito-atlanto-axial complex. These decompressive procedures in themselves do not necessarily induce instability, however, they may potentiate instability if pathologic bone deterioration or ligamentous laxity is present.

We will review the basic occipitocervical and atlantoaxial stabilization/fusion techniques with respect to their proposed advantages and disadvantages. Occipitocervical wiring and fusion techniques have been indicated in cases of atlanto-occipital dislocation, unstable Chiari malformations, status post wide decompression, rheumatoid arthritis, and congenital osseous malformation such as C1-C2 dysgenesis, Down's syndrome and Klippel-Feil syndrome [36,46]. Occasionally, tumor or complex fractures of C1-C2 may require decompression and C0-C2 stabilizations. The primary drawback of the occipitocervical fusion is the significant loss of cervical range of motion. The normal rotation at C1-C2 (approximately 45 degrees) accounts for one half of all cervical rotation. The C0-C2 articulation allows for less than 10 percent of cervical rotation. Flexion, extension and lateral bending at C0-C1-C2 account for 5-25 degrees [3-4,42]. The second major drawback is that occipitocervical fusion typically has a higher pseudarthrosis rate and requires a longer post-operative external immobilization period (5-6 months) than

C1-C2 fusions [47]. Failure rates are more commonly observed in rheumatoid arthritis and Down's syndrome [18,47]. Methylmethacrylate can be used to augment bony fusion but higher infection rates have been observed.

Occipitocervical plates have the same limitations with respect to decreased range of motion as other occipitocervical fixations/fusions, but have the advantage of immediate rigid internal fixation which allows for earlier mobilization and less extensive external orthoses [33-35]. Goel has described a modified plate and screw fixation of the occipito-atlanto-axial complex with 100 percent fusion rate and no mortality/morbidity or instrumentation failure [33]. A similar plate/screw construct has been used by Smith and Anderson at the craniocervical junction and all patients fused with minimal complications [35]. An inverted Y-plate in combination with screws and transarticular atlantoaxial screw fixation has likewise shown 100 percent fusion rates with the absence of severe complications [34].

The contoured loop/rod has the advantage of immediate rigid internal fixation allowing early mobilization and minimal external support [32,42,47]. Occipital burr holes with segmental sublaminar wiring/cables and autologous bone graft allow for a technically less demanding fixation than occipitocervical plates with good fusion rates and minimal complications observed. Titanium plates may be used in conjunction with titanium cables to optimize post-operative CT and MRI (Figure 2).

Atlantoaxial fixation and fusion techniques such as the Gallie Brooks and "Interspinous" methods have all been thoroughly described [38,48-50]. The Gallie fusion has only one sublaminar wire passed at C1, the Brooks technique has sublaminar wires passed at both C1 and C2, and the interspinous method has a sublaminar wire passed at C1. Both the Brooks and interspinous methods have the advantage of cancellous to cancellous interface between the graft and C1 and C2 laminae, and the advantage of a graft under compressive forces. Both the Brooks and "Interspinous" methods rely on structural maintenance of the graft such that wires/cables do not loosen and result in loss of alignment. The Brooks technique provides a more rigid fixation than the Gallie technique and provides additional rotational stability. Methylmethacrylate can be used to supplement these constructs, however, bony fusion is relied on for long-term stability. The integrity of the posterior arch of C1 is assumed during posterior C1-C2 wiring techniques.

Posterior C1-C2 transarticular screws provide immediate internal fixation of C1-C2 even in the presence of an incomplete posterior C1 arch. Frequently C1-C2 wiring such as the "interspinous" technique is used to provide additional stability until bony fusion occurs. Stillerman achieved 95 percent fusion with posterior transarticular screws and onlay graft [39]. Earlier mobilization and less extensive orthoses are also advantages in using transarticular screws to supplement C1-C2 wiring and fusion. The contraindications of posterior transarticular screw fixation include ectasia of the vertebral artery into the body of C1, altered anatomy or bony destruction in the region of the proposed screw placement, and inadequate fluoroscopic images [22,37]. Fusion rates have been very good (95-100%), even when used to salvage a pseudarthrosis of C1-C2 or OS odontoideum.

Interlaminar clamps have been used to stabilize the atlantoaxial articulation [38-39,50]. Halifax clamps have the advantage of avoiding sublaminar passage of wires and are thought to provide similar biomechanical strength to that of the Brooks technique. Fusion rates have been lower (80%) and instrumentation failure rates higher due to clamp detachment with extreme rotation and extension. Moskovich and Crockard have modified the interlaminar clamp technique by using interposed bone graft [40].

Anterior decompression of C1-C2 via a transoral resection is most commonly performed on patients who present with signs or symptoms of spinal cord and/or brain-stem dysfunction. Rheumatoid arthritis and congenital osseous malformation are the most frequent pathologies requiring anterior decompression [23]. If pre-operative reduction using cervical traction is successful, occipitocervical fusion only may be necessary. If pre-operative reduction cannot be obtained, transoral resection is performed and instability is re-accessed. If instability is present, posterior fixation is then performed once in the reduced position [47]. Dickman found that transoral odontoid resection resulted in 40 percent experiencing instability after transoral surgery, however, the instability may occur in a delayed fashion [3].

Anterior stabilization may be performed using anterior transarticular screws through the C2 superior articular facet into the lateral mass of C1 but this technique is much less frequently used than the direct anterior screw fixation of the odontoid [24,47]. Much has been published regarding the advantages of odontoid screw fixation with special emphasis on the ability to gain odontoid fracture fixation without altering the natural motion characteristics of the atlantoaxial complex [22,28,30,43]. The anterior odontoid screw fixation provides the highest fusion rate for acute unstable Type II odontoid fractures [28]. Posterior C1-C2 wiring is typically accredited with a 90-95 percent fusion rate when combined with a cervical halo or Minerva orthosis for a three month period post-operatively. Posterior transarticular screws with or without C1-C2 wiring achieve a 95-100 percent fusion rate in a

less extensive cervical orthosis. C1-C2 wiring with or without transarticular screw fixation results in sacrifice of C1-C2 motion in particular normal rotation. The primary advantage of anterior odontoid screw fixation is that of immediate stability while preserving normal rotation at C1-C2 [49]. If the transverse atlantal ligament is disrupted (which can typically be assessed with MRI) resulting in odontoid fracture with atlantoaxial subluxation, posterior C1-C2 wiring and fusion alone or in combination with posterior transarticular screws is recommended as early surgical intervention [2]. Biomechanical studies have been performed on the efficacy of direct anterior fixation of odontoid fracture [26-27,29,31,41]. Doherty performed biomechanical studies on Type II and Type III odontoid fractures in a cadaver model. Single screw fixation of odontoid fractures was found to provide stability equal to approximately one-half that of unfractured bone [26]. A subsequent study by Sasso and Doherty revealed no significant differences between one and two screw techniques under loading to failure, however, the two screw technique provided increased stiffness in extension [26,31]. Graziano also found direct odontoid fixation, with one or two screws, offers similar stability [41].

References

[1] Williams PL, Warwick R. *Gray's Anatomy*. 36th Edition. WB Saunders, Philadelphia 1980: 1578 pp.

[2] Dickman CA, Greene KA, Sonntag VKH. Injuries involving the transverse atlantal ligament: Classification and treatment guidelines based upon experience with 39 injuries. *Neurosurgery* 1996:38(1): 44-50.

[3] Dickman CA, Locantro J, Fessler RG. The influence of transoral odontoid resection on stability of the craniovertebral junction. *J Neurosurg* 1992:77: 525-530.

[4] White AA III, Panjabi MM. *Clinical Biomechanics of the Spine*. 2nd Edition. JB Lippincott Co., Philadelphia, PA, 1990: 722 pp.

[5] Papadopoulos SM. Biomechanics of occipito-atlanto-axial trauma. In: *Spinal Trauma: Current Evaluation and Management*. GL Rea, CA Miller (eds). The American Association of Neurological Surgeons, Park Ridge, IL, 1993: 17-23.

[6] Panjabi MM, Vasavada A, White AA III. Cervical spine biomechanics. *Seminars in Spine Surgery* 1993:5 (1): 10-16.

[7] Menezes AH, Piper JG. Anatomy and radiographic pathology of injury to the occipito-atlanto-axial complex. In: *Spinal Trauma: Current Evaluation and Management*. GL Rea, CA Miller (eds). The American Association of Neurological Surgeons, Park Ridge, IL, 1993: 1-16.

[8] Kathol MH, El-Khoury GY. Diagnostic imaging of cervical spine injuries. *Seminars in Spine Surgery* 1996:8 (1): 2-18.

[9] Colamaria V, Mazza C, Beltramello A, Polo A, Boner A, Antoniazzi F, Polo M, Luchini P, Sgro V, Dalla Bernardina B. Irreversible respiratory failure in an achondroplastic child: The importance of an early cervicomedullary decompression, and a review of the literature. *Brain Dev* 1991:13(4): 270-279.

[10] Ferrante L, Acqui M, Celli P, Santoro A, Fortuna A. Achondroplasia: Unusual bone abnormalities of the cervical spine. *Neurosurg Rev* 1992:15: 143-145.

[11] Hecht JT, Butler IJ. Neurologic morbidity associated with achondroplasia. *J Child Neurol* 1990:5: 84-97.

[12] Gabriel KR, Mason DE, Carango P. Occipito-atlantal translation in Down's syndrome. *Spine* 1990:15(10): 997-1002.

[13] Thomas IT, Frias JL, Williams JL, Friedman WA. Magnetic resonance imaging in the assessment of medullary compression in achondroplasia. *AJDC* 1988:142: 989-992.

[14] Boden SD, Dodge LD, Bohlman HH, Rechtine GR. Rheumatoid arthritis of the cervical spine. A long-term analysis with predictors of paralysis and recovery. *J Bone Joint Surg* 1993:75A(9): 1282-1297.

[15] Dickman CA, Ronderos JF, Sonntag VKH. Stabilization of the craniovertebral junction in rheumatoid arthritis. Part I: Pathophysiology, diagnosis, and surgical criteria. *Contemp Neurosurg* 1995:17(11): 1-6.

[16] Dickman CA, Ronderos JF, Sonntag VKH. Stabilization of the craniovertebral junction in rheumatoid arthritis. Part II: Surgical techniques. *Contemp Neurosurg* 1995:17(12): 1-6.

[17] Zeidman SM, Ducker TB. Rheumatoid arthritis. Neuroanatomy, compression, and grading of deficits. *Spine* 1994:19(20): 2259-2266.

[18] Zoma A, Sturrock RD, Fisher WD, Freeman PA, Hamblen DL. Surgical stabilisation of the rheumatoid cervical spine. *J Bone Joint Surg* 1987:69B: 8-12.

[19] Rousselin B, Helenon O, Zingraff J, Delons S, Drueke T, Bardin T, Moreau J-F. Psuedotumor of the craniocervical junction during long-term hemodialysis. *Arthritis Rheum* 1990:33(10): 1567-1573.

[20] Dickman CA, Papadopoulos SM, Sonntag VKH, Spetzler RF, Rekate HL, Drabier J. Traumatic occipitoatlantal dislocations. *J Spinal Disorders* 1993:6(4): 300-313.

[21] Lee C, Woodring JH, Goldstein SJ, Daniel TL, Young AB, Tibbs PA. Evaluation of traumatic atlantooccipital dislocations. *AJNR* 1987:8: 19-26.

[22] Apfelbaum RI. Ventral and upper cervical spine fixation techniques. In: *Neurological Topics: Spinal Instrumentation.* EC Benzel (ed). The American Association of Neurological Surgeons, Park Ridge, IL, 1994: 63-96.

[23] Crockard HA. Anterior approaches to lesions of the upper cervical spine. In: *Clinical Neurosurgery* 1988:34: 389-416.

[24] Dickman CA, Sonntag VKH, Marcotte PJ. Techniques of screw fixation of the cervical spine. *BNI Quarterly* 1993:9(4): 27-39.

[25] Dickman CA, Foley KT, Sonntag VKH, Smith MM. Cannulated screws for odontoid screw fixation and atlantoaxial transarticular screw fixation. *J Neurosurg* 1995:83: 1095-1100.

[26] Doherty BJ, Heggeness MH, Esses SI. A biomechanical study of odontoid fractures and fracture fixation. *Spine* 1993:18(2): 178-184.

[27] Esses SI, Bednar DA. Screw fixation of odontoid fractures and nonunions. *Spine* 1991:16(10): S483-S485.

[28] Konstantinou D, Levi ADO, Sonntag VKH, Dickman CA. Odontoid screw fixation. *BNI Quarterly* 1997:13(2): 14-19.

[29] McBride AD, Mukherjee DP, Kruse RN, Albright JA. Anterior screw fixation of Type II odontoid fractures. *Spine* 1995:20(17): 1855-1860.

[30] Rainov NG, Heidecke V, Rurkert W. Direct anterior fixation of odontoid fractures with a hollow spreading screw system. *Acta Neurochir* 1996:138: 146-153.

[31] Sasso R, Doherty BJ, Crawford MJ, Heggeness MH. Biomechanics of odontoid fracture fixation. *Spine* 1993:18(14): 1950-1953.

[32] Flint GA, Hockley AD, McMillan JJ, Thompson AG. A new method of occipitocervical fusion using internal fixation. *Neurosurgery* 1987:21(6): 947-950.

[33] Goel A, Laheri V. Plate and screw fixation for atlanto-axial subluxation. *Acta Neurochir* 1994:129: 47-53.

[34] Grub D, Dvorak J, Panjabi M, Froehlich M, Hayek J. Posterior occipitocervical fusion. A preliminary report of a new technique. *Spine* 1991:16(3): S17-S24.

[35] Smith MD, Anderson P, Grady MS. Occipitocervical arthrodesis using contoured plate fixation. An early report on a versatile fixation technique. *Spine* 1993:18(14): 1984-1990.

[36] Wertheim SB, Bohlman HH. Occipitocervical fusion. *J Bone Joint Surg* 1987:69A(6): 833-836.

[37] Apfelbaum R. Posterior transarticular C1-2 screw fixation for atlantoaxial instability. *Aesculap Scientific Information 25* 1993, Aesculap Ag, D-7200 Tuttlingen, Germany, 12 pp.

[38] Coyne TJ, Fehlings MG, Wallace MC, Bernstein M, Tator CH. C1-C2 posterior cervical fusion: Long-term evaluation of results and efficacy. *Neurosurgery* 1995:37(4): 688-693.

[39] Stillerman CB, Wilson JA. Atlanto-axial stabilization with posterior transarticular screw fixation: Technical description and report of 22 cases. *Neurosurgery* 1993:32(6): 948-955.

[40] Moskovich R, Crockard HA. Atlantoaxial arthrodesis using interlaminar clamps. An improved technique. *Spine* 1992:17(3): 261-267.

[41] Graziano G, Jaggers C, Lynch W. A comparative study of fixation techniques for Type II fractures of the odontoid process. *Spine* 1993:18(16): 2383-2387.

[42] Sonntag VKH, Kalfas I. Innovative cervical fusion and instrumentation techniques. In: *Clin Neurosurg* 1991:37: 636-660.

[43] Verheggen R, Jansen J. Fractures of the odontoid process: Analysis of the functional results after surgery. *Eur Spine J* 1994:3: 146-150.

[44] Menezes AH, Traynelis VC, Gantz BJ. Surgical approaches to the craniovertebral junction. *Clinical Neurosurgery*:1994:41: 187-203.

[45] Menezes AH. Complications of surgery at the craniovertebral junction - avoidance and management. *Pediatr Neurosurg* 1991-92:17: 254-266.

[46] McAfee PC, Cassidy JR, Davis RF, North RB, Ducker TB. Fusion of the occiput to the upper cervical spine. A review of 37 cases. *Spine* 1991:16(10): S490-S494.

[47] Menezes AH, Ryken TC. Instrumentation of the craniocervical region. In *Neurosurgical Topics: Spinal Instrumentation*. EC Benzel (ed). The American Association of Neurological Surgeons, Park Ridge, IL, 1994: 47-62.
[48] Cooper PR. Posterior stabilization of the cervical spine. *Clinical Neurosurgery* 1993:40: 286-320.
[49] Dickman CA, Sonntag VKH. Wire fixation for the cervical spine: Biomechanical principles and surgical techniques. *BNI Quarterly* 1993:9(4): 2-16.
[50] An HS, Coppes MA. Posterior cervical fixation for fracture and degenerative disc disease. *Clin Orthop* 1997:335: 101-111.

Figure Captions

Figure 1a: Craniocervical Anatomy (axial view).

Figure 1b: Craniocervical Anatomy (sagittal view).

Figure 2a: Pre-operative MRI of cervical spine of a myelopathic rheumatoid arthritis patient.

Figure 2b: Occipitocervical contoured Titanium rod/cable instrumentation and fusion.

Figure 2c: Post-operative MRI following transoral resection of pannus and occipitocervical contoured rod/cable instrumentation and fusion. Note minimal artifact from Titanium rod.

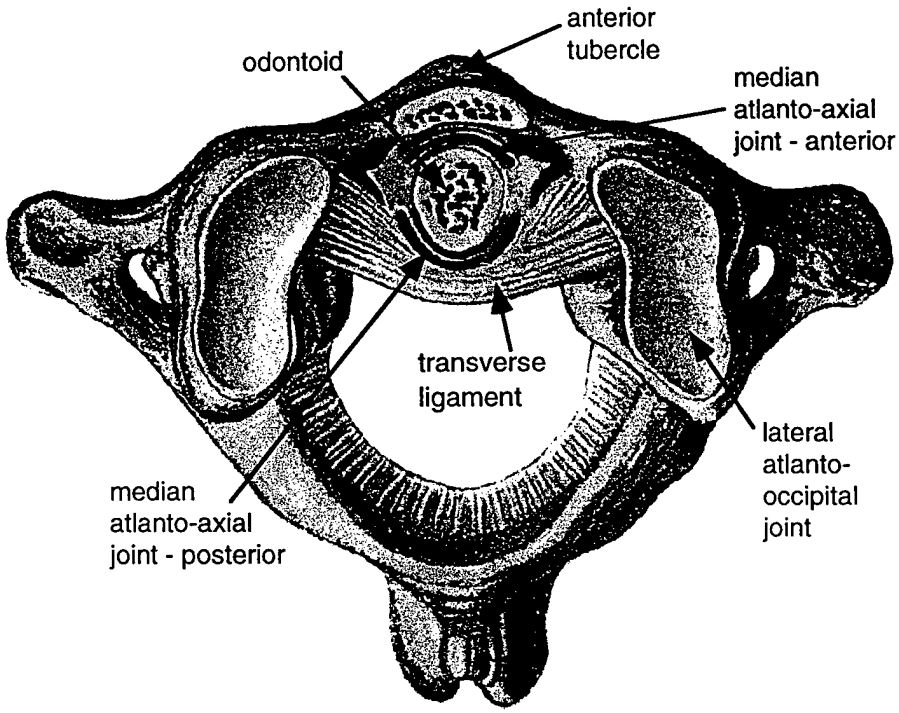
anterior
tubercle
odontoid
median
atlanto-axial
joint - anterior
transverse
ligament
lateral
atlanto-
occipital
joint
median
atlanto-axial
joint - posterior

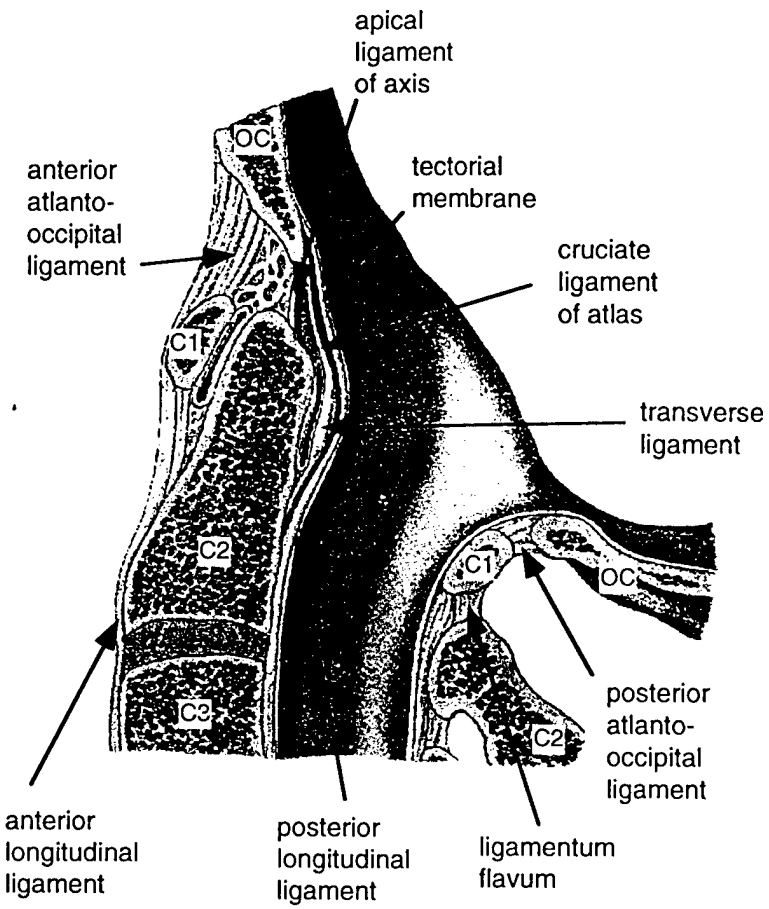
apical
ligament
of axis
OC
anterior
atlanto-
occipital
ligament
tectorial
membrane
cruciate
ligament
of atlas
C1
transverse
ligament
C2
C1
OC
C3
C2
posterior
atlanto-
occipital
ligament
anterior
longitudinal
ligament
posterior
longitudinal
ligament
ligamentum
flavum

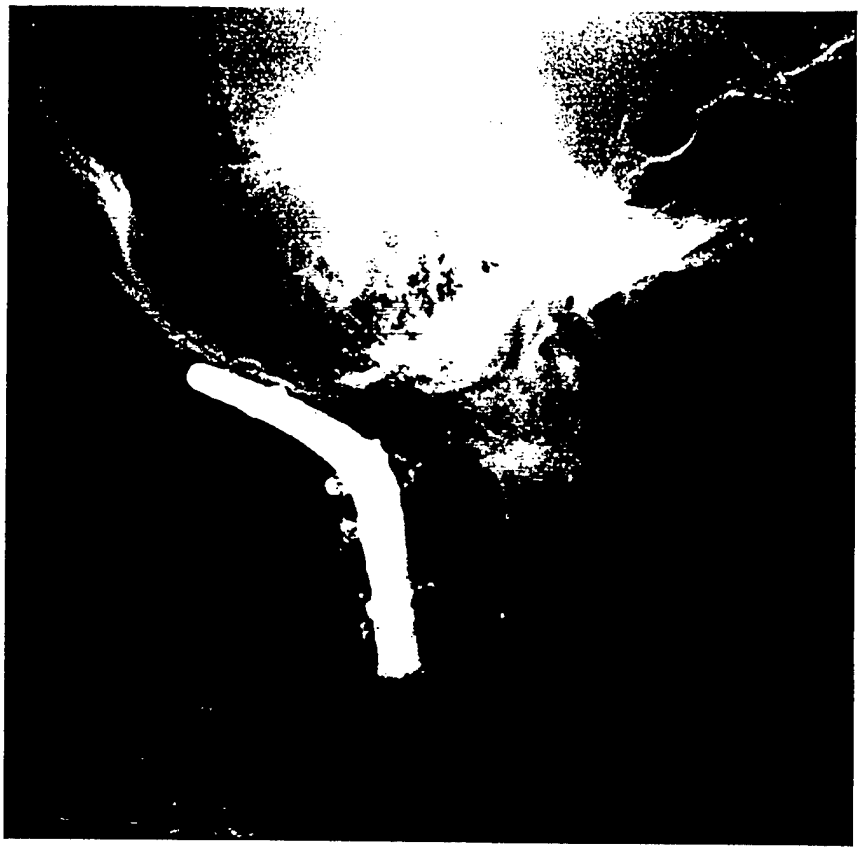

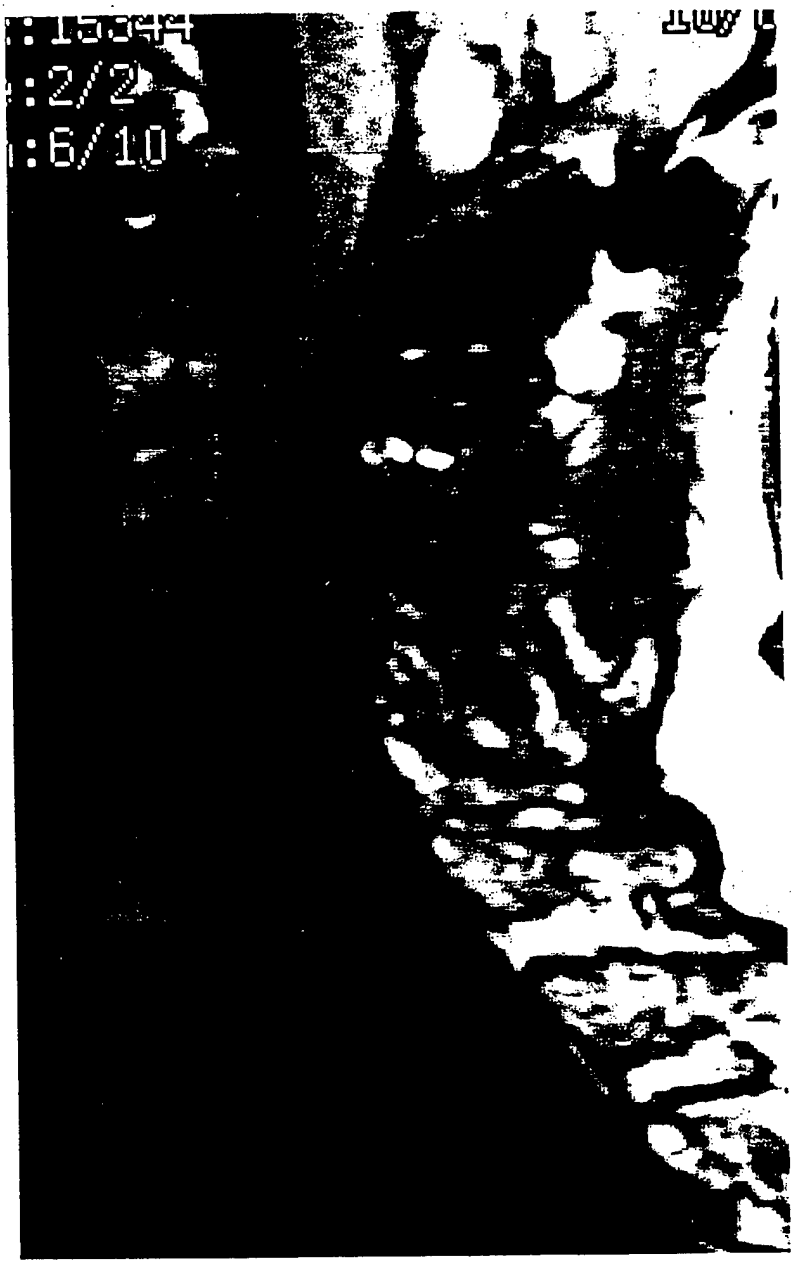
:2/2
:6/10

POSTERIOR CERVICAL SPINE INSTRUMENTATION: SUBAXIAL FIXATION PROCEDURES

Joseph F. Cusick, Jamie L. Baisden

Abstract

A variety of posterior cervical surgical fixation techniques are available to assist in alleviating instability or deformity of the injured cervical spinal column. Resolution of these alterations will improve the load bearing capacity of the column and assist in avoiding compromise of associated neural structures. Each method however, possesses an individual value and needs to be applied in a manner to correct the major forces of injury and limit secondary complications. Wiring techniques of the spinous processes, lamina and facets will offer selective strengthening of the column with understanding of the individual effectiveness necessary to define the appropriate use of the various proposed techniques. The absence of midline structures, especially with inherent changes induced by extensive multilevel dissection or injury to posterior column components, may necessitate the need to consider innovative facet wiring procedures or lateral mass screw-plate fixation techniques. This chapter addresses the role of the posterior cervical fixation techniques including the limitations and advantages offered by each procedure.

1. Introduction

Instability of the cervical spine may be defined as the inability of the spine to be altered in alignment or curvature by exposure to physiological forces. These conditions, actual and potential with resultant damage to associated neural structures, indicate the risk of impending catastrophic sequelae. Cervical spine injuries are

therefore, the result of complex loads and moments which result in differing levels of deforming forces on the various components (facets, vertebral bodies, intervertebral disc, ligaments). If these deforming forces result in segmental changes to the vertebral column resulting in increasing deformity under physiological loads, the process is unstable. In evaluating these situations, Panjabi & White proposed that > 3.5 mm of anterolisthesis or > 11 degrees of angulation constitutes instability in the lower cervical spine [1]. Certain patients with recent trauma and cervical pain may not demonstrate radiologic evidence of instability on routine cervical spine films, but the clinical suspicion may indicate performance of flexion-extension lateral radiographs. Dynamic radiographs however, should be approached with a level of caution, and frequently the situation is initially best approached by computerized tomography (CT) with sagittal reconstruction for full definition of the possible injury patterns. If instability is not demonstrated with the above studies, yet suspected from the increased pre-vertebral soft tissue swelling and the severe neck pain, these patients should be placed in a firm cervical collar and dynamic radiographs repeated in 10 to 14 days. This time allows muscle spasm to abate with the improved potential to demonstrate ligamentous instability.

These situations may suggest the consideration of prophylactic intervention, but basic to the details of therapeutic intervention, either operative or nonoperative, is an understanding of the biomechanical principles of cervical spine function. Attention to these considerations will permit the most efficacious planning of a specific treatment, especially the details of surgical intervention. Generally in the cervical region, the major mechanism of injury is transmission of force through the head and the corresponding changes are usually related to either flexion, extension or rotation with associated axial compression or distraction. Clarification of each of these factors will assist the surgeon in designing the most appropriate procedure, and permits an operative design to counteract the major force vectors responsible for the principal injury pattern.

Many cervical spine abnormalities with instability may not require open surgical intervention, but instead may be treated by a variety of means including prolonged immobilization in traction or external orthotics as well as open reduction with or without internal fixation and bony fusion.

2. Spinous Process Wiring

A variety of wiring techniques of the spinous processes, lamina and facets have been proposed for the treatment of cervical spinal instability. Wire or cable can be passed through and around spinous processes, facet joints or lamina with spinous process wiring remaining one of the most popular methods in the treatment of many traumatic cervical spine injuries. Each of these techniques has a varying capacity to correct the injurious forces that caused the destabilizing injury. Since Rogers reported a high rate of success for cervical fusion with a single interspinous wiring, a variety of techniques have been proposed [2]. Murphy and Southwick, modified Rogers' technique to obtain improved tension band effect at the area of injury and therefore, the potential for correction of alignment abnormalities [3]. Presently, one of the favored spinous process wiring techniques is the Bohlman triple wire method which is a biomechanically proven method of accomplishing this midline fixation of the spinous processes. In this technique, a drill hole is made at the base of the spinous process and a single 20 gauge wire is passed through the drill hole and looped around the superior border of the rostral process. The wire is then passed distally through the drill hole in the lower process and then looped around the base of the spinous process at that level. Two separate 22 gauge wires are passed through the same holes to secure the bone graft in a compression arrangement. If cables are used, the surgeon will need to drill a more superior hole through the upper and lower spinous process. Biomechanical studies have verified the strength of this construct and case reviews have described excellent union with this technique [3]. Recent development of commercially available braided wire constructs (cables) with improved malleability and strength has improved the application of many of these techniques.

Most wiring techniques are effective in restricting flexion but less effective in limiting extension and rotation. Modification of wire fixation has been developed to assist in the treatment of rotational instability, especially as encountered with facet dislocation and, if concerns are present regarding rotational stability, the oblique wiring technique will be of value [4]. The spinous processes and facets are exposed and the facet joint is opened with sharp dissection. In order to open the facet joint and ease the wire passage, it is advisable to burr down the superior facet. Frequently the frustration of facet wire passage is based upon the lack of widely opening the facet joint. The drill hole is made at the center of the inferior facet, angled slightly medially and inferiorly. Twenty gauge wire or cable is passed through the drill hole. The wire is passed around the spinous process to be wired [Figure 1]. The application, in a bilateral fashion, will further establish both flexion and rotational stability [5]. This construct can

be extended to include segments with compromised facets, again using additional spinous process inclusion in the distal wire loop.

3. Facet Wiring Techniques

Extensive posterior cervical procedures such as multilevel laminectomy or laminoplasty, may result in alignment or flexibility changes of the cervical vertebral column that may adversely affect therapeutic outcome. These dynamic alterations may be a significant factor if posterior decompressive procedures fail to resolve or avoid additional neurologic deterioration [6-10]. Under certain conditions therefore, posterior internal fixation in conjunction with decompression may improve long-term clinical outcomes [7,11-12]. The majority of biomechanical studies of posterior arthrodesis generally have concentrated on the techniques of intraspinous or intralaminar fixation and frequently have used these evaluations as a basis for comparison of all posterior cervical spine fixation techniques [11,13-16]. The absence of midline structures following laminectomy and related procedures obviates such approaches and, in this setting, facet wiring or lateral mass screw and plate fixation techniques have been advocated [5,12,17-20]. The alternative methods of facet wires positioned through drill holes in the facet offer an increased comparative safety by avoiding these neurovascular complications, and this form of facet wiring has been advocated for translational and rotational stability after laminectomy [4-5,12,18,21-22].

The facet joints are major determinants of cervical motion, and numerous studies have demonstrated that facet joint instability occurs with posterior ligamentous and bony injuries. Functional unit studies have shown an approximate 30 percent increase to flexion-compression load with unilateral facetectomy, and an approximate 50 percent decrease in stiffness with bilateral facetectomies. Facet to facet or facet to spinous process fixation resulted in significant restoration to intact levels, but did demonstrate persistent interspinous motion [23]. This latter finding suggests that facet wiring techniques be associated with spinous process wiring. Other "in vitro" studies have verified the relative contribution of the facet joint to stability and the merits of fixation [24-25].

Robinson and Southwick originally described multilevel facet fixation accomplished by individual facet wires passed through corticocancellous grafts as a method to avoid instability following extensive and wide laminectomy [22]. This technique was later modified to include additional wire passage about the bony strut and through the spinous process caudal to the laminectomy [3]. These surgical techniques, especially inclusion of wiring through the intact spinous processes above and below the levels of laminectomy, require an extensive bone strut with potential donor site problems, bone displacement or attenuation of the bone-wire interface. To alleviate some of these difficulties, especially the technical limitation of obtaining adequate autologous bone struts of unlimited length, Garfin et al., recommended the use of threaded Harrington rods as struts rather than the autologous bone grafts [21]. In this technique the individual facet wires were supplemented only by inclusion of spinous process wiring to the rods at the levels distal to the laminectomy (T2 or T3). In an extension of this concept that metal rods may offer immediate stability without the limitations imposed by autologous bone grafts, Maurer et al., reported nine patients with advanced cervical spondylotic myelopathy who demonstrated sustained neurologic improvement following multilevel laminectomy combined with Luque rectangle fixation from C2 through T1 [26]. This rectangle was secured by individual facet wires at the laminectomized segments as well as sublaminar wires at C2 and T1 [Figure 2].

Cross-linking bony or metal struts above and below the levels of facet wiring, as in the Luque rectangle preparations, improves the biomechanical quality of the fixation, but does require additional extension of the process beyond the levels of the laminectomy. This procedure, which usually spans C2 through T1, reportedly has offered satisfactory clinical results, but the procedure requires the potentially hazardous use of sublaminar wiring, the need to establish multilevel bony fusion to avoid wire fatigue with fixation compromise, and additional loss of cervical motion segments including compromise of lateral flexion-rotation. These limiting factors may temper enthusiasm for such inclusive fixation, but attempts to use fixation without the midline extension above and below the areas of decompression, irrespective of the strut material used in the present study, failed to offer the same desired level of rigid internal fixation [27]. All these methods of facet wire fixation have as a basis individual facet wires placed through drill holes in the middle position of the facet and directed caudally through the inferior facet to exit from the facet joint. This part of the procedure requires a wide exposure of that joint, including almost total violation of the capsular ligaments, and, because these ligaments have been shown to impart a significant degree of restraint at the maximum levels of applied flexion motion, the loss of facet joint integrity would be expected to cause an increasing

flexibility at the upper levels of flexion or flexion-compression forces [10-12,28]. In laboratory setting where such wires only were secured about a strut following a multilevel laminectomy, application of a flexion-compression load resulted in increasing flexibility and segmental motions, including occasions when these changes were of great magnitude even when compared to laminectomy preparations. Such changes occurred irrespective of the inclusion of wiring through the spinous process distal to the laminectomy [27]. This inability to restore some of the functional integrity of the altered cervical column is the result of a process that can be termed "the loosest shoelace." The excess motion is the probable result of the motion from compensated facet joints failing to be restrained by the individual wires that have failed to offer internal fixation. This method therefore, appears to only secure the bone to the facet surfaces without any other redeeming biomechanical characteristics. Although subsequent arthrodesis with this technique may achieve increased mechanical stability, the occurrence of this process will be independent of any immediate rigid internal fixation.

The necessity to achieve levels of structural stiffness approaching or exceeding the intact specimen as a method to avoid the potential for adverse alignment has not been established. It does seem reasonable however, that the expectation for a type of internal fixation to correct some of the biomechanical alterations induced by multilevel laminectomy would require restoration of column strength to levels exceeding that seen after laminectomy without fixation. Methods that not only fail to accomplish such improvement in structural stiffness, but also occasionally result in greater mechanical compromise of the column would be inadequate. To achieve this desired effect of improved strength and decreased segmental motion with present methods of facet fixation, cross-linking of individual facet fixation above and below the levels of laminectomy is recommended.

All previous proposed techniques of facet wiring associated with the necessary cross-linking, whether dependent upon autologous bone or metallic struts, will incur the loss of additional motion segments by the necessity to incorporate the levels above and below the region of laminectomy. In many instances, the requirement will include the C2 segment with resultant additional reduction of lateral rotation-flexion. The use of sublaminar wires in the Luque rectangle technique raises the consideration of possible neural compromise during wire passage. In those methods where autologous bone struts are the major component, the fixation will be limited by the ability to obtain bone grafts of the desired length and configuration. Substituting metallic rods or rectangles will help resolve this latter consideration, but will also require customizing of the devices, compromise follow-up magnetic imaging studies, and incur the possibility of device failure at the bone-metal interface. The limitations and disadvantages of these proposed methods suggest that a facet wiring technique that would offer effective internal fixation, be less inclusive, avoid sublaminar wire passage, and not require extensive bony or metallic struts would be preferable. The following is a description of the operative technique and resultant mechanical effects of such a method which has been given the descriptive terminology of the "crisscross" technique of cervical facet wire (cable) fixation. Individual facet cables are positioned in a manner that results in cable passage across each facet joint. The cables are secured in a sequential pattern in a rostral-caudal cinch and fasten technique. This sequence of cable fixation is depicted in Figure 3. In fastening the cables, it is not necessary to affect tension until completing the most inferior connection which in this example would be cable 4 to cable 6. When tightening this last connection, after the cable has passed around the spinous process, all previous connections that have been crimped will tighten and secure the connections across each facet. In this respect, the lower connection on each side is the only connection requiring tightening before crimping. Potential areas of system failure at the cephalad inferior facet and at the last cable connection which were defined during application of a flexion-compression load were resolved by incorporation of a grommet at the upper level and doubling the crimps at the lower connection. The sequence of cable connections can be continued through additional levels of facet fixation maintaining the same pattern (cable 1 to 3; cable 2 to 5; cable 4 to 7; and cable 6 to 8). The last connection always remains the cable exiting from the penultimate facet joint to the cable exiting from the last joint after passage about the spinous process below the level of laminectomy [Figure 3]. Prior to tightening the cables, the facet joints are packed with morcellized bone graft material obtained from the spinous processes. Final tightening and crimping are done only after bilateral cable placement has been completed. Before final trimming of the cable ends, the surgeon may secure a strip of autograft over the posterior surface of the facets by crimping cable ends in superior-inferior and lateral planes.

"In vitro" biomechanical studies demonstrated that the overall loss of stiffness incurred by multi-segmental laminectomy was resolved by crisscross wiring (76.6% vs. 95.5%). Crisscross wiring also caused a decrease in overall motion which was only slightly diminished from intact levels. The crisscross technique of facet wiring therefore, offers the advantages of immediate mechanical stability of the cervical spine at the levels determined by the surgeon without potential excessive stresses being applied to the levels adjacent to the fixation or incurring risk of potential neurovascular injury. The process is also not limited by significant alterations of facet joint topography or

variability of interfacet distances as well as permitting potential realignment and curvature preservation. The only disadvantages of the technique are those imposed by problems in achieving adequate penetration of the facet necessary to accomplish easy cable passage, and this limitation is easily resolved with modest experience and attention to detail.

4. Lateral Mass Plate and Screw Fixation

This technique is also applicable when posterior midline structures (spinous process and lamina) are not present or violated. These constructs offer rigid internal fixation which probably approaches that offered by the Luque loop approach, including flexion, extension and rotation, and therefore, present the opportunity to avoid the need for external immobilization by halo or Minerva fixation. As previously noted however, lateral mass plates have the risk for neurovascular injury (nerve root, vertebral artery), foraminal narrowing, dislodgment or facet joint violation. The quality of recipient bone must be determined with concerns directed towards the avoidance of severe osteoporosis as well as the difficulties in topographical facet anatomy incurred by severe spondylotic degenerative changes. Additionally, these constructs are limited in their capacity to correct alignment or curvature abnormality realignments of significant magnitude which may necessitate different techniques. The surgeon must conceptualize that the spine will be fixated in the configuration existing at operative exposure.

The details regarding implementation of these constructs will have some variations depending upon the various commercial products, but the techniques for screw placement are fairly well defined. Initially the appropriate length plate or rod is selected and contoured to the lordotic curve. The details regarding placement of screw holes into the lateral masses have advocates for various locations of screw placement and direction [17,29-32]. All methods require the careful definition of the topographical anatomy of the articular pillars. The surgeon outlines the superior aspect at the level of the tip of the inferior facet, medially at the junction of the lamina and facet (the valley), lateral aspect at the outer facet margin, and the inferior aspect at the caudal inferior facet tip for C3 through C6. A general consensus of these various opinions favors the placement of the drill hole at a point 1 mm medially and 1 mm rostral to the midpoint of this rectangle. The drill is angled 15 to 20 degrees rostrally and 30 degrees laterally with a depth of 10 to 11 mm. This trajectory should place the screw in the "safe quadrant" and avoid nerve root or vertebral artery compromise. Magerl recommends angling 30 degrees rostrally in order to maintain a parallel trajectory to the facet joints and recommends that placement of a fine needle in the facet joint will aid in defining this angulation. The distance between holes is 13 to 16 mm and placement of self-tapping screws of 15 to 16 mm in length and 3.5 mm in width are sufficient in the majority of cases. The authors' approach shares many of the details of the Magerl technique and therefore, may present some biomechanical superiority to the Roy-Camille approach. It is again necessary to emphasize that any reduction will need to be achieved by other methods prior to fixation of the plate. At C7, the lateral mass is transitional in character with reduction in size and increased variability. These changes increase risk of nerve root or facet joint disruption, especially since the surgeon desires to achieve bicortical purchase [31].

Pedicle screw placement, rather than lateral mass, is recommended for C7 and T1 levels with the screw directed 25 to 30 degrees medially and 10 degrees caudally. This trajectory will align with the plane of the pedicle and avoid the potential complications of attempted lateral mass placement at these transitional levels.

5. Conclusion

A variety of methods to achieve posterior fixation with individual inherent advantages and disadvantages emphasize the need to tailor the desired method to the individual situation and not to depend upon a singular technique to offer the most efficacious treatment. In this regard, factors such as the patient's ability to accept external immobilization, the presence of significant curvature or alignment alterations, violation of midline structures and quality of recipient bone all will influence the effectiveness of the selected technique.

Acknowledgment: This research was supported by the Department of Veterans Affairs Medical Research.

References

[1] White AA, Panjabi M. The role of stabilization in the treatment of cervical spine injuries. *Spine* 1984:9: 512-522.

[2] Rogers WA. Fractures and dislocations in the cervical spine: An end result study. *J Bone Joint Surg* 1957:39A: 341-346.

[3] Murphy MJ, Southwick WO. Posterior approaches and fusions. In: *The Cervical Spine.* Second Edition. HH Sherk, HJ Dunn, FJ Eismont, JW Fielding, DM Long, K Ono, L Penning, R Raynor (eds). JB Lippincott Co., Philadelphia, PA, 1989: 781-787.

[4] Edwards CC, Matz SO, Levine AM. The oblique wiring techniques for rotational injuries of the cervical spine. *Orthop Trans* 1986:10: 455.

[5] Cusick JF, Yoganandan N, Pintar FA, Myklebust JB, Hussain H. Biomechanics of cervical spine facetectomy and fixation techniques. *Spine* 1988:13: 808-812.

[6] Batzdorf U, Batzdorf A. Analysis of cervical spine curvature in patients with cervical spondylosis. *Neurosurgery* 1988:22 (5): 827-836.

[7] Braakman R. Management of cervical spondylotic myelopathy and radiculopathy. *J Neurol Neurosurg Psychiatry* 1994:57: 257-263.

[8] Cusick JF, Pintar FA, Yoganandan N. Biomechanical alterations induced by multilevel cervical laminectomy. *Spine* 1995:20(22): 2392-2398.

[9] Mikawa Y, Shikata J, Yamamuro T. Spinal deformity and instability after multilevel cervical laminectomy. *Spine* 1987:12 (1): 6-11.

[10] Yasuoka S, Peterson HA, MacCarty CS. Incidence of spinal column deformity after multilevel laminectomy in children and adults. *J Neurosurg* 1982:57: 441-445.

[11] Cusick JF, Steiner RE, Berns T. Total stabilization of the cervical spine in patients with cervical spondylotic myelopathy. *Neurosurgery* 1986:18:(4): 491-495.

[12] Fairbanks TJ. Spinal fusion after laminectomy for cervical myelopathy. *Proc R Soc Med* 1971:64: 8-10.

[13] Bohlman HH. Acute fractures and dislocations of the cervical spine: An analysis of 300 hospitalized patients and review of the literature. *J Bone Joint Surg* 1979:61A: 1119-1142.

[14] Panjabi MM, Summers DJ, Pelker RR, Videman T, Friedlaender GE, Southwick WO. Three-dimensional load-displacement curves due to forces on the cervical spine. *J Orthop Res* 1986:4: 152-161.

[15] Stauffer ES. Management of spine fractures C3 to C7. *Orthop Clin North Am* 1986:17(1): 45-53.

[16] Traynelis VC, Donaher PA, Roach RM, Kojimoto H, Goel VK. Biomechanical comparison of anterior Caspar plate and three-level posterior fixation techniques in a human cadaveric model. *J Neurosurg* 1993:79: 96-103.

[17] Anderson PA, Henley MB, Grady S, Montesano PX, Winn HR. Posterior cervical arthrodesis with AO reconstruction plates and bone graft. *Spine* 1991:16(Suppl)(3): S72-79.

[18] Callahan RA, Johnson RM, Margolis RN, Keggi KJ, Albright JA, Southwick WO. Cervical facet fusion for control of instability following laminectomy. *J Bone Jt Surg* 1977:59A: 991-1002.

[19] Cooper PR, Cohen A, Rosiello A, Koslow M. Posterior stabilization of cervical spine fractures using plates and screws. *Neurosurgery* 1988:23(3): 300-306.

[20] Heller JG. Complications of posterior cervical plating. *Seminars in Spine Surgery* 1993:5(12): 128-138.

[21] Garfin SR, Moore MR, Marshall LF. A modified technique for cervical facet fusions. *Clin Orthop* 1988:230: 149-153.

[22] Robinson RA, Southwick WO. Indications and techniques for early stabilization of the neck in some fracture dislocations of cervical spine. *South Med J* 1960:53: 565.

[23] Cusick JF, Yoganandan N, Pintar FA, Hussain H: Biomechanics of cervical spine facetectomy and fixation techniques. *Spine* 13:808-812, 1988.

[24] Goel VK, Clark CR, Harris KG, Schulte KR. Kinematics of the cervical spine: Effects of multiple total laminectomy and facet wiring. *J Orthop Res* 1988:6(4): 611-619.

[25] Zdeblick TA, Zau DD, Warden KE, McCabe R, Cunz D, Vanderby R. Cervical stability after foraminotomy. *J Bone Joint Surg* 1992:74A: 22-29.

[26] Maurer PK, Ellenbogen RG, Ecklund J, Simonds GR, van Dam B. Cervical spondylotic myelopathy: Treatment with posterior decompression and Luque rectangle bone fusion. *Neurosurgery* 1991:28: 680-684.

[27] Cusick JF, Pintar FA, Yoganandan N, Baisden J. Wire fixation techniques of the cervical facets. *Spine* 1997:22(9): 970-975.

[28] Raynor RB, Moskovich R, Zidel P, Pugh J. Alterations in primary and coupled neck motions after facetectomy. *Neurosurgery* 1987:21: 681-687.

[29] Roy-Camille R, Saillant G, Mazel C. Internal fixation of the unstable cervical spine by a posterior osteosynthesis with plates and screws. In: *The Cervical Spine.* Second Edition. HH Sherk, HJ Dunn, FJ Eismont, JW Fielding, DM Long, K Ono, L Penning, R Raynor (eds). JB Lippincott Co., Philadelphia, PA, 1989: 390-403.

[30] Heller JG, Carlson GD, Abitbol JJ, Garfin Sr. Anatomic comparison of the Roy-Camille and Magerl techniques for screw placement in the lower cervical spine. *Spine* 1991:16(Suppl): S552-557.

[31] An HS, Gordin R, Renner K. Anatomic considerations for plate-screw fixation of the cervical spine. *Spine* 1991:16(Suppl): S548-551.

[32] Weidner A. Posterior plating. In: *The Cervical Spine: An Atlas of Surgical Procedures.* First Edition. HH Sherk, HJ Dunn, FJ Eismont, et al (eds). JB Lippincott Co., Philadelphia, PA, 1994: 163-175.

Figure Legends

Figure 1: Bilateral facet to spinous process wiring of C4 to C5 provides excellent stability against rotational as well as anterior horizontal displacement.

Figure 2: Securing of sublaminar wires above and below the levels of laminectomy and individual facet wires at the levels of laminectomy.

Figure 3: Illustration of a commonly used technique of facet wiring consisting of individual facet wires incorporated about a bony strut and inclusive of wiring of the strut to the spinous process below the levels of laminectomy.

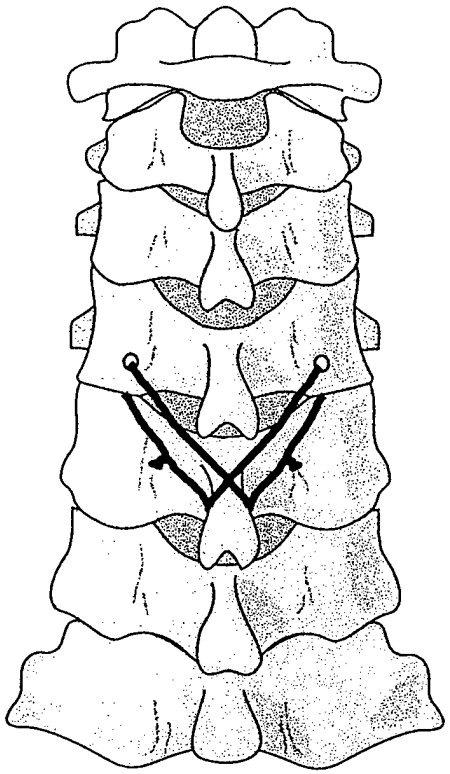

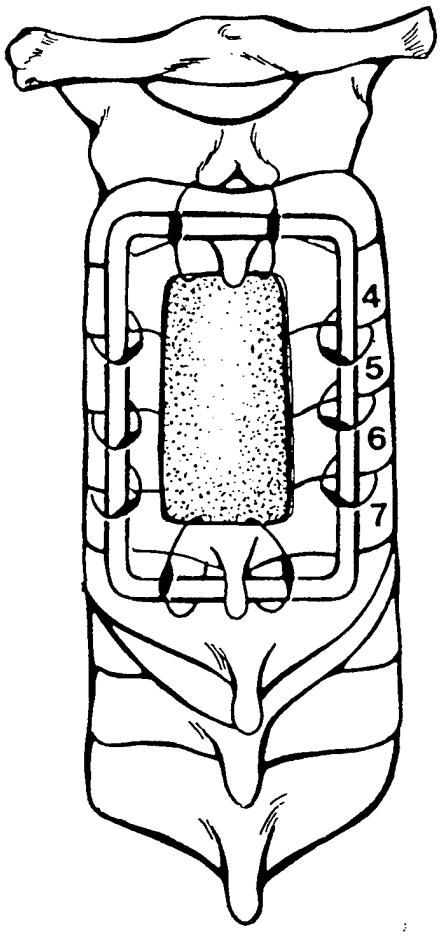
4
5
6
7

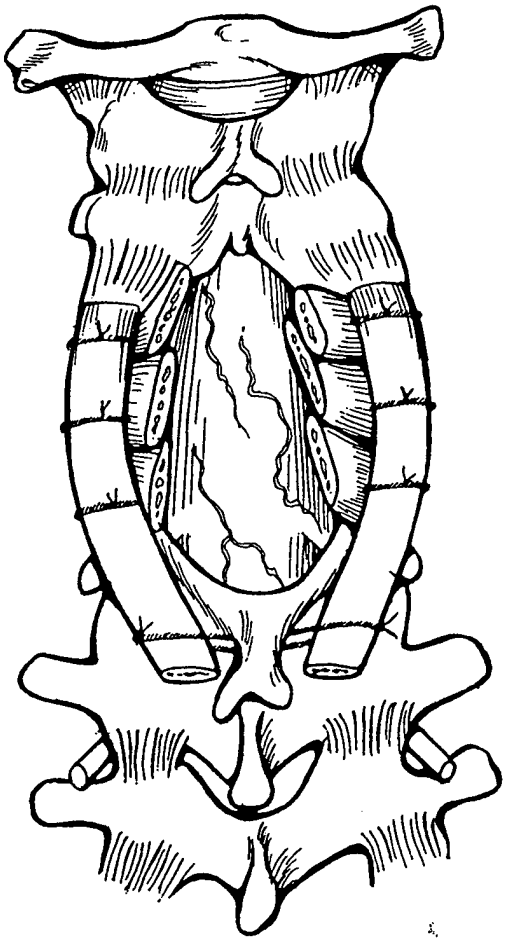

BIOMECHANICAL ANALYSIS OF CERVICAL LAMINECTOMY AND FACETECTOMY USING FINITE ELEMENT METHOD

Srirangam Kumaresan, Narayan Yoganandan
Frank A. Pintar, Joseph F. Cusick

Abstract

An anatomically accurate three-dimensional finite element model of the human cervical spine (C4-C5-C6) was used to study the external and internal biomechanics of laminectomy with and without graded facetectomy. The finite element model was developed using the geometric details from multi-planar CT images and cryomicrotome anatomic sections. The intact model was validated under flexion, extension, lateral bending and axial torsion loading modes with experimental data. The overall external (angular motion) and internal (superior and inferior intervertebral disc stresses indicative of load sharing) responses were determined under the four physiological loading modes for these iatrogenic changes. Laminectomy considerably altered the cervical angular motion and the disc stress under flexion compared to other loading modes. Facetectomy increased the angular motion and the inferior disc stress notably under flexion but did not affect the adjacent superior disc stress. Facet resection of more than one-half caused significant increases in angular rotation and intervertebral disc stresses. The present anatomically accurate and validated three-dimensional finite element model provides both internal and external responses to better understand the clinical biomechanics of the iatrogenically altered spine. These findings suggest an accentuated role for the internal biomechanical variables to be more sensitive and better characterize the response of the cervical spine under iatrogenically altered conditions. This increased stress magnitude in the intervertebral disc anulus may lead to degenerative changes at the facetectomized spinal level. It is well known that the bone remodeling is the response of bone tissue to mechanical stress. Soft tissues may also change structural properties as an adaptation to higher stress environment. The above internal biomechanical response variations in terms of the soft and hard tissue stresses before and after facetectomy may better reveal the true nature of the accelerated degenerative process in the cervical column.

1. Introduction

Cervical laminectomy accompanied by facetectomy is performed to decompress the spinal cord and treat various spinal disorders [1-3]. This procedure involves the removal of the lamina, posterior ligaments and facet masses. Biomechanically, such structural alterations affect the strength and motion characteristics of the spine [4,5]. Clinical and biomechanical experimental studies have been conducted to evaluate the effects of laminectomy with and without the alteration of facet integrity [1-2,4-10]. Clinical observations have the ability to assess post-operative outcomes such as changes in the spinal curvature. Experimental biomechanical research can provide information regarding the stability of the iatrogenically altered spine based on external response such as sagittal rotations and segmental motions [11-13]. However, the quantification of external and internal responses of the spine provides additional information to better understand the iatrogenic changes to the spine. The finite element (FE) model is an ideal tool to accomplish this objective [14-26]. This chapter presents the application of the anatomically accurate three-dimensional (3-D) finite element model of the human lower cervical spine (C4-C5-C6) to evaluate the effects of laminectomy with and without graded facetectomy in terms of external angular rotation and internal intervertebral disc stresses under physiologic flexion, extension, lateral bending and axial torsion loadings.

2. Surgical Simulation

The FE model of the three-segment (C4-C5-C6) human cervical spine was developed using geometric details from sagittal and coronal computed tomography images and cryomicrotome anatomic sections. Details of the model construction, development and experimental validation under physiologic loading modes are presented in an earlier chapter. Figure 1 shows the intact finite element model of the cervical spine. The intact finite element model was modified to simulate laminectomy by resecting the C5 lamina along with the interconnecting interspinous ligaments and ligamentum flavum [27]. To this laminectomized model, bilateral graded facetectomies were performed. At the level of the C5-C6 intervertebral joint, facetectomy was simulated by removing the facet masses of the superior articular process of the C6 vertebra and the inferior articular process of the C5 vertebra along with the corresponding capsular ligaments posteriorly (from medial to lateral). The lateral border of the facetectomized mass was the medial margin of the pedicle. According to the grade level, facetectomized mass was excised towards the lateral side. These iatrogenic alterations were designed to replicate the common methods of surgical exposure [28]. Figure 2 illustrates the model with laminectomy and facetectomy. Different grades of facetectomy (25, 50, 75, 100%) were selected to represent the exposure of nerve root. The intact and iatrogenic altered models were exercised under flexion, extension, lateral bending and axial torsion. The angular rotations (C4 with respect to C6), and the von Mises stress for the superior (C4-C5) and inferior (C5-C6) intervertebral discs were obtained [17]. These output variables were normalized with intact model output according to accepted methods.

3. Results and Discussion

Under laminectomy, the percentage increase in angular rotation (Figure 3) was the highest under flexion compared to the other loading modes. Such considerable increase of motion only under flexion demonstrates the restrictive role of the posterior elements. The observed higher angular rotation appears to confirm the clinical observation that patients undergoing laminectomy may be more susceptible to develop instability or alignment changes leading to progressive curvature alterations [8,29]. In general, increasing levels of facet resection resulted in increased changes in the angular rotations under all the four physiologic load vectors. In addition, the flexion response was the most affected and the axial torsion response was the least affected due to

graded facetectomy. Under extension and lateral bending modes, graded facetectomy responses were essentially similar. An examination of these changes demonstrated that one-half resection of facet results in a considerable increase in the angular motion under all loading modes. Similar observations were reported by Zdeblick et al., in their *in vitro* experimental study of cervical spine foraminotomy under pure moment flexion and torsion loading [30]. They also concluded that foraminotomy with a resection of more than one-half of the facet joint results in segmental hypermobility. Raynor et al., reported that facet resection of more than 50 percent results in instability [10]. These findings agree with the present results of pronounced increase in motion beyond one-half facet resection.

Figure 4 illustrates the superior and inferior intervertebral disc stress alterations with respect to the intact spine under the various iatrogenic conditions. Spinal component stresses represent internal load sharing in the cervical structure. In general, the percentage change in the disc stress (internal response) was higher under all loading modes compared to the angular rotation (external response). The increase in the inferior disc stress was the highest under flexion compared to the other loading modes. Such increase of disc stress emphasizes the transfer of the internal resisting load vector from the posterior to the anterior region of the spine. These data concur with literature emphasizing the destabilizing effects of laminectomy in terms of shifting the load to the anterior components [5]. This observation may support the theory that cervical laminectomy accentuates degenerative changes in the intervertebral disc structures [6,31]. Furthermore, like the angular rotation, the inferior disc stress also demonstrated a considerable change secondary to one-half facetectomy combined with laminectomy. The higher inferior disc stress noted for facet resection of more than 50 percent emphasizes the importance of integrity of the facet for intervertebral strength. If clinical conditions require wider facet resection (i.e., more than 50%), the present data suggests that it may be necessary to use fixation techniques to restore the strength and stability of the cervical spine [4].

4. Conclusion

Laminectomy with partial or full facet resection alters the structural integrity of the spine affecting the motion of the intervertebral joint, and induces additional loads to the remaining components of the spine [17]. The present FE approach revealed that laminectomy considerably altered the angular motion and the disc stress under flexion compared to all other loading modes [15]. Facetectomy increased the angular motion and the inferior disc stress notably under flexion but did not affect the adjacent superior disc stress. Facet resection of more than 50 percent caused significant increases in angular rotation and intervertebral disc stresses. It should be emphasized that these responses cannot be obtained by any experimental study and consequently, the present 3-D anatomically accurate FE model offers an additional facet to better understand the effects of surgical alterations on the biomechanics of cervical spine [14,17]. These findings suggest an accentuated role for the internal biomechanical variables to be more sensitive and better characterize the response of the cervical spine under iatrogenically altered conditions. This increased stress magnitude in the intervertebral disc anulus may lead to degenerative changes at the facetectomized spinal level. It is well known that bone remodeling is the response of bone tissue to mechanical stress. Soft tissues may also change structural properties as an adaptation to a higher stress environment. The above internal biomechanical response variations in terms of the soft and hard tissue stresses before and after facetectomy may better reveal the true nature of the accelerated degenerative process in the cervical column. Clinically, hypermobility may lead to spinal curvature alterations following laminectomy, and the excessive disc loading represented by accentuated levels in the disc stresses may accelerate the degenerative changes in the disc. This may result in further formation of osteophytes and a progressive deterioration in the biomechanical load carrying capacity of the human cervical spine. The finite element model stress analysis response therefore, provides an additional understanding of the extrinsic as well as intrinsic responses.

References

[1] Scoville WB. Cervical spondylosis treated by bilateral facetectomy and laminectomy. *J Neurosurg* 1961:18: 423-428.

[2] Hirabayashi K, Satomi K. Expansive open-door laminoplasty for cervical spinal stenotic myelopathy. *Spine* 1983:8: 693-699.

[3] Allen BJ, Tencer AF, Ferguson RL. The biomechanics of decompressive laminectomy. *Spine* 1987:12: 803-808.

[4] Cusick JF, Yoganandan N, Pintar FA, Myklebust JB, Hussain H. Biomechanics of cervical spine facetectomy and fixation techniques. *Spine* 1988:13(7): 808-812.

[5] Cusick JF, Pintar FA, Yoganandan N, Reinartz JM. Biomechanical alterations induced by multilevel cervical laminectomy. *Spine* 1995:20(22): 2393-2399.

[6] Cahill DW, Bellegarrigue R, Ducker TB. Bilateral facet to spinous process fusion: A new technique for posterior spinal fusion after trauma. *Neurosurgery* 1983:13: 1-4.

[7] Callahan RA, Johnson RM, Margolis RN, Keggie KJ, Albright JA, Southwick WO. Cervical facet fusion for control of instability following laminectomy. *J Bone Jt Surg* 1977:59A: 991-1002.

[8] Cattell HS, Clark GL. Cervical kyphosis and instability after multiple laminectomy. *J Bone Jt Surg* 1967:49A: 713-720.

[9] Mikawa Y, Shikata J, Yamamuro T. Spinal deformity and instability after multilevel cervical laminectomy. *Spine* 1987:12: 6-11.

[10] Raynor RB, Pugh J, Shapiro I. Cervical facetectomy and its effect on spine strength. *J Neurosurgery* 1985:63: 278-282.

[11] Yoganandan N, Pintar FA, Maiman DJ, Reinartz J, Sances A Jr, Larson SJ, Cusick JF. Kinematics of the lumbar spine following pedicle screw plate fixation. *Spine* 1993:18(4): 504-512.

[12] Yoganandan N, Maiman DJ, Pintar FA, Bennett GJ, Larson SJ. Biomechanical effects of laminectomy on thoracic spine stability. *Neurosurgery* 1993:32(4): 604-610.

[13] Pintar FA, Cusick JF, Yoganandan N, Reinartz J, Mahadevappa M. Biomechanics of lumbar facetectomy under compression flexion. *Spine* 1992:17(7): 804-810.

[14]. Kumaresan S, Yoganandan N, Pintar F. Finite element analysis of anterior cervical spine interbody fusion. *J Bio-Medical Materials & Engineering* 1997(9): 1-10.

[15] Kumaresan S, Pintar FA, Yoganandan N. Finite element analysis of cervical laminectomy with graded facetectomy. In: *ASME Winter Bioengineering Conference,* 1996, pp 27-28.

[16] Kumaresan S, Yoganandan N, Voo L, Pintar FA, Cusick J. Finite element analysis of cervical laminectomy. In: *11th Annual North American Spine Society*, Vancouver, Canada, 1996, pp 271-272.

[17] Kumaresan S, Yoganandan N, Pintar F, Voo L, Cusick J, Larson S. Finite element modeling of cervical laminectomy with graded facetectomy. *J Spinal Disord* 1997:10(1): 40-47.

[18] Kumaresan S, Yoganandan N, Pintar FA. Adult and pediatric human cervical spine finite element analyses. In: *ASME Summer Bioengineering Conference*, Sun River, OR, 1997, pp 515-516.

[19] Kumaresan S, Yoganandan N, Pintar FA. Nonlinear finite element analysis of human cervical spine facet joint. In: *ASME Summer Bioengineering Conference*, Sun River, OR, 1997, pp 447-448.

[20] Kumaresan S, Yoganandan N, Pintar FA. Importance of material properties on spinal components load sharing. *Mathematical Modelling and Scientific Computing* 1997:8: 6-10.

[21] Kumaresan S, Yoganandan N, Pintar FA. Sensitivity of cervical spine finite element model to material property variations. In: *ASME Winter Bioengineering Conference,* Dallas, TX, November 16-21, 1997.

[22] Yoganandan N, Myklebust JB, Ray G, Sances A Jr. Mathematical and finite element analysis of spinal injuries. *CRC Review Biomed Eng* 1987:15(1): 29-93.

[23] Yoganandan N, Kumaresan S, Voo L, Pintar F. Finite element applications in human cervical spine modeling. *Spine* 1996:21(15): 1824-1834.

[24] Yoganandan N, Kumaresan S, Voo L, Pintar F. Finite element model of the human lower cervical spine. *J Biomech Eng* 1997:119(1): 87-92.

[25] Yoganandan N, Voo L, Pintar FA, Kumaresan S, Cusick JF, Sances A Jr. Finite element analysis of the cervical spine. In: *CDC Injury Prevention Through Biomechanics*, Detroit, MI, 1995, pp 149-155.

[26] Yoganandan N, Kumaresan S, Voo L, Pintar F, Larson S. Finite element modeling of the C4-C6 cervical spine unit. *Med Eng Phy* 1996:18(7): 569-574.

[27] Kumaresan S, Voo LM, Yoganandan N, Pintar FA. Finite element biomechanics of the cervical spine. In: *6th Injury Prevention Through Biomechanics Symposium*, Wayne State University, Detroit, MI, 1996, pp 77-84.

[28] Voo LM, Kumaresan S, Yoganandan N, Pintar FA, Cusick JF. Finite element analysis of cervical facetectomy. *Spine* 1997:22(9): 964-969.

[29] Franklin HS, Hendrik JS, William HB, Joseph MJ. Swan-neck deformity following extensive cervical laminectomy. *J Bone Jt Surg* 1974:56A: 564-580.

[30] Zdeblick TA, Zou D, Warden KE, McCabe R, Kunz D, Vanderby R. Cervical stability after foraminotomy. *J Bone Joint Surgery* 1992:74A(1): 22-27.

[31] Ishida Y, Suzuki K, Ohmori K, Kikata Y, Hattori Y. Critical analysis of extensive cervical laminectomy. *Neurosurgery* 1989:24: 215-222.

Figure Captions

Figure 1: Finite element model of an intact cervical spine (C4-C5-C6 unit).

Figure 2: Finite element model of the cervical spine illustrating laminectomy and bilateral facetectomy.

Figure 3: The change in angular rotation from the intact unit due to laminectomy with graded facetectomies under flexion (FLE), extension (EXT), lateral bending (LB) and axial torsion (AT).

Figure 4: The change in the superior and inferior intervertebral disc stresses from the intact condition due to laminectomy (L) with and without graded facetectomies (25%, 50%, 75% and 100% FR) under flexion, extension, lateral bending and axial torsion.

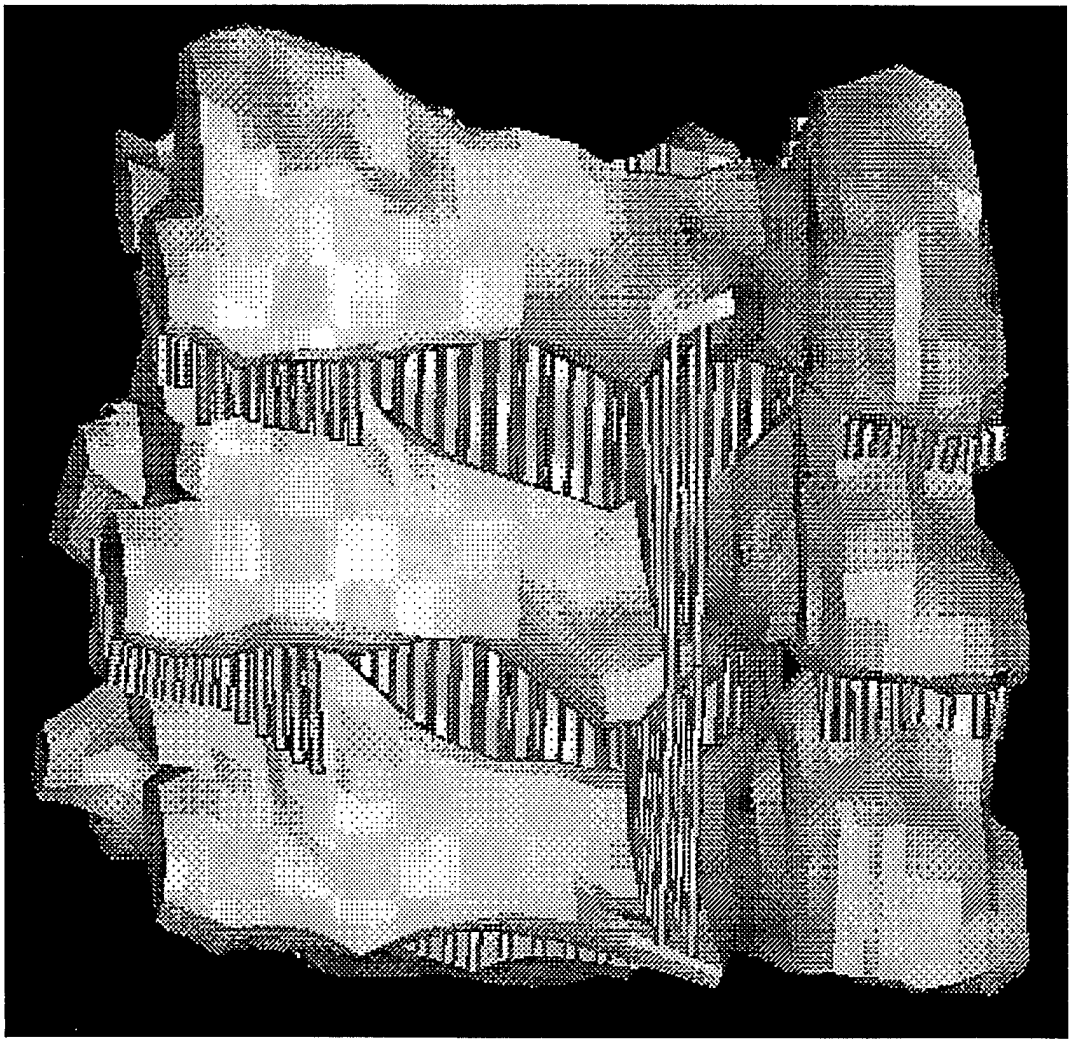

Figure 1: Finite element model of an intact cervical spine (C4-C5-C6 unit)

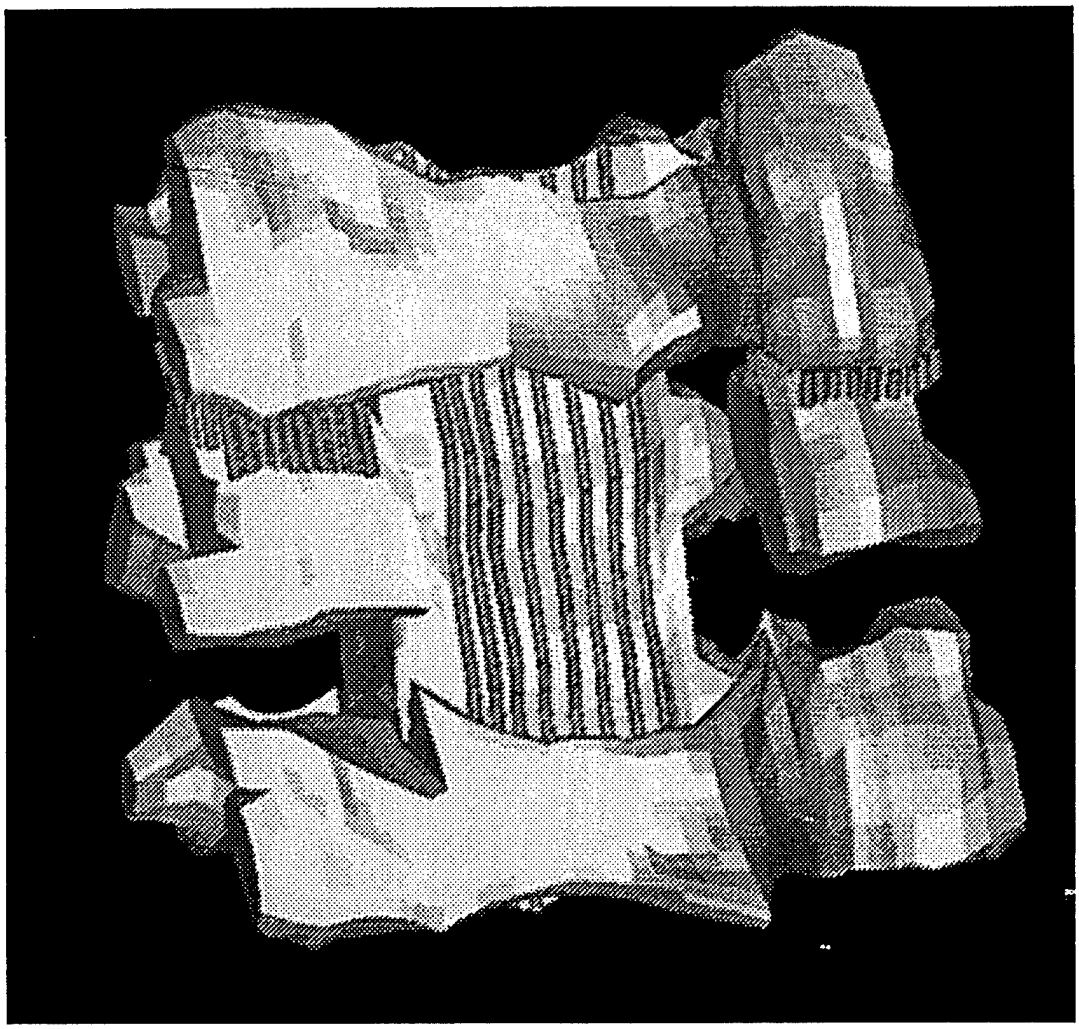

Figure 2: Finite element model of the cervical spine illustrating laminectomy and bilateral facetectomy

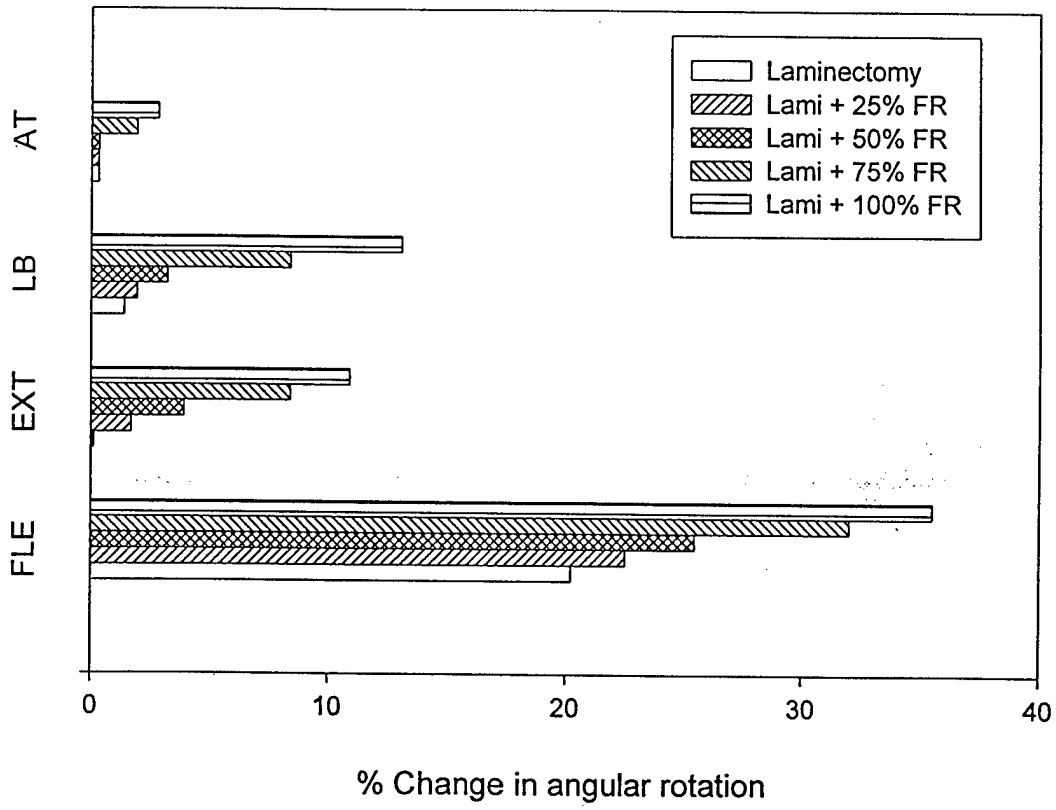

Figure 3: The change in angular rotation from the intact unit due to laminectomy with graded facetectomies under flexion (FLE), extension (EXT), lateral bending (LB), and axial torsion (AT).

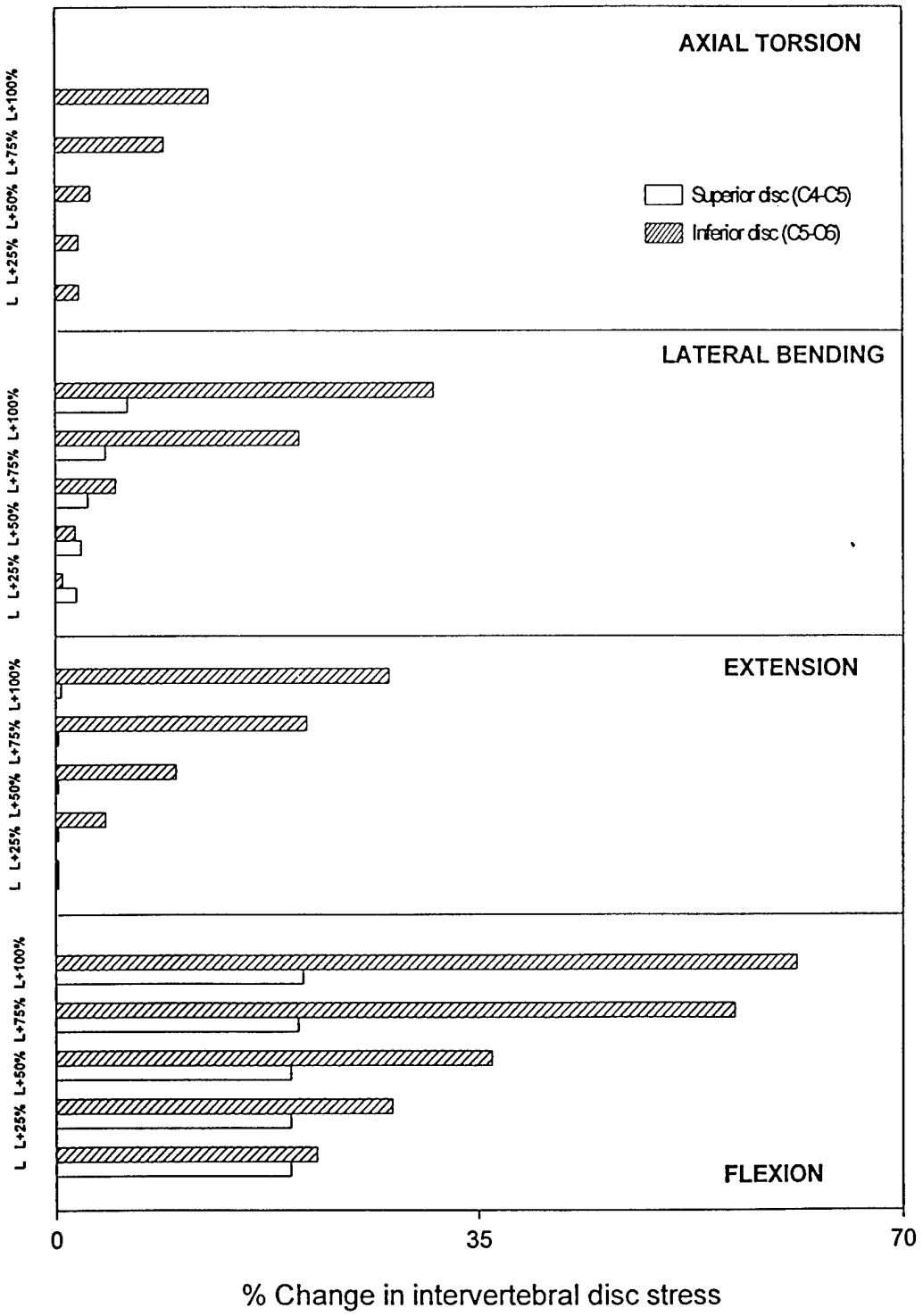

Figure 4: The change in the superior and inferior intervertebral disc stresses from the intact condition due to laminectomy (L) with and without graded facetectomies (25%, 50%, 75% and 100% FR) under flexion, extension, lateral bending, and axial torsion.

PATHOPHYSIOLOGY OF CERVICAL SPONDYLOTIC MYELOPATHY

Joseph F. Cusick

Abstract

A variety of factors have been proposed to explain the pathogenesis and natural history of cervical spondylotic myelopathy. Progressive restriction of the confines of the cervical canal and the resultant spinal cord compression, vascular compromise, motion alterations and spinal cord tethering has been implicated, acting singularly or in combination, as causative mechanisms in the development and progression of the myelopathy. Analysis of the influence of these factors suggests that the mechanical compromise induced by the spondylotic degenerative changes of the cervical spine when coupled with levels of increased flexibility or segmental hypermobility is the predominant event that results in progressive neural compromise. The various anatomical changes in the components of the cervical spine may also present an environment for increasing adverse effects to act upon the spinal cord and nerve roots. In this chapter, these considerations are explored and the relationship to the myelopathy will be described. In these settings the cervical spondylotic myelopathy may not represent a relatively benign disease entity, but a process requiring active intervention.

1. Introduction

Defining the natural history and pathogenesis of cervical spondylotic myelopathy (CSM) will enhance the ability to design effective treatment regimens. The majority of individuals over 50 years of age will demonstrate significant radiological evidence of spondylotic degenerative disease

of the cervical spine, but only a small percentage will develop compromise of underlying neurological structures. Clarification of those individuals at risk for such alterations and the potential for subsequent deterioration therefore, became the predominant issues in the therapeutic decision process. The varying pattern of anatomic alterations in this disease entity results in possible mechanical and structural changes in many vertebral column components initiating with the intervertebral degeneration. Associated slackening of the anulus fibrosis and associated ligamentous structures may result in osteophytosis or relative hypermobility or instability. This disease therefore, sets in motion a series of possible alterations of the cervical vertebral column that may result in compromise of the spinal canal and foramen or motion changes with abnormalities in both translational and angular motions [1-2]. These processes of increasing stiffness, canal compromise or segmental hypermobility may cause adverse forces to act singularly or in combination on the spinal cord, nerve roots and adjoining structures. In contrast to the variable clinical presentation and variety of potential causative factors in CSM, the pattern of histological impairment is surprisingly consistent. The major changes are a consistent demyelination and degeneration in lateral columns, especially the corticospinal tracts and frequent degeneration in the posterior columns, especially the anteromedial portion. There is relative sparing of the anterior spinal tracts. Atrophic alterations of the dorsal and ventral roots and some neurophagia of the anterior horn cells (Figure 1) may also be present [3-7]. These pathological findings were further defined by Ogino et al., who correlated the degree of cord destruction and neurosurgical impairment in the clinical pathological studies of nine patients. In defining the ratio of the anteroposterior and transverse diameters as the compression ratio, these investigators noted that developmental narrowing of the spinal canal with increased transverse cord distortion was the major predicator of disease severity. The most severely affected individuals also were the subjects showing extensive degeneration and infarction of the gray matter with diffuse degeneration of the lateral white matter columns [5]. These authors also verified in their clinicopathological studies the relative sparing of the anterior white matter tracts.

Cervical spondylotic myelopathy therefore, is a multi-factorial process resulting from abnormal stresses imposing on the spinal cord by varying alterations of the spinal column architecture, and the degree and type of these stresses will vary relative to the location of spinal cord compromise, pre-existing size of the spinal column, and the forms of spinal column motion [3,8-10]. The relationship of the specific spinal column abnormality and the biomechanical tolerances of spinal cord to these stresses must be defined to ascertain the most efficacious form of therapy. The individual significance of these factors is not only necessary to determine the need for surgical intervention, but assists in defining the value of specific surgical approaches [11]. The proposal that mechanical compression of the spinal cord is the cause of CSM has been proposed by many investigators. The definition of critical canal size and the corresponding possible effects on neural structures have implications in CSM. Normal cervical spinal canal anteroposterior dimensions have been documented to range from 16 to 18 mm at C3-C7 and spinal cord diameter to range from 8.5 to 11.5 mm [12]. The capacity of the spinal canal decreases at lower cervical regions with the spinal cord filling approximately 50 percent of the canal at the C1 level and 75 percent at the C6 level [2,10,13-15]. Adams and Logue in 1971, found an average canal diameter of 11.8 mm in CSM patients, and Wolf et al., found that an anteroposterior (A-P) diameter of less than 10 mm was likely to be associated with myelopathy [16-17]. Kallen analyzed canal dimensions by comparing developmental A-P diameter (DAD) and spondylotic A-P diameter (SAD) with the findings that patients with increased segmental stenotic index (DAD - SAD = SSI) were likely to develop myelopathy [18]. This contention was supported by Nurick and implicated pre-disposition of patients with congenitally shallow canals to develop myelopathy. Edwards and LaRocca indicated that patients with normal A-P diameters of the canal had a longer pre-diagnostic course [2,19-20]. These latter investigators emphasized Ogino's observations of the importance of increased transverse cord diameter resulting from decreasing sagittal A-P canal size, and found irreversible neurological injury when critical levels of this ratio were exceeded. This recognition of the potential importance of spinal cord distortion in the transverse plane will have possible importance in the development of vascular compromise of the spinal cord. All of these studies however, share the quality of being static evaluations, and it is not an unusual clinical finding to

have severe cervical spinal canal stenosis of less than 10 mm without any evidence of myelopathy. In this regard, it has been clearly shown that patients with congenitally narrow canals are predisposed to progressive CSM. It would be fair to acknowledge however, that compromise of the cervical spinal canal is an important component in the pathogenesis of CSM, but as a singular entity may not explain fully the causative mechanisms. In this regard, Barnes and Saunders have argued that hypermobility or subluxation may be a major contributing factor in patients manifesting severe disability in CSM [21]. In that study, minimum canal size and degree of subluxation or amount of osteophytosis had no predictive value, but the range of head and neck movement did differentiate between those who deteriorated and those who remained unchanged resulting from an advanced disease process. Jeffreys however, noted that subluxation was an important factor in only 2.9 percent of his patients, whereas Nurick noted this abnormality in 28.7 percent [22,20]. Jeffreys suggested that this difference in his series of patients was indicative of spinal column rigidity in a retrospective series of conservatively managed patients.

The importance of vascular factors in the pathogenesis of CSM has been a controversial subject over the last 25 years. Mair and Druckman initiated much of the debate with their hypothesis that compression of the anterior spinal artery by spondylotic ridges caused ischemic damage to the anterior two-thirds of the spinal cord [23]. Brain extended the causative factors of spinal cord ischemia in CSM to include compromise of the anterior spinal veins, radicular arteries at the foraminal region, and vertebral artery narrowing as a participant in degenerative changes in the blood vessels in an aging group of patients [8]. Ten years later, Taylor reinforced the probable importance of occlusion of extramedullar vessels in the production of the myelopathy with cervical spondylotic degeneration [24]. Breig et al., in their classic monograph, implicated the stretching and occlusion of intramedullary arteries running in the transverse plane during anterior-posterior compression of the spinal cord [25]. Shimomura et al., in the canine model, showed that anterior spinal artery occlusion resulted in ischemia to the anterior one-third of the spinal cord with relative sparing of the posterior-lateral and posterior regions [26]. These authors implicated the probable importance of surface and intramedullary vessel occlusions rather than the anterior spinal artery compromise as the basis for ischemic changes causing the usual pathological damage found in CSM. Jellinger in an autopsy series (1037 necropsies) found only the rare occurrence of atheroma in intramedullary and radicular vessels, and was unable to implicate arteriosclerotic disease as a probable contributor to CSM [27]. In an extension of previous studies, Hukuda and Wilson noted the additive effects of compression and ischemia in the production of myelopathy and spinal cord damage [28]. In 1973, Gledhill et al., correlated the degree of demyelination with the severity of neurological injury following acute spinal cord compression [29]. The importance of demyelination, rather than gray matter or intramedullary infarction, was further emphasized by Gooding, Wilson et al., who demonstrated severe demyelination, especially in the lateral columns, with combined ischemia (anterior spinal and radicular artery occlusions) and compression [30]. Hoff, in later microangiography studies in the canine model, again demonstrated the additive effects of ischemia and compression [31]. Larson et al., using neurophysiological parameters in the monkey, also verified this association but stressed the comparative importance of mechanical compromise [32]. Doppman, in studies of the effects of segmental epidural balloon compression, reemphasized Breig's observation that flattening of the spinal cord during either posterior or anterior compression caused severe narrowing of the intramedullary arteries (Figure 2) [1].

Summation of these investigations permits certain conclusions. First, anterior spinal artery and radicular artery occlusion do not reproduce the consistent histological pattern of injury demonstrated in the majority of clinicopathological studies in CSM, but the majority of laboratory studies indicate that the effects of ischemia and compression are additive. The blood vessels undergoing the most notable alterations during spinal cord compression are the intramedullary arteries, especially those vessels coursing transversely to the anterior-posterior compression. This latter consideration would also recognize the possible contribution of increasing shear forces acting on the intramedullary vasculature in the more centrally located portions of the spinal cord during compression and bending (Figure 2). Secondly, demyelination rather than axonal damage or gray matter infarction, is the predominant injury, especially in the earlier stages. These findings indicate

a greater susceptibility of the myelin and its supportive cells to mechanical stresses which may be exacerbated by ischemia.

2. Basic Considerations

The degenerative process of cervical spondylosis through acquired narrowing of the spinal canal or segmental hypermobility of the spinal column, either singularly or in combination, may result in injury to the spinal cord or supportive vasculature. Although the vertebrae are rigid structures, the spinal column is a dynamic entity that undergoes changes in configuration during the processes of flexion, extension and lateral bending. These changes have increased importance when associated with compromise of the cross-sectional area of a spinal canal by the spondylotic process, and illustrate the importance of understanding the functional biomechanics of both the spinal column and the spinal cord relative to the disease state of CSM. Numerous investigators have demonstrated that in flexion, the cervical spinal canal is lengthened, and in extension it is shortened [33,25,10,6]. When the cervical spine is placed in flexion, the canal becomes longer at both the anterior and posterior walls, with the posterior vertebral contour becoming convex. It has been estimated that the cervical canal lengthens 2.8 cm from full extension to full flexion, and in both flexion and extension, the largest change in dimension takes place at the posterior wall. During maximal extension, the backward movement of the upper vertebra upon the inclined facet of the lower vertebra may result in laminar impingement and induce further shortening of the canal. The movement of the lamina and the possible enfolding of the ligamentum flavum may contribute to a decrease in the cross-sectional diameter of the canal. During flexion and extension, the relative ranges of motion of specific levels are determined by the geometric design of the bony components, the physical characteristics of the associated ligamentous structures, and the distance from the center of rotation of the cervical spine. The facet joints at the lower cervical levels allow the cervical vertebrae to tilt and slide over the corresponding articular surfaces. Further, the ligaments at these levels are relatively distensible [34]. These factors, together with the distance from the cervical center of rotation, result in increased mobility at these levels [35]. The increased motion accelerates deterioration of the vertebral joint and intervertebral disc with the increased incidence of cervical spondylotic degeneration at the C5-C6 level, corresponding to the more marked range of flexion-extension movement at this interspace. In subsequent discussions of the advisability for certain surgical approaches in the treatment of CSM, the recognition of these increased degenerative changes at the lower cervical segments (C4-C7) with the corresponding increased canal stenosis and the reciprocal potential for increased motion at the upper levels (C1-C4) of the spinal column will be considered [36]. Bohlman reported on the problem of compensatory subluxation in the upper cervical spine adjacent to the stiff spondylotic lower segments [37]. Hayashi et al., in a comparative analysis of the aging cervical spinal column, found increased degeneration with decreased motion at C5-C6 and C6-C7 and corresponding vertebrolisthesis (retrolisthesis) of C3-C4 and C4-C5 [38]. These investigators also noted that a consequence of the aging process was a greater comparative narrowing of the dynamic canal than the static canal.

3. Biomechanical Properties of the Cervical Spinal Cord

The spinal cord participates with the vertebral column in configurational changes relative to alterations in functional positioning, and the susceptibility to injury will vary with specific abnormalities of the vertebral column. The majority of information regarding the physical properties of the spinal cord and related nerve roots, dentate ligaments, pia, and dura mater has its basis in the studies of Breig and co-workers [33,25]. In considering the physical properties of the spinal cord, it is important to note Breig's clarification that the spinal cord is part of a continuous tissue tract originating in the mesencephalon and extending to the point where the nerve roots exit. This structure participates in physical alterations as a whole with the predominant effects occurring

at the local level of distortion. This concept indicates however, that abnormalities influencing the spinal cord may have compounding effects at distant sites along this brain stem-spinal cord tissue tract. In the cadaver preparation, distraction of the spinal cord demonstrates a load displacement curve with two distinct phases. Large initial displacements are accomplished with small amounts of force, demonstrating the elastic qualities of the spinal cord, but these initial stages are followed by an abrupt stiffening in which additional small increments of stretch require larger load levels. These biomechanical findings agree with the physiological evidence obtained in our axial distraction studies, in which initial load levels resulted in mild reversible distortion of axonal conduction until a critical level of stretch was accomplished [39]. At this later stage, additional force resulted in marked deterioration of axonal conduction that was usually irreversible. This situation mirrors a frequent clinical dilemma of distinguishing between physiological (reversible) impairment of axonal conduction or anatomic (irreversible) damage to these neural elements in patients with developing myelopathy. In addition to giving insight into the physical properties of the spinal cord in distraction, Breig demonstrated that the spinal cord does not move in the longitudinal plane, but adapts itself to the length of the spinal canal by plastic deformation [25].

In flexion, the cord elongates with the spinal canal and narrows in anteroposterior diameter. This induces increased axial tension in the axon cylinders of the white matter tracts and lesions of the vertebral canal that compromise cross-sectional area (especially those processes anterior to the spinal cord) which applies further local and generalized increases in axial tension within the spinal cord. Reid, in cadaver dissections, noted the anterior component of the force exerted by the cord and dura undergoing a 3 mm displacement of the neck in flexion, was found to reach 207-275 MPa, whereas with the neck in the neutral position, an anterior pressure of only 14 MPa was exerted on the cord and dura [40]. In contrast to the elongation of the spinal cord during flexion, the spinal cord in extension shortens and increases in anteroposterior diameter with a relative relaxation of the axon cylinders. The corresponding decreased cross-sectional area of the spinal canal occurring from posterior bulging of the anulus, as well as the enfolding of the ligamentum flavum and scaffolding of the lamina in extension, may result in a pincer-like action upon the cord (Figure 2). In this setting, irreversible spinal cord damage becomes more likely when compression exceeds one-third of the normal cord diameter [33,25]. An important consideration in defining the risk for spinal cord compromise is consideration of both the degree and axis of applied forces. Tensile forces applied to the spinal cord in the neutral position will produce a relatively even load distribution across the structure, but if the cord undergoes bending, compressive forces will increase on the concave side causing increasing tensile (stretch) forces on the convex side (Figure 3). Shear forces, in contrast to tensile forces, are maximal towards the center of the spinal cord and act in a perpendicular plane to the tensile forces. The interaction of these three different forces being applied to varying areas of the spinal cord during flexion (bending), indicates the potential for a complex pattern of injury relative to the individual magnitude of each of the stresses and their possible interaction. Variation in injuries therefore, can be anticipated, such as marked increased shear stresses in the central cord during the pincer action compromise of the spinal cord incurred during a sudden forceful hyperextension. This occurrence can be contrasted to an intermittent application of sub-threshold injuries in flexion, causing a potential cumulative effect of posterior and posterior-lateral tensile stresses on the spinal cord during the bending configuration [35].

The role of the dentate ligaments in the transmission of potentially injurious forces on the spinal cord has been controversial. In 1947, Kahn proposed that the dentate ligaments firmly fixed the cord against any anterior compressing lesion and therefore, prevented equal transmission of applied pressures. He charted lines of stress, showing that the maximum burden was incurred by the posterior-lateral region with relative sparing of the anterior columns [14]. Bedford and co-workers later supported this concept and suggested that because of this visual fixation, the cord was vulnerable to abnormal neck movements [41]. Reid's observations during elevation of the cadaver cord led him to postulate that the normal function of the dentate ligaments appears to be the transmission of axial stresses between the cord and dura, rather than provision of a mechanism to hold the cord in any particular dorsal or ventral position [40]. Breig however, demonstrated that the spinal cord does not move in the longitudinal axis, but adapts itself to the length of the spinal canal by plastic deformation. His cadaver studies revealed that in flexion of the spine, the lateral

bands and dentate ligaments are straightened both axially and transversely with slight resultant tension set up in them. This tension, as well as the position of the dural attachment of the dentate ligaments, which is slightly near the ventral and dorsal regions, results in a retaining action by these ligaments [25]. Thus, the cord with the spine in flexion does not yield beyond the middle of the canal. Stoltmann and Blackwood were unable to demonstrate in their cadaver studies, any limitation of movement of the spinal cord by the dentate ligaments in the anterior-posterior direction, and hypothesized that the probable function of the dentate ligaments was to limit the movement of the spinal cord in the longitudinal axis [26]. They used en bloc sections of the cervical and upper thoracic vertebral columns with both posterior and anterior bone removal and subsequent intradural exposure performed in formalin-fixed preparations or the anterior exposure in frozen specimens. The subsequent evaluations of the restrictive action of the dentate ligaments were examined without subjecting the canal to alterations in functional positions.

Experiments in our laboratory using the canine preparations tend to support Breig's observations. Cord-to-cord evoked potentials were used to measure the functional integrity of the spinal cord with the cord in a moderate degree of flexion. A sling was passed about the spinal cord and a force transducer with micrometer drive was used to carry out elevation of the spinal cord and record tension measurements (Figure 4). This study demonstrated that at levels of posterior elevation usually within the confines of the canine canal, the dentate ligaments were the most significant element increasing tension requirements and alterations of the somatosensory-evoked potential [42]. Human cadaver studies also showed an approximate 50 percent reduction of force during posterior elevation after dentatomy. These findings suggest that after dentate ligament section, the applied tension is distributed over a longer segment of the cord with a reduction in the tension and disruption of axonal conduction at the level at which the force was applied. Case studies also indicate that the dentate ligament may undergo individual hypertrophy by the additional formation of collagen as they are exposed to a series of intermittent and elongating tension loads. As the tension strength and tensile rigidity of these structures increase, the amount of elongation developed under subsequent loads of similar magnitude will decrease. Although such alterations occur only with intermittent tension loads, it appears reasonable to assume that the dentate ligaments, in certain instances of cervical spondylosis, undergo stretch hypertrophy resulting from tension occurring intermittently when the cord is in ventral flexion. Recently, a spinal cord model that permits calculation of the pattern of stresses at level of ventral bar formation was compared to the well recognized and previously described topography of neuropathological damage [43]. The results again implicated the potential role of the dentate ligaments in injurious force application to the lateral columns.

4. Conclusion (Pathogenesis)

The majority of clinical studies of the pathogenesis of CSM indicate that mechanical compromise of the spinal cord neural substrate and possible corresponding stretching and narrowing of intramedullary blood vessels are the predominant causative factors. The character and degree of these stresses being applied to the spinal cord are usually exaggerations of the normal biomechanical properties of the spinal canal and spinal cord caused by the degenerative spondylotic process. The effects of these various stresses will depend upon the location (anterior, posterior, lateral) of the spinal canal compromise and the possible coexistence of segmental hypermobility, which may be accentuated by positional (flexion, extension, rotation) movements of the cervical spine. The combined effects of the compressive, tensile and shear forces induced by the spondylotic process with the corresponding alterations of the physical properties of the spinal cord usually exhibit their effects in a subacute manner with each component dependent upon the positional configuration of the spinal canal. The usual temporal sequence of CSM suggests that these stresses act in a sub-threshold and cumulative fashion with the major accentuation of stresses related to increased tensile forces acting on the lateral and posterior aspects of the spinal cord as the canal compromise increases in anterior-posterior restriction [44]. Corresponding transverse

distortion of the spinal cord will further accentuate these tensile stresses in the region of the lateral and posterior columns.

Clinicopathological studies of CSM illustrate a consistent pattern of histological damage, which mainly consists of lateral and posterior white matter tract involvement with varying degrees of gray matter degenerative changes and sparing of the anterior white matter tracts. Laboratory studies that have attempted to replicate these injuries suggest that the abnormal stresses applied to the spinal cord can be exacerbated by corresponding ischemia, but gray matter infarction is a late consequence of the process. The consistent demyelination in the lateral columns unassociated with evidence of severe neuronal injury in the gray matter suggests an early vulnerability of the myelin and its supportive cells, and this relative absence of significant neuronal and axonal destruction indicates a reversibility of this injury. All of these considerations indicate that CSM is a potentially treatable process when relief of the abnormal stresses being placed on the spinal cord and its intramedullary blood vessels can be accomplished before the stresses cause irreversible neural damage. This understanding therefore, of the pathogenesis of CSM is necessary to define the most effective treatment methods.

References

[1] Doppman JL. The mechanism of ischemia in anteroposterior compression of the spinal cord. *Invest Radiol* 1975:10: 543-554.

[2] Edwards WC, LaRocca H. The development segmented sagittal diameter of the cervical spinal cord in patients with cervical spondylosis. *Spine* 1983:8: 20-27.

[3] Braakman R. Management of cervical spondylotic myelopathy and radiculopathy. *J Neurol Neurosurg Psychiatry* 1994:57: 257-263.

[4] Ogino H, Tada K, Okada K, Yonenobu K, Yamamoto T, Ono K, Namiki H. Canal diameter, anteroposterior compression ratio, and spondylotic myelopathy of the cervical spine. *Spine* 1983:8: 1-15.

[5] Ono K, Ota H, Tada K, Yamamoto T. Cervical myelopathy secondary to multiple spondylotic protrusions: A clinico-pathologic study. *Spine* 1977:2: 109-125.

[6] Penning L. *Functional Pathology of the Cervical Spine.* Williams and Wilkins, Baltimore, MD, 1968.

[7] Wilkinson M. *Cervical Spondylosis. Its Early Diagnosis and Treatment.* WB Saunders, Philadelphia, PA, 1971: 175 pp.

[8] Brain R. Cervical spondylosis. *Ann Int Med* 1954:41: 12-180.

[9] Cusick JF. Pathophysiology and treatment of cervical spondylotic myelopathy. *Clin Neurosurg* 1991:37: 661-681.

[10] Ehni G. *Cervical Arthrosis. Diseases of the Cervical Motion Segments.* Year Book Medical, Chicago, IL, 1984: 258 pp.

[11] Gonzalez-Feria L, Peraita-Peraita P. Cervical spondylotic myelopathy: A cooperative study. *Clin Neurol Neurosurg* 1975:1: 19-26.

[12] Burrows HR. The sagittal diameter of the spinal canal in cervical spondylosis. *Clin Radiol* 1963:14: 77-86.

[13] Hashimoto I, Tak YK. The true sagittal diameter of the cervical spinal canal and its diagnostic significance in cervical myelopathy. *J Neurosurg* 1977:47: 912-916.

[14] Kahn EA. The role of the dentate ligaments in spinal cord compression and the syndrome of lateral sclerosis. *J Neurosurg* 1947:4: 191-199.

[15] Payne EE, Spillane JD. The cervical spine: An anatomico-pathologic study of 70 patients. *Brain* 1957:70: 557-596.

[16] Adams CBT, Logue V. Studies in cervical spondylotic myelopathy. II. The movement and contour of the spine in relation to the neural complications of cervical spondylosis. *Brain* 1971:94: 569.

[17] Wolf BS, Khilnani M, Malis L. The sagittal diameter of the bony cervical spinal canal and its significance in cervical spondylosis. *J Mount Sinai Hospital* 1956:23: 283-292.

[18] Kallen F, Simmons EH, Marzo JM. Recognition of cervical spondylotic myelopathy using plain lateral x-rays. Thesis, Department of Anatomical Sciences and Orthopaedics, School of Medicine, State University of New York at Buffalo, Buffalo, NY, 1986.

[19] Mann KS, Khosla VK, Gulati DR. Cervical spondylotic myelopathy treated by single-stage multilevel anterior decompression. A Prospective study. *J Neurosurg* 1984:60: 81-87.
[20] Nurick S. The natural history and the results of surgical treatment of the spinal cord disorder associated with cervical spondylosis. *Brain* 1972:95: 101-108.
[21] Barnes MP, Saunders M. The effect of cervical mobility on the natural history of cervical spondylotic myelopathy. *J Neurol Neurosurg Psychiatry* 1984:47: 17.
[22] Jeffreys RV. The surgical treatment of cervical myelopathy due to spondylosis and disc degeneration. *J Neurol Neurosurg Psychiatry* 1986:49: 353-361.
[23] Mair WGP. Druckman R. The pathology of spinal cord lesions and their relation to the clinical features in protrusions of cervical intervertebral discs. *Brain* 1953:76: 70-91.
[24] Taylor AR. Vascular factors in the myelopathy associated with cervical spondylosis. *Neurology* 1964:14: 62-65.
[25] Breig A, Turnbull IM, Hassler O. Effects of mechanical stresses on the spinal cord in cervical spondylosis: A study of fresh cadaver material. *J Neurosurg* 1966:25: 45-56.
[26] Shimomura Y, Hukuda S, Mizuno S. Experimental study of ischemic damage to the cervical spinal cord. *J Neurosurg* 1968:28: 565-581.
[27] Jellinger K. Spinal cord arteriosclerosis and progressive vascular myelopathy. *J Neurol Neurosurg Psychiatry* 1967:30: 195-206.
[28] Hukuda S, Wilson CB. Experimental cervical myelopathy: Effects of compression and ischemia on the canine cervical cord. *J Neurosurg* 1972:37: 631-652.
[29] Gledhill RF, Harrison BM, McDonald NI. Demyelination and remyelination after acute spinal cord compression. *Exp Neurol* 1973:38: 472-475.
[30] Gooding MR, Wilson CB, Hoff JT. Experimental cervical myelopathy: Effects of ischemia and compression of the canine cervical spinal cord. *J Neurosurg* 1975:43: 9-17.
[31] Hoff J, Nishimura M, Pitts L, Vilnis V, Turek K, Lagger R. The role of ischemia in the pathogenesis of cervical spondylotic myelopathy: A review and new microangiographic evidence. *Spine* 1977:2: 100-108.
[32] Larson SJ, Walsh PR, Sances A Jr, Cusick JF. Evoked potentials in experimented myelopathy. *Spine* 1980:5(4): 299-302.
[33] Breig A. *Biomechanics of the Central Nervous System.* Year Book Medical, Chicago, IL, 1960: 187 pp.
[34] Myklebust JB, Pintar FA, Yoganandan N, Cusick JF. Tensile strength of spinal ligaments. *Spine* 1988:13(5): 526-531.
[35] Panjabi MM, White AA III. Basic biomechanics of the spine. *Neurosurgery* 1980:7: 76-93.
[36] Cusick JF, Steiner RE, Berns T. Total stabilization of the cervical spine in patients with cervical spondylotic myelopathy. *Neurosurgery* 1986:18: 491-495.
[37] Bohlman HH. Cervical spondylosis with moderate to severe myelopathy: A report of seventeen cases treated by Robinson anterior cervical discectomy and fusion. *Spine* 1977:2: 151-161.
[38] Hayashi H, Okada K, Hamada M, Tada K, Ueno R. Etiologic factors of myelopathy. A radiographic evaluation of the aging changes in the cervical spine. *Clin Orthop* 1987:214: 200-209.
[39] Cusick JF, Myklebust J, Zyvoloski M, et al. Effects of vertebral column distraction in the monkey. *J Neurosurg* 1982:57: 651-659.
[40] Reid JD. Effects of flexion-extension movements of the head and spine upon the spinal cord and nerve roots. *J Neurol Neurosurg Psychiatry* 1960:23: 214-221.
[41] Bedford PD, Bosanquist FD, Russell WR. Degeneration of the spinal cord associated with cervical spondylosis. *Lancet* 1952:2: 55-57.
[42] Cusick JF, Ackmann, JJ, Larson SJ. Mechanical and physiological effects of dentatotomy. *J Neurosurg* 1977:46: 767-775.
[43] Levine DH. Pathogenesis of cervical spondylotic myelopathy. *J Neurol Neurosurg Psychiatry* 1997:62: 334-340.
[44] Turnbull IM. Microvasculature of the human spinal cord. *J Neurosurg* 1971:35: 141-147.

Figure Captions

Figure 1: A compendium illustration derived from clinicopathological studies showing the selective areas of degenerative changes in the spinal cord.

Figure 2: a) Illustration demonstrating the effects of anterior compression during flexion with corresponding narrowing of the intramedullary arteries in the transverse plane as the transverse diameter of the spinal cord increases. b) Similar illustration demonstrating the "pincer" effect of forces during extension with increased shear stresses acting on the more centrally located vessels.

Figure 3: Cord-to-cord and sensorimotor corter (SMC) to conus medullaris (CM) evoked responses during application of an increasing axial distractive load in the monkey. Both responses, except for some temporal dispersion during load application, remain intact until a critical level of sustained load results in sudden and almost complete loss of these conductive responses through the posterior and posterior-lateral white matter tracts.

Figure 4: Illustrations depicting the relative levels of increased local and regional stresses applied on the cord by an anterior force and the limitation in posterior migration imposed by the dentate ligaments.

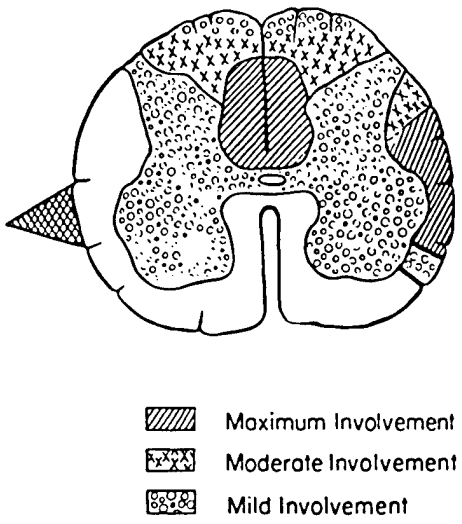

Figure 1: A compendium illustration derived from clinicopathological studies showing the selective areas of degenerative changes in the spinal cord.

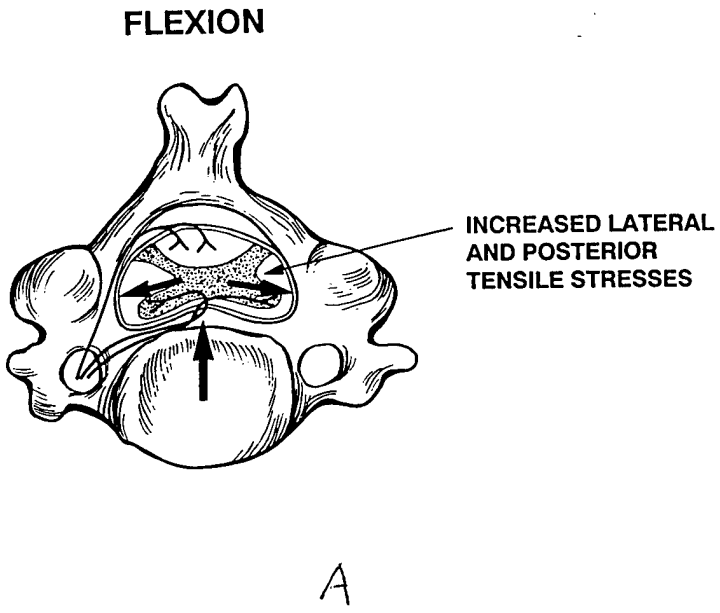

Figure 2: A) Illustration demonstrating the effects of anterior compression during flexion with corresponding narrowing of the intramedullary arteries in the transverse plane as the transverse diameter of the spinal cord increases. B) Similar illustration demonstrating the "pincer" effect of forces during extension with increased shear stresses acting on the more centrally located vessels.

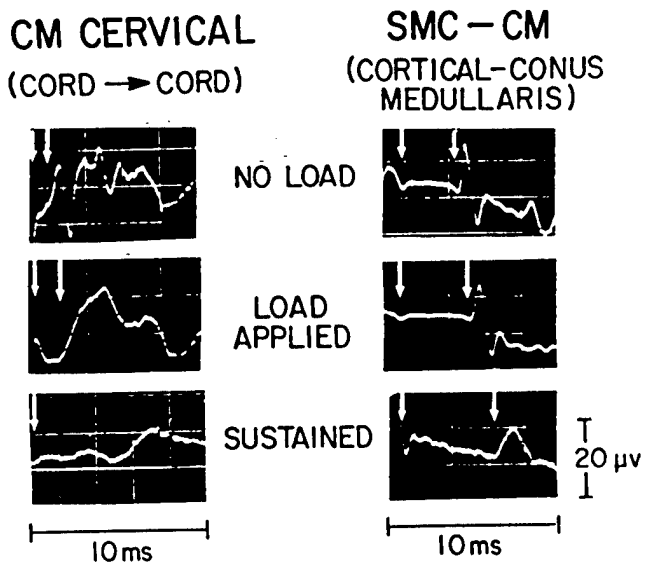

Figure 3: Cord-to-cord and sensorimotor corter (SMC) to conus medullaris (CM) evoked responses during application of an increasing axial distractive load in the monkey. Both responses, except for some temporal dispersion during load application, remain intact until a critical level of sustained load results in sudden and almost complete loss of these conductive responses through the posterior and posterior-lateral white matter tracts.

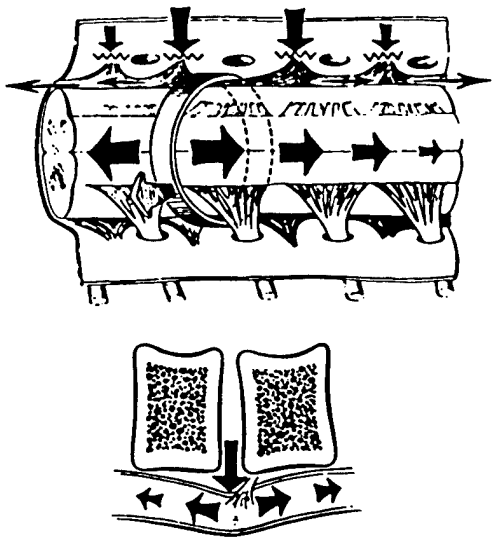

Figure 4: Illustrations depicting the relative levels of increased local and regional stresses applied on the cord by an anterior force and the limitation in posterior migration imposed by the dentate ligaments.

HEAD AND NECK INJURY ISSUES IN NAVAL AVIATION

John J. Quartuccio, Phillip E. Whitley

Abstract

Head and neck injury can occur to naval aviators during missions employing maneuvering accelerations, ejection from fighter/attack aircraft, and mishaps in helicopter crashes. The risk of head and neck injury in naval aviation is increased by wearing helmet mounted mission enhancement devices which have poor centers of gravity and excessive weight, and by the influx of smaller anthropometry aviators (male and female) without concomitant decrease in added head weight or reduction of acceleration forces. The lack of environment specific injury and design criteria make the task of designing a safe system difficult. These issues are discussed in this chapter.

1. Introduction

Prevention and reduction of severity of head and neck injuries are of primary importance in life support and protection of naval aviators. While the wearing of a helmet protects from a variety of focal head injuries, facial impact and neck injuries remain as unprotected problem areas. Additionally, the occurrence of diffuse axonal injury is not known and probably lost in reports due to vague descriptions of the post-traumatic state. The areas where head and neck injuries primarily generate are during fighter/attack combat missions involving high sustained acceleration, ejection

from fighter aircraft, and crashes in crashworthy aircraft such as helicopters. With these environments being normally quite severe, the added complications of head-worn systems for mission enhancement (e.g., night vision goggles) and the expansion of the aviator population to include smaller occupants, male and female, further complicate an already difficult system design task. This chapter will discuss these injury environments, the incidence and severity of head and neck injuries, and especially difficult head and neck injury issues encountered in naval aviation.

2. Neck Injury During Maneuvering Acceleration

Neck injury during normal mission operations has been reported during sustained acceleration operations for fighter aircraft [1-5]. The primary aircraft acceleration of interest in this environment is +Gz. This nomenclature for the acceleration vector directed head-to-toe, +Gz, is standard in this area of research and will be used throughout. Acceleration in the +Gz direction is consistent with ejection from fixed wing aircraft and vertical crash of rotary wing aircraft. This acceleration vector directly increases the loading of the spine (transmission of forces) due to the mass the head, any item worn on the head, as well as the mass of the neck. Air crew routinely wear a helmet to protect from direct impact and to serve as a mounting platform for communications and an oxygen mask. The weight of a typical helmet configuration is 1.6 to 1.8 kg. Items such as night vision goggles and chemical defense masks may also be worn as the mission dictates, adding additional weight. The fighter combat mission requires that out-of-the-cockpit vision be maintained at all times to either visually acquire a target or to avoid becoming a target. Forward and rearward vision are crucial with head and neck motion being extreme at times. Side-to-side axial head and neck rotation as well as looking rearward over the shoulder either right or left are routine. The air crew is restrained to the ejection seat at the shoulders which impedes body position for maximum rearward vision. This rearward vision is then achieved by forcible head rotation to the desired location plus pushing off with the opposite side hand to gain a little more visual angle.

The acceleration domain for various fighter aircraft is shown in Table 1 [6]. These data were taken from air combat maneuvering training ranges. While a small amount of time is spent at high acceleration, the predominance of time is spent at lower levels. The ranges of maximum onset rates for the USAF data, shown for comparison, were from 1.1 to 2.1 G/sec while the average maximum onset rate for the USN data was 3.1 G/sec. These measured data are far below the capabilities of the aircraft. For example, an F/A-18 can achieve 18 G/sec onset rates. The time histories of acceleration exposure can be complex and unpredictable. Figure 1 shows the acceleration profile for a fighter avoiding a surface-to-air missile [7]. While the acceleration levels are not high, only +6.2 Gz, the total duration was 5 minutes. This type of exposure can be extremely fatiguing physically as well as mentally. The pilot is in control of the aircraft and will have a good idea of the onset and level of acceleration. Still many pilots are actively rotating their head and neck during the acceleration event to set-up the next maneuver. The "back-seater", some aircraft have two crew members, does not generally know the onset and level of acceleration. The back seat air crew member can be caught completely unaware of maneuvers with his head and neck unprepared or in poor position. The combination of possibly long mission duration which cause baseline neck muscle fatigue, excessive head and neck motion during acceleration, added head weight due to helmets, +Gz load, as well as possibly high G onset rates are contributing occupational stresses to the potential for neck injury.

Table 1: Time Duration of Acceleration Exposures During Air Combat Training

G Level	Average G-Level Duration (sec)			
	USAF Nellis AFB[1]			USN Oceanana[2]
	F-4	F-15	F-16	F-14/F-16N
5 G	13	22	20	14
6 G	1.2	8.4	7.8	6.1
7 G	0	1.3	2.0	2.2
8 G	0	0.01	0.15	0.58
9 G	0	0	0	0.06
Average G*	6	6.8	7.1	7.0
Peak G	6.8	8.2	8.4	9.0
Average Sortie Duration (sec)	178	144	160	230

*: - Weighted time series average
1: - Gillingham
2: - Whitley

2.1 Injury Data

The injury surveys performed to date have spanned the US Navy, Air Force, as well as foreign air forces. Perhaps the first published neck injury during aerial combat was suffered by a Norwegian Air Force flight surgeon who was seated in the back seat of an F-16B [1]. The flight surgeon was looking over his shoulder to visually acquire the target when the pilot of the aircraft performed an abrupt climbing turn of the F-16B to +8 Gz. This maneuver caught the flight surgeon completely unaware which resulted in his head being thrust between his knees. Upon return from flight, the flight surgeon complained of neck pain and nausea. The muscles of the neck and shoulders were tightly contracted. An area of pain was found between C5 and C6 with a degree of hypermobility suggesting a C5-C6 subluxation. Further x-ray assessment revealed a possible wedge compression fracture of C6. This case report led the way to further analysis. Vanderbeek in a questionnaire study of F-5, F-15 and F-16 pilots found that over a three month period, nine percent reported major injury (injury severe enough to impede further flying until recovery), and 42 percent suffered minor injury [5]. A marked increase in major injury from about five percent to 13 percent was incurred with increased aircraft capability when the F-16 is compared to the F-15 and F-5. The percentage for minor injuries increased from 27 percent to 46 percent and 45 percent when the F-5 was compared to the F-15 and F-16, respectively. An age related two-fold increase (6-7% compared to 15%) in major injury was seen between either the 20-29 or 30-34 years as compared to the 35 years and older age group. No difference was noted on minor injury rate across age. A US Navy survey found that in a group of 148 F/A-18, A-7, and A-4 pilots, 60 percent reported neck pain during flight while eight percent were temporarily removed from flight status [3]. Again, the highest performance aircraft, the F/A-18 had the largest percentage of neck pain reports with the largest percentage of reports of mission impairment. A Belgian survey of their F-16 pilots revealed 50 percent reported neck pain, but no serious structural injuries were reported [2]. Mission impairment was also noted.

A case report study on diagnosed neck injuries during aerial combat maneuver training in F-15 and F-16 aircraft helps to delineate the involved mechanism [4]. In eight case studies, the

types of injuries reported were two cervical vertebrae compression fractures, a spinous process fracture, an interspinous ligament tear, a nerve injury affecting the right myofacial nerve, and two nucleus pulposus herniations. Two factors were apparent from this case study. The first factor is that the injuries were predominantly in the lower cervical vertebrae C5-C7, and the second factor is that some injured pilots either had their heads in a lateral position (looking right or left with chin also facing right or left) or were axially rotating their heads under acceleration from one lateral position to another. These injuries can be attributed to the total load on the lower cervical vertebrae, the moment of the center of gravity of that total load with respect to the point of injury, and lastly to the potential for stress concentration by lateral rotation of head and neck.

2.2 *Analysis of Factors Contributing to Neck Injury*

Operational neck injury data indicates four origins of neck injury. First, neck injury related to neck muscle strain, the total weight of the head and any head-mounted system represents the mass that must be held in place about the occipital condyles. The head is held in an upright position so the eyes can acquire the target. When the weight increases as a function of acceleration, neck strain increases. As the length and numbers of engagements increase, fatigue increases which contributes to the total injury potential. Neck strengthening and flexibility exercises would aid the neck muscles in coping with the acceleration stress. Survey studies have shown a decrease in neck strain reports for pilots who perform any type of strength training [8]. Decreasing the weight of any head-mounted system would also help. Increasing the strength of the neck muscles has the additional problem however, of increasing the pressure on the intervertebral discs. Second, neck injury related to a herniated nucleus pulposus is a direct result of chronic exposure to acceleration. When a pilot fights to keep the head erect, extreme neck muscle force is required which in turn creates compressive forces on the cervical vertebrae and the intervertebral discs. Decreasing the loading of the disc by helmet system weight reduction would help reduce this risk. Imposing longer periods of rest between flights would also allow time for the mechanical properties of the disc to return to normal. The third and fourth origins of neck injury involve cervical vertebrae fractures. The first origin of cervical vertebrae fractures is related to the fact that pilots are constantly searching the sky for the target even at high acceleration. The rearward view is especially difficult due to the fact that the ejection seat has a head rest that is essential for ejection. When the pilot at high acceleration axially rotates the head to acquire the target, the normal load distribution is disrupted which leads to stress concentration at locations on the vertebrae susceptible to injury. The second origin of cervical vertebrae fractures comes from the rapid neck flexion induced by a high G onset to a poorly positioned, unprepared individual crew member.

3. Injury During Ejection From High Performance Aircraft

3.1 *Ejection Sequence*

The ejection sequence can be broken down into the following general phases. The air crew initiates ejection by forcibly pulling the ejection handle; the body position is critical in reducing risk to the air crew (initiation phase). After initiation, the ejection seat is accelerated up the ejection seat rails by a pyrotechnic charge (catapult phase). As the seat separates from the rails, the seat transitions from translating along a fixed orientation to free stream dynamics. The seat will rotate relative to the aircraft due to the balance of aerodynamic and inertial loading. At approximately the same time, the seat rocket motor initiates automatically and provides further clearance away from the aircraft and ground (rocket motor phase). After the rocket motor has fired and depending upon altitude and air speed, the seat typically activates a drogue parachute to slow the seat down to the point where seat-man separation and parachute deployment can occur (drogue phase). Seat-man separation is accomplished by the initiation of cartridge-actuated devices to free the occupant from the seat restraint attachment points. At seat-man separation, parachute

deployment commences. Upon inflation of the parachute, the occupant is removed from the seat (seat-man separation phase). After which, the empty seat falls freely to the ground. As the parachute deploys, the occupant is ideally aligned with the parachute risers however, in many conditions the orientation of the occupant relative to the wind stream has had drastic effects on the loading applied to the body. When the canopy of the parachute inflates, the risers transmit the deceleration forces to the occupant (parachute recovery phase). Once under a full canopy the occupant descends to the ground, beginning survival skills until rescued.

3.2 Head Injury

The head should be protected by a helmet through the catapult phase. If the air crew ejects through the aircraft canopy, ideally, any contact with the canopy is with previously fractured glass. If canopy fracture has not taken place, then the head impact has a potential to cause head and neck injury. However, during high-speed ejection, the helmet can be extracted by the windblast forces. If the helmet is to stay on, then proper helmet fit is essential. The helmet is needed throughout the ejection process to reduce the injury risk from riser slap to the head; however, helmet retention may also induce high tension and shear loads at high ejection air speeds. Unless the seat system reduces the loads applied to the head, retaining the helmet in this case may actually induce injury.

3.3 Neck Injury

Because the catapult phase was historically high in vertical axis acceleration and onset rate, compression fractures of the lumbar and thoracic vertebrae plus disc herniation in these areas were likely during ejection. Over the years, ejection seat performance has improved, and injury potential during the catapult phase has decreased for the thoracic and lumbar areas. The cervical vertebrae were also injured during early ejection seats and remain a concern for modern seats. Guill et al., in a study of the causal factors of neck injury during ejection from Navy aircraft, outlined several driving forces required to induce neck injuries during ejection [9]. Inertial forces before, during or after ejection; poor cervical alignment; windblast effects on head aerodynamic lifting, seat instability and the forces generated during parachute riser deployment and parachute canopy inflation; and system malfunction contribute to the complexity of this event and the difficulty in placing the injury during a particular point during ejection. The neck injury rate during the reported period was 12 percent of which approximately 10 percent were "minor" and two percent were "major". The minor injuries were sprains and strains and the major injuries were fractures of predominantly C2, C5 and C6 cervical vertebrae. Some cervical distractions with accompanying ligament damage of predominantly the upper cervical vertebrae were noted. With the introduction of mission enhancing head-mounted systems, the potential for neck injury will increase from increased head born weight. The potential for neck injury during windblast and parachute opening has only just begun to be studied through testing and computer modeling, but indications are that the heavier system may have an even greater injury potential during parachute opening. Ideally, if the air crew ejects through the canopy any contact with the canopy is with previously fractured glass. If this is not the case, then head impact has a potential to cause severe neck injury. The angle of head impact can determine severity of neck injury.

4. Injury During Helicopter Crash

4.1 Crash Sequence

Helicopter platforms, to widely varying degrees, incorporate a level of crashworthiness by design. [10,11]. When a helicopter crashes in a nominal "belly first" configuration, the landing gear first compress to failure. Once the landing gear has failed, the air frame structure crushes. This force transmitted to the floor of the cockpit and cabin causes the floor and other structures to deform and transmit the loading to the seat assembly. Some helicopter platforms utilize air crew

seats equipped with energy absorbing technologies which attenuate the force and thereby limit the resulting acceleration (on the order of 15 Gz) to be transmitted to the occupant. The seat strokes and the occupant lags the seat in this event. The stroking distance of the seat is limited, and if this distance is fully utilized with remaining relative velocity of the seat to the aircraft, the seat will experience excessive acceleration loading when contacting a hard stop of the system. This loading is translated to the occupant. The force is transmitted up the spine to the head and accounts for the significant concern over lumbar and thoracic vertebrae fracture. Limitations on the allowable loads have been dictated by the Eiband Curves, but a lumbar compressive load limit of 6670 N has been suggested as the maximum allowable in civil aircraft which would correspond to nine percent probability of detectable spinal column injury [12]. The crash event is not however, limited only to the vertical axis. The horizontal and lateral crash loads can be extreme. Most commonly, the horizontal loads are of concern. Once the occupant bottoms out, the occupant begins pitching forward in the seat. With the restraint systems used, typically a five-point restraint, forward movement occurs due in part to the stretch of the webbing material. Once this stretch is complete, the occupant's thorax is abruptly halted, but the head and neck continue to translate and rotate. This motion of the head and neck results in cervical tension and shear that approaches and can exceed suggested neck distraction limits [13]. Chin-to-chest contact as well as head contact with the cabin structures, sighting systems and flight controls are also a hazard. De-lethalization of the cockpit is a major concern. Application of inflatable restraint systems provides some measure of limitation of body excursion and could provide some head support. Airbags have greatly reduced catastrophic injury in automobiles. Implementation of airbag systems in military helicopter crew stations is just underway and may also provide protection. As is seen in automotive crashes, contact of the expanding airbag with a slightly out-of-position occupant can cause rather than prevent injury. Troops and passengers riding in the helicopter receive some protection during a crash through the troop seats, but they are poorly restrained. Troops or passengers in the cargo area of the helicopter experience the same vertical acceleration threat but the horizontal and vertical loads are more threatening due to the poor restraint. During the period 1972-1981 for Navy and Marine Corps helicopters, 25 percent of the major injuries and fatalities across the board were attributed to crash forces and poor restraint [14].

4.2 Head Injury

The primary head injury modes in a helicopter crash are due to head contact with the crew station or cabin structures, sighting systems and flight controls. In some cases, survivable crashes have recorded fatalities due to the occupant contacting the interior of the aircraft. In a recent study performed by the Navy on the H-53 from 1977 through 1992, the injuries for 86 pilots and co-pilots, 79 crew members, and 124 passengers from survivable, partially survivable, and nonsurvivable mishaps were analyzed [15]. For survivable and partially survivable mishaps, 8.7 percent of pilots and co-pilots, 4.2 percent of crew members, and 8.8 percent of passengers suffered cranial injuries of which 48 percent were fatal. The types of injuries seen were skull fractures (simple, comminuted), avulsion, decapitation and LeFort fractures.

4.3 Neck Injury

The neck injury potential in helicopter crashes is due to force transmission from the vertical acceleration component, extreme head and neck motion which places the neck in hyperflexion and distraction, and neck compression with shear due to head contact with the crew station or cabin structures, sighting systems and flight controls. In the previous study cited for the H-53, for survivable and partially survivable mishaps, 5.4 percent of pilots and co-pilots, 2.5 percent of crew members, and two percent of passengers suffered cranial injuries of which 42 percent were fatal. The types of injuries seen were cervical vertebrae compression fractures, avulsions and distractions. Few, if any, of these crashes involved the use of head-worn mission enhancement devices which would increase the incidence and severity of these crashes for the pilot and co-pilot.

5. Current Concerns in Naval Combat Aviation Head and Neck Injury

5.1 Neck Tension During Ejection Windblast

The primary role of the helmet in ejection is to provide protection from injury. The helmet with its visor and mask provides protection from explosion, fire, birdstrike, shrapnel and loose objects while the air crew is still in the cockpit. During the initial and descent phases of ejection, the helmet with its visor and mask provides a level of protection from fire, loose objects, windblast, rain, thermal exposure, blunt force trauma, abrasions, hypoxia and chemical-biological agent contact. During the parachute landing phase, the helmet protects from blunt force trauma, abrasion, penetration and fire. Even in the survival and rescue phases the helmet provides protection from thermal effects and mishaps during helicopter hoist operations. With all the benefits of the helmet, the retention of this protective device would seem of paramount importance. However, the helmet may not be retained during ejection, depending on ejection air speed. Guill et al., found in their comprehensive study of neck injury during US Navy ejection from 1949 to 1989 that helmets are lost during ejection at a percentage of approximately five percent at the lower air speeds (100-200 KEAS) rising exponentially to approximately 50 percent at 500 KEAS [9]. Of those ejectees losing helmets, 21.7 percent suffered neck injuries while only 10.8 percent of those who retained helmets suffered neck injuries. The difference in injury percentages between those losing and those retaining helmets was most marked at the moderate air speed (200-300 KEAS) which tend to be the most common ejection air speeds. In a recent analysis of USAF and USN ejection data since 1989, Travis noted that the helmet loss rate for USAF and USN was 10.56 percent and 18.65 percent, respectively [16]. For those USAF air crew losing helmets, 26.7 percent resulted in major head injury or fatality while for those retaining helmets no major head injuries or fatalities were recorded. For the Navy, 17 percent of those losing the helmet suffered major or fatal head injury while only one percent of those retaining the helmet had major or fatal head injury. For neck injury in both services no significant difference was found in percentage of air crew with neck injury and retention of the helmet. For both services, the average air speed for those losing the helmet was 262 KTS, and 209 KTS for those retaining the helmet. The average air speed for the major or fatal neck injuries regardless of helmet retention was 448 KTS with a 215 KTS average for no or minor neck injury. The average air speed for major or fatal head injury regardless of helmet retention was 312 KTS with a 213 KTS average for no or minor head injury. The opposing argument is that while the helmet may be necessary, the fact remains that the retention of the helmet comes at the expense of increased tension on the neck. Several studies have demonstrated this effect.

Studies performed by the US Navy have shown significant neck tension during windblast [17]. Neck tension values with the HGU-68/P were as high as 1780 N at 600 KEAS. Additional studies performed on the Zvezda windblast facility in Russia at air speeds above 600 KEAS show even greater tension loads [18]. Using an HGU-55/P and an HGU-68/P a joint team of USAF and USN scientists collected inertial data during windblast exposures up to 708 KEAS. At 708 KEAS with the HGU-68/P neck tension values between 2890 to 3115 N were measured. The HGU-55/P was not retained at high windblast levels while the HGU-68/P was retained. The reason for the HGU-86/P retention was an integrated chin-nape strap. This integrated strap wraps around the occipital area of the head and then under the chin. The tightening-up of the strap caused the entire assembly to tighten around the occipital-chin area giving a good fit. However, such a good fit may be injurious.

5.2 Neck Injury During Parachute Opening Shock

The parachute opening shock concerns are significant issues for the seats that utilize drogue stabilization systems, and are an area of concern for all seats during the opening of the main personnel recovery parachute. The Articulated Total Body Model (ATB) has been used extensively in order to identify potential injury modes of the body when subjected to the opening shock due to stabilization as well as personnel recovery [19]. Typically, the body simulation model requires a

precise description of the seat or body motion. Initial efforts have been conducted using the measured rotational velocity and linear acceleration of the manikin thorax segment to predict the corresponding inertial response of the head and neck segment. For the evaluation of added head mass systems, related parameters such as center of gravity, mass and moments of inertia can be varied independently through simulation. As previously discussed, increases in size, mass and complexity of air crew head-mounted equipment is an ongoing trend. These systems become incorporated by modifying the parameters of the head and helmet, but all loading is transferred to the spine at the occipital condyles. In general, the modes of injury to the head and neck system include excessive acceleration and velocity as well as excessive joint forces and torques. One may expect that increased mass and moments of inertia of the head and helmet system reduces the acceleration and velocity; while the increased mass properties also increase the resulting forces and moments applied to the body joints. The body simulation model enabled these related properties (mass, moments of inertia, center of gravity) to be varied independently and potentially defining a range of values that minimizes the risk to the air crew.

An extensive effort has been developed by the Naval Air Warfare Center in Patuxent River, Maryland to link the ejection seat trajectory computer simulation with the ATB model [20]. The body motion derived from this analysis may then be used for more detailed analysis of the head and neck response. Previously, this type of analysis would have required the use of ejection test data to define the seat motion, and then, predict the body response. In this case, the analysis of the body response is limited to the conditions of the ejection test. These ejection tests are extremely expensive in labor hours, use of an elaborate facility, as well as the expenditure of hardware. Now that the seat and body model are incorporated together, this type of analysis may take into account conditions which were not tested. These conditions include variations in the seat installation, seat type, seat system components, occupant size and shape, and occupant initial orientation. The final result is an analytical method of establishing design parameters to the helmet system manufacturer based on the specific system application. Results have indicated that small variations of these properties induce significantly different results, even affecting the mode of the response, inducing extension versus flexion loading.

5.3 Mission Enhancement Devices

Mission enhancement devices that are worn on the head provide air-to-air and air-to-ground targeting, night vision and flight control information. As the number of features increase, the total weight of the system increases. Earlier systems that provided a number of features in addition to the basic functions of a helmet weighed in excess of 2.72 kg. More modern systems are approaching 2.17 kg or less. While the total weight is important, the major factor in the injury potential is the location of the center of gravity (CG) of the head and helmet system combined. Typically, the CG is placed forward of the occipital condyles and results in high pitch moments about the occipital condyles and C7-T1 during the catapult phase of an ejection which are consistent with cervical hyperflexion injury.

5.4. Female Specific Concerns

Female air crew are currently a part of combat missions. The ejection and crashworthiness design criteria based on a male population will not be applicable to females. Gender differences are probably not a factor for the younger air crew age groups when one examines strength of ligaments, tendons and bone. A review of the literature indicates significantly less mechanical strength for females in several bones tested, but this difference is mostly based on dimensional factors. However, a gender-related difference in trabecular bone strength has been reported. The body dynamic response of females to ejection and crash, and the accompanying injury risk continues to be a critical area. Escape and energy absorption systems were designed for male occupants and their protective capabilities especially for a small occupant are in question. An initial assumption was made in this accommodation problem that same size males and females (height, weight) would be at the same level of spinal injury risk during ejection and crash. Due to recent data using quantitative computed tomography to compare the vertebral size and density of males

and females, this assumption appears to be invalid [21]. In a matched set of males and females, the cross-sectional area of the females was 25 percent less than their male counterparts with no difference in bone density noted. This decrease in spinal load bearing capacity for females places them at higher risk for lumbar vertebral fracture. Vertebral strength actually depends on four factors: vertebral size (height, cross-sectional area), bone density, endplate cortical bone thickness, and trabecular bone architecture [21]. In order to design better escape and crash systems, the differences between male and female vertebral characteristics and loading must be determined in order to assess injury. The muscular strength difference between genders would render females more susceptible to injury for the following reasons. The gender correction factors for strength moments generated about the major joint centers indicate a 50 percent decrease in strength moments for females [22]. The total strength of a joint center is dependent upon the strength of the ligaments, tendons and muscular development surrounding the joint. This lack of strength can be carried to the neck musculature as well. With the trend towards added head weight for mission enhancement devices this injury potential will only increase. Injury potential for females during normal mission activities may also be greater with these head-mounted systems.

5.5 Injury Risk Assessment in Naval Combat Aviation Head and Neck Injury.

Current methods of injury risk assessment rely on force and moment measurement of manikins in the region of the spine roughly representative of the occipital condyles and the base of the cervical spine (C7-T1). Results of these data are then evaluated by considering the peak loading and associated time domain or duration of pulse. Based on this analysis of peak loading, general conclusions can be reached concerning an indication of injury, by considering the results with respect to limit values. This limit value however, remains as only a rough order of magnitude. On the other hand, likelihood of injury, taking into account probability of specific modes, gender and variation of the response of organic elements are not currently considered. Therefore, the answer to a fundamental question of what was the probability of injury induced by the impact acceleration event is not yet attainable. The probability of injury remains a critical question for the Navy so that the effectiveness of support gear or other design solutions can be evaluated, and priority can be given to the efforts that have the most benefit or payoff, measured in lives saved and injury risk reduced. Therefore, continued research in the area of head and neck trauma is a critical need for Navy aviators.

6. Conclusion

In a combat situation, the post-ejection or crash surroundings necessitate that the air crew be able to escape and evade the enemy while trying to assist a helicopter rescue team in the recovery from the ejection or crash area. If the air crew is injured, then this task is made more difficult. Emergency egress on land requires sufficient strength to get out of the crashed aircraft. The badly injured air crew on land is more likely to become a prisoner of war who may in turn die in captivity. To compound the problem, a badly injured air crew, downed over water, may not be able to survive at sea even under peacetime operations. Because of these issues, greater emphasis in the military environment is placed on providing the lowest probability of injury that still allows escape, evasion and mission performance.

References

[1] Andersen HT. Neck injury sustained during exposure to high G forces in the F16B. *Aviat Space Environ Med* 1988:59: 356-8.

[2] Biesemans I, Ingels M, Vandenbosch P. A survey of cervical pain in pilots of a Belgian F.16 Air Defense Wing. In: *Neck Injury in Advanced Military Aircraft Environments.* In: *AGARD Conference Proceedings No. 471*, 1989.

[3] Knudson R, McMillan D, Doucette D, Seidel M. A comparative study of G-induced neck injury in pilots of the F/A-18, A-7, and A-4. *Aviat Space Environ Med* 1988:59: 758-60.

[4] Schall DG. Non-ejection neck injuries in high performance aircraft. in neck injury in advanced military aircraft environments. In: *AGARD Conference Proceedings No. 471*, 1989.

[5] Vanderbeek RD. Period prevalence of acute neck injury in U.S. Air Force pilots exposed to high G forces. *Aviat Space Environ Med* 1988:59: 1176-80.

[6] Gillingham K, Plentzas S, Lewis N. G Environments of F-4, F-5, F-15, and F-16 Aircraft During F-15 Tactics Development and Evaluation. USAFSAM-TR-85-51, 1985.

[7] Forster EM, Morrison JG, Hitchcock EH, Scerbo MW, Schmorrow D. Performance during a simulator surface to air missile avoidance G profile. *Aviat Space Environ Med* 1995:66: 465.

[8] Hamalainen O, Vanharanta H, Bloigu R. Determinants of +Gz-related neck pain: A preliminary survey. *Aviat Space Environ Med* 1993:64: 651-2.

[9] Guill F, Herd G. An evaluation of proposed causal mechanisms for "Ejection Associated" neck injuries. *Aviat Space Environ Med* 1989:60(7S): A26-47.

[10] Department of the Army. Aircraft Crash Survival Design Guide. USAAVSCOM TR 89-D-22, 1989.

[11] Shanahan DF. Basic Principles of Helicopter Crashworthiness. Technical Report USAARL 93-15, 1993.

[12] Chandler RF. Development of Crash Injury Protection in Civil Aviation. In: *Accidental Injury: Biomechanics and Prevention.* AM Nahum, JW Melvin (eds). Springer-Verlag, New York, 1993.

[13] Hubbard RP, Bergman PC. Biomechanical performance of a new head and neck support. SAE Paper 902312. In: *Proceedings 34th Stapp Car Crash Conference*, Society of Automotive Engineers, 1990.

[14] Coltman JW. Evaluation of the crash environment and injury-causing hazards in U.S. Navy helicopters. *SAFE Journal* 16(1).

[15] Tillman N, Kennedy G, Kinker L, Federman P, Speidel D. Advanced Crashworthy Air crew Survival System (ACASS) H-53 Mishap Analysis, NAWCAD Technical Report, May 1994 (unpublished as yet).

[16] Travis T, Passmore, JD, Lee R. USAF/USN helmet loss and head/neck injury experience in ejections 1989-1995. In: *Proceedings 67th Science Aerospace Medical Association*, May 1996, Atlanta, GA.

[17] McConnel R. Windblast Testing of the Crusader and HGU-68/P Helmets. NAWCAD Technical Report June, 1995 (unpublished as yet).

[18] Reh G. K-36 Foreign comparative testing program: Helmet testing. In: *Proceedings Safety and Flight Equipment Symposium*, Reno, NV, November 1994.

[19] Obergefell LA, Fleck JT, Kaleps I, Gardner TR. Articulated Total Body Model Enhancements, Volume 2: User's Guide, Armstrong Aerospace Medical Research Laboratory, AAMRL-TR-88-043, January 1988.

[20] Quartuccio J. Ejection seat and body dynamic simulation model. In: *1996 Safety and Flight Equipment Symposium*, Reno, NV, October 1996.

[21] Gilsanz V, Boechat MI, Gilzantz R, Loro ML, Roe TF, Goodman WG. Gender differences in vertebral sizes in adults: Biomechanical implications. *Radiology* 1994:190: 678-682.

[22] Chaffin DB, Andersson GBJ. *Occupational Biomechanics*, 2nd Edition. Wiley-Interscience, New York, 1991: 250-251.

Figure Caption

Figure 1: Time history of acceleration while avoiding a surface-to-air missile (Whitley).

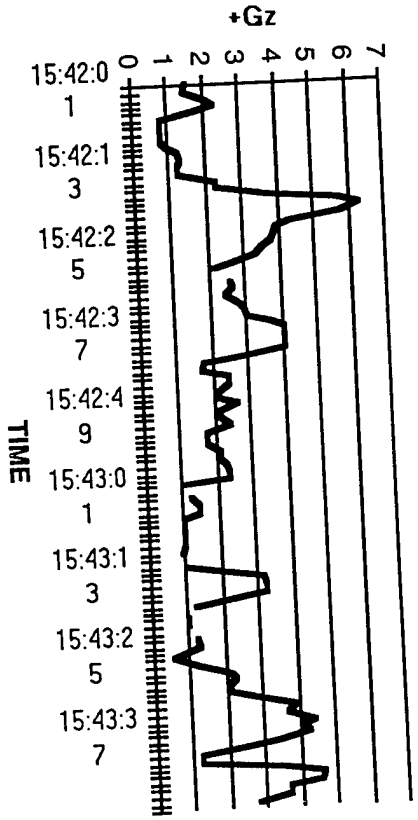
+Gz
0
1
2
3
4
5
6
7
TIME
15:42:01
15:42:13
15:42:25
15:42:37
15:42:49
15:43:01
15:43:13
15:43:25
15:43:37